Radiative corrections to the photon + 1 jet rate at LEP

Aude Gehrmann De-Ridder

Radiative Corrections to the Photon + 1 Jet Rate at LEP

Aude Gehrmann–De Ridder

Department of Physics
University of Durham

A thesis submitted to the University of Durham
for the degree of Doctor of Philosophy
April 1997

Declaration

I declare that the material presented in this thesis has not been submitted for a degree at this or any other university.
The research work presented in this thesis has been carried out primarily together with Dr. E.W.N. Glover and partly with T. Gehrmann. It will largely appear in the following publications:

- *Radiative Corrections to the Photon +1 Jet Rate at LEP*
  A. Gehrmann–De Ridder, T. Gehrmann and E.W.N. Glover, University of Durham preprint DTP/97/24, submitted to Phys. Lett. **B**.

- *A complete $\mathcal{O}(\alpha\alpha_s)$ calculation of the Photon +1 Jet Rate in e^+e^--annihilation*
  A. Gehrmann–De Ridder and E.W.N. Glover, University of Durham
  preprint DTP/97/26, (in preparation).

Acknowledgements

Firstly, I would like to thank Nigel Glover for his considerate guidance and continuous support throughout the completion of this Ph.D thesis.
I am very grateful to him for the confidence he showed to me from the instant at which I became his Ph.D student until the fulfillment of this rather difficult research project. I would like to thank him to have followed step by step and with continuous interest and confidence the progresses I made solving the problems arising in this many-sided and thereby even more challenging calculation. I also greatly appreciated to have had the opportunity to share his interest and enthusiasm on current topics of Particle Physics during the numerous discussions we had together.

The Particle Theory Group at Durham University provided a warm and friendly working atmosphere which contributed to render my stay in Durham in the last three years pleasant and enjoyable. I am grateful to all his members.

This work was financially supported by a research studentship of the University of Durham which is hereby gratefully acknowledged.

I would like to thank Prof. W. Buchmüller for his kind hospitality in the DESY Theory Group, where this work has been finalized.

Finally, I would like to thank my dear husband Thomas for his invaluable help and continuous encouragement during the completion of this Ph.D thesis. I am grateful to him for the numerous and enlightening discussions we had together and which helped me to find the answers to various physics questions directly related or not to the topic of my Ph.D dissertation. Most important of all however, I would like to thank him for his love and tenderness which rendered these three years spent together in Durham the most enjoyable and naturally, unforgettable.

Aude Gehrmann–De Ridder

A thesis submitted to the University of Durham
for the degree of Doctor of Philosophy
April 1997

Radiative Corrections to the Photon + 1 Jet Rate at LEP

Abstract

We present a complete calculation of the photon +1 jet rate in e^+e^- annihilation up to $\mathcal{O}(\alpha\alpha_s)$. Although formally of next-to-leading order in perturbation theory, this calculation contains several ingredients appropriate to a next-to-next-to-leading order calculation of jet observables. No such calculation has been performed before, and the work discussed here represents a first step in that direction. In particular, we describe a generalization of the commonly used phase space slicing method to isolate the singularities present when more than one particle is unresolved. More precisely, we provide an analytic evaluation of the following multiple unresolved factors: triple collinear factor, soft/collinear factor and double single collinear factor. By comparing the results of our calculation with the existing data on the photon +1 jet rate from the ALEPH Collaboration at CERN, we make a new determination of the process-independent non-perturbative quark-to-photon fragmentation function $D_{q\to\gamma}(z,\mu_F)$ at $\mathcal{O}(\alpha\alpha_s)$. As a first application of this measurement allied with our improved perturbative calculation, we determine the dependence of the isolated photon +1 jet cross section in a democratic clustering approach on the jet resolution parameter $y_{\rm cut}$ at next-to-leading order. Inclusion of the next-to-leading order corrections to this observable considerably improves the agreement between theoretical prediction and experimental data.

Contents

Chapter 1

Introduction

One of the main goals of particle physics is to identify the structureless constituents of matter and to understand the nature of forces acting between them. At the smallest distances currently probed in high energy accelerators ($\approx 10^{-18}$ m), there are two types of matter units: the *leptons* and the *quarks*, which both have spin 1/2. One distinguishes charged leptons, like the electron, which can interact both electromagnetically and weakly and the lepton-neutrinos which only interact weakly. The quarks – which are the constituents of hadrons – can interact via all three interactions: strong, electromagnetic and weak. These three fundamental interactions form the basis of our current understanding of particle physics, the Standard Model, which, up to now, appears to be in very good agreement with the experimental observations.

The remainder of this introductory chapter will be organized as follows. In the first part we shall present the fundamental features of *Quantum Chromodynamics* (QCD), the theory of the strong interaction (Sections 1.1 – 1.4), with particular emphasis on the perturbative domain of QCD. Essential properties of the weak interaction will be outlined in Section 1.5. In the second part we shall discuss the production of hadronic jets in e^+e^- annihilation experiments. In particular we shall describe how jet cross sections can be calculated within the framework of perturbative QCD and how the results of these calculations compare with experiment. Finally, within this context, we shall present the

a hadron. An example of a particle which seems to contradict this principle is the spin-3/2 resonance Δ^{++}. It consists of three 'up' quarks, with all spins pointing in the same direction.

This conceptual difficulty could be overcome by the introduction of a new quantum number, *colour* [3]. Quarks are assumed to carry one of the three colours (red, green or blue) and antiquarks one of the corresponding anticolours. The introduction of colour provides a way of categorizing which combinations of quarks are allowed. In fact, only colour singlet states can exist. If the group of colour transformation is SU(3), then the basic colour singlet states are precisely the observed baryons and mesons. The baryons are made of three quarks of different colours while the mesons consist of a quark-antiquark pair of the same colour.

Since the quark model was suggested, three more quarks (charm, bottom, top) have been discovered, all being heavier than u, d and s. Furthermore, experimental evidence of the validity of the 'colour SU(3) hypothesis' now exists. For example, the ratio R between the e^+e^- total hadronic cross section and the cross section for the production of a pair of muons provides one stringent piece of evidence for the existence of three colours.

1.1.2 Dynamical properties of quarks: Quantum chromodynamics (QCD)

One of the fundamental ideas of QCD [4] is that the quarks carry colour and that these colour 'charges' of the quarks act as sources of the strong or chromodynamic force between quarks, just as the electric charges act as sources of the electromagnetic force. As the quarks carry both colour and electric charge, they experience both the strong and electromagnetic forces, as well as the more feeble weak and gravitational interactions. However, the chromodynamic force is by far the strongest in the region of our interest ($\approx 10^{-18}$ m or equivalently for energies ranging between 1 GeV and few hundred GeV) and so can be examined independently from the others.

In analogy to QED, where the electromagnetic force between charged particles is me-

diated by one gauge boson, the photon, the chromodynamic interaction between coloured quarks is mediated via the gauge bosons of QCD, the *gluons*. The conservation of colour in quark-quark interactions is a consequence of the invariance under a redefinition of the colour label associated with a quark inside the hadron, i.e. it is a consequence of the invariance under the colour symmetry group $SU(3)_c$ of the theory. The structure of $SU(3)_c$ is more complicated than the structure of the electromagnetic symmetry group U(1) since the 8 massless spin-1 gluons themselves carry colour. These can therefore also act as source of the chromodynamic force and consequently can interact among themselves too. A hadron within this theory remains a colour singlet which is built of quarks which continually exchange gluons and consequently change colour.

The Lagrangian density of QCD is given by[1]

$$\mathcal{L} = -\frac{1}{4} F^a_{\mu\nu} F^{\mu\nu}_a + \sum_q \bar{\psi}_q \left[i\gamma^\mu D_\mu - m_q \right] \psi_q \ , \tag{1.1}$$

with

$$\begin{aligned} F^a_{\mu\nu} &= \partial_\mu A^a_\nu - \partial_\nu A^a_\mu - g f^{abc} A^b_\mu A^c_\nu, \\ D_\mu &= \partial_\mu + i g A^a_\mu T_a. \end{aligned} \tag{1.2}$$

The $SU(3)_c$ symmetry determines the algebra of the T^a matrices in fixing the structure constants f_{abc}:

$$\left[T^a, T^b \right] = i f^{abc} T^c.$$

From the above equation (1.1), we can read off the QCD interactions: the covariant derivative D_μ gives rise to a quark–gluon vertex, the contraction of the field strength tensors $F^a_{\mu\nu} F^{\mu\nu}_a$ yields 3-gluon and 4-gluon vertices. The parameter g is the strong coupling and can only be determined experimentally.

The colour structure of QCD is contained in the T^a matrices and their algebra. These can be factored out in practical calculations, yielding overall colour factors. Denoting by

[1] We give here only a brief outline of the quantum field theory of QCD, a more formal and complete treatment can for example be found in [5].

N the number of colours, the most common colour factors are:

$$\sum_{k=1}^{N}\sum_{a=1}^{N^2-1} \quad \underset{T^a_{ik}\quad T^a_{kj}}{\text{i k j}} \quad \equiv \quad C_F\,\delta_{ij} = \left(\frac{N^2-1}{2N}\right)\delta_{ij}\ ,$$

$$\sum_{i,j=1}^{N} \quad \underset{T^a_{ij}\quad T^b_{ji}}{\text{a i b, j}} \quad \equiv \quad T_F\,\delta^{ab} = \frac{1}{2}\delta^{ab}\ ,$$

$$\sum_{c,d=1}^{N^2-1} \quad \underset{f_{acd}\quad f_{bcd}}{\text{a c b, d}} \quad \equiv \quad C_A\,\delta^{ab} = N\delta^{ab}\ , \tag{1.3}$$

and furthermore $T_f \equiv n_f\,T_F$. Thus for the specific case of SU(3) we have

$$C_F = \frac{4}{3}, \quad C_A = 3.$$

In the remainder of this thesis we shall keep the number of colours to be N and the only colour factor which will be present in the calculation of the photon + 1 jet rate at $O(\alpha\alpha_s)$ is C_F. Systematically, we shall write this colour factor as $\left(\frac{N^2-1}{2N}\right)$ to avoid confusion with the unresolved single collinear factor.

1.1.3 Asymptotic freedom and confinement

The essential physical idea is the following. The strong interaction between two coloured entities can be characterized by a coupling which is a function of the distance between them rather than a constant. In fact, when the distance probed is very small, or equivalently when the energy is sufficiently high (typically greater than 10 GeV), the coupling tends to zero, i.e. the quarks only interact very weakly with each other and can be treated as free particles. The theory in this regime is called *asymptotically free*. This property of QCD is essential to guarantee that calculations at the quark level are meaningful. Indeed as in QED, where the coupling constant is also small ($\alpha = \frac{1}{137}$), in this high energy regime calculations of physical quantities are possible because the increasingly complicated higher-order processes become decreasingly important. Such calculations will then be performed using a perturbative expansion – a series in the strong coupling constant α_s.

On the other hand, when the distance between the two coloured entities increases and becomes macroscopic, the coupling between them becomes large and possibly even bigger than 1. This strong coupling is responsible for the observed confinement of quarks within hadrons. A phenomenon which is presently not yet fully understood theoretically, as non-perturbative methods are still under development.

The origin of the running of the QCD coupling with the scale (i.e. the distance at which the interaction is probed) can be understood as follows. Let us consider a physical process which depends on one hard scale Q only. When this process is evaluated as a perturbative series in the strong coupling α_s, ultraviolet divergences may appear. These divergences can only be renormalized by a redefinition of the coupling α_s. As a result, α_s becomes a function of the renormalization scale, which is typically taken to be Q, i.e. it runs. The derivation of the scale dependent strong coupling α_s is outlined in Section 2.5. A more formal and complete derivation of the renormalization procedure of ultraviolet divergences in QCD can be found in [6].

In the evaluation of the photon +1 jet rate at $\mathcal{O}(\alpha\alpha_s)$, no ultraviolet divergences occur as no pure quark or pure gluon self energy loops are included at this first order in α_s and in α. The coupling α_s does therefore not need to be renormalized.

1.2 Perturbative QCD: Essential theorems

At high energies, the evaluation of physical observables involving the production of quarks as a perturbative expansion in α_s is considerably simplified if the masses of the quarks can be neglected. For the class of processes we will focus on in this thesis, the production of quark-antiquark pairs in e^+e^- annihilation, this is the case. This process depends on one large scale, the mass of the Z-boson ($M_Z = 91$ GeV). Compared to this scale, the masses of the quarks produced by the decay of the Z-boson (u, d, s, c, b) can be consistently neglected.

1.2.1 The KLN theorems

The consideration of massless quarks and on-shell gluons in the calculation of cross sections leads however to *soft* and *collinear* divergences. Indeed, as an example, let us consider the production of a quark-antiquark pair with an additional gluon radiated on the quark side. In the massless limit, the inverse quark-gluon propagator given by[2] $s_{qg} = 2E_qE_g(1 - \cos\theta_{qg})$ vanishes if either the gluon is soft, $E_g \to 0$, or it is collinear to the quark, $\theta_{qg} \to 0$. Consequently the matrix element squared which contains terms proportional to $\left\{\frac{1}{s_{qg}}\right\}$ diverges in these limits. The cross section for the production of a quark-antiquark pair and a real gluon which is obtained as the result of the integration of the $\{q\bar{q}g\}$-matrix element squared over the 3-particle phase space is also infinite; the phase space integrals are not calculable as their integrand contain infinities. However, the total cross section at $\mathcal{O}(\alpha_s)$, which includes both real radiation and the contribution where a virtual gluon is exchanged between the quark and antiquark is finite. This is a consequence of the Bloch, Nordsieck and Kinoshita, Lee, Nauenberg (KLN) theorems [7] which guarantee that for any suitably defined[3] physical quantity, calculable as a perturbative series, the infinities present in individual terms of the real and virtual contributions arising in the calculation cancel amongst each other.

In order to evaluate these real and virtual contributions present at this order in α_s and which contain singularities, a regularization procedure is required. The procedure used in this dissertation is *dimensional regularization*[4]. Within this procedure, the number of space time dimensions is considered to be $d = 4 - 2\epsilon$ with $\epsilon < 0$, the regularization parameter. Going to $d \neq 4$ affects both the phase space and matrix elements of the $q\bar{q}(g)$ process. As a result the integrals become feasible, the soft and collinear singularities arising in both real and virtual contributions appear as poles in ϵ. When the two contributions are added together, the poles exactly cancel, and the limit $\epsilon \to 0$ can be safely

[2]The invariant mass $\{s_{qg}\}$ defined by $s_{qg} = (p_q + p_g)^2$ is given by $2p_qp_g$ in the massless limit.

[3]We shall come back to explain what is meant by 'suitably defined' physical quantities later.

[4]For a formal derivation of the dimensional regularization procedure, see [8].

taken yielding a finite result for the total cross section. In Section 1.5.3 we shall explicitly demonstrate how soft and collinear divergences manifest themselves as poles in ϵ for this particular $\{q\bar{q}(g)\}$ production cross section. Furthermore we shall show for this example how the cancellation of singularities present in the real and virtual contributions occurs.

The suitably defined quantities to which the theorems above apply are *infrared safe* quantities. These are independent of the masses of the light quarks in the high energy domain. Such quantities possess a perturbative expansion in the small coupling α_s that is free of soft or collinear singularities. Consequently they are *calculable* in perturbation theory. As the masses of the light partons are only negligible at short distances, infrared safe quantities correspondingly depend only on the short-distance (or high energy) behaviour of QCD and not on the long-distance effects which produce the confinement of quarks. An example of infrared safe quantity is given by the total hadronic cross section in e^+e^- annihilation.

1.2.2 The factorization theorem

For quantities which are 'infrared-sensitive', i.e. that have infrared and collinear singularities, perturbation theory cannot make absolute predictions. The theory may however be able to predict their behaviour. Indeed, such quantities can still be handled provided the singularities can be collected into an overall non-perturbative factor which describes the dependence of the quantity on long distance physics. Through this factorization procedure, an arbitrary scale, the factorization scale, often denoted by μ_F is introduced. It can be thought of as the scale which separates the long distance hadronic physics from the short distance partonic physics. The infrared-sensitive quantity becomes dependent on this scale and can therefore ultimately only be determined experimentally. Nevertheless, once the factorization procedure has been carried out, perturbation theory can still be used to predict how the non-perturbative factor varies or 'evolves' with different choices of the factorization scale. The factorization properties of particular infrared-sensitive quantities can be proven to all orders in perturbation theory. For more details concerning

the factorization theorems, see [9]. Together with the KLN theorem, this factorization theorem constitutes the necessary theoretical basis allowing the description of scattering processes involving hadrons within the framework of perturbative QCD.

1.2.3 Fragmentation processes

A typical class of infrared-sensitive quantities to which the factorization theorem applies are cross sections involving the fragmentation of quarks into hadrons in e^+e^- annihilation processes. The probability of obtaining a hadron as a result of the fragmentation process can be described by a fragmentation function which is a dimensionless, universal and process independent quantity. Generally, the leading-order cross section for the production of a hadron in a hard collision may be expressed as a sum over all partons of a convolution between a partonic (or short-distance) cross section and the parton-to-hadron fragmentation function. The collinear quark-gluon singularities appearing in the perturbative expansion of the hard scattering cross section get absorbed into the fragmentation function. Through this procedure, the fragmentation function becomes dependent on the factorization scale and can therefore only be determined experimentally. The perturbative expansion of the hard scattering cross section is rendered finite and calculable but also dependent on the factorization scale.

If the hadron under consideration is a photon the situation is slightly different as the quarks can emit a photon via the electromagnetic interaction too [10]. Consequently, the leading order cross section (which is of $\mathcal{O}(\alpha)$) for the production of a quark-antiquark pair with an additional photon receives two contributions, the processes $e^+e^- \to q\bar{q}\gamma$ and $e^+e^- \to q\bar{q}$ with associated quark-to-photon fragmentation. In this case, the quark-photon collinear singularities present in the first contribution need to be factorized in the quark-to-photon fragmentation function of the second process. As a result both contributions become finite and μ_F-dependent.

The reason why these two above processes should be considered together will be discussed in detail in Section 2.1. Furthermore, in Section 2.4 we shall derive the factorization

of the quark-photon collinear singularities for the lowest order process $e^+e^- \to q\bar{q}+\gamma$. The factorization of these collinear singularities together with the derivation of the factorization scale dependence of the quark-to-photon fragmentation function at next-to-leading order ($O(\alpha\alpha_s)$) is one of the goals of this dissertation and will be explicitly shown in Chapter 8. Using these results, we shall be able to determine the factorization scale dependent quark-to-photon fragmentation function at $\mathcal{O}(\alpha\alpha_s)$ from experimental data on final state photons in e^+e^- annihilation. This determination will be described in Chapter 10.

1.2.4 Importance of a precise determination of the quark-to-photon fragmentation function

The quark-to-photon fragmentation function is of particular importance to estimate the cross section for final state photon radiation in hadron–hadron collisions; e.g. the process $pp \to \gamma\gamma + X$ forms an important background to the Higgs decay $pp \to H + X \to \gamma\gamma + X$ process, which is a preferred channel for the discovery of the Standard Model Higgs with intermediate mass at LHC.

Let us first examine the different QCD processes contributing to $pp \to X + \gamma\gamma$. At leading order, two photons are produced through the Born process $q\bar{q} \to \gamma\gamma$ and important contributions of $\mathcal{O}(\alpha_s)$ and $\mathcal{O}(\alpha_s^2)$ are the box graph and the fragmentation processes. Those three processes are illustrated in Fig.(1.1). The box graph process $gg \to \gamma\gamma$ is mediated by a quark loop while the fragmentation processes $qg \to \gamma(q \to \gamma)$ or $gg \to (q \to \gamma)(\bar{q} \to \gamma)$ contain one or two photons which are radiated approximately collinearly from final state quarks. These processes may be evaluated in terms of the quark-to-photon fragmentation function. So far those fragmentation processes have been estimated by P.Aurenche et al. and E.Berger et al. in [11] using the quark-to-photon fragmentation function [12] available in the literature[5]. It was found [13] that the total cross section is dominated by the fragmentation processes.

[5]We will return to the form of this lowest order fragmentation function in Section 2.5.

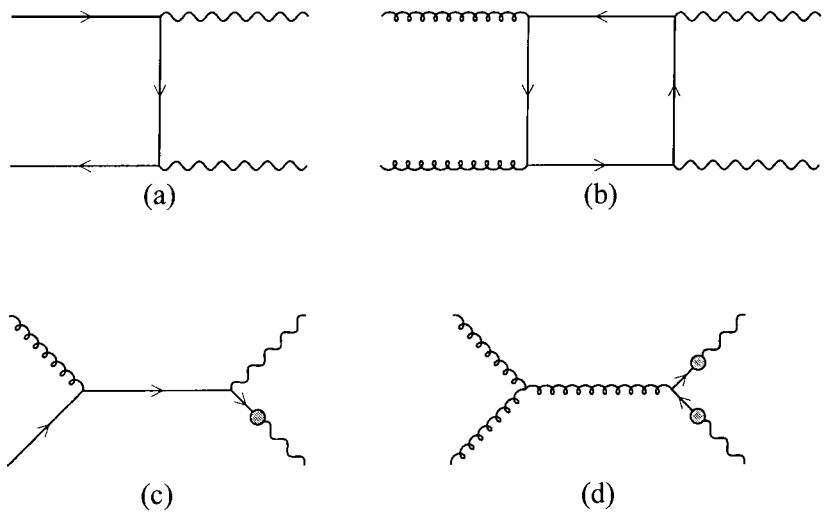

Figure 1.1: Examples for Standard Model background processes to the $H \to \gamma\gamma$ signal at hadron colliders: (a) Born process, (b) box graph, (c) single fragmentation, (d) double fragmentation.

One of the main difficulties in the determination of a possible discovery channel for the Higgs boson comes from the arbitrariness of its mass. This leads a priori to a multitude of possible production and decay scenarios. However from the non-detection of the Higgs boson at LEP so far, lower bounds on the mass of the Higgs boson can be derived. Moreover, theoretical arguments yield some upper bounds on it, as outlined in [14]. The Higgs mass can be constrained as follows, 65 GeV $< M_H <$ 1 TeV. A light Higgs ($M_H <$ 85 GeV) may still be found[6] at LEP2 while a heavy Higgs ($M_H >$ 180 GeV) has a clear signature at LHC through its Z^0Z^0 or WW decays. The intermediate Higgs mass range (85 GeV $\leq M_H \leq$ 180 GeV) seems to be more problematical[7]. Although the Higgs production cross section is very large, the normally preferred decay mode into a pair of heavy b quarks suffers from a large QCD two jet background to the extent that only

[6]Details on Higgs searches at LEP2 can be found in [15].

[7]Details on searches for the Higgs in this intermediate mass range have been discussed in the Proceedings of the LHC workshop (Aachen 1990), [13].

rare decay modes with a clean and distinct signature (such as $H \rightarrow \gamma\gamma$) are considered worthwhile. For an intermediate mass Higgs, this decay mode may be detectable despite its small branching ratio ($\approx 10^{-3}$) because of the large Higgs production cross section. This process has a clear signature: the production of a pair of isolated high p_T photons and essentially no missing p_T. One serious source of background is however due to: the "irreducible" $\gamma\gamma$ background (i.e. same final state as the signal) from $q\bar{q} \rightarrow \gamma\gamma$ and $gg \rightarrow \gamma\gamma$.

As we mentioned in the previous paragraph the main contribution to the total $\gamma\gamma$ cross section comes from the fragmentation processes (roughly one order of magnitude bigger than the box and Born graphs). As these contributions are related to the presence of a collinear photon in the final state, the fragmentation contributions could in principle be reduced by imposing some isolation cuts. However it is not clear whether the imposition of such cuts is sufficient to obtain a clear distinction between signal and background. It depends on how important those fragmentation contributions are. A precise determination of this irreducible background and therefore of the quark-to-photon fragmentation function is needed. The results obtained in the remainder of this thesis should help to contribute to this determination.

1.3 The weak interaction

As we mentioned before, at the energies we are particularly interested in, the quarks and gluons are the fundamental entities between which the strong interactions can be described within perturbative QCD and between which the weak interactions are largely negligible. In e^+e^- annihilation processes, however, the quarks are produced via the weak decay of a Z-boson. We shall therefore briefly outline essential features of the weak interaction to conclude the first part of this introductory chapter.

Prior to the early 60's one of the most common processes where a weak interaction takes place was the neutron β-decay into a proton, an electron and an antineutrino. It was also predominantly this reaction which formed the basis of the first description of a

theory of the weak interactions by Fermi in 1934 [16]. Within this description the four fermions interact at a single point. This interaction is characterized by a single coupling G_F, ($G_F = 1.1 \times 10^{-5}\text{GeV}^{-2}$), the Fermi coupling constant which measures the strength of the weak force and an a priori unknown function Γ which contains the essence of the weak interactions and is responsible for the transformations of the particles. Just after the essential experimental discovery of the parity-violation property of the weak interactions [17], in 1956 Feynman and Gell-Mann suggested that this function Γ should be a mixture of vector and axial vector quantities [18] to account for these parity-violating effects of the weak interaction. Within this pointlike interaction model for the weak force with couplings which are a mixture of a vector and an axial vector, one is able to explain all the data from low-energy weak interaction processes. However, the Fermi theory makes unacceptable predictions for the high energy behaviour of the weak interactions.

Nowadays the weak interactions may be described together with the electromagnetic interactions in a unified theory, the electroweak theory. Within this framework, the weak interactions are mediated by three gauge bosons: $W^{\pm}$ and Z^0, which couple to a quantum number called, weak isospin[8] . Through the Higgs mechanism, the symmetry between electromagnetic and weak interactions is spontaneously broken and the weak gauge bosons acquire mass ($M_W \sim 80.4$ GeV, $M_Z \sim 91.2$ GeV).

A particular feature of the W and Z bosons is their coupling structure to fermions. As a result of the violation of parity by the weak interactions, the W couples only to the left-handed fermions, and the coupling of the Z boson to the left-handed and right handed fermions are non-identical. This is expressed in couplings with vector and axial vector contributions.

At low energies this electroweak model reproduces the Fermi model, provided that the weak charge g_W is related to the Fermi constant G_F as follows:

$$\frac{G_F}{\sqrt{2}} = \frac{g_W^2}{8M_W^2}. \tag{1.4}$$

[8]We mention here only basic features of the electroweak model, more complete treatments can be found in the literature, for example in [19].

	e_f	v_f	a_f	Particles		
Quarks	$\frac{2}{3}$	$\frac{1}{2} - \frac{4}{3}\sin^2\Theta_W$	$\frac{1}{2}$	u	c	t
	$-\frac{1}{3}$	$-\frac{1}{2} + \frac{2}{3}\sin^2\Theta_W$	$-\frac{1}{2}$	d	s	b
Leptons	0	$\frac{1}{2}$	$\frac{1}{2}$	ν_e	ν_μ	ν_τ
	-1	$-\frac{1}{2} + 2\sin^2\Theta_W$	$-\frac{1}{2}$	e	μ	τ

Table 1.1: Particle content of the Standard Model, electric charges e_f, vector- and axialvector-couplings v_f, a_f with $\sin^2\Theta_W = 0.232$ the ratio of electromagnetic and weak coupling constant. All particles are spin–1/2 fermions.

The particle content of the Standard Model can be grouped into three generations of quarks and leptons, which are listed in Table 1.1.

1.4 Jet Physics at LEP

1.4.1 Introduction

Electron-positron annihilation into hadrons is one of the most precise tools to study the properties of QCD. The success of these studies is partly due to the fact that the hadronic cross section near the Z resonance is large, 40 nb. Below and above the Z peak the e^+e^- annihilation hadronic cross section is significantly smaller. In an electron-positron annihilation event, the produced Z boson decays into a quark-antiquark pair. Subsequently, these quarks radiate gluons which themselves decay into gluons or quark-antiquark pairs. At a certain point, these *partons* (quarks or gluons) transform themselves into the experimentally observed hadrons. In a typical such event, two or sometimes three or more sprays of approximately comoving hadrons are produced. These sprays or clusters of hadrons are called *jets*.

The first evidence for a *jet structure* in hadron production by e^+e^- annihilation processes was reported back in the year 1975 [20]. The data, taken at the Stanford Laboratory,

showed an increasingly two-jet like event structure when the centre of mass energy, E_{cm} was raised from 3 to 7.4 GeV. The jet structure manifests itself in a decrease of the mean sphericity, a measure of the global shape of hadronic events (ideal back-to-back two-jet events have a spericity value of 0, while spherical events have $S = 1$). In 1979, a small fraction of planar, well separated three-jet events were observed by the PETRA experiments around $E_{cm} \approx 30$ GeV [21]. Finally, the year 1982 brought first evidence for four-jet like events, observed by the JADE experimental collaboration [22] at $E_{cm} = 33$ GeV. We shall comment on the occurence of these different n-jet like events at the end of this section[9].

Although the formation of these hadrons in e^+e^- annihilation is the consequence of a *non-perturbative* process, various measurable cross sections with final state hadrons can be calculated within the theoretical framework of perturbative QCD. The reason is that the production process of a primary quark-antiquark pair, the basic process leading to the formation of hadrons, occurs at a much earlier time than the production of hadrons. The non-perturbative interactions which change the quarks and the gluons into hadrons occurs "too late" to modify the original probability for the event to happen. Consequently, the production of hadrons, and in particular of *jets* can be calculated in perturbation theory.

1.4.2 Jet definition

Most commonly, one measures the cross section for the final state to contain exactly 2, 3, 4,... jets. A *jet definition* provides then a procedure to classify experimentally final state hadronic events according to the number of jets they contain. Furthermore as jet cross sections shall be calculated in perturbative QCD, the *same* jet definition should be used in the parton-level calculation, to classify the quarks and gluons into parton level jets. To be applicable in a perturbative calculation, a jet definition must satisfy the following criteria: It should lead to cross sections which are free of soft and collinear singularities, in other words, the definition must be infrared safe. Furthermore it should also be relatively

[9] Further details on these experimental determinations together with an experimental overview of jet physics as a quantitative test ground of QCD properties can be found in [23].

insensitive to the transformation of quarks and gluons into hadrons.

The possibility of measuring and calculating infrared safe jet cross sections was first explored by Sterman and Weinberg [24]. In their picture, the jets are defined with the aid of cones surrounding the produced hadrons. The definitions used nowadays for electron-positron collisions involve a clustering algorithm which successively combines the final state hadrons into jets. In the corresponding theoretical calculations, the same algorithm is used to combine the partons into jets. More precisely, a test variable d_{ij} is constructed for all possible pair of momenta p_i and p_j in an event. The pair with the smallest d_{ij} are then combined to form a pseudoparticle provided d_{ij} is smaller than some fixed value of the experimental jet resolution parameter commonly denoted by y_{cut}. This process is repeated until no further clusterings occur. The number of jets and their momenta are then given by the remaining pseudoparticles. The recombination procedure can ensure that the resulting pseudoparticles are massless or that they preserve energy-momentum but cannot ensure both properties at the same time. The way the partons (hadrons) momenta are combined to give the pseudoparticle momentum defines a particular *recombination* scheme[10]. The definition of the test function d_{ij} defines the *jet algorithm*. There are several distinct algorithms used at LEP and here we shall focus on the JADE [26] and k_T- or DURHAM [27] algorithms.

For the JADE algorithm, the test variable is simply given in the e^+e^- centre-of-mass frame in terms of the dimensionless invariant quantity,

$$d_{ij} = y_{ij} = \frac{s_{ij}}{s} = 2E_iE_j(1 - \cos\theta_{ij}). \tag{1.5}$$

Notice that with this definition, this algorithm is infrared safe: A particle that has only a small amount of energy will not affect the final number of jets or their four-momenta, since it will only contribute to a small amount of the final four-momentum of the jet in which it is included. Similarly if two particles are nearly collinear, then the first step of the algorithm is to combine them into one jet.

[10]The definitions of the most commonly used scheme can for example be found in [25]

The k_T or Durham algorithm was introduced when it has been realized that the JADE algorithm sometimes reconstructs "spurious" jets, i.e. clusters of hadrons or partons whose momenta do not correspond to any set of approximately comoving particles in the event. For example, this can happen when soft gluons are emitted close to one of the quarks or antiquarks. In this case the JADE algorithm has the tendency to cluster the soft particles together instead of combining them separately with the quark and the antiquark. In the Durham algorithm defined in the e^+e^- centre-of-mass frame by,

$$d_{ij} = 2\,\min(\mathrm{E_i^2}, \mathrm{E_j^2})\,\frac{(1-\cos\theta_{\mathrm{ij}})}{\mathrm{s}}, \tag{1.6}$$

the soft particles are clustered more naturally with the quark and the antiquark [27][11]. The Durham algorithm is also infrared safe and can therefore be used to measure and to calculate cross sections with a fixed number of jets. We shall use this jet algorithm to ultimately evaluate the photon +1 jet rate at $\mathcal{O}(\alpha alpha_s)$ numerically. For any jet algorithm, at lowest order, each parton is identified with a jet, such that the jet cross section is simply given by the partonic cross section. This jet cross section is obtained integrating numerically the partonic matrix element squared over the phase space defined by the recombination algorithm. At higher orders the evaluation of jet cross sections requires more thought. Section 1.5 will be dedicated to this study.

1.4.3 Jet rates

To conclude this section on generalities of the physics of jets at LEP we shall discuss the occurrence of n-jet like events as a function of the jet resolution parameter y_{cut}. In particular, in Figure 1.2, taken from [14], the jet rates measured by the OPAL Collaboration are compared with the rates obtained from a fixed order perturbative calculation. Both rates are functions of y_{cut}.

[11] For a more detailed description of these two algorithms, see for example the contributions of Dokshitzer and Brown in the proceedings to the Durham workshop on Jet Studies at LEP and HERA (1991) [27, 28].

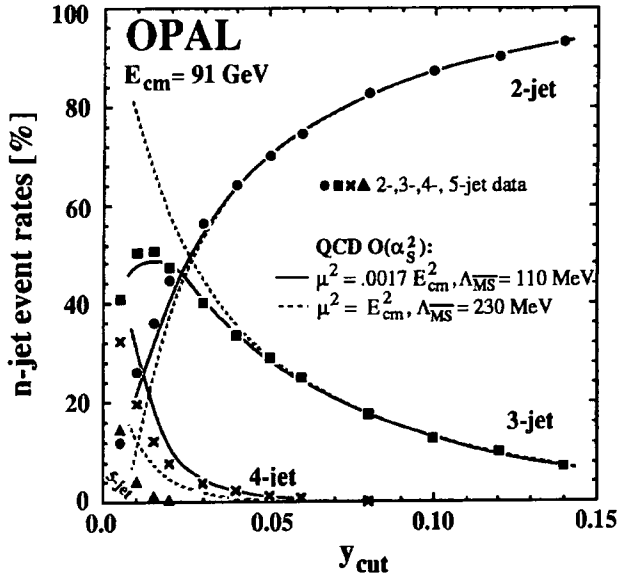

Figure 1.2: Jet rates as a function of the jet resolution parameter $y_{\rm cut}$ obtained using the JADE algorithm.

Concerning the measured rate, at large y_{cut} the events are essentially all classified as 2-jet events. As y_{cut} decreases, the jets become narrower, fewer events are two jet like and the number of multijet events increases. For some small y_{cut} the number of 2-jet events tends to zero. For an even smaller value of y_{cut} the 3-jet rate tends to zero and so on for higher number of jets and smaller values of y_{cut}. For the calculated rates, at $\mathcal{O}(\alpha_s^2)$, the results are slightly different. At large y_{cut} one observes a similar behaviour as for the measured rates, however the results differ significantly for small values of y_{cut}. For sufficiently small values of y_{cut} in fact, the 2-jet rate tends to $-\infty$ while the 3-jet rate tends to $+\infty$. Indeed, for small values of y_{cut} the presence of large logarithms of y_{cut} induces the breakdown of the perturbative approach. These logarithms must be resummed to all orders to obtain a reliable prediction. It is only by resumming these large logarithms to all orders in perturbation theory that the turn-over observed for example at $y_{cut} = 0.02$ for the 3-jet rate in Fig.1.2 can be reproduced.

1.5 Calculation of jet cross sections at higher orders

At lowest order, as we have seen in Section 1.4 the individual partons in the final state can be identified as jets. The jet cross sections can be obtained by integrating numerically the parton cross section over the phase space defined by the jet algorithm.

As higher order corrections are included, more and more partons are admitted in the final state. In contrast to the lowest order interpretation, the partons cannot be directly identified as jets anymore. Two things could happen: Either, a parton although it is hard, can be clustered to other partons to form a jet. This jet is then defined with the aid of a jet algorithm with an *experimental* resolution criterion y_{cut} as discussed in Section 1.4. Or, when higher order corrections are included, the partons in the final state can also be *collinear* and/or *soft*.

As the presence of soft and/or collinear partons in the final state induces divergences in different contributions to the partonic cross section, it is not possible anymore to evaluate this cross section directly numerically. As mentioned in Section 1.2.1, the Bloch-Nordsieck and Kinoshita-Lee-Nauenberg theorems guarantee us however that similar divergences are also present in the virtual contributions to the jet cross section. Furthermore, those theorems ensure that these divergences present in the real and virtual contributions (which manifest themselves as poles in ϵ in dimensional regularization) cancel against each other. To evaluate the partonic cross section in such a way that the cancellation of soft and collinear singularities is possible, one would therefore in principle need to calculate the matrix element and to perform the phase space integrals analytically in d dimensions. This becomes rapidly unfeasible as the number of particles in the final state increases [29]. An alternative is to find a way to split the calculation of jet cross sections into analytic and numerical parts. In this way, the divergent contributions are calculated analytically in d-dimensions while the finite terms can be evaluated numerically using standard techniques, such as Monte Carlo integration. There are essentially three different methods which render the evaluation of higher order jet cross sections possible: the *subtraction*, *phase space slicing* and *hybrid subtraction* methods. We shall briefly explain these three methods

in the following.

1.5.1 Three numerical methods

The basic features of these numerical methods may be understood by means of the evaluation of a simple one-dimensional integral as suggested by Z.Kunszt and D.Soper in [30],

$$\mathcal{I} = \lim_{\epsilon \to 0} \left\{ \int_0^1 \frac{dx}{x} x^\epsilon F(x) - \frac{1}{\epsilon} F(0) \right\}. \tag{1.7}$$

$F(x)$ is a complicated function, which renders the evaluation of $\mathcal{I}$ analytically impossible. $\mathcal{I}$ could represent a n-jet cross section while $F(x)$ could stand for the $n+1$-parton bremsstrahlung matrix elements and x for an invariant mass s_{ij}. As $x \to 0$, which corresponds in the framework of jet cross sections to the case when one of the final state particles becomes soft or collinear, the integrand is regularised by the x^ϵ factor as in dimensional regularization. The first term is however still divergent as $\epsilon \to 0$. This divergence is cancelled by the second term - which is the equivalent of the n-parton one-loop contribution - so that the integral is finite.

The first method we shall describe is the method used first by R.K.Ellis, Ross and Terrano in [31] for the evaluation of $\mathcal{O}(\alpha_s^2)$ quantities in electron-positron annihilation, also known as the *subtraction* method. It was then further developed by Z.Kunszt and D.Soper in [30] to be applied to the evaluation of jet cross sections in hadron collisions. Here, a divergent term is subtracted from the first term and added to the second,

$$\begin{aligned} \mathcal{I} &= \lim_{\epsilon \to 0} \left\{ \int_0^1 \frac{dx}{x} x^\epsilon (F(x) - F(0)) + F(0) \int_0^1 \frac{dx}{x} x^\epsilon - \frac{1}{\epsilon} F(0) \right\} \\ &= \int_0^1 \frac{dx}{x} \left(F(x) - F(0) \right), \end{aligned} \tag{1.8}$$

so that the integral is manifestly finite. The first term shall be evaluated numerically in 4 space time dimensions whereas the second one needs to be calculated analytically in d-dimensions. This method has the advantages of requiring no extra theoretical cutoffs and making no approximations. A disadvantage is however that it does require the analytical evaluation of the subtraction term, the analogue of $F(0) \int_0^1 \frac{dx}{x} x^\epsilon$, for each process

individually. An attempt to systematize the evaluation of these subtraction terms has been recently suggested by S.Catani and M.H.Seymour in [32]. Details of their method can be found in [32]. For further applications of the subtraction method, see [33].

An alternate approach which is known as the phase space slicing method was first introduced by [34] and further developed by W.T.Giele and E.W.N.Glover in [25]. In this review, the method was elaborated to evaluate higher order jet cross sections in e^+e^- annihilation. The essential tool of this approach is the decomposition of the integration region into two parts, $0 < x < \delta$ and $\delta < x < 1$. In the first region, the function $F(x)$ can be approximated by $F(0)$ provided the arbitrary cutoff, which is a purely theoretical separation criterion, $\delta \ll 1$,

$$\begin{aligned} \mathcal{I} &\sim \lim_{\epsilon \to 0} \left\{ \int_\delta^1 \frac{dx}{x} x^\epsilon F(x) + F(0) \int_0^\delta \frac{dx}{x} x^\epsilon - \frac{1}{\epsilon} F(0) \right\} \\ &\sim \int_\delta^1 \frac{dx}{x} F(x) + F(0) \ln(\delta). \end{aligned} \tag{1.9}$$

In the first region of phase space the integration can be performed numerically as $F(x)$ is convergent over the whole range of integration, whereas in the second region it needs to be calculated analytically. However the evaluation of the analogue of $F(0) \int_0^\delta \frac{dx}{x} x^\epsilon$ should be easier to evaluate than the subtraction term in eq.(1.8). In the language of jet cross sections, the evaluation of $F(0) \int_0^\delta \frac{dx}{x} x^\epsilon$ corresponds to the evaluation of the approximated matrix element squared over the approximated phase space in a singular, i.e. soft or collinear, region. As these soft/collinear approximations of matrix elements and phase space are universal [25], the application of the phase space slicing method to a wide variety of physical processes is possible and facilitated.

A main drawback of this approach however is the presence of the arbitrary cutoff δ. The integral $\mathcal{I}$ or equivalently any physical process should not depend on δ. The δ dependence of the two terms in eq.(1.9) should cancel. In the evaluation of a jet cross section, the cancellation of the δ dependence is realised numerically by a Monte Carlo program. This is not a straightforward point for the following reasons. The soft/collinear approximations used in the analytic part of the calculation are reliable only when δ is

small and are best when δ is the smallest possible. For the numerical cancellation of the δ dependence on the other hand, "not too small" values of δ are preferred since smaller values of δ induce the cancellation of larger logarithms, possibly giving rise to numerical instability problems. In practice δ is chosen in such a way that the approximations performed in the analytic calculation are valid and that the instability problems are avoided. The phase space slicing method has been applied so far to $e^+e^- \to 2$ jets, $e^+e^- \to 3$ jets [25], $p\bar{p} \to W, Z + 1$ jet, $p\bar{p} \to 2$ jets [35] and $ep \to e + 2$ jets [36].

Finally, a third method is a hybrid of the two previous techniques, called the *hybrid subtraction* method [37]. To preserve the portability of the phase space slicing method, we add and subtract only the universal soft/collinear approximations for $0 < x < \delta$,

$$\begin{aligned}
\mathcal{I} &\sim \lim_{\epsilon\to 0}\left\{\int_0^1 \frac{dx}{x}x^\epsilon F(x) - F(0)\int_0^\delta \frac{dx}{x}x^\epsilon + F(0)\int_0^\delta \frac{dx}{x}x^\epsilon - \frac{1}{\epsilon}F(0)\right\} \\
&\sim \lim_{\epsilon\to 0}\left\{\int_\delta^1 \frac{dx}{x}x^\epsilon F(x) + \int_0^\delta \frac{dx}{x}x^\epsilon\left[F(x) - F(0)\right]\right. \\
&\quad \left. + F(0)\int_0^\delta \frac{dx}{x}x^\epsilon - \frac{1}{\epsilon}F(0)\right\} \\
&\sim \left\{\int_\delta^1 \frac{dx}{x}F(x) + \int_0^\delta \frac{dx}{x}\left[F(x) - F(0)\right] + F(0)\ln(\delta)\right\}. \qquad (1.10)
\end{aligned}$$

Eq.(1.10) reflects how the calculation of jet cross sections is performed using this method. The first and last term in this equation are identical to those in the equation describing the phase space slicing method, eq.(1.9). Consequently, when applying these two methods to the evaluation of jet cross sections, the isolation of soft/collinear divergences and the evaluation of the matrix element squared integrated over the non-singular region will be performed in the same way within both methods. Moreover the cancellation of the δ dependence is also realised on a numerical basis within the hybrid subtraction method.

The difference between the latter two approaches is given by,

$$\int_0^\delta \frac{dx}{x}\left(F(x) - F(0)\right). \qquad (1.11)$$

In the "language" of jet cross sections this term corresponds to the evaluation of the difference between the full matrix element squared and its approximation integrated over

the phase space restricted to the region where $0 < x < \delta$. Clearly, the difference between the two approaches tends to zero as $\delta \to 0$. Furthermore, provided δ is chosen small enough, all three methods should give equivalent results. This was shown to be indeed the case for a particular physical quantity, the energy-energy correlation function [38] in [37] where the small unphysical parameter is labelled $y_{\min}$. In particular, in this letter the authors discuss for which particular choice of $y_{\min}$ the results obtained applying the phase space slicing or hybrid subtraction method, agreed reasonably well with the results obtained using the subtraction method. They found that at large $y_{\min}$ the predictions varied rapidly with $y_{\min}$. This is understandable since for large $y_{\min}$ values, the approximations used to perform the analytic integrations are inaccurate. For $y_{\min} < 10^{-4}$, this variation was found to be small. A reasonable approximation to the $y_{\min} \to 0$ limit, which does not lead to numerical instability problems was therefore chosen to be $y_{\min} = 10^{-5}$.

Nevertheless, it is worth noting that it can also happen that the difference between phase space slicing and hybrid subtraction methods as given in eq.(1.11) leads to important discrepancies in the final numerical results obtained applying one or the other method.

Within the phase space slicing method, the matrix element squared and phase space are approximated in a given singular region and generally the approximations are accurate in that singular region. At the edges of the singular region it can however happen that this approximation is not appropriate anymore. In such cases, using the phase space slicing method could lead to erroneous results. Indeed, within this method, the pole part is obtained as the result of the analytic integration of the approximate matrix elements over the corresponding singular region of phase space. The finite contributions are obtained as the sum of the finite terms of the analytic integration and the result of the numerical integration of the matrix element squared over the resolved region of phase space. If the approximation of the matrix element squared is not appropriate this finite part may not be correct.

Using the hybrid subtraction method, the integration over the singular region of the approximated matrix element squared is added and subtracted and such a problem is

avoided. The pole part is obtained as in the phase space slicing method. However, an additional finite contribution arises through the evaluation of the difference of the full matrix element squared and the approximated matrix element squared integrated over a given singular region, the analogue of $\int_0^\delta \frac{dx}{x}[F(x) - F(0)]$ in eq.(1.10). Clearly, if the approximation is accurate this difference term tends to zero. If not on the other hand it generates an additional finite contribution to the jet cross section, such that the results obtained applying one or the other method are different.

When evaluating the photon +1 jet rate at $\mathcal{O}(\alpha\alpha_s)$, as we shall discuss in more detail when describing the numerical part of this calculation in Chapter 9, at the boundaries of any single collinear regions, it turns out that the single collinear approximation of the four-particle matrix element squared is not an appropriate approximation anymore. As we shall illustrate in Chapter 9, the large particle multiplicity in the process is responsible for this subtle inaccuracy. For this reason, in our numerical program evaluating the photon +1 jet rate at $\mathcal{O}(\alpha\alpha_s)$, we will apply the hybrid subtraction method.

1.5.2 An example: The $e^+e^- \to$ 2 jets cross section at $\mathcal{O}(\alpha_s)$

To illustrate how the hybrid subtraction method can be applied to yield a finite jet cross section, we shall consider a particular example, the $e^+e^- \to 2$ jet cross section at $\mathcal{O}(\alpha_s)$. We will first present how the different contributions to the cross section should be combined to yield a finite result using the phase space slicing method. We shall then specify which additional contribution shall be taken into account when the hybrid subtraction method is used instead.

The essential tool of the phase space slicing method as we saw in the previous subsection, is the decomposition of the phase space into different regions, one where all final state particles are considered to be *theoretically resolved* (or seen) and others where at least one of the particles is said to be *theoretically unresolved.* The separation criterion between resolved and unresolved regions is given by a theoretical resolution parameter: s_{min}. Two partons are considered as *theoretically resolved* if the invariant mass of the parton pair is

greater than $s_{\min}$, they are said to be *theoretically unresolved* (i.e soft and/or collinear) otherwise. It is only in the *unresolved regions*, where at least one of the invariant masses of a parton pair s_{ij} is less than $s_{\min}$, that the calculation needs to be carried out in d dimensions. As a consequence of this slicing procedure of the phase space, the divergences associated with the presence of soft or collinear partons lie in the *unresolved* phase space regions and can be isolated and analytically cancelled against the divergences present in the virtual contributions. We shall explicitly show how this cancellation happens in Section 1.5.3 for the evaluation of the $e^+e^- \to 2$ jet cross section at $\mathcal{O}(\alpha_s)$. After the analytic cancellation of poles, the matrix element and the phase space restricted to the region where all final state particles are theoretically resolved can be evaluated in four space time dimensions. The jet algorithm can be applied to select the two-jet events.

At lowest order the sole contribution to the $e^+e^- \to 2$ jet cross section comes from the two-parton process $e^+e^- \to q\bar{q}$. The partons q and $\bar{q}$ form the two jets. At next-to-leading order there are two contributions. One contribution comes from the tree level three-parton process $e^+e^- \to q\bar{q}g$. The other is related to the next-to-leading order two-parton process $e^+e^- \to q\bar{q}$, where a virtual gluon is exchanged. The three-particle phase space can be split into *resolved* and *single unresolved* regions. In these single unresolved or so-called one-particle unresolved regions, the gluon is "theoretically" unseen, i.e. it is collinear to the quark or to the antiquark or it is soft. Partons i and j are considered as collinear when the invariants built with their momenta is less than the theoretical parameter $s_{\min}$, i.e. $s_{ij} < s_{\min}$. Parton k is soft when the invariants involving the momentum of parton k are less than $s_{\min}$. Before deriving these divergent contributions explicitly, let us first see how all the different contributions to the $\mathcal{O}(\alpha_s)$ $e^+e^- \to 2$ jet cross section combine to yield a finite result.

Schematically, following the notation in [25], the differential cross section associated with the three-parton process $e^+e^- \to q\bar{q}g$ reads[12]

$$\mathrm{d}\sigma(e^+e^- \to 3 \text{ partons}) \;=\; \Big[\theta(s_{qg} - s_{\min})\theta(s_{\bar{q}g} - s_{\min})$$

[12]The step function $\theta(x)$ is 1 if $x \geq 0$ and 0 otherwise.

$$+\theta(s_{\min}-s_{qg})\theta(s_{\bar{q}g}-s_{\min})+\theta(s_{\min}-s_{\bar{q}g})\theta(s_{qg}-s_{\min})$$
$$+\theta(s_{\min}-s_{qg})\theta(s_{\min}-s_{\bar{q}g})\Big]\times \mathrm{d}\sigma(e^+e^-\to 3\text{ partons}). \tag{1.12}$$

In this equation, the first term represents the contribution to the three-parton cross section when all three partons $q, \bar{q}$ and g are resolved and can therefore be evaluated numerically, $\mathrm{d}\sigma^{(R)}(e^+e^-\to 3\text{ partons})$. The second and third terms represent the divergent contribution when the gluon is either collinear to the quark or to the antiquark $\mathrm{d}\sigma^{C}(e^+e^-\to 2\text{ partons})$; the fourth term represents the divergent contribution arising when the gluon is soft $\mathrm{d}\sigma^{S}(e^+e^-\to 2\text{ partons})$. Eq.(1.12) can be reexpressed as follows,

$$\begin{aligned}\mathrm{d}\sigma(e^+e^-\to 3\text{ partons}) &= \mathrm{d}\sigma^{(R)}(e^+e^-\to 3\text{ partons})\\ &\quad+\mathrm{d}\sigma^{C}(e^+e^-\to 2\text{ partons})+\mathrm{d}\sigma^{S}(e^+e^-\to 2\text{ partons}).\end{aligned}$$

As the soft and collinear divergences present in $\mathrm{d}\sigma^{C}$ and $\mathrm{d}\sigma^{S}$ are expected to cancel against the divergences present in the virtual contributions, it seems natural to combine them and to define the two-parton resolved contribution as the sum of these contributions,

$$\begin{aligned}\mathrm{d}\sigma^{(R)}(e^+e^-\to 2\text{ partons}) &= \Big[\mathrm{d}\sigma^{V}(e^+e^-\to 2\text{ partons})\\ &\quad+\mathrm{d}\sigma^{C}(e^+e^-\to 2\text{ partons})+\mathrm{d}\sigma^{S}(e^+e^-\to 2\text{ partons})\Big].\end{aligned} \tag{1.13}$$

As will be shown in Section 1.5.3, the divergences are all proportional to the lowest order two-parton cross section $\mathrm{d}\sigma^{tree}(e^+e^-\to 2\text{ partons}) \equiv \sigma_0$. The resolved two-parton contribution $\mathrm{d}\sigma^{(R)}(e^+e^-\to 2\text{ partons})$ then reads,

$$\mathrm{d}\sigma^{(R)}(e^+e^-\to 2\text{ partons}) = \Big[\mathcal{K}(s_{q\bar{q}}, s_{\min})\ \mathrm{d}\sigma^{tree}(e^+e^-\to 2\text{ partons})\Big]. \tag{1.14}$$

The so-called dynamical $\mathcal{K}$ factor is finite and needs to be evaluated analytically. It depends on the theoretical resolution criterion $s_{\min}$ and on the invariant mass of the final

state $s_{q\bar{q}}$. The $\mathcal{O}(\alpha_s)$ two-jet cross section is then finally obtained as the sum of the resolved two-parton cross section $\mathrm{d}\sigma^{(R)}(e^+e^- \to 2 \text{ partons})$ and the two-jet contribution from the resolved three-parton cross section $\mathrm{d}\sigma^{(R)}(e^+e^- \to 3 \text{ partons})$,

$$\mathrm{d}\sigma(e^+e^- \to 2 \text{ jets}) = \left[\mathrm{d}\sigma^{(R)}(e^+e^- \to 2 \text{ partons}) + \Theta \times \int \mathrm{d}\sigma^{(R)}(e^+e^- \to 3 \text{ partons})\right]. \tag{1.15}$$

The integration represents the projection of the three-parton phase space onto the two-jet phase space while Θ contains the experimental definition for a two-jet final state. $\mathrm{d}\sigma(e^+e^- \to 2 \text{ jets})$ is finite as it is the sum of two finite contributions. $\mathrm{d}\sigma^{(R)}(e^+e^- \to 2 \text{ partons})$ is finite but obtained after the analytic cancellation of poles as in eq.(1.13), $\mathrm{d}\sigma^{(R)}(e^+e^- \to 3 \text{ partons})$ can be evaluated numerically in four space time dimensions. Finally, the jet finding algorithm can be applied to the three parton final state according to the experimental definition Θ to select the two-jet events. The $e^+e^- \to 2$ jet cross section at $\mathcal{O}(\alpha_s)$ is then obtained using the phase space slicing method, applying eq.(1.15).

To evaluate the $e^+e^- \to 2$ jet cross section at $\mathcal{O}(\alpha_s)$ using the hybrid subtraction method, one needs to consider some additional contributions which will be evaluated numerically. More precisely, for each singular region one needs to consider the contribution resulting from the numerical integration of the difference between the three-particle matrix element squared and the approximated matrix element squared over the three-particle phase space restricted to the particular singular region. For example, in the region of phase space where the gluon is soft, additionally to the terms present in eq.(1.15), we need to consider,

$$\left[\Theta \times \int \left(|\mathcal{M}_{q\bar{q}g}|^2 - |\mathcal{M}_{soft}|^2\right) \mathrm{d}P_3^{(4)}(M, p_q, p_{\bar{q}}, p_g)\theta(s_{\min} - s_{qg})\theta(s_{\min} - s_{\bar{q}g})\right],$$

where $|\mathcal{M}_{q\bar{q}g}|^2$ is the 4-dimensional three particle matrix element squared, $|\mathcal{M}_{soft}|^2$ its soft approximation, and $\mathrm{d}P_3^{(4)}(M, p_q, p_{\bar{q}}, p_g)$ the 4-dimensional three particle phase space, which analogue in d-dimensions is given in Appendix B. The integration and Θ symbols are defined as in eq.(1.15). In order to evaluate the $e^+e^- \to 2$ jet cross section at $\mathcal{O}(\alpha_s)$ using the hybrid subtraction method, similar terms need to be considered in the region

where the gluon is collinear to the quark and in the region where it is collinear to the antiquark.

1.5.3 The isolation of soft and collinear divergences

In this subsection we shall see how the introduction of the theoretical resolution criterion $s_{\min}$ enables us to isolate soft and single collinear divergences. We shall present the factorization properties of matrix element squared, phase space and cross section in soft and collinear limits. In particular, the soft and single collinear contributions to the cross section for the process $\gamma^* \to q\bar{q}$ at $\mathcal{O}(\alpha_s)$ will be explicitly derived and the cancellation between the soft/collinear real divergences and those present in the virtual contributions will be shown. The generalization to the process $e^+e^- \to q\bar{q} + n$ gluons where one gluon becomes soft or collinear can be found in [25].

For convenience we use the following notation

$$q \equiv 1, \qquad \bar{q} \equiv 2, \qquad g \equiv 3. \tag{1.16}$$

Following this notation, the invariants $s_{qg}, s_{\bar{q}g}$ and $s_{q\bar{q}}$ are denoted by s_{13}, s_{23} and s_{12} respectively; The d-dimensional three particle matrix element squared and phase space are given as follows.

For massless quarks of unit charge, $|\mathcal{M}_{q\bar{q}g}|^2 \equiv |\mathcal{M}_{123}|^2$ reads:

$$|\mathcal{M}_{123}|^2 = \left[(1-\epsilon)\left(\frac{y_{23}}{y_{13}} + \frac{y_{13}}{y_{23}}\right) + \frac{2y_{12} - \epsilon y_{13}y_{23}}{y_{13}y_{23}}\right], \tag{1.17}$$

where $y_{ij} = \frac{s_{ij}}{M^2}$. M is the mass of the final state. The d-dimensional three particle phase space is given in the Appendix B by eq.(B.4) and reads,

$$\int \mathrm{d}P_3^{(d)}(M, p_1, p_2, p_3) = (2\pi)^{3-2d} \int \mathrm{d}R_3^{(d)}(M, p_1, p_2, p_3)$$

with,

$$\begin{aligned}\int \mathrm{d}R_3^{(d)}(M, p_1, p_2, p_3) \;=\; & \frac{1}{4\,2^{d-1}} \int (s_{12}s_{13}s_{23})^{\frac{d-4}{2}}\; \mathrm{d}s_{12}\, \mathrm{d}s_{13}\mathrm{d}s_{23}\mathrm{d}\Omega_{d-1}\, \mathrm{d}\Omega_{d-2} \\ & \delta(s_{12}+s_{13}+s_{23}-M^2)\,(M^2)^{\frac{2-d}{2}}.\end{aligned}$$

The soft limit of the three-particle differential cross section

a.The soft limit of the matrix element squared $|\mathcal{M}_{q\bar{q}g}|^2$

When the gluon is soft[13], $E_g \to 0$ and the invariants containing the momentum of the gluon p_g, i.e. $s_{qg} \equiv s_{13}$ and $s_{\bar{q}g} \equiv s_{23}$, tend to 0. The soft gluon limit is therefore defined requiring,

$$s_{13} < s_{\min} \qquad s_{23} < s_{\min}. \tag{1.18}$$

In this limit, as $s_{\min}$ tends to 0, the matrix element squared $|\mathcal{M}_{123}|^2$ given by (1.17) is singular and factorizes. It becomes,

$$|\mathcal{M}_{123}|^2 \to |\mathcal{M}_{12}|^2 \, f_{12}(3). \tag{1.19}$$

$f_{ab}(c)$ is sometimes called the *eikonal factor* [39] and reads

$$f_{ab}(c) = \frac{4s_{ab}}{s_{ac}s_{bc}}. \tag{1.20}$$

Thus in the soft gluon limit, the three-particle matrix element squared is written as the matrix element squared "without the gluon", $|\mathcal{M}_{12}|^2$, multiplied by a factor $f_{12}(3)$ which contains all the soft gluon singularities. The product $|\mathcal{M}_{12}|^2 \; f_{12}(3)$ is the soft gluon approximation of the full matrix element squared $|\mathcal{M}_{123}|^2$.

b.The soft behaviour of the phase space

In the soft gluon limit defined above, the d-dimensional three-particle phase space also factorizes,

$$\mathrm{d}P_3^{(d)}(M, p_1, p_2, p_3) \to \mathrm{d}P_2^{(d)}(M, p_1, p_2)\, \mathrm{d}P_{soft}^{(d)}(p_1, p_2, p_3). \tag{1.21}$$

$\mathrm{d}P_2^{(d)}(M, p_1, p_2)$ is the two-particle phase space given in Appendix B by

$$\int \mathrm{d}P_2^d(M, p_1, p_2) \;=\; \int (s_{12})^{\frac{4-d}{2}} \, (2\pi)^{2-d} \frac{\mathrm{d}\Omega_{d-1}}{2^{d-1}} \, \mathrm{d}s_{12} \, \delta(s_{12} - M^2) \; ,$$

whereas the soft phase space factor $\mathrm{d}P_{soft}^{(d)}(p_1, p_2, p_3)$ reads

$$\mathrm{d}P_{soft}^{(d)}(p_1, p_2, p_3) = \frac{1}{4}\mathrm{d}\Omega_{d-2} s_{12}^{\frac{2-d}{2}} \, \mathrm{d}s_{13}\mathrm{d}s_{23} \, [s_{13}s_{23}]^{\frac{d-4}{2}} \, (2\pi)^{1-d} \theta(s_{\min} - s_{13})\theta(s_{\min} - s_{23}).$$

[13]Recall, that in the massless limit, $s_{ij} = (p_i + p_j)^2 \; = \; 2E_iE_j(1 - cos\theta_{ij})$.

Performing the angular integrals, and setting $d = 4 - 2\epsilon$, this soft phase space factor reads:

$$\mathrm{d}P^{(d)}_{soft}(p_1,p_2,p_3) = \frac{(4\pi)^\epsilon}{16\pi^2\Gamma(1-\epsilon)}\frac{\mathrm{d}s_{13}\mathrm{d}s_{23}}{s_{12}}\left[\frac{s_{13}s_{23}}{s_{12}}\right]^{-\epsilon}\theta(s_{\min}-s_{13})\theta(s_{\min}-s_{23}). \quad (1.22)$$

When multiplied with the the soft matrix element squared $f_{12}(3)$ we see that the soft phase space factor regulates the singularities in s_{23} and s_{13}.

c.The soft behaviour of the cross section

We just saw how the three particle matrix elements and phase space factorize when the gluon becomes soft. We can now combine these results to obtain the soft behaviour of the cross section for $\gamma^* \to q + \bar{q} + g$. The 3-particle cross section $\mathrm{d}\sigma_{q\bar{q}g} \equiv \mathrm{d}\sigma_{123}$ is given by

$$\mathrm{d}\sigma_{123} \equiv g_s^2\left(\frac{N^2-1}{2N}\right)\int |\mathcal{M}_{123}|^2\ \mathrm{d}P^{(d)}_3(M,p_1,p_2,p_3), \quad (1.23)$$

where g_s is the strong charge and $(N^2-1)/2N$ is the colour factor. In the soft gluon limit this cross section becomes,

$$\mathrm{d}\sigma_{123} \to \underbrace{\int |\mathcal{M}_{12}|^2\ \mathrm{d}P^{(d)}_2(M,p_1,p_2)}_{\sigma_{12}\equiv\sigma_0} \times\left[\int g_s^2\left(\frac{N^2-1}{2N}\right) f_{12}(3)\mathrm{d}P^{(d)}_{soft}(p_1,p_2,p_3)\right]. \quad (1.24)$$

All the dependence on the soft gluon momenta p_3 has factorized and is included in the square bracket in eq.(1.24), it multiplies the cross section "without the gluon", σ_0. The integrated soft gluon behaviour finally reads,

$$\begin{aligned} S_F &= \int g_s^2\left(\frac{N^2-1}{2N}\right) f_{12}(3)\mathrm{d}P^{(d)}_{soft}(p_1,p_2,p_3) \\ &= \frac{\alpha_s}{2\pi}\left(\frac{(4\pi\mu^2)^\epsilon}{\Gamma(1-\epsilon)}\right)\left(\frac{N^2-1}{2N}\right)\frac{2}{s_{12}}\int_0^{s_{\min}}\mathrm{d}s_{23}\int_0^{s_{\min}}\mathrm{d}s_{13}\ \left[\frac{s_{23}s_{13}}{s_{12}}\right]^{-\epsilon-1} \\ &= \frac{\alpha_s}{2\pi}\left(\frac{4\pi\mu^2}{M^2}\right)^{+\epsilon}\left(\frac{N^2-1}{2N}\right)\frac{1}{\Gamma(1-\epsilon)}\frac{2}{\epsilon^2}\ (y_{\min})^{-2\epsilon}(y_{12})^\epsilon. \end{aligned} \quad (1.25)$$

Here μ is an arbitrary scale which is introduced to keep the strong coupling constant $\alpha_s = g_s^2\mu^{-2\epsilon}/4\pi$, dimensionless in $d = 4 - 2\epsilon$ dimensions. The product $S_F\sigma_0$ constitutes

the soft gluon approximation of the three particle cross section σ_{123}. Furthermore, note that in this particular example of a three-parton final state process, $s_{12} = M^2$ and consequently $y_{12} = 1$ so that the factor y_{12}^{ϵ} can be omitted in eq.(1.25). If, however, we are interested to know the soft gluon behaviour of the cross section for a process which has an additional photon in the final state, as in the remainder of this thesis, this factor needs to be kept as y_{12} is not equal to one anymore.

Finally, when evaluating the soft approximation of the matrix element squared we have neglected all terms of $\mathcal{O}(1)$ (or higher) in s_{13} and s_{23}. From this last equation, we see that it was justified to do so, as in the soft region of phase space (defined by $s_{13} < s_{\min}$ and $s_{23} < s_{\min}$) those terms lead to contributions to the soft factor, S_F, which are of $\mathcal{O}(y_{\min})$ and therefore negligible.

The single collinear limit of the differential cross section

a.The single collinear limit of $|\mathcal{M}_{q\bar{q}g}|^2$

The matrix element squared, in addition to being singular in the soft gluon region is also singular in the collinear regions. It is singular when $q \equiv 1$ and $g \equiv 3$, for example, are collinear and cluster to form a new parton Q such that:

$$p_1 + p_3 = p_Q.$$

p_3 and p_1 carry respectively a fraction z and $1 - z$ of the parent parton momentum p_Q,

$$p_1 = (1 - z)\, p_Q, \qquad p_3 = z\, p_Q. \tag{1.26}$$

As 1 and 3 are collinear s_{13} tends to 0, we consider the quark-gluon collinear limit to be:

$$s_{13} < s_{\min} \ll M^2. \tag{1.27}$$

In this limit, we can ignore terms of order 1 in s_{13} in the matrix element squared and the invariants s_{12} and s_{23} become

$$s_{12} = (1 - z)\, M^2, \qquad s_{23} = z\, M^2. \tag{1.28}$$

The matrix element squared $|\mathcal{M}_{123}|^2$ exhibits an overall factorization,

$$|\mathcal{M}_{123}|^2 \to P_{13\to Q}(z, s_{13})|\mathcal{M}_{Q2}|^2. \tag{1.29}$$

$|\mathcal{M}_{Q2}|^2$ is the two particle matrix element squared obtained replacing partons 1 and 3 by the parent parton Q. The collinear matrix element squared, $P_{13\to Q}(z, s_{13})$ is singular as $s_{13} \to 0$. It is given by,

$$P_{13\to Q}(z, s_{13}) = \frac{1}{s_{13}} P_{13\to Q}(z). \tag{1.30}$$

$P_{13\to Q}(z) \equiv P_{qg\to Q}(z)$ is the d-dimensional *Altarelli-Parisi splitting function*, [40] and corresponds to the probability that a quark emits a collinear gluon thereby losing a fraction z of its initial momentum. It is given by,

$$P_{13\to Q}(z) = \frac{1 + (1-z)^2 - \epsilon z^2}{z} \tag{1.31}$$

This particular splitting function has been originally derived in the context of collinear photon emission off electrons by von Weizsäcker and Williams [41].

Throughout this thesis we will encounter both the d-dimensional splitting function $P_{ab\to Q}(z)$ as given in eq.(1.31) which we shall sometimes also denote $P^{\epsilon}_{ab}(z)$ (or $P^{\epsilon}(z)$) and its counterpart in 4 dimensions. We will denote the 4-dimensional splitting function by $P_{ab}(z)$ or simply by $P(z)$.

b.The collinear behaviour of the phase space

The d-dimensional three-particle phase space for $M \to p_1 + p_2 + p_3$ is given in (B.4). In the single collinear region, when $s_{13} < s_{\min}$ the invariants s_{12} and s_{23} are defined according to eq(1.28) and the three particle phase space factorizes,

$$\mathrm{d}P_3^{(d)}(M, p_1, p_2, p_3) \to \mathrm{d}P_2^{(d)}(M, p_Q, p_2)\,\mathrm{d}P_{col}^{(d)}(p_1, p_3, z), \tag{1.32}$$

where $\mathrm{d}P_2^d(M, p_Q, p_2)$ is the known two-particle phase space in d-dimensions given by eq.(B.3) with p_Q instead of p_1. Performing the angular integrations and fixing $d = 4 - 2\epsilon$, the collinear phase space factor $\mathrm{d}P_{col}^{(d)}(p_1, p_3, z)$ reads:

$$\mathrm{d}P_{col}^{d}(p_1, p_3, z) = \frac{(4\pi)^{\epsilon}}{16\pi^2\Gamma(1-\epsilon)} \mathrm{d}s_{13}\,\mathrm{d}z \Big[s_{13} z(1-z)\Big]^{-\epsilon} \theta(s_{\min} - s_{13})\theta(s_{23} - s_{\min}). \tag{1.33}$$

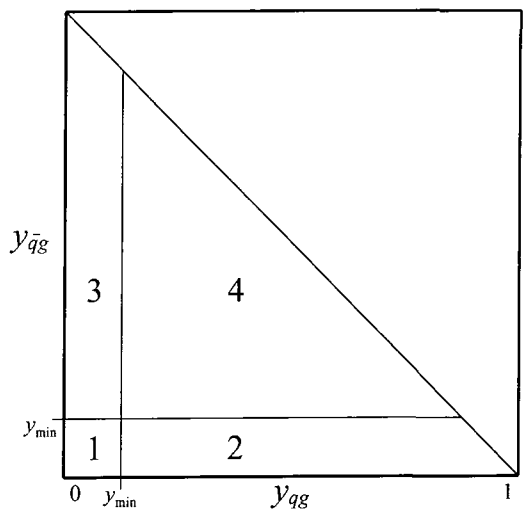

Figure 1.3: Dalitz plot for the $q\bar{q}g$ final state phase space in terms of the invariants y_{qg} and $y_{\bar{q}g}$. The kinematically allowed region is limited by $y_{qg} + y_{\bar{q}g} < 1$. In region 1, the gluon is soft, in regions 2 and 3, the gluon is collinear to the quark or antiquark respectively. The region 4 is the 'theoretically resolved' region.

c.The collinear behaviour of the cross section

In order to determine the quark-gluon collinear contribution to the cross section, we must integrate the collinear matrix element squared over the single collinear region. We must ensure however that this single unresolved region does not overlap with the soft region; we must match this collinear region precisely onto the soft region so that there is no double counting and no omitted singular region. We must therefore require that $s_{qg} < s_{\min} \equiv s_{13} < s_{\min}$, while $s_{\bar{q}g} > s_{\min} \equiv s_{23} > s_{\min}$. It is shown in Fig. 1.3 how the matching of the two regions of phase space is then realised. The requirement $s_{23} > s_{\min}$ avoids the soft region and determines the lower boundary of the integration for z. $s_{23} > s_{\min}$ corresponds to $zs_{2Q} > s_{\min}$. In other words, as $s_{2Q} = M^2$, z has to be greater than $y_{\min}$. In the quark-gluon collinear limit the cross section $\mathrm{d}\sigma_{123}$ becomes,

$$\mathrm{d}\sigma_{123} \to \mathrm{d}\sigma_{Q2} \times \left[\int g_s^2 \left(\frac{N^2-1}{2N} \right) P_{13\to Q}(z, s_{13}) \mathrm{d}P_{col}^{(d)} \right]. \tag{1.34}$$

All the divergences related to the collinear gluon have been factored and multiply the two-particle cross section $\mathrm{d}\sigma_{Q2}$. Integrating out the collinear behaviour gives,

$$\begin{aligned} C_F &= \int g_s^2 \left(\frac{N^2-1}{2N}\right) P_{13\to Q}(z, s_{13}) \mathrm{d}P_{col}^{(d)}(p_1, p_3, z) \\ &= \frac{\alpha_s}{2\pi}\left(\frac{N^2-1}{2N}\right)\frac{(4\pi\mu^2)^\epsilon}{\Gamma(1-\epsilon)}\int_0^{s_{\min}} \mathrm{d}s_{13}\, s_{13}^{-\epsilon-1}\left[\int_{y_{\min}}^1 \mathrm{d}z\,[z(1-z)]^{-\epsilon} P_{13\to Q}(z)\right] \\ &= -\frac{1}{\epsilon}\frac{\alpha_s}{2\pi}\left(\frac{N^2-1}{2N}\right)\frac{1}{\Gamma(1-\epsilon)}\left(\frac{4\pi\mu^2}{M^2}\right)^{+\epsilon}(y_{\min})^{-\epsilon} \\ &\quad \left[\frac{2}{\epsilon}(y_{\min})^{-\epsilon} - \frac{(1-\epsilon)(4-\epsilon)}{2\epsilon(1-2\epsilon)}\frac{\Gamma^2(1-\epsilon)}{\Gamma(1-2\epsilon)}\right]. \end{aligned} \tag{1.35}$$

The full contribution from unresolved phase space

We can combine the results from the previous subsections to give an expression for the sum of all contributions to the process $\gamma^* \to q\bar{q}g$ where the gluon is real and unresolved. It yields,

$$\begin{aligned} \sigma_R^{(U)} &= [S_F + 2C_F]\,\sigma_0 \\ &\equiv R_{q\bar{q}}\,\sigma_0. \end{aligned} \tag{1.36}$$

σ_0 is the tree level cross section for the process $\gamma^* \to q\bar{q}$. As the gluon can be collinear to the quark *or* to the antiquark, and since the resulting contribution is the same in both cases, the factor C_F needs to be multiplied by two. $R_{q\bar{q}}$ reads,

$$\begin{aligned} R_{q\bar{q}} &= \frac{\alpha_s}{2\pi}\left(\frac{N^2-1}{2N}\right)\frac{1}{\Gamma(1-\epsilon)}\left(\frac{4\pi\mu^2}{M^2}\right)^{+\epsilon} \\ &\quad \times\left[\frac{2}{\epsilon^2} - 2\ln^2(y_{\min}) + \frac{3}{\epsilon} - 3\ln(y_{\min}) + 7 - \frac{2\pi^2}{3}\right] + \mathcal{O}(\epsilon). \end{aligned} \tag{1.37}$$

Note that we have neglected terms of $\mathcal{O}(s_{\min})$ such that this equation for the two-particle resolved factor $R_{q\bar{q}}$ is only valid in the small $s_{\min}$ limit. Furthermore, the complete contribution to the $\mathcal{O}(\alpha_s)$ cross section for $\gamma^* \to q\bar{q}$ with one unresolved gluon in the final state can be obtained by adding the one-loop virtual contribution σ_V to the unresolved

real contribution $\sigma_R^{(U)}$. The matrix element "squared" $|\mathcal{M}_V|^2$ associated with the loop diagram is obtained by interfering the tree level amplitude $\mathcal{T}$ with the loop amplitude $\mathcal{L}$,

$$|\mathcal{M}_V|^2 \equiv 2Re(\mathcal{L}\mathcal{T}^*).$$

An explicit calculation of $|\mathcal{M}_V|^2$ yields

$$|\mathcal{M}_V|^2 = |\mathcal{M}_{tree}|^2 V_{q\bar{q}},$$

where $V_{q\bar{q}}$ is given by

$$V_{q\bar{q}} = \frac{\alpha_s}{2\pi}\left(\frac{N^2-1}{2N}\right)\left(\frac{4\pi\mu^2}{M^2}\right)^{+\epsilon}\frac{\Gamma^2(1-\epsilon)\Gamma(1+\epsilon)}{\Gamma(1-2\epsilon)}\Big[-\frac{2}{\epsilon^2}+\pi^2-\frac{3}{\epsilon}-8\Big]. \tag{1.38}$$

Integrating $|\mathcal{M}_V|^2$ over the two-particle phase space yields,

$$\sigma_V = \sigma_0 V_{q\bar{q}},$$

such that the two-parton contribution to the $\mathcal{O}(\alpha_s)$ cross section for the $\gamma^* \to q\bar{q}$ process then finally reads,

$$\sigma_R^{(U)} + \sigma_V = \sigma_0 \mathcal{K}_{q\bar{q}} \tag{1.39}$$

which is finite. The two-quark $\mathcal{K}$ factor is obtained combining $V_{q\bar{q}}$ with the two-particle resolved factor $R_{q\bar{q}}$ and reads,

$$\begin{aligned}\mathcal{K}_{q\bar{q}} &= R_{q\bar{q}} + V_{q\bar{q}} \\ &= \frac{\alpha_s}{2\pi}\left(\frac{N^2-1}{2N}\right)\left(\frac{4\pi\mu^2}{M^2}\right)^{+\epsilon}\Big[-2\ln^2(y_{\min})+\frac{\pi^2}{3}-3\ln(y_{\min})-1\Big] \\ &\quad +\mathcal{O}(\epsilon).\end{aligned} \tag{1.40}$$

In the second part of this first chapter we have discussed how jet cross sections may be calculated at higher orders in perturbative QCD. We have seen for the particular example of the $\mathcal{O}(\alpha_s)$ process $e^+e^- \to 2$ jets how the phase space may be decomposed into theoretically resolved and single unresolved regions. And in these last regions we explicitly derived the soft and collinear contributions to the cross section. In the remainder

of this thesis, for the evaluation of the photon +1 jet rate at order $\alpha\alpha_s$ we shall extend this method to decompose the four-particle phase space and to analytically isolate collinear or/and soft divergences present in different contributions to the cross section. In this calculation we will have to deal with contributions which can have up to two particles simultaneously theoretically unresolved. Such configurations had so far never been considered in the calculation of jet cross sections. In a pure QCD calculation, they will only appear at next-to-next-to-leading order (NNLO). As a consequence, the calculational methods developed in this thesis to evaluate these double unresolved contributions will be applicable in a variety of calculations of jet observables at NNLO. Possible applications are $e^+e^- \to 3$ jets at $\mathcal{O}(\alpha_s^3)$ [42] or $p\bar{p} \to 2$ jets at $\mathcal{O}(\alpha_s^3)$.

Chapter 2

Photons in hadronic Z decays

Electron-positron annihilation provides a very clean environment in which to test perturbative QCD. The production of hadrons in e^+e^- collisions at LEP ($\sqrt{s} = M_Z$) can be viewed as the production of a Z boson which subsequently decays into a quark-antiquark pair. During the subsequent *QCD parton evolution* process the quarks produced in the hard interaction radiate gluons which themselves decay into gluons or quark-antiquark pairs. Ultimately, these partons are transformed into clusters of observable hadrons through the non-perturbative *hadronization* process. With the aid of a suitable *jet* definition it is possible to analyse these hadronic final state events and to classify them experimentally according to the number of jets they contain. A given jet algorithm leads therefore to measurable jet cross sections. Furthermore, as we saw in Section 1.2, it is possible to match the theoretical parton level calculations performed in the framework of perturbative QCD to the experimentally observed hadronic jet rates. This correspondence is realized by subjecting both parton and hadron momenta to the same recombination algorithm characterized by a resolution criterion y_{cut}. Jet cross sections become then also calculable in perturbation theory.

In a small fraction of events, in addition to the jets of hadrons one may observe a highly energetic photon. Experimentally, highly energetic photons are identified by a shower in the electromagnetic calorimeter, which is accompanied by "no charged tracks" pointing to

it. We distinguish two possible sources for the emission of a photon in hadronic Z decays, depending whether the photon is emitted at an early or late stage of the QCD parton evolution process. We shall discuss these two sources in Section 2.1. Most earlier studies of photon $+n$ jet events have concentrated their interest on *isolated* photons. After having explained how isolated final state photons can be defined, we shall present the results of theoretical analyses and the results of a comparison with experimental data on the isolated photon $+n$ jets rate in Section 2.2.

An alternative analysis of final state photons is obtained by treating the photon like any other parton and to cluster it together with the other partons in jets. The photon in this case is called *non isolated.* We shall present the calculation of the lowest order photon $+1$ jet rate performed following this *democratic* approach in Section 2.4. Section 2.5 will be dedicated to a brief discussion of alternative approaches to analyse final state photon events widely used in the literature. Finally, in Section 2.6 we will describe how the experimental measurement of the photon $+1$ jet rate is realized by the ALEPH Collaboration at CERN.

2.1 Two sources of final state photons

In events where a photon is emitted in addition to the jets of hadrons, the photon can have two possible origins. The photon may have been emitted at an early stage in the QCD parton evolution process initiated from the primary quark-antiquark pair. Such photons are generally well separated from the other hadrons in the event. Indeed, considering the process $e^+e^- \rightarrow q\bar{q}\gamma$ in the massless limit with the photon emitted on the quark leg, the inverse propagator $s_{q\gamma}$ is given by,

$$s_{q\gamma} = 2E_q E_\gamma [1 - \cos\theta_{q\gamma}]$$

where E_q, E_γ are the energy of the quark and the photon and $\theta_{q\gamma}$ is the angle between the quark and the photon. For fixed energies of quark and photon, a large separation angle $\theta_{q\gamma}$ corresponds to a large invariant mass of the parent quark propagator. By the

uncertainty principle, this implies that the quark propagates for a short time. Consequently, the radiation of a photon by a quark at large angles occurs at an early stage of the hadronization process.

Alternatively the photon may have been radiated somewhat later during the hadronization process. Following the above argument, it is then more likely that it has been emitted collinearly to one of the primary quarks. However, if it is travelling for a long time, the emission could take place during the hadronization process. This non-perturbative quark-to-photon fragmentation process is characterized by the universal and process-independent quark-to-photon fragmentation function which is not calculable in perturbation theory and must be measured. The fragmentation process must be considered together with the collinear emission of a photon from a quark, as both processes happen at a later stage of the QCD parton evolution procedure.

From a theoretical point of view, these two contributions are associated with each other in perturbative QCD calculations since quark-photon collinear singularities may be factorized into the quark-to-photon fragmentation function as mentioned in Section 1.2.3 and as we shall see when evaluating the γ +1 jet rate at order α in Section 2.4. In experiments, such final state photons are generally not well separated from the other hadrons, and are therefore harder to detect. We shall discuss the experimental detection of these *non isolated* photons in hadronic Z decays in Section 2.6.

Clearly, as the two sources for the emission of a photon in the final state are easily distinguishable from each other, by imposing some kind of isolation criteria on the photon, one is able to reduce or even to completely eliminate the second source of final state photons in Z decays. One can then study *isolated* final state photon events. This is exactly what was performed in the earlier experimental [43, 44] and theoretical [45, 46, 47, 48] analyses which we shall describe below.

2.2 Isolated Photons

In all these earlier analyses, the candidate photon is isolated from the hadronic debris in an event using a geometrical cone centred around its direction inside of which a minimal accompanying hadronic energy is allowed[1]. In the next step, the photon is removed from the event and the partons are clustered together according to a jet algorithm with resolution criterion $y_{\rm cut}$, i.e. all partons i, j are required to fulfill $y_{ij} < y_{\rm cut}$. Finally an event is retained only if the restored candidate photon remains apart from the jets in a second application of the clustering algorithm. In particular, we require

$$y_{c\gamma} > y_{\rm cut} \tag{2.1}$$

for all clusters c then formed. Thus it is worth noting that using this procedure to isolate the photon, any particles associated with the photon will be incorporated in the other jets.

In leading order QCD, the only process contributing to the isolated photon $+n$ jet rate is $e^+e^- \to q\bar{q}\gamma$ and the number of jets produced can be one or two. If two jets and a photon are observed, each parton builds a jet and the photon is well separated from the other partons. If one jet is observed in addition to the photon, the event configuration is the following. The photon is placed in one hemisphere and the quark-antiquark are clustered together in the other hemisphere, back to back to the photon. Thus for an identified photon event we require,

$$\theta_{q\gamma}, \theta_{\bar{q}\gamma} > \theta_{min}, \qquad E_\gamma > E_{min}. \tag{2.2}$$

In particular, for the process $e^+e^- \to q\bar{q}\gamma$, following [46] we have,

$$1 - x' \;=\; x(2 - x - x')\frac{1}{2}(1 - \cos\theta_{q\gamma}),$$

[1]Notice that, we need to allow some minimal hadronic energy inside the cone surrounding the photon since a perfectly isolated photon is not an infrared safe quantity. As we shall see later in this section, this point induces some differences in the way isolated photons are defined in the various theoretical calculations [45, 46, 47, 48].

$$1-x \;=\; x'(2-x-x')\frac{1}{2}(1-\cos\theta_{\bar{q}\gamma}), \tag{2.3}$$

where x, x' and x_γ are the energy fractions carried by the quark, the antiquark and the photon. These fractions are defined as follows:

$$x = 2E_q/\sqrt{s}, \quad x' = 2E_{\bar{q}}/\sqrt{s} \quad \text{and} \quad x_\gamma = 2-x-x'. \tag{2.4}$$

In terms of these energy fractions, the scaled pair invariant masses $y_{ij} = s_{ij}/s$ with $s_{ij} = (p_i + p_j)^2$ are given by,

$$y_{q\gamma} = 1-x', \qquad y_{\bar{q}\gamma} = 1-x, \qquad y_{q\bar{q}} = 1-x_\gamma, \tag{2.5}$$

and in terms of the energy fractions x and x' the isolation conditions for the photon are,

$$\begin{aligned} 1-x' &> x(2-x-x')\delta, \\ 1-x &> x'(2-x-x')\delta, \\ 2-x-x' &> \varepsilon, \end{aligned} \tag{2.6}$$

where,

$$\begin{aligned} \delta &= \frac{1}{2}(1-\cos\theta_{min}), \\ \varepsilon &= \frac{2E_{min}}{\sqrt{s}} \quad (0 \le \delta, \varepsilon \le 1). \end{aligned} \tag{2.7}$$

At next-to-leading order the isolated photon + n jet cross sections receive contributions from the one loop $e^+e^- \to q\bar{q}\gamma$ and the tree level $e^+e^- \to q\bar{q}\gamma g$ processes. At most three jets can be identified in the final state, in which case only the $q\bar{q}\gamma g$ process contributes to the cross section. If three jets are identified, all the partons are well separated from each other and from the photon and each of them forms a jet . If one or two jets are observed in addition to the photon, both processes contribute and the $\mathcal{O}(\alpha\alpha_s)$ cross section is given by

$$\mathrm{d}\sigma(\gamma + n\text{jets}) = \Theta\left[\mathrm{d}\sigma^1(q\bar{q}\gamma) + \mathrm{d}\sigma^0(q\bar{q}\gamma g)\right] \tag{2.8}$$

where Θ represents the photon and jet definitions to be applied to the partons and the photon. Although the physical $\gamma + 1, 2$ jet cross sections are finite, both the virtual and gluon bremsstrahlung contributions contain soft/collinear singularities. In order to numerically evaluate these next-to-leading order jet cross sections, we must first analytically cancel the divergences present in the real contributions against the explicit divergences present in the virtual graphs so that the cross sections are finite. Once the divergences have cancelled, the finite next-to leading order jet cross section can be evaluated numerically, the jet algorithm and isolation criteria can be applied to the partons and the photon to select photon +1, 2 jet events. This can be achieved using the phase space slicing method, in a similar way as for the evaluation of the $e^+e^- \rightarrow 2$ jets cross section which we described in Section 1.5.2. Details of the application of the phase space slicing method to the calculation of the $\gamma + 1, 2$ jet cross sections can be found in [46].

As we already mentioned, a perfectly isolated photon is not an infrared safe quantity and therefore some amount of hadronic energy needs to be allowed inside the cone surrounding the photon. The definition of an isolated photon is not the same in the various theoretical calculations [45, 46, 47, 48] as different amounts of gluon energy are allowed inside the cone for each of them. More precisely, in [46], soft gluons which are defined by $s_{qg} < s_{\min}$ and $s_{\bar{q}g} < s_{\min}$ are allowed to exist inside the cone. In [47], soft gluons are allowed inside the photon cone if the deposited energy is less then a fraction ε of the photon energy while in [45] the gluon is combined with the quark if $y_{(qg)\gamma} > y_{q\gamma}$.

It is worth noting that in all these theoretical calculations, gluons and quarks are treated differently with respect to the photon. Soft gluons are allowed inside the cone surrounding the photon while quarks are not. In the experimental analysis, clearly the situation is different, the amount of energy inside the cone is required to be less than the experimental hadronic energy resolution threshold E_{had} which is typically of a few hundred MeV.

All three calculations are found to be in reasonably good agreement with each other and with the available data [43, 44] for the photon +1,2 jet rates. However, for the case of photon + 1 jet rate, it was pointed out by E.W.N.Glover and W.J.Stirling in [46] that

relatively large negative corrections over the whole range of $y_{\rm cut}$ are necessary in order to obtain a reasonable agreement between the theoretical and experimental results. This conclusion is not very satisfactory, and in [46], it is suggested that these large effects could be a consequence of the "two step" procedure used to identify the photon in all these previous analyses.

2.3 Non Isolated Photons

A safer approach would be to apply the recombination algorithm *simultaneously* to all partons in the event, including the photon. After clustering, one of the clusters contains the electromagnetic shower and is called "photon" if the fraction of the electromagnetic energy inside the cluster is larger than the experimentally determined value $z_{\rm cut}$ (typically equal to 0.7),

$$z_\gamma \equiv \frac{E_\gamma}{E_\gamma + E_{\rm Had}} > z_{\rm cut}. \tag{2.9}$$

Within this *democratic* approach, one can expect that particles which are associated with the photon in the event will be combined with it by the cluster algorithm independently of whether these particles are quarks or gluons, unlike in the isolated photon analysis.

However within this democratic approach, the second source of final state photons is not suppressed anymore; to evaluate photon $+n$ jets cross sections one also needs to consider the contributions arising from the collinear emission of a photon by one of the quarks and related to the non-perturbative quark-to photon fragmentation process. We shall present a theoretical and experimental analysis of such *non isolated* final state photons in the next sections. In particular we shall see how the comparison between the results of a lowest order calculation of the photon + 1 jet cross section and the measurement of this cross section enables us to determine the non-perturbative quark-to-photon fragmentation function at $\mathcal{O}(\alpha)$.

2.4 The photon +1 jet rate at $\mathcal{O}(\alpha)$

As there is no $e^+e^- \to \gamma$ +1 parton process, the first non trivial contributions to the photon +1 jet rate comes from $e^+e^- \to q\bar{q}\gamma$ and $e^+e^- \to q\bar{q}$ where one of the quarks fragments into a photon. The quark-to-photon fragmentation function is present at leading order. As this fragmentation function depends on the fraction of the parent parton energy carried by the photon, we will formulate the cross section in terms of z rather than the energy of the photon, E_γ. We shall evaluate,

$$\frac{1}{\sigma_0}\frac{\mathrm{d}\sigma}{\mathrm{d}z}$$

where σ_0 is the tree level cross section for the process $\gamma^* \to q\bar{q}$.

A simplification follows from this formulation too. The initial state configuration becomes irrelevant for this calculation of the photon + 1 jet rate. Instead of considering the two contributions to be $e^+e^- \to q\bar{q}\gamma$ and $e^+e^- \to q\bar{q}$ with associated quark-to-photon fragmentation function, we can as well consider the two contributions to be $\gamma^* \to q\bar{q}\gamma$ and $\gamma^* \to q\bar{q}$ with associated quark-to-photon fragmentation function. This is what we shall do in the rederivation of the photon +1 jet rate at $\mathcal{O}(\alpha)$ in this section and in the evaluation of the next-to-leading order corrections to it in the forthcoming chapters of the dissertation[2].

The contributions related to the three parton final state process $\gamma^* \to q\bar{q}\gamma$ are all "experimentally unresolved". The three partons need to be clustered together according to a jet algorithm with a jet resolution parameter y_{cut} to form a two-jet event. Furthermore as one of the jets has to form the "photon" jet, the fraction of the electromagnetic energy z inside one of the clusters needs to be greater than the experimental cut, z_{cut}.

These real contributions can be either *theoretically* resolved, if all the final state particles are clearly distinguishable, they can be *theoretically* unresolved when the photon becomes collinear to the quark (or to the antiquark), $s_{q\gamma}$ (or $s_{\bar{q}\gamma}$) is less than the theoretical

[2]Note that we are finally interested in the quark-to-photon fragmentation in $Z \to q\bar{q}$. The transition $\gamma^* \to Z$ is however just a mere replacement of the coupling factors.

slicing parameter $s_{\min}$ in this case. The introduction of this theoretical parton resolution parameter $s_{\min}$, as we have seen in Section 1.5.2, enables us to isolate analytically these collinear divergences. Furthermore, as the physical cross section is finite, these collinear divergences will be "absorbed" into the *bare* quark-to-photon fragmentation function. To start with, we shall concentrate on the contributions to the photon + 1 jet rate where the three partons in the final state are *resolved* theoretically. Second, we will explicitly show how the collinear singularities are factorized into the *bare* fragmentation function.

2.4.1 The resolved contributions

The d-dimensional three particle matrix element squared (for massless quarks of unit charge) is given by eq.(1.17) and the d-dimensional three particle phase space can be found in the Appendix B (c.f. eq.(B.4)). In the region of the three-particle phase space where all the final state particles are clearly distinct, we have

$$s_{q\gamma} > s_{\min}, \qquad s_{\bar{q}\gamma} > s_{\min}. \tag{2.10}$$

And the matrix element squared is finite. The theoretically resolved contributions to the photon +1 jet rate, $\mathrm{d}\sigma^{(R)}$ can therefore be obtained by integrating the four dimensional three-parton matrix elements over the "photon +1 jet phase space".

If we work in the JADE jet algorithm [26], for example[3] , with a jet resolution parameter $y_{\rm cut} \leq 1/3$ then, for a photon cluster with a fraction of electromagnetic energy greater than $z_{\rm cut}$, the photon +1 jet region is defined by,

$$\begin{aligned} 1: &\quad y_{q\bar{q}} < y_{\rm cut}, \\ 2: &\quad y_{q\gamma} < y_{\rm cut} \text{ and } \frac{E_\gamma}{E_\gamma + E_q} > z_{\rm cut}, \\ 3: &\quad y_{\bar{q}\gamma} < y_{\rm cut} \text{ and } \frac{E_\gamma}{E_\gamma + E_{\bar{q}}} > z_{\rm cut}. \end{aligned} \tag{2.11}$$

[3]The definition of the photon +1 jet region is defined slightly differently in the DURHAM algorithm [27], it can be found in [49].

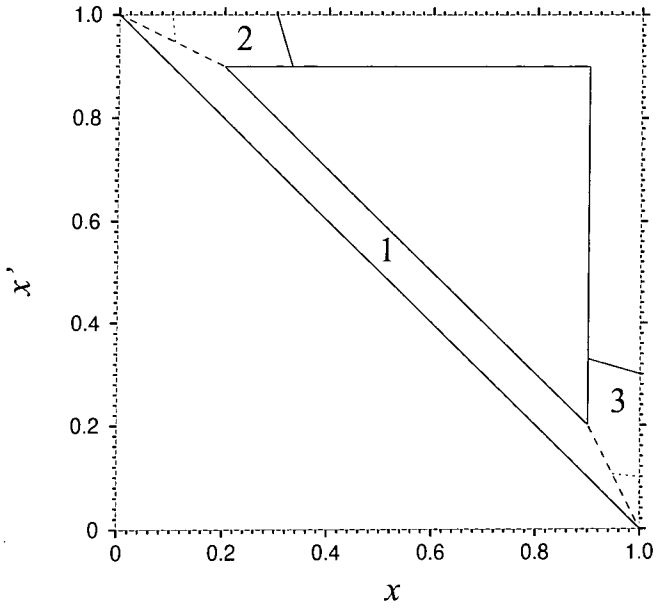

Figure 2.1: Dalitz plot for the $q\bar{q} + \gamma$ final state in terms of the quark and antiquark energy fractions x and x'. The regions 1, 2 and 3 show the photon + 1 jet phase space for $y_{\rm cut} = 0.1$ and $z_{\rm cut} = 0.7$ in the E0 scheme. The dotted lines show regions 2 and 3 for $z_{\rm cut} = 0.9$. Region 1 where the quark-antiquark combine to form a jet is separated from the regions where the quark (antiquark) combines with the photon by a dashed line.(Figure taken from [49])

The corresponding Dalitz plot is shown in Fig. 2.1 for $y_{\rm cut} = 0.1$ and $z_{\rm cut} = 0.7$. In region 1, the quark and antiquark combine to form the jet, while in regions 2 (3), the photon coalesces with a quark (antiquark) to form a mixed electromagnetic/hadronic cluster. x, x' are the quark energy fractions defined as in the isolated photon analysis, c.f. eq.(2.5).

In the region of phase space where quark and photon combine (regions 2 and 3), the fraction of electromagnetic energy in the cluster, z, is related to x and x' by,

$$z = \frac{2 - x - x'}{2 - x'}, \tag{2.12}$$

in region 2 and by eq.(2.12) with $x \leftrightarrow x'$ in region 3. In region 1 the quark and the

antiquark combine to form a jet, thus leaving the photon completely isolated. In this case the photon cluster has $z = 1$.

By integrating over $y_{\bar{q}\gamma}$ in these three phase space regions building the photon +1 jet phase space, it is straightforward to obtain the *resolved* contribution, $d\sigma^{(R)}$ to the photon +1 jet cross section as a function of z and $y_{\min}$[4],

$$\frac{1}{\sigma_0}\frac{d\sigma^{(R)}(\gamma + 1 \text{ jet})}{dz}(z, y_{\min}, y_{\text{cut}}) = \frac{1}{\sigma_0}\frac{d\hat{\sigma}^{(R)}(\gamma + 1 \text{ jet})}{dz}(z, y_{\min}, y_{\text{cut}}) + R_\Delta(z, y_{\text{cut}})\delta(1 - z). \quad (2.13)$$

Let us first note that R_Δ, which represents the contribution to the resolved cross section where quark and antiquark combine leaving the photon isolated, is independent of the slicing parameter $y_{\min}$. This is because there is no singularity associated with the $y_{q\bar{q}} \to 0$ limit in the matrix element. $d\hat{\sigma}^{(R)}$ is the contribution to the resolved cross section, where quark and photon, or antiquark and photon are clustered into one jet, and depends on $\log(y_{\min})$. So does $d\sigma^{(R)}$. However when combined with the theoretically unresolved contributions, $d\sigma^{(U)}$, all $y_{\min}$ dependence vanishes.

Because of the low parton multiplicity in the final state, some analytic results can be obtained for the resolved photon +1 jet cross section at $\mathcal{O}(\alpha)$, $d\sigma^{(R)}$. The constraints on the invariants defining the γ +1 jet region of phase space given in eq.(2.11) fix the boundaries of the phase space integrals which can be evaluated analytically. The explicit expressions for (2.13) have been derived by E.W.N.Glover and A.G.Morgan and can be found in [49]. Note that the evaluation of resolved contributions to the γ +1 jet rate at $\mathcal{O}(\alpha\alpha_s)$ will have to be performed numerically as will be presented in Chapter 9.

2.4.2 The quark-photon collinear contribution

In the region of phase space defined by $s_{q\gamma} < s_{\min}$, but $s_{\bar{q}\gamma} > s_{\min}$ the quark and the photon are collinear and cluster to form a new parton Q such that:

$$p_\gamma + p_q = p_Q.$$

[4] $y_{\min} = \frac{s_{\min}}{M^2}$, where M is the mass of the final state.

p_γ and p_q carry respectively a fraction z and $1-z$ of the parent parton momentum p_Q,

$$p_q = (1-z)\,p_Q, \qquad p_\gamma = z\,p_Q. \tag{2.14}$$

In the quark-photon collinear limit ($s_{q\gamma} < s_{\min}$) the invariants $s_{q\bar{q}}$ and $s_{\bar{q}\gamma}$ become

$$s_{q\bar{q}} = (1-z)\,M^2, \qquad s_{\bar{q}\gamma} = z\,M^2. \tag{2.15}$$

In this limit, the matrix elements and phase space related to $\gamma^* \to q\bar{q}\gamma$ exhibit an overall factorization in exactly the same factors as the matrix elements and phase spaces related to the process $\gamma^* \to q\bar{q}g$ in the quark-gluon collinear limit discussed in Section 1.5.3. We have respectively,

$$|\mathcal{M}_{123}|^2 \to P_{q\gamma\to Q}(z, s_{q\gamma})|\mathcal{M}_{Q2}|^2, \tag{2.16}$$

with, $P_{q\gamma\to Q}(z, s_{q\gamma})$ the *collinear factor* given by[5]

$$P_{q\gamma\to Q}(z, s_{q\gamma}) = \frac{1}{s_{q\gamma}} P_{q\gamma\to Q}(z). \tag{2.17}$$

As $s_{q\gamma}$ tends to 0, the three particle phase space also factorizes,

$$\mathrm{d}P_3^{(d)}(M, p_q, p_{\bar{q}}, p_\gamma) \to \mathrm{d}P_2^{(d)}(M, p_Q, p_{\bar{q}})\,\mathrm{d}P_{col}^{(d)}(p_q, p_\gamma, z). \tag{2.18}$$

$\mathrm{d}P_2^d(M, p_Q, p_{\bar{q}})$ is the known two-particle phase space in d dimensions given in the Appendix B by eq.(B.3) and the collinear phase space factor $\mathrm{d}P_{col}^{(d)}(p_q, p_\gamma, z)$, reads,

$$\mathrm{d}P_{col}^{(d)}(p_q, p_\gamma, z) = \frac{(4\pi)^\epsilon}{16\pi^2\Gamma(1-\epsilon)} \mathrm{d}s_{q\gamma}\,\mathrm{d}z \Big[s_{q\gamma} z(1-z)\Big]^{-\epsilon} \theta(s_{\min} - s_{q\gamma}). \tag{2.19}$$

The result we will obtain for quark-photon collinear limit of the differential cross section $\mathrm{d}\sigma_{q\bar{q}\gamma}$ is however somewhat different than the result obtained in eq.(1.35) for the quark-gluon collinear limit of differential cross section $\mathrm{d}\sigma_{q\bar{q}g}$. In the quark-photon collinear limit, $\mathrm{d}\sigma_{q\bar{q}\gamma}$ factorizes in a collinear factor and the two particle cross section. We formally have,

$$\mathrm{d}\sigma_{q\bar{q}\gamma} \to \sigma_{Q\bar{q}} \times \left[\int g^2 P_{q\gamma\to Q}(z, s_{q\gamma}) \mathrm{d}P_{col}^{(d)}\right]. \tag{2.20}$$

[5]Recall, $P_{q\gamma\to Q}(z)$ is the d-dimensional Altarelli-Parisi splitting function defined in eq.(1.31). It is given by $P_{q\gamma\to Q}(z) = \frac{1+(1-z)^2-\epsilon z^2}{z}$.

g^2 stands here for $(\alpha e_q^2)4\pi\mu^{2\epsilon}$, where μ^2 is introduced to maintain a dimensionless electromagnetic coupling α. To evaluate the quark-gluon collinear factor as in eq.(1.35) we integrated the collinear matrix element over all unresolved variables defined in this collinear region. These unresolved variables were,

$$s_{qg} \quad \text{and} \quad z,$$

where z was the fractional momentum carried by the gluon.

In the quark-photon collinear limit of the differential cross section $\mathrm{d}\sigma_{q\bar{q}\gamma}$, z represents the fractional momentum carried by the photon. As the photon is observed in the final state the collinear differential cross section will be a function of z. In other words z does not count as "unresolved variable" anymore. To evaluate the quark photon collinear differential cross section we only need to integrate over $s_{q\gamma}$. The quark-photon collinear factor $C_{F\gamma}\,\mathrm{d}z$ reads,

$$\begin{aligned} C_{F\gamma}\mathrm{d}z &\equiv \int g^2 P_{q\gamma\to Q}(z, s_{q\gamma})\mathrm{d}P_{col}^{(d)}(p_q, p_\gamma, z)\,\mathrm{d}z \\ &= \frac{\alpha e_q^2}{2\pi}\frac{(4\pi\mu^2)^\epsilon}{\Gamma(1-\epsilon)}\left[z(1-z)\right]^{-\epsilon} P_{q\gamma\to Q}(z)\mathrm{d}z \int_0^{s_{\min}} \mathrm{d}s_{q\gamma}\, s_{q\gamma}^{-\epsilon-1} \\ &= -\frac{1}{\epsilon}\frac{\alpha e_q^2}{2\pi}\frac{1}{\Gamma(1-\epsilon)}\left(\frac{4\pi\mu^2}{M^2}\right)^{+\epsilon}(y_{\min})^{-\epsilon}\left[z(1-z)\right]^{-\epsilon}\mathrm{d}z P_{q\gamma\to Q}(z). \end{aligned} \tag{2.21}$$

The quark-photon collinear contribution, $\mathrm{d}\sigma_C^{(U)}$ to the photon +1 jet rate, which is a function of z and $y_{\min}$ is therefore given by,

$$\frac{1}{\sigma_0}\frac{\mathrm{d}\sigma_C^{(U)}}{\mathrm{d}z}(z, y_{\min}) = C_{F\gamma}. \tag{2.22}$$

2.4.3 The factorization of collinear singularities

We first recall the results obtained so far for the contributions to the γ +1 jet rate at $\mathcal{O}(\alpha)$. We have,

$$\begin{aligned} \frac{1}{\sigma_0}\frac{\mathrm{d}\sigma(\gamma+1\text{ jet})}{\mathrm{d}z} &= 2\frac{\mathrm{d}\sigma^{(R)}(\gamma+1\text{ jet})}{\mathrm{d}z}(y_{\min}, y_{\mathrm{cut}}, z) + 2\frac{\mathrm{d}\sigma^{(U)}(\gamma+1\text{ jet})}{\mathrm{d}z}(y_{\min}, z) \\ &\quad + 2D_{q\to\gamma}^{bare}(z). \end{aligned} \tag{2.23}$$

As the three parton phase space and matrix elements are completely symmetric in the variables $y_{q\gamma}$ and $y_{\bar{q}\gamma}$, the contributions obtained considering the photon collinear on the quark leg are identical to those obtained considering the photon collinear to the antiquark leg. To evaluate the photon + 1 jet rate at $\mathcal{O}(\alpha)$ we therefore only consider the contributions where the photon is collinear on the quark leg, and multiply the result by two. The same procedure will be considered for the calculation of the photon + 1 jet rate at $\mathcal{O}(\alpha\alpha_s)$. Moreover, by charge conjugation invariance, we can assume that $D_{\bar{q}\to\gamma} = D_{q\to\gamma}$.

As the left-hand side of the equation (2.23) is a finite experimentally observable quantity, the explicit $\frac{1}{\epsilon}$ divergence present in the unresolved contribution $C_{F\gamma}$ has to be compensated by a similar divergence present in the *bare* quark-to-photon fragmentation function. Hence, we can decompose[6] the *bare* fragmentation function into a finite renormalized non-perturbative component $D_{q\to\gamma}(z,\mu_F)$ and a perturbative infinite counter term. It reads,

$$D^{bare}_{q\to\gamma}(z) = D_{q\to\gamma}(z,\mu_F) + \frac{1}{\epsilon}\left(\frac{4\pi\mu^2}{\mu_F^2}\right)^{\epsilon}\frac{1}{\Gamma(1-\epsilon)}\left(\frac{\alpha e_q^2}{2\pi}\right)\left(\frac{1+(1-z)^2}{z}\right). \qquad (2.24)$$

To keep both fragmentation functions dimensionless, a mass factorization scale μ_F has to be introduced compensating the unphysical scale μ. The renormalized fragmentation function $D_{q\to\gamma}(z,\mu_F)$ now depends on the chosen mass factorization scale, μ_F. The perturbative counter term in eq.(2.24) ensures that the right hand side of equation (2.23) is finite. Indeed, we obtain,

$$\begin{aligned}\frac{1}{\sigma_0}\frac{\mathrm{d}\sigma(\gamma+1\text{ jet})}{\mathrm{d}z}(z,\mu_F) &= 2\frac{\mathrm{d}\sigma^{(R)}(\gamma+1\text{ jet})}{\mathrm{d}z}(y_{\min},y_{\mathrm{cut}},z) + 2D_{q\to\gamma}(z,\mu_F)\\ &\quad + \left(\frac{\alpha e_q^2}{\pi}\right)\left[\left(\frac{1+(1-z)^2}{z}\right)\log\left(\frac{s_{\min}z(1-z)}{\mu_F^2}\right)+z\right].\end{aligned}$$

[6]This decomposition is not unambiguous, as one could add an arbitrary finite term into the bare quark-to-photon fragmentation function. The particular choice of finite terms defines the renormalization/factorization scheme. The results given here correspond to the so-called *modified minimal* subtraction ($\overline{\mathrm{MS}}$)-scheme [50].

(2.25)

Considering the explicit expression for the resolved contributions $d\sigma^{(R)}(\gamma + 1 \text{ jet})$, as given in [49], it can be noticed that as $z \to 1$ this cross section grows like $\log(1-z)^2$. Furthermore the cancellation of the $y_{\min}$ dependence in the γ +1 jet cross section becomes manifest such that eq.(2.25) may be rewritten as,

$$\begin{aligned}\frac{1}{\sigma_0}\frac{d\sigma(\gamma+1\text{ jet})}{dz}(z,\mu_F) &= 2D_{q\to\gamma}(z,\mu_F) + \left(\frac{\alpha e_q^2}{2\pi}\right)\left(\frac{1+(1-z)^2}{z}\right)\log\left(\frac{s}{\mu_F^2}\right) \\ &+ \left(\frac{\alpha e_q^2}{\pi}\right)\left(\frac{1+(1-z)^2}{z}\right)\log\left(\frac{z(1-z)^2}{1+z}\right) \\ &+ \left(\frac{\alpha e_q^2}{\pi}\right) f(z,y_{\text{cut}}) + R_\Delta(z,y_{\text{cut}})\delta(1-z), \qquad (2.26)\end{aligned}$$

where $f(z, y_{\text{cut}})$ is a known regular function with $f(z=1)=1$ and R_Δ the perturbative component for isolated photon production defined as in eq. (2.13). Note that, when the higher order corrections to this process will be included in the following chapters of this dissertation, as the resolved contributions will be evaluated numerically, the cancellation of the $y_{\min}$ dependence in the finite answer will also be shown on a numerical basis only.

2.4.4 A possible form for $D_{q\to\gamma}(z,\mu_F)$

The non-perturbative quark-to-photon fragmentation function is unknown. It is a universal and process independent function which is incalculable in perturbation theory and needs to be measured by experiment. Its variation with the factorization scale μ_F may however be determined within the framework of perturbative QCD. Indeed, requiring the *bare* quark-to-photon fragmentation function $D^{bare}_{q\to\gamma}$ to be independent of the unphysical factorization scale μ_F, yields an *evolution equation* for the non-perturbative fragmentation function $D_{q\to\gamma}(z,\mu_F)$. This evolution equation is determined by the perturbative content of $D^{bare}_{q\to\gamma}(z)$ and reads,

$$\frac{\partial D_{q\to\gamma}(z,\mu_F)}{\partial \ln(\mu_F^2)} = \left(\frac{\alpha e_q^2}{2\pi}\right)\left(\frac{1+(1-z)^2}{z}\right). \qquad (2.27)$$

A general form of the fragmentation function which satisfies the above evolution equation is given by,

$$D_{q\to\gamma}(z,\mu_F) = A\left(z,\frac{\mu_F^2}{\mu_0^2}\right) + B(z,\mu_0). \tag{2.28}$$

where the scale μ_0 and the associated function $B(z,\mu_0)$ are nothing more than the constants of integration which shall be determined by the data. μ_0 can also be viewed as the scale below which the physics is non-perturbative. Requiring that the cross section is "well behaved" as z tends to one allow us to constrain further $D_{q\to\gamma}(z,\mu_F)$. A possible choice for $D_{q\to\gamma}(z,\mu_F)$ which balances the singular behaviour of the resolved cross section $\mathrm{d}\sigma^{(R)}$ (given by eq.(2.26)) is,

$$D_{q\to\gamma}(z,\mu_F) = \left(\frac{\alpha e_q^2}{2\pi}\right)\frac{1+(1-z)^2}{z}\ln\left(\frac{\mu_F^2}{\mu_0^2(1-z)^2}\right). \tag{2.29}$$

It corresponds to choose $B = 0$ in eq.(2.28). This fragmentation function is an exact solution of the leading order evolution equation, the factorization scale dependence is therefore eliminated. Furthermore, since the $\log(1-z)$ behaviour is cancelled, the total differential cross section is positive for all values of z. Finally, it is also worth noting that within this approach, the quark-to-photon fragmentation function $D_{q\to\gamma}(z,\mu_F)$ is proportional to the electromagnetic coupling constant α.

At the electron-positron collider, both up- and down- type quarks are produced such that the measured quark-to-photon fragmentation function, $D_{q\to\gamma}^{\mathrm{LEP}}(z,\mu_F)$ is a combination of up- and down-type quark-to-photon fragmentation functions. More precisely it is given by,

$$D_{q\to\gamma}^{\mathrm{LEP}}(z,\mu_F) = \frac{2\,(v_u^2+a_u^2)D_{u\to\gamma}(z,\mu_F) + 3\,(v_d^2+a_d^2)D_{d\to\gamma}(z,\mu_F)}{2\,(v_u^2+a_u^2) + 3\,(v_d^2+a_d^2)}, \tag{2.30}$$

where v_q and a_q are the vector and axial vector couplings of quark q with the Z boson. We shall present the measurement of the quark-to-photon fragmentation function in photon +1 jet events at LEP in Section 2.6.

2.5 An alternative approach

As a result of the factorization of collinear singularities, we saw in the last section that the bare quark-to-photon fragmentation function can be decomposed into a renormalized fragmentation function $D_{q\to\gamma}(z,\mu_F)$ and a perturbative counter term. As a consequence the renormalized fragmentation function satisfies an evolution equation given by eq.(2.27). A parametric form for $D_{q\to\gamma}(z,\mu_F)$ could then be suggested by requiring that the fragmentation function satisfies the evolution equation and imposing that the lowest order photon +1 jet cross section is well behaved as z tends to one. An alternative procedure to determine a parametric form for $D_{q\to\gamma}(z,\mu_F)$ is obtained by considering the next-to-leading order evolution equation and solving it in the leading logarithmic approximation. We shall explain what we mean by this statement in the following.

One can consider that the renormalized quark-to-photon fragmentation function evolves with variations of μ_F, just as usual fragmentation or parton distribution functions do, as a result of gluon bremsstrahlung and quark-antiquark pair production [51]. At next-to-leading order the resulting evolution equations[7] are given [12] by,

$$\frac{\partial D_{q\to\gamma}(z,\mu_F)}{\partial \ln(\mu_F^2)} = \frac{\alpha\epsilon_q^2}{2\pi}\,\frac{1+(1-z)^2}{z} + \frac{\alpha_s(\mu_F^2)}{2\pi}\int_z^1 \frac{\mathrm{d}y}{y} D_{q\to\gamma}(y,\mu_F) P_{qq}^{(0)}\left(\frac{z}{y}\right) \qquad (2.31)$$

where $P_{qq}^{(0)}(z)$ is the lowest order quark-to-quark Altarelli-Parisi splitting function defined as in [40] by $\left(\frac{N^2-1}{2N}\right)\left(\frac{1+z^2}{1-z}\right)_+$. The first term describes the $q \to q\gamma$ splitting and is also present in eq.(2.27). The second term is not present in eq.(2.27) and represents the convolution of a quark-to-quark splitting via the emission of a bremsstrahlung gluon "convoluted" with the quark-to-photon fragmentation function. It is worth noting too, that the strong coupling α_s is running in this evolution equation, i.e. it is a function of μ_F^2.

Indeed, for the evaluation of a quantity as a perturbative series in the coupling α_s,

[7] Note that in comparison with the evolution equations given by J.F.Owens in [12], we do not consider the gluon-to-photon fragmentation function in eq.(2.31). In [12], it is claimed that for $z > 0.5$ this fragmentation function can be consistently neglected as it is phenomenologically suppressed.

as higher orders are incorporated ultraviolet divergences can arise. Through the renormalization procedure necessary to remove these infinities, the strong coupling constant becomes dependent on a momentum scale characteristic of the process considered (which is typically given by $Q^2 = M_z^2$ in e^+e^- annihilation). Moreover, when the process of renormalization is implemented, it is necessary to specify a point at which the coupling of the theory is defined. This renormalization point is denoted by a momentum transfer μ. Since α_s is dimensionless, its dependence on the renormalization point μ is expressed through dimensionless ratios of the form Q^2/μ^2. The running coupling $\alpha_s(Q^2)$ can then be related to the logarithm of Q^2 in the following way,

$$\frac{\mathrm{d}\alpha_s(t)}{\mathrm{d}t} = \beta\left[\alpha_s(t)\right], \tag{2.32}$$

where $t = \ln(Q^2/\mu^2)$ and the function β determines the change in the coupling as the renormalization point μ is changed. The function β is calculated up to four loops using perturbative methods, [52]. For the next-to-leading order calculations discussed in this thesis (which are leading order in the strong coupling constant), the one-loop result is sufficient, it yields,

$$\beta(\alpha_s) = -b\alpha_s^2, \tag{2.33}$$

with $b = \frac{33-2n_f}{12\pi}$, n_f denoting the number of quark flavours. If the equation (2.32) is integrated, one finds

$$\alpha_s(t) = \frac{\alpha_s(0)}{1+\alpha_s(0)bt}. \tag{2.34}$$

The explicit dependence on $\alpha_s(0)$ can be removed by defining a scale parameter Λ by,

$$\Lambda^2 = \mu^2 e^{-1/\alpha_s(0)b},$$

so that,

$$\alpha_s(Q^2) = \frac{12\pi}{(33-2n_f)\ln(Q^2/\Lambda^2)}. \tag{2.35}$$

The scale parameter Λ is approximately the scale around which perturbation theory is not valid anymore. Experimental measurements yields a value approximately equal to 200 MeV for $n_f = 5$, [53]. Furthermore, considering the factorization scale μ_F to be the

large momentum variable Q, eq.(2.35) yields a relation between $\alpha_s(\mu_F^2)$ and $\ln(\mu_F^2)$ as we wanted.

In order to solve completely the inhomogeneous evolution equation, i.e. eq.(2.31), it is necessary to specify appropriate boundary conditions and therefore to know the quark-to-photon fragmentation function at a given initial scale μ_0. This must be taken either from the data or from some set of model-dependent assumptions[8]. At asymptotically large values of the factorization scale μ_F however, the solutions of the evolution equation (2.31) become independent of the initial boundary conditions.

The leading logarithmic approximation relies on the presence of a single large momentum scale that characterizes the process under consideration. In e^+e^- annihilation processes, the mass of the incoming Z-boson plays this role whereas in $p\bar{p}$ collisions the transverse momentum of the photon p_T is the scale which characterizes the process. Solving the evolution equation (eq.(2.31)) in the leading logarithmic approximation means to consider the asymptotic limit where $\mu_F^2 \to \infty$ and to solve the evolution equation while retaining only the terms in $\ln(\mu_F^2)$ or more precisely the terms which are proportional to $\ln\left(\frac{\mu_F^2}{\Lambda^2}\right)$. The asymptotic solution reads,

$$\lim_{\mu_F \to \infty} D_{q\to\gamma}(z,\mu_F) = \frac{\alpha}{2\pi} \ln\left(\frac{\mu_F^2}{\Lambda^2}\right) a_{q\to\gamma}(z). \tag{2.36}$$

Exact analytic expressions for $a_{q\to\gamma}(z)$ can be found using Mellin transformations and inverse Mellin transformations in [55]. A parametric formula which accurately reproduces the exact leading logarithmic solution is given by D.W.Duke and J.F.Owens in [12] as,

$$a_{q\to\gamma} = e_q^2 \frac{1}{z}\left[\frac{2.21 - 1.28z + 1.29z^2}{1 - 1.63\ln(1-z)} z^{0.049} + 0.002\,(1-z)^2\, z^{-1.54}\right]. \tag{2.37}$$

A particular feature of this asymptotic solution is the logarithmic growth with $\ln(\mu_F^2)$. More precisely, as these solutions are proportional to $\alpha \ln\left(\frac{\mu_F^2}{\Lambda^2}\right)$, from eq.(2.35), they

[8]In the literature it is often called Vector Meson Dominance (VMD) contribution [54]. This (VMD) model is based on the assumption that the photon may fluctuate mainly into ρ and ω mesons.

can be considered to be proportional to α/α_s. What is often encountered in the literature [12, 56] is the assumption that the quark-to-photon fragmentation function, (like its asymptotic limit) is also of order α/α_s. Within this assumption, the second term in the evolution equation (2.31) which at first appeared to be a higher order correction turns out to be of $\mathcal{O}(\alpha)$ and as important as the first term in the evolution equation.

Moreover, for the evaluation of processes involving the quark-to-photon fragmentation function at a given order in α_s, the perturbative contributions which need to be taken into account will of course vary depending whether one interprets the quark-to-photon fragmentation function as being of order α as in [49] or of order α/α_s as in [12, 56]. Applications of the second interpretation are widely used in the literature. It is applied to e^+e^- annihilation processes by [12, 56, 57], to the production of isolated photons in ep-collisions by [58] and to analyse isolated large p_T photon production in proton-antiproton collisions by [59, 60].

Finally, as the quark-to-photon fragmentation function is a process independent function, one could also try to implement the quark-to-photon fragmentation function evaluated in the leading logarithmic approximation as given by eq.(2.36, 2.37) in the evaluation of the photon +1 jet rate, as given by eq.(2.26). Within the leading logarithmic approximation, when the quark-to photon fragmentation is evaluated, the terms in $\ln(\mu_F^2)$ are considered to be dominant and all terms not proportional to $\ln(\mu_F^2)$ are neglected. In the case of the photon +1 jet rate given by eq.(2.26) where the fractional momentum z carried by the photon is relatively large ($z > 0.7$), neglecting those "non-logarithmic" terms does not necessarily appear to be a good thing to do. Indeed, as was pointed out by B.R.Webber in [61], the leading logarithmic approach is expected to yield an accurate prediction for any quark-to-hadron fragmentation function for *intermediate* values of z *only*. For large and small values of z however, the leading logarithmic (or leading log) approach is inadequate, because it does not take into account the terms proportional to $\ln z$ or $\ln(1-z)$.

Precisely in the case of the photon +1 jet rate, z is large and inserting the quark-to-photon fragmentation function obtained in the leading logarithmic approach the following

happens. As $z \rightarrow 1$ the perturbative contribution to the cross section, $d\sigma^{(R)}$ has an explicit $\ln(1-z)$ behaviour (as seen in eq.(2.26)) which, unlike in the first approach we presented, is not cancelled by a similar behaviour in the leading log quark-to-photon fragmentation function. It is not clear in this context, that the logarithmic terms of μ_F^2 are really much larger than the other terms and we therefore do not expect the quark-to-photon fragmentation function to be adequately obtained using the leading logarithmic approach.

However, the quark-to-photon fragmentation function is a priori unknown and will be measured at LEP. It is only by comparing the theoretical calculation of the photon + 1 jet rate and the experimental measurements that the form of the quark-to-photon fragmentation function can be determined. We shall present the experimental measurement of photon +1 jet events, and the comparison between the calculated (up to $\mathcal{O}(\alpha)$) and measured photon +1 jet rate in Section 2.6. The comparison between the calculated (up to $\mathcal{O}(\alpha\alpha_s)$) and measured rates will take place in Chapter 10.

2.6 The experimental measurement of the photon +1 jet rate

2.6.1 The selection of photon + 1 jet events at LEP

In this study of the ALEPH Collaboration at CERN [62], a sample of 1.17 million selected hadronic Z decay events are subdivided into 1 jet $+\gamma$, 2 jets $+\gamma$, and ≥ 3 jets $+\gamma$ topologies using the DURHAM algorithm [27] with the resolution parameter $y_{\rm cut}$, varied between 0.001 and 0.33. The photon is clustered together with all the other particles, as in the parton-level calculation (c.f. Section 2.4) and events are kept when at least one of the reconstructed hadronic jets contains a photon ($E_\gamma > 5$ GeV) carrying at least 70% of the total energy of the jet. The fractional energy, z of such a photon within a jet is defined as,

$$z = \frac{E_\gamma}{E_\gamma + E_{had}} \tag{2.38}$$

where E_{had} is the energy of all accompanying hadrons in the "photon-jet" determined by the cluster algorithm. Thus, events with completely isolated photons appear at $z = 1$. Currently, the measured z range is limited to $0.7 < z < 1.0$ by hadronic decay backgrounds which are very large when $z < 0.7$. The z distribution is divided into 6 equal bins between 0.7 and 1 for each topology. Furthermore, in order to separate more clearly the large contribution coming from the isolated photon component near $z = 1$ the last bin is split into two parts: $0.95 < z < 0.99$ and $0.99 < z < 1$.

The backgrounds are very large and mainly due to multi-photon clusters which remain indistinguishable from single photons. To a lesser extent initial state radiation (ISR) from the incoming leptons is also a background source. The first source arises mainly from the electromagnetic decays of hadrons and is important over the whole z range as highlighted in Fig. 2.2. Typical and relevant processes are $\pi^0 \to \gamma\gamma$ and $\eta \to \gamma\gamma$. Since ISR photons are mainly isolated, this background is very small for $z < 0.9$ but becomes the dominant background for $z > 0.99$. (5–10%). All these backgrounds are determined by Monte Carlo simulations and subtracted statistically from the data bin-by-bin in z for each value of $y_{\rm cut}$ after direct experimental confirmation that the principal components, namely $\pi^0 \to \gamma\gamma$ are adequately simulated.

The residue of the measured rate not accounted for after this statistical subtraction of all backgrounds described above is ascribed to *final state radiation* (FSR) photons. These events correspond to photons emitted from a primary quark-antiquark pair and will be taken into account in the measurement of the photon +1 jet rate.

2.6.2 The determination of $D_{q\to\gamma}(z,\mu_F)$ for $0.7 < z < 0.95$

In Section 2.4 we saw that the lowest order photon +1 jet cross section, given in eq.(2.26), could be written as,

$$\frac{1}{\sigma_0}\frac{\mathrm{d}\sigma(\gamma+1\ \mathrm{jet})}{\mathrm{d}z}(z,\mu_F) = 2D_{q\to\gamma}(z,\mu_F) + \left(\frac{\alpha e_q^2}{2\pi}\right)\left(\frac{1+(1-z)^2}{z}\right)\log\left(\frac{s}{\mu_F^2}\right) + \left(\frac{\alpha e_q^2}{\pi}\right)\left(\frac{1+(1-z)^2}{z}\right)\log\left(\frac{z(1-z)^2}{1+z}\right)$$

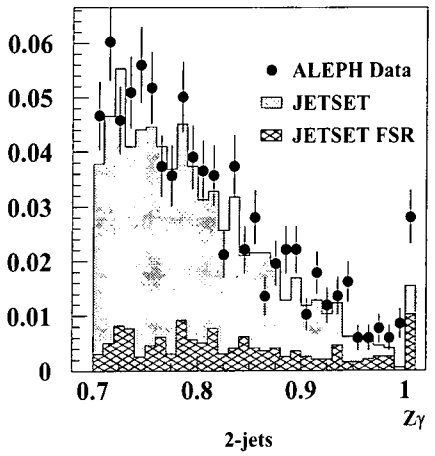

Figure 2.2: Observed z_γ distribution before background subtraction. The cross-hatched areas show the signal component in the JETSET Monte Carlo selected sample. Figure taken from [62].

$$+\left(\frac{\alpha e_q^2}{\pi}\right) f(z, y_{\rm cut}) + R_\Delta(z, y_{\rm cut})\delta(1-z), \qquad (2.39)$$

where $f(z, y_{\rm cut})$ is a known regular function with $f(z=1)=1$ and R_Δ is the the perturbative component to the cross section for an isolated photon as defined as in eq. (2.13). In this context, we also saw that the quark-to-photon fragmentation function $D_{q\to\gamma}(z,\mu_F)$ could be parametrized as in eq.(2.28) by,

$$D_{q\to\gamma}(z,\mu_F) = A\left(z, \frac{\mu_F^2}{\mu_0^2}\right) + B(z,\mu_0).$$

The A-term is an exact solution of the leading order evolution equation for $D_{q\to\gamma}(z,\mu_F)$ which is constructed to cancel both the μ_F dependence and the logarithms of $(1-z)$. The second term, $B(z,\mu_0)$ is required in order to specify the starting value of the non-perturbative fragmentation function $D_{q\to\gamma}(z,\mu_F)$ at $\mu_F=\mu_0$, the starting scale.

Inserting this parametrization into eq.(2.39) yields,

$$\frac{1}{\sigma_0}\frac{{\rm d}\sigma(\gamma+1\ {\rm jet})}{{\rm d}z}(z,\mu_F) = \left(\frac{\alpha e_q^2}{\pi}\right)\left(\frac{1+(1-z)^2}{z}\right)\log\left(\frac{s}{\mu_0^2}\frac{z}{1+z}\right)$$

$$+2B(z,\mu_0)+\frac{\alpha e_q^2}{\pi}f(z,y_{\rm cut})+R_\Delta(z,y_{\rm cut})\delta(1-z). \quad (2.40)$$

The free parameters to be determined are the cut-off scale μ_0 and the function $B(z,\mu_0)$. Various parametrizations have been tried in fitting $\frac{1}{\sigma_0}\frac{{\rm d}\sigma(\gamma+1\ {\rm jet})}{{\rm d}z}(z,\mu_F)$ to the five data points in the range $0.7 < z < 0.95$ at one particular value of $y_{\rm cut}$ ($y_{\rm cut} = 0.06$). The parametrizations tried include $(\alpha e_q^2)/2\pi$ multiplied by a constant C, $C_1 + C_2(1-z)$, and $C + (1-z)^\beta$. The ALEPH Collaboration found that $B(z,\mu_0) = 0$ does not give a sensible fit, whereas the data cannot differentiate between the other parametrizations. For simplicity, $B(z,\mu_0) = (\alpha e_q^2)/2\pi\ C$ is chosen as providing an adequate description of the data. The shape of the cross section, $\frac{1}{\sigma_0}\frac{{\rm d}\sigma(\gamma+1\ {\rm jet})}{{\rm d}z}(z,\mu_F)$ is well described with the A-term alone, but the normalization to the data requires the addition to this term of a negative constant. A corresponding double parameter fit having $\chi^2/4 = 0.24$ gives [62],

$$\mu_0 = 0.22^{+1.3}_{-0.19}{\rm GeV} \quad \text{and} \quad C = -12.1 \pm 4.3, \quad (2.41)$$

where statistical and systematic errors are combined in quadrature. The values of C and μ_0 are found to be strongly correlated. Indeed, as an alternative, considering that when $z \to 1$ the only contribution to the cross section should come from the isolated contribution to it, i.e. from R_Δ, yields the following relation between C and μ_0,

$$C = -1 - \ln\left(\frac{s}{2\mu_0^2}\right). \quad (2.42)$$

A one parameter fit having $\chi^2/5 = 0.31$ then yields,

$$\mu_0 = 0.14^{+0.21+0.22}_{-0.08-0.04}\ \ {\rm GeV}. \quad (2.43)$$

This single parameter fit was then used to evaluate the photon +1 jet rate for different values of $y_{\rm cut}$, [62]. The results are shown in Fig. 2.3 where we see that the data are adequately described by the leading order calculation including the parametrized quark-to-photon fragmentation function as in eq.(2.40) with the fitted value of μ_0 and $B(z,\mu_0) = (\alpha e_q^2)/2\pi)\ C$.

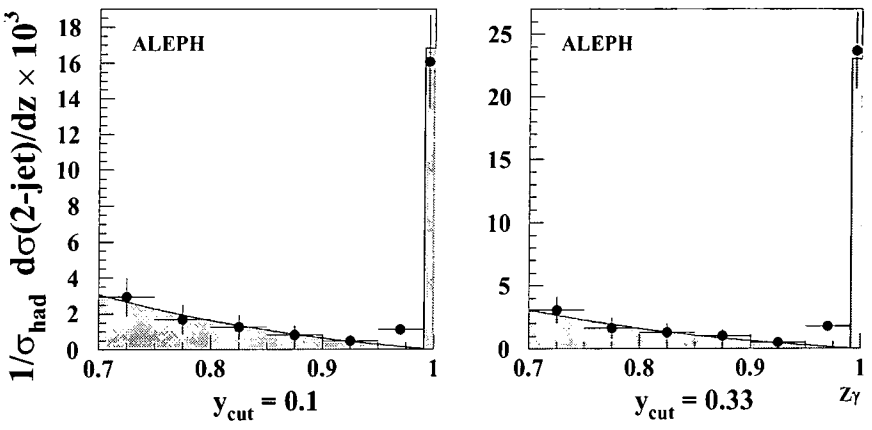

Figure 2.3: Comparison of the photon +1jet rates measured for different values of $y_{\rm cut}$ to a universal fragmentation function (see text). Figure taken from [62].

However, there seems to be a discrepancy between theory and experimental data for $z > 0.95$. Before discussing this difference and defining an isolated photon cross section in the same way at parton and hadron level as in Section 2.6.4, we shall first see how the quark-to-photon fragmentation obtained within the leading logarithmic approximation by D.W.Duke and J.F.Owens in [12] compares with the experimental data on the photon +1 jet rate.

2.6.3 A comparison with the fragmentation function obtained in the leading logarithmic approximation

In the leading logarithmic approximation the factorization scale μ_F is chosen to be the large momentum characterizing the process, so $\mu_F = M_Z$ and the initial scale μ_0 is set equal to Λ_{QCD}=200 MeV. The leading log quark-to-photon fragmentation function which is proportional to $\ln(Q^2/\Lambda^2)$ is given by eq.(2.36, 2.37). Inserting this parametrization of the fragmentation function with these values for μ_F and μ_0 into the leading order expression for the photon +1 jet cross section as given by eq.(2.39) gives a very poor

agreement with the experimental data as can be seen in Fig. 2.4.

A first improvement is obtained if one considers μ_F not to be the characteristic large scale of the process but rather the *maximum transverse momenta* of the photon within the photon-jet[9],

$$p_T = \sqrt{\frac{z(1-z)^2}{(1+z)}s}. \tag{2.44}$$

In the case where $\mu_F = p_T$, the factorization scale ranges from 17 GeV at z=0.7 to zero at z=1, [62]. The lower-cut off scale Λ is kept to be 0.2 GeV. Fig. 2.4 shows the comparison of the theoretical prediction and the data at $y_{\rm cut} = 0.06$. The prediction now follows the shape of the measured distribution but the rate is still too large. A second improvement yielding an acceptable fit to the data in the range $0.7 < z < 0.95$ can be obtained by allowing the initial scale to vary also. This is shown in Fig. 2.4 where Λ is found to be equal to $1.30^{+0.70}_{-0.45}$ GeV.

However by choosing $\mu_F = p_T$, which is clearly not a hard scale, and by allowing Λ to be different from the characteristic hadronization scale, we are not satisfying the criteria needed to justify the application of the leading logarithmic approximation. Neglecting non-logarithmic terms in the quark-to-photon fragmentation function is clearly not appropriate anymore. We therefore deduce that the quark-to-photon fragmentation function obtained using the framework of the leading logarithmic approximation seems to be ruled out by the data.

2.6.4 The isolated photon region: $z > 0.95$

From Fig. 2.3 it appears that the cross section decreases up to $z = 0.95$ and an isolated photon peak in the final bin $0.99 < z < 1$ is clearly noticeable. But, it also appears that a fraction of this isolated component populates the $0.95 < z < 0.99$ bin. The following is happening. A photon which had $z = 1$ at the parton level can, in the process of

[9]From kinematical constraints the transverse momenta is related to the invariants $s_{q\gamma}$ by $p_T^2 = z(1-z)s_{q\gamma}$. Furthermore $s_{q\gamma} = (1-z)/(1+z)s$, is the maximal allowed value for $s_{q\gamma}$ from phase space constraints for sufficiently high values of $y_{\rm cut}$, here chosen to be $y_{\rm cut} \geq 0.06$, as in [62].

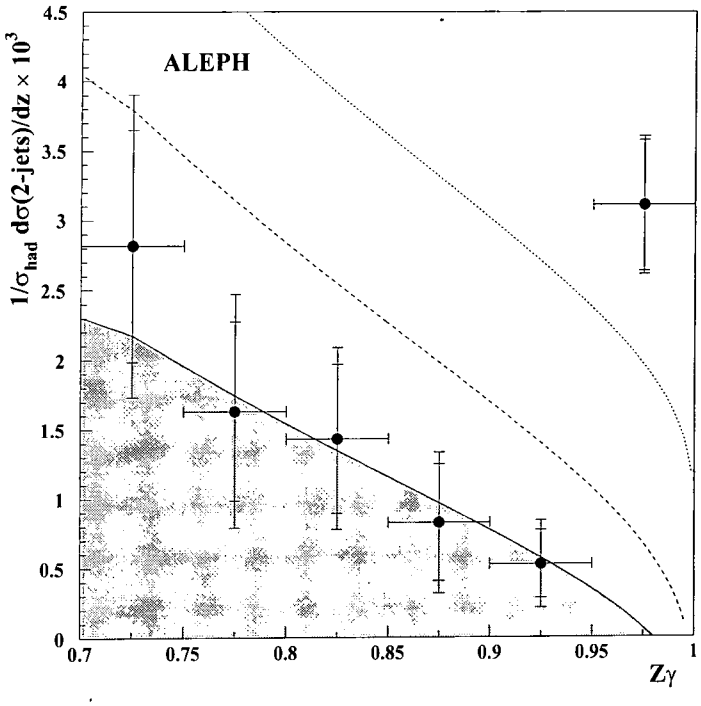

Figure 2.4: Comparison of measured $D(z_\gamma)$ function extracted from the photon +1jet rates at $y_{\rm cut} = 0.06$ to the Duke-Owens fragmentation function for $Q = p_T$ (dashed) and $Q = M_Z$ (dotted) with $\Lambda = 0.2$ GeV. The darkened area shows a fit to the (DO) function with $Q = p_T$ yielding $\Lambda = 1.30$ GeV. Figure taken from [62].

hadronisation, emit a soft gluon and become less energetic, thereby ending up with a momentum fraction z less than one. Moreover, these hadronization effects, which give rise to a discrepancy between the parton level calculation and hadron level data appear to be more and more pronounced with increasing $y_{\rm cut}$.

This discrepancy can be relieved if one defines an *isolated* photon to yield a fractional momentum z inside the "photon jet" to be greater than some fixed value ($z > 0.95$) at both parton **and** hadron level. Indeed, the agreement between parton level calculation and hadron level data is restored if in Fig. 2.3 one combines the two highest z bins into one single bin containing isolated photon events. This provides us with a safe way to define

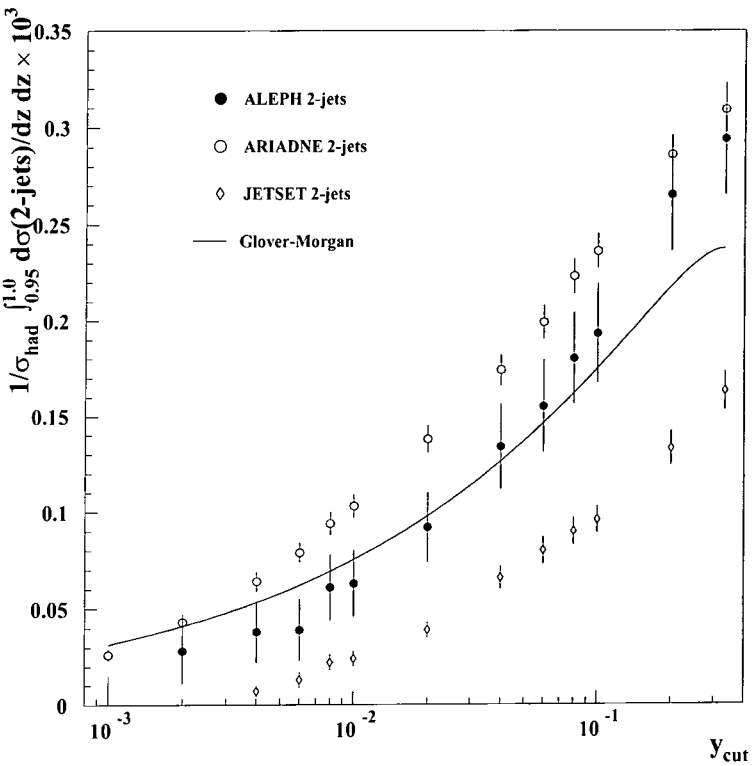

Figure 2.5: Integrated photon +1jet rate above $z_\gamma = 0.95$ as function of $y_{\rm cut}$, compared with the calculation of Glover and Morgan [49] including the fitted non-perturbative component of the $D(z_\gamma)$ function. Figure taken from [62].

isolated photons within the democratic approach at parton and hadron level, unlike in the previous analysis described in Section 2.2 where an isolated photon was defined in a two-step approach.

Furthermore, with this definition of an isolated photon and using the measured quark-to-photon fragmentation function yields a leading order prediction for the *integrated* rate above $z > 0.95$ as a function of $y_{\rm cut}$. As shown in Fig. 2.5, the agreement is adequate over the full range of $y_{\rm cut}$.

For large values of $y_{\rm cut}$ however, the theoretical prediction appears to be 2σ away from the data points. This may be explained as follows: Let us consider the simplest process

$e^+e^- \rightarrow q\bar{q}$. At large $y_{\rm cut}$, as can be seen from Fig. 1.2 in Section 1.2, events with 3 partons in the final state resulting from the additional emission of a real gluon in the process above, fall into the two-jet rate at hadron level. Such events are of course not counted in the lowest order parton level calculation so that the discrepancy between data and theory in this case may be accounted for by higher order corrections. The next-to-leading order corrections to the photon +1 jet rate shall be calculated in the remainder of this thesis and one of the aims of this calculation is to obtain a better agreement between the theoretical calculation and the data for the integrated rate for $z > 0.95$ and in particular at large $y_{\rm cut}$. Finally, note that the slight discrepancy between theory and experiment at small $y_{\rm cut}$ may be explained with the help of Fig. 1.2 too. The theoretical calculation is a fixed order calculation which may not be reliable for small values of y_{cut} due to the presence of large logarithms of y_{cut}. When next-to-leading order corrections are included this discrepancy should also be reduced.

In summary, in this chapter we have reviewed the phenomenology of photons in hadronic Z decays. In particular, after having described previous analyses of "isolated" photon +1 jet events where a two-step approach was used to identify the photon in Section 2.2, we have presented the lowest order calculation of the photon +1 jet rate at $\mathcal{O}(\alpha)$ in Section 2.3. This calculation is performed using a democratic approach where the photon is clustered together with all other partons in the final state. To be identified the photon is required to carry a large fraction of the energy inside the "photon jet". This lowest order calculation could be used to extract the non-perturbative quark-to-photon fragmentation function at $\mathcal{O}(\alpha)$ as presented in Section 2.6.2. A reasonable agreement between this lowest order parton level calculation and the experimental measurement is achieved. Finally, using the quark-to-photon fragmentation function determined in this way, a prediction for the isolated photon + 1 jet rate could be made and a reasonable agreement between the theoretical prediction and the data is obtained, as discussed at the end of Section 2.6. It appears however to be necessary to implement next-to-leading order corrections into the theoretical calculation. Their inclusion is expected to provide a better description of the data especially for large values of $y_{\rm cut}$. The comparison between

the next-to-leading order photon +1 jet rate and the data will be shown in Chapter 10.

Chapter 3

The Photon +1 jet rate at $\mathcal{O}(\alpha\alpha_S)$

In the previous two chapters, we have presented the necessary tools to evaluate jet cross sections at higher orders. In particular, in Section 1.5.2 we have seen how the introduction of a parton resolution criterion $s_{\min}$ enabled us to divide the phase space of higher order jet cross sections into *resolved* and *single unresolved* regions. In a simple example we have shown how soft and collinear divergences could be analytically isolated and cancelled against divergences present in the virtual contributions. On the other hand, in Section 2.4, we have presented the calculation of the the photon +1 jet rate at lowest order. We had contributions from the process $\gamma^* \to q\bar{q}\gamma$ and from the process $\gamma^* \to q\bar{q}$ with one of the quarks fragmenting into a photon. In particular, we have shown how the collinear quark-photon singularity is absorbed into the *bare* $\mathcal{O}(\alpha)$ fragmentation function $D_{q\to\gamma}$.

At next-to-leading order, the contributions to the photon +1 jet rate involve the processes $\gamma^* \to q\bar{q}\gamma$ and $\gamma^* \to q\bar{q}$ where one of the quark fragments into a photon, dressed with an additional real or virtual gluon. In addition, a generic $\mathcal{O}(\alpha\alpha_s)$ contribution to the *bare* quark-to photon fragmentation function (or counter term) has to be taken into account as well. As in the lowest order case we shall evaluate,

$$\frac{1}{\sigma_0}\frac{\mathrm{d}\sigma}{\mathrm{d}z},$$

where z is the fractional energy carried by the photon inside the "photon jet". σ_0 is the

tree level cross section for the process $\gamma^* \to q\bar{q}$.

Although the above cross section is finite at $\mathcal{O}(\alpha\alpha_s)$, we expect some of the contributions to contain divergences. A direct numerical evaluation incorporating the experimental jet algorithm is therefore not possible straightaway. We need to separate the calculation into two parts: an analytical and a numerical part. We have to calculate all potentially divergent contributions and cancel the singularities amongst them analytically. An important feature of this analytical part of the calculation is the need to extend the decomposition of the phase space into resolved and single unresolved regions to regions where *more than one* particle is theoretically "unseen". After a large analytic cancellation between real and virtual contributions has taken place, we expect that the remaining divergences, essentially due to collinear quark-photon singularities, will be factorized into the *bare* $\mathcal{O}(\alpha\alpha_s)$ fragmentation function, rendering the differential cross section finite. Finally once the divergences have cancelled, the different contributions to the cross section can be evaluated numerically while the jet algorithm is applied to select the photon +1 jet events.

It is the purpose of this chapter to present the plan of the calculation of the photon +1 jet rate at $\mathcal{O}(\alpha\alpha_s)$. In Section 3.1 we shall discuss the different classes of processes which enter in the calculation of this cross section. As we will see, we need to consider processes with two, three and four particles in the final state. Experimentally, all contributions involving more than two final state particles are *unresolved.* The additional particles present in the final state need to be clustered together according to a jet algorithm with jet resolution parameter y_{cut} so that only the photon-jet and one further jet remain. On the other hand, the contributions with three and four particles in the final state can be theoretically resolved or unresolved. In Sections 3.2–3.4 we will explicitly give the criteria, which define the phase space region where all particles are theoretically well separated and specify each theoretically unresolved region. We shall also outline how the different contributions to the cross section will be calculated analytically in the remainder of this thesis. Finally, Section 3.5 gives an outline of the calculation with particular emphasis on the expected pole structures and cancellations of singularities between the different

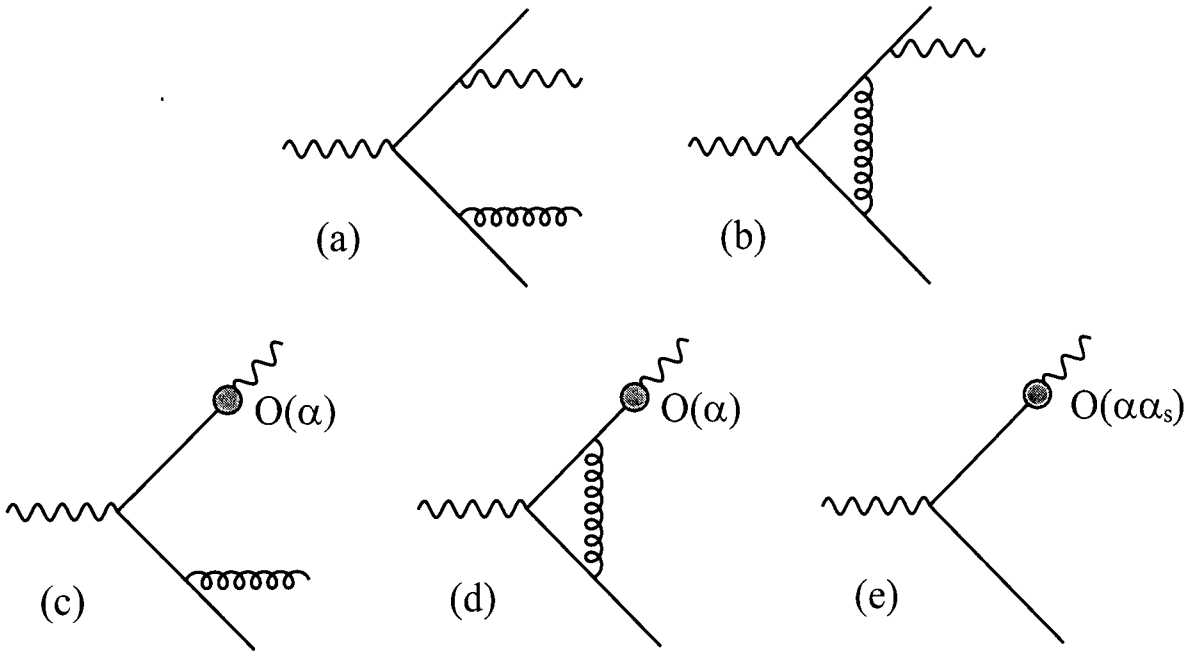

Figure 3.1: Final state configurations contributing to the photon +1 jet rate

contributions.

3.1 Contributions to the photon +1 jet rate at $\mathcal{O}(\alpha\alpha_s)$

At next-to leading order, one finds five classes of contributions to the photon +1 jet rate, which are represented schematically in Fig 3.1:

(a) the tree level process $\gamma^* \to q\bar{q}g\gamma$, where the final state particles are clustered together such that a "photon jet" and one additional jet are observed in the final state. As we will see in the next subsection, the photon can be isolated, in that case quark, antiquark and gluon are clustered together to form one jet. But it can also be clustered with one or two of the three other final state particles.

(b) the one loop gluon correction to the $\gamma^* \to q\bar{q}\gamma$ process, where the photon and one of the quarks are clustered together; for this process it can also happen that the photon is isolated and that quark and antiquark are combined into one jet.

(c) the process $\gamma^* \to q\bar{q}g$, where one of the quarks fragments into a photon while the remaining partons form only a single jet.

(d) the one loop gluon correction to $\gamma^* \to q\bar{q}$, where one of the quarks fragments into a photon.

(e) the tree level process $\gamma^* \to q\bar{q}$ with a generic $\mathcal{O}(\alpha\alpha_s)$ counter term present in the *bare* quark-to-photon fragmentation function.

We will discuss the detailed structure of the contributions to the photon + 1 jet rate associated with each of this classes of processes below. Some of these contributions may involve complicated phase space structure, with theoretically resolved, single unresolved and double unresolved regions. In this section we shall however not quantify the phase space configurations as Sections 3.2–3.4 are devoted to a detailed study of the individual phase space regions.

3.1.1 $\gamma^* \to q\bar{q}\gamma$ with real gluon bremsstrahlung

The tree level process $\gamma^* \to q\bar{q}g\gamma$ contributes to the photon +1 jet rate, if the final state configuration is such that only the photon jet and an associated jet are observed. As the photon has to be identified in the final state, it cannot be soft. Various different configurations are possible and a schematic overview is given in Fig. 3.2. Note that topologies where the role of quark and antiquark are exchanged are also present, but are not shown. The contributions arising when the photon is unresolved through clustering with either the quark or antiquark are in fact equal. Therefore, as in the calculation of the γ +1 jet at leading order described in Section 2.4, we consider only the contributions corresponding to the Feynman diagrams where the photon is emitted on the quark leg. When summing

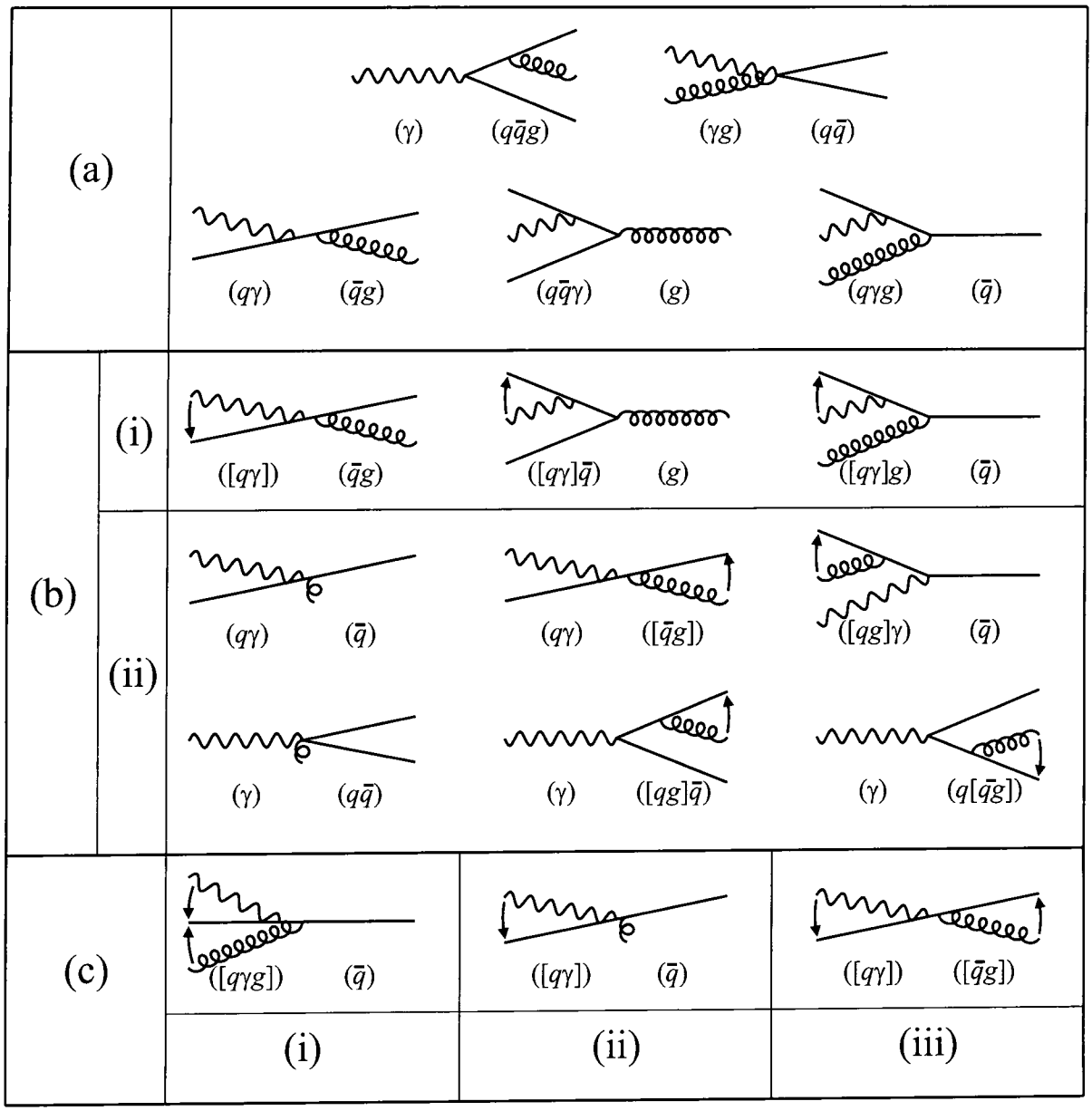

Figure 3.2: Different contributions from the tree level $\gamma^* \rightarrow q\bar{q}\gamma g$ process. Square brackets denote theoretically unresolved particles, round brackets experimental clusters.

all the contributions, the result obtained considering the photon associated with the quark will be multiplied by two.

The individual contributions can be structured as follows:

(a) **Theoretically resolved contributions**

If all particles are resolved, a γ +1 jet event can only be formed if some final state particles are clustered together by the jet algorithm. The possible configurations yielding a photon + 1 jet event are displayed in Fig. 3.2.a.

(b) **Single theoretically unresolved contributions**

One has to distinguish two classes of single (or one-particle) theoretically unresolved contributions, depending whether the gluon or the photon is unresolved.

(i) If the photon is unresolved, it is collinear to the quark while the gluon is *hard*, i.e. the gluon is theoretically resolved but combined with the photon-quark cluster or with the antiquark by the experimental jet algorithm. Alternatively, the gluon forms a jet on its own while the antiquark is clustered into the photon jet.

(ii) If the gluon is theoretically unseen, it can be soft or collinear to the quark or antiquark, while the photon is experimentally combined with the quark to form the photon jet or is isolated while all other partons form a single jet.

The possible configurations of single unresolved contributions yielding a photon + 1 jet event are displayed in Fig. 3.2.b.

(c) **Double theoretically unresolved contributions**

These contributions arise when the photon and the gluon are theoretically "unseen" in the final state. We count three double unresolved contributions:

(i) *Triple collinear contribution*

The photon and the gluon are simultaneously collinear to the quark.

(ii) *The soft/collinear contribution*

The photon is collinear to the quark while the gluon is soft.

(iii) *The double single collinear contribution*

The photon is collinear to the quark while the gluon is collinear to the antiquark.

For these three contributions, the final state configuration corresponds already to a photon +1 jet event. Hence, the final state particles will not be clustered further by the jet algorithm. These contributions are schematically displayed in Fig. 3.2.c.

3.1.2 $\gamma^* \to q\bar{q}\gamma$ with a virtual gluon

The one loop correction to $\gamma^* \to q\bar{q}\gamma$ contributes to the photon +1 jet rate, if two of the final state partons coincide in a single jet. One has to separate the theoretically unresolved collinear photon contribution from the contributions where a *hard* photon is clustered with the quark to form the photon jet or isolated while quark and antiquark form a single jet.

3.1.3 $\gamma^* \to q\bar{q}g$ with the fragmentation function

The tree level three parton production process with associated fragmentation contributes to the photon +1 jet cross section if, in addition to the photon-jet, only a single jet is formed. This is the case if,

(i) the gluon is resolved, but clustered into the photon or antiquark jet or forms a jet on its own, while the antiquark is clustered into the photon jet.

(ii) the gluon is unresolved, i.e. it is collinear to the quark or the antiquark or it is soft.

These configurations are illustrated in Fig. 3.3. Since this process is already of $\mathcal{O}(\alpha_s)$, only the $\mathcal{O}(\alpha)$ counter term in the bare fragmentation function contributes.

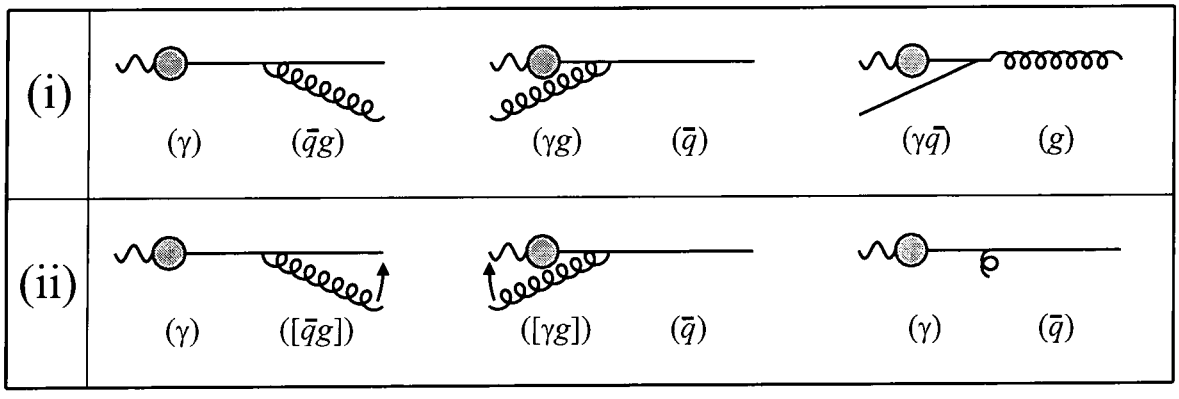

Figure 3.3: Different contributions from the tree level $\gamma^* \rightarrow q\bar{q}g$ process with subsequent fragmentation of the quark into a photon. Square brackets denote theoretically unresolved particles, round brackets represent experimental clusters.

3.1.4 $\gamma^* \rightarrow q\bar{q}$ with a virtual gluon and the fragmentation function

The one loop correction to the quark antiquark with associated photon fragmentation process always yields a final state with a photon +1 jet. As in the previous case, only the $\mathcal{O}(\alpha)$ counter term in the bare fragmentation function contributes.

3.1.5 $\gamma^* \rightarrow q\bar{q}$ with the fragmentation function

On top of all the processes described above involving a real or virtual gluon, one has to consider a contribution to the photon +1 jet rate from the generic $\mathcal{O}(\alpha\alpha_s)$ counter term present in the *bare* fragmentation function. Inclusion of this contribution absorbs all left over singularities of the processes cited above.

3.1.6 Summary

The contributions to the photon +1 jet cross section from all these processes will be calculated in the remainder of this thesis. The theoretically resolved, but experimentally unresolved contributions can be obtained numerically straightaway and will only be considered in Chapter 9. All single or double theoretically unresolved contributions need to be evaluated analytically to extract their divergent pole parts before they can be included in the numerical evaluation of the cross section. Their numerical implementation relies on the *hybrid subtraction* method introduced in Section 1.5.1 and will be discussed in Chapter 9. We will present the calculation of the single unresolved real contributions associated with the process $\gamma^* \to q\bar{q}\gamma g$ in Chapter 4, while the double unresolved contributions will be evaluated in Chapter 5. The resolved and unresolved virtual corrections to $\gamma^* \to q\bar{q}\gamma$ are derived in Chapter 6. Finally, Chapter 7 contains the calculation of all contributions involving the $\mathcal{O}(\alpha)$ counter term in the quark-to-photon fragmentation function. The $\mathcal{O}(\alpha\alpha_s)$ fragmentation counter term will be introduced when we add up all divergent contributions in Chapter 8, yielding a finite result.

So far we have only presented the different topologies of the contributions to the cross section under consideration, without quantifying the relevant regions of phase space for each contribution. The decomposition of the phase space into theoretically resolved and unresolved regions will be presented in great detail in the following three sections.

3.2 The phase space decomposition of the real contributions

In the previous section we have outlined the generic structure of all individual contributions to the photon +1 jet differential cross section at $\mathcal{O}(\alpha\alpha_s)$. To each specific contribution corresponds a particular region of the final state phase space. In this section, we shall give the criteria which define the different phase space regions associated with the individual contributions to the tree level process $\gamma^* \to q\bar{q}\gamma g$. We shall also present schematically

how these contributions will be calculated in the remainder of this dissertation.

These real contributions can be separated into three categories: the theoretically resolved, single unresolved or double unresolved contributions. The final state phase space therefore needs to be divided into corresponding regions.

The d-dimensional four-particle phase space $\mathrm{d}R_4^{(d)}(p_q, p_{\bar{q}}, p_\gamma, p_g)$ is derived in Appendix B in eq.(B.6) and reads,

$$\begin{aligned}\mathrm{d}R_4^{(d)} &= \frac{(\Delta_4)^{-1/2}}{Q^2\, 2^9} \int \mathrm{d}\Omega_{d-1}\, \mathrm{d}\Omega_{d-2}\, \mathrm{d}\Omega_{d-3}\, \delta(s_{q\bar{q}} + s_{q\gamma} + s_{qg} + s_{\bar{q}\gamma} + s_{\bar{q}g} + s_{g\gamma} - M^2) \\ &\quad \left(\frac{-\Delta_4}{M^2}\right)^{\frac{d-4}{2}} \mathrm{d}s_{q\bar{q}} \mathrm{d}s_{q\gamma} \mathrm{d}s_{qg} \mathrm{d}s_{\bar{q}\gamma} \mathrm{d}s_{\bar{q}g} \mathrm{d}s_{g\gamma},\end{aligned}$$

where Δ_4 is the Gram determinant defined in eq.(B.7). The separation of the four particle phase space into different resolved and unresolved regions is one of the most subtle points in this calculation. As one sees from the equation above, the four particle phase space includes five independent integration variables $\mathrm{d}s_{ij}$. The different phase space regions will be defined by specifying whether the invariants s_{ij} are greater or less than a theoretical parton resolution parameter $s_{\min}$ (or a cut proportional to $s_{\min}$). In contrast to the three particle phase space which has only two independent integration variables (and is easy to draw (Fig. 1.3)) the four particle phase space is difficult to visualize. To split this phase space into different regions which do not overlap and without leaving out any of them is therefore not a trivial task. In particular, it is not easy to ensure that no singular region is omitted. In a singular phase space region, the four-particle matrix element squared, $|\mathcal{M}|^2$ is singular, as one of the invariants s_{ij} present in the denominator tends to 0.

Before we define each singular phase space region it is worth noting that all the integration variables cited above will not have to be constrained in the same manner. For example, $s_{g\gamma}$ does not need to be limited as it does not appear in the denominator of the four-particle matrix element squared, $|\mathcal{M}|^2$. Furthermore this matrix element squared vanishes in the soft quark limit, i.e. $s_{q\bar{q}}$ does not need to be constrained either. We already saw that this was the case for the $\gamma^* \to q\bar{q}g$ process in Section 1.5.3. The only

variables that are constrained are thus,

$$s_{q\gamma}, \qquad s_{\bar{q}\gamma}, \qquad s_{qg}, \qquad s_{\bar{q}g},$$

although in the *double unresolved* region, we shall choose to constrain the combinations,

$$s_{q\gamma g}, \qquad s_{\bar{q}\gamma g},$$

for certain configurations. The decomposition of the four-particle phase space is summarized in Fig. 3.4. In this table, we have specified which invariants are less than $s_{\min}$ (or a cut proportional to $s_{\min}$) for each singular region of phase space. We have also noted which invariants are greater than $s_{\min}$ to eliminate overlaps between regions determined by the same combinations of invariants less than $s_{\min}$. Invariants that are not specified are completely unconstrained.

Moreover, for each of the singular phase space regions we shall specify how the fraction z of energy carried by the photon inside the "photon jet" is obtained. For each of these contributions we will require that the energy fraction z reconstructed by the jet algorithm is greater than the experimental cut z_{cut}.

The four-particle phase space can be divided into the following regions.

3.2.1 The single unresolved regions

We count four (five including the antiquark-photon collinear region) different single unresolved phase space regions as the photon or the gluon can be theoretically not identified. By analogy with the definitions of the single unresolved regions of the 3-parton final state phase space, it would seem natural to define the single unresolved regions of the 4-parton final state phase space by specifying which single invariant s_{ij} is less than $s_{\min}$ in the collinear regions and which pair of invariants is less than $s_{\min}$ in the soft region. However in the presence of an additional particle in the final state these cuts are not appropriate anymore. Indeed the single unresolved regions are defined as follows:

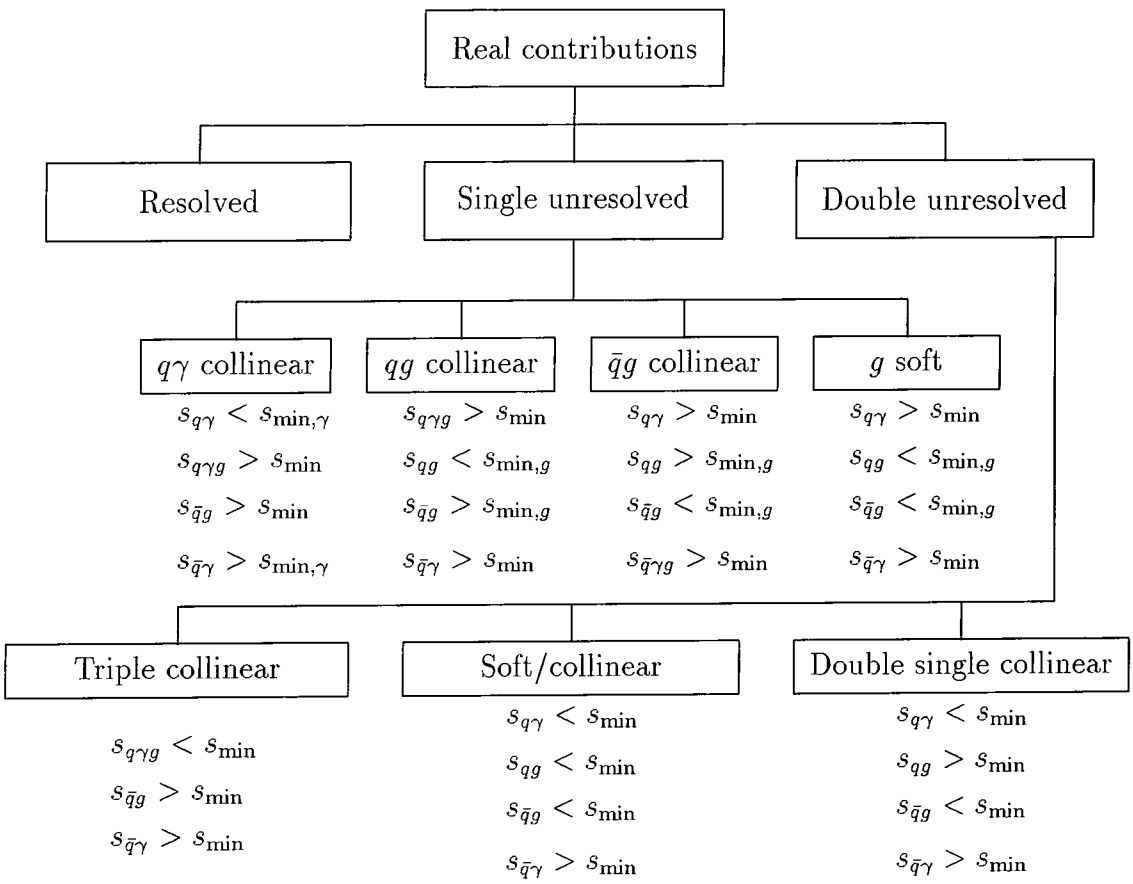

Figure 3.4: Phase space decomposition of the real $\gamma^* \to q\bar{q}\gamma g$ contributions. For abbreviation, we have introduced $s_{\min,\gamma} \equiv s_{\min}\, s_{q\bar{q}\gamma}/M^2$ and $s_{\min,g} \equiv s_{\min}\, s_{q\bar{q}g}/M^2$. Note that the single and double unresolved regions where the photon clusters with the antiquark are not shown. For these regions, the necessary cuts are obtained by exchanging q and $\bar{q}$. Altogether, there are five single unresolved and six double unresolved regions.

(i) The *single collinear quark-photon* region[1]

$$s_{q\gamma} < s_{\min}\frac{s_{q\bar{q}\gamma}}{M^2} \qquad s_{\bar{q}\gamma} > s_{\min}\frac{s_{q\bar{q}\gamma}}{M^2}, \qquad s_{q\gamma g} > s_{\min}, \qquad s_{\bar{q}g} > s_{\min}, \tag{3.1}$$

[1] M is the mass of the final state

(ii) The *single collinear quark-gluon* region

$$s_{qg} < s_{\min}\frac{s_{q\bar{q}g}}{M^2}, \qquad s_{\bar{q}g} > s_{\min}\frac{s_{q\bar{q}g}}{M^2}, \qquad s_{q\gamma g} > s_{\min}, \qquad s_{\bar{q}\gamma} > s_{\min}, \tag{3.2}$$

(iii) The *single collinear antiquark-gluon* region

$$s_{\bar{q}g} < s_{\min}\frac{s_{q\bar{q}g}}{M^2}, \qquad s_{qg} > s_{\min}\frac{s_{q\bar{q}g}}{M^2}, \qquad s_{q\gamma} > s_{\min}, \qquad s_{\bar{q}\gamma g} > s_{\min}, \tag{3.3}$$

(iv) The *soft gluon* region

$$s_{qg} < s_{\min}\frac{s_{q\bar{q}g}}{M^2}, \qquad s_{\bar{q}g} < s_{\min}\frac{s_{q\bar{q}g}}{M^2}, \qquad s_{q\gamma} > s_{\min}, \qquad s_{\bar{q}\gamma} > s_{\min}. \tag{3.4}$$

We shall justify the boundaries of the different single unresolved regions as given above in Chapter 4. For now, let us just say that with these boundaries no singular region of the 4-parton phase space is omitted or double counted.

In Section 1.5.3 we have presented the calculation of the soft and single collinear contributions to the cross section related to the process $\gamma^* \to q\bar{q}$ at $\mathcal{O}(\alpha_s)$. We saw that in these single unresolved regions of the three-particle phase space, one could write the cross section as the product of a universal "*one-particle unresolved factor*" and the two-particle tree level cross section σ_0. These single unresolved factors were C_F in eq.(1.35) and S_F in eq.(1.25) for the collinear and soft gluon case. In Section 2.4 we discussed also the collinear quark-photon behaviour of the three-particle cross section $\sigma_{q\bar{q}\gamma}$. The related collinear factor $C_{\gamma F}$ is a function of z. These three factors were obtained by integrating the approximated matrix elements over the corresponding single unresolved phase space regions.

The contributions to the photon +1 jet rate at $\mathcal{O}(\alpha\alpha_s)$ in the single unresolved regions of the 4-particle phase space will be obtained in a similar manner and will even yield single unresolved factors analogous to C_F, S_F and $C_{\gamma F}\mathrm{d}z$. These factors will be slightly modified to take into account the change in the boundaries between the single unresolved regions of the three and four parton phase space. In the 4-parton phase space those

single unresolved factors shall be denoted by $\tilde{C}_F, \tilde{S}_F$ and $\tilde{C}_{\gamma F}\mathrm{d}z$ and will be evaluated in Chapter 4. Furthermore, to yield the single unresolved contributions to the photon +1 jet differential cross section, these factors will be multiplied with the following three particle cross sections,

(i) $\sigma_{q\bar{q}\gamma}$, if the gluon is unresolved,

(ii) $\sigma_{Q\bar{q}g}$, if the photon is collinear to the quark[2].

The three particle cross sections, $\sigma_{q\bar{q}\gamma}$ and $\sigma_{Q\bar{q}g}$ are free of divergences and will be evaluated numerically. Moreover, the jet algorithm will be applied to cluster these three-particle final state events into γ +1 jet events. The different single unresolved configurations are depicted in Fig. 3.2.b. The fraction of energy carried by the photon inside the photon jet, z, is obtained when this jet is constructed with the help of the jet algorithm. However, for the quark-photon collinear contribution it is worth noting the following. In the quark-photon cluster, the photon carries a fraction z of the parent momentum p_Q. When the jet algorithm is applied, an additional parton could be clustered with this parent parton Q. Hence the reconstructed value of z, the fractional momentum of the photon in the Q+parton cluster, will be sometimes less than the value used in the analytic calculation of the collinear factor $C_{\gamma F}$. It is this reconstructed or "experimental" value of z which has to be greater than z_{cut}.

3.2.2 The double unresolved regions

In the double unresolved regions, the gluon and the photon are theoretically not identified. As the photon has to be seen in the final state, it can only be collinear to the quark and cannot be soft[3]. The gluon on the other hand can be collinear to the quark or to the antiquark or it can be soft. Corresponding to these different final state configurations we

[2] Q is the parent parton of the quark and the photon, as in Section 2.4.

[3] Recall that we only list the contributions associated with the processes where the photon is emitted on the quark leg.

decide to define three double unresolved phase space regions: the *triple collinear* region, the *soft/collinear* region and the *double single collinear* region. As before, these regions are matched by three analogous double unresolved regions where the photon clusters with the antiquark.

In the introduction to this subsection, we mentioned that the different phase space regions are determined by specifying which invariants appearing in the four-particle phase space are greater or less than $s_{\min}$. This is not exactly true in the double unresolved regions. In particular, in the triple collinear region we need to constrain the "triple" invariant $s_{q\gamma g} \equiv s_{q\gamma} + s_{qg} + s_{\gamma g}$ as it appears in the denominator of the four-particle matrix element; we will require: $s_{q\gamma g} < s_{\min}$. The three different double unresolved regions are defined more precisely as follows.

(i) The *triple collinear* region

In this region, the photon and the quark are simultaneously collinear,

$$s_{q\gamma g} < s_{\min} \quad \text{and} \quad s_{\bar{q}g} > s_{\min}. \tag{3.5}$$

We require $s_{\bar{q}g} > s_{\min}$ since in this region the gluon is collinear but not soft. The fractional energy z of the photon inside the quark-photon-gluon cluster is given by,

$$z = \frac{E_\gamma}{E_\gamma + E_q + E_g} = y_{\bar{q}\gamma}, \tag{3.6}$$

where E_γ,E_q,E_g are the energy of the photon, the energy of the quark and the energy of the gluon respectively.

(ii) The *soft/collinear* region

In this region the photon is collinear to the quark while the gluon is soft. We require,

$$s_{q\gamma} < s_{\min}, \quad s_{qg} < s_{\min} \quad \text{and} \quad s_{\bar{q}g} < s_{\min}. \tag{3.7}$$

For this configuration, z the fractional energy of the photon inside the quark-photon cluster is given by,

$$z = \frac{E_\gamma}{E_\gamma + E_q} = y_{\bar{q}\gamma}, \tag{3.8}$$

since the energy of the gluon is close to zero.

(iii) The *double single collinear* region

In the double single collinear region, the photon is collinear to the quark and the gluon is collinear to the antiquark and we have:

$$s_{q\gamma} < s_{\min}, \quad \text{and} \quad s_{qg} > s_{\min} \quad \text{and} \quad s_{\bar{q}g} < s_{\min}. \tag{3.9}$$

For this configuration, z the fractional energy of the photon inside the quark-photon cluster is given by

$$z = \frac{E_\gamma}{E_\gamma + E_q} = y_{\bar{q}\gamma}, \tag{3.10}$$

as in the soft gluon case.

As mentioned in the previous section, these two-particle unresolved contributions correspond already to a photon +1 jet final state configuration. The configurations corresponding to these three two-particle unresolved contributions are shown in Fig. 3.2.c. Unlike in the single unresolved regions, the jet algorithm cannot cluster the particles further. The fraction z defined in the analytic evaluation will also be the "experimental" z.

Moreover, in the single unresolved region we have seen that the different contributions to the cross section may be written as the product of single unresolved factors and a resolved three-particle cross section. Similarly, in these two-particle unresolved regions cited above we shall write the differential cross sections as the product of a "*two-particle unresolved*" factor and the tree level parton cross section σ_0. In order to evaluate analytically these *as yet unknown* two-particle unresolved factors in each particular two particle unresolved region defined above, we need to determine the particular approximations of matrix elements and phase space and to perform the phase space integrations over the "unresolved variables". This is the same procedure as used to evaluate the quark-photon collinear factor $C_{\gamma F}$, for example, where we have integrated the approximated matrix element in this single collinear region over the unresolved variable $s_{q\gamma}$. The determination of the matrix elements, phase space and differential cross section in these three two-particle

unresolved regions of the four-particle phase space will be extensively discussed in Chapter 5.

3.2.3 The fully resolved region

In principle this region is defined by requiring that all constrained invariants are greater than the theoretical parton resolution parameter, $s_{\min}$, i.e. by requiring that,

$$s_{q\gamma} > s_{\min}, \qquad s_{\bar{q}\gamma} > s_{\min}, \qquad s_{qg} > s_{\min}, \qquad s_{\bar{q}g} > s_{\min}. \tag{3.11}$$

However, it turns out that the boundaries of this region are more subtle than that and must be chosen so as to match onto the boundaries of the unresolved regions. Consequently, the resolved region is defined as being the remaining phase space region of the four parton phase space when all unresolved regions are excluded. In this *non singular* region, the four-particle matrix element squared is finite and can be evaluated numerically. The phase space integrals can be performed using standard Monte Carlo techniques and the jet algorithm can be directly applied to select photon +1 jet final states. Furthermore, the fraction z of energy carried by the photon inside the photon jet is determined entirely by the jet algorithm. The numerical evaluation of this contribution will be discussed in Chapter 9. A picture of the different resolved configurations can be found in Fig. 3.2.a.

3.2.4 Summary

In this section we have given the criteria which allow us to split the four-particle final state phase space into *resolved*, *single unresolved* and *double unresolved* regions. These criteria are summarized in Fig. 3.4. As we mentioned in the beginning of this section, since the phase space is five-dimensional, it is difficult to visualise. Furthermore, as the boundaries of different unresolved regions involve triple invariants, we are unable to illustrate how these different regions match onto each other.

3.3 Phase space decomposition of the virtual contributions

As mentioned previously, the virtual contributions to the $\gamma^* \to q\bar{q}\gamma$ process are of two types corresponding to the presence of a theoretically resolved or unresolved photon in the final state. The three particle phase space given by eq.(B.4) divides therefore as follows:

(a) The *resolved photon* region

$$s_{q\gamma} > s_{\min}, \qquad s_{\bar{q}\gamma} > s_{\min}. \tag{3.12}$$

(b) The *unresolved quark-photon collinear* region

$$s_{q\gamma} < s_{\min}, \qquad s_{\bar{q}\gamma} > s_{\min}, \tag{3.13}$$

plus a similar region for the collinear antiquark-photon configuration.

However, the virtual contributions contain divergences independently of what the phase space region is. In Section 1.5.3 we have seen that the complete finite $\mathcal{O}(\alpha_s)$ cross section for the process $\gamma^* \to q\bar{q}$ is obtained by adding the one loop virtual contributions σ_V to the unresolved soft and collinear contributions $\sigma_R^{(U)}$. Similarly here, we expect that the divergences present in the virtual contributions with a *hard photon* will cancel against the divergences present in the single unresolved real contributions where a *hard* photon is emitted together with a soft or collinear gluon in the final state. On the other hand, in the unresolved photon region, the virtual contributions will need to be associated with the two particle unresolved real contributions described earlier. The calculation of these virtual contributions will be detailed in Chapter 6.

3.4 Phase space decomposition of the contributions with the fragmentation function

As we saw in Section 3.1, two classes of processes with a quark fragmenting into a photon give rise to contributions to the photon +1 jet cross section:

(a) The process $\gamma^* \to q\bar{q}$ with a virtual gluon and associated fragmentation of the quark, which always yields a photon and another jet in the final state.

(b) The tree level process $\gamma^* \to q\bar{q}g$ with associated fragmentation of the quark.

Depending on whether the gluon is theoretically seen or not in the final state the real contributions with associated fragmentation can be subdivided further into resolved and unresolved contributions. The corresponding three particle final state phase space needs therefore to be divided accordingly. We distinguish four regions of the three-particle final state phase space:

(i) The *resolved gluon* region

$$s_{qg} > s_{\min}, \qquad s_{\bar{q}g} > s_{\min}. \tag{3.14}$$

(ii) The *single collinear quark-gluon* region

$$s_{qg} < s_{\min}, \qquad s_{\bar{q}g} > s_{\min}. \tag{3.15}$$

(iii) The *single collinear antiquark-gluon* region

$$s_{qg} > s_{\min}, \qquad s_{\bar{q}g} < s_{\min}. \tag{3.16}$$

(iv) The *soft gluon* region

$$s_{qg} < s_{\min}, \qquad s_{\bar{q}g} < s_{\min}. \tag{3.17}$$

Concerning the calculation of the contributions involving $D_{q\to\gamma}$, in Section 1.2.2 we saw that for processes involving a fragmenting parton in the final state the cross section is obtained as the *convolution* of the underlying *bare* partonic cross section with the *bare* fragmentation function. It is commonly denoted by,

$$\sigma_{q\bar{q}g} \otimes D_{q\to\gamma}.$$

The exact meaning of this convolution, together with a detailed presentation of the calculation of all contributions involving the $\mathcal{O}(\alpha)$ quark-to-photon fragmentation counter term will be given in Chapter 7.

In this and in the previous two sections, we have presented the decomposition of the phase space for all the contributions entering in the calculation of the photon +1 jet rate at $\mathcal{O}(\alpha\alpha_s)$. At the end of each section, we have attempted to explain how the individual contributions shall be calculated in the remainder of this thesis. While doing so, we have also mentioned that divergences present in some contributions will cancel against those present in other contributions. Throughout this chapter, we have so far not quantified the divergences in terms of poles in ϵ. This shall be schematically presented in the last section of this chapter. More precisely, in the next section we shall summarize the plan of the calculation of all the contributions to the photon +1 jet rate at $\mathcal{O}(\alpha\alpha_s)$ with particular emphasis on the expected pole structure in the different contributions. We shall outline how this calculation will yield a finite $s_{\min}$-independent result.

3.5 Outline of the calculation

Before starting the detailed calculation of the various contributions to the photon +1 jet rate at $\mathcal{O}(\alpha\alpha_s)$ in the forthcoming chapters, we shall specify in this section which contributions should be grouped together, as they yield the same structure and in particular, as by doing so, some divergences cancel[4]. We will first present the expected pole structure of the different pieces and summarize the expected cancellations of singularities between the different contributions in Figs. 3.5–3.6. Finally, we also note that, although the various contributions depend on the theoretical parameter $s_{\min}$, the physical γ +1 jet cross section will not.

For the contributions "without fragmentation", unless all the particles are theoretically seen in the final state (in which case there are no divergences) the contributions can be

[4]Recall that these divergences manifest themselves in dimensional regularisation where $d = 4 - 2\epsilon$, as poles in ϵ.

written as a product of an "unresolved factor", which contains all the singularities, and a tree level cross section. These "unresolved factors" can be of two types, depending on whether one or two particles in the final state are theoretically not identified, i.e. soft or collinear.

In Sections 1.5.3 and 2.4.2, we have derived the single unresolved factors, C_F, S_F and $C_{F\gamma}\mathrm{d}z$. From eqs. (1.25), (1.35) and (2.21), we see that C_F and $C_{F\gamma}\mathrm{d}z$ contain at most $1/\epsilon$ poles, whereas S_F is proportional to $1/\epsilon^2$. We expect the slightly modified unresolved factors $\tilde{C}_F, \tilde{S}_F$ and $\tilde{C}_{F\gamma}\mathrm{d}z$ to have the same pole structure. Depending whether it is the photon or the gluon which is unresolved, these single unresolved factors will be multiplied by the tree level cross sections, $\sigma_{q\bar{q}g}, \sigma_{q\bar{q}\gamma}$. Furthermore, we saw in Section 1.5.3 that soft and collinear divergences due to the emission of a soft or collinear gluon in the real diagram are cancelled against similar divergences in the virtual graphs. In particular the sum of the real and virtual unresolved factors $R_{q\bar{q}}$ and $V_{q\bar{q}}$ yields the two-particle finite $\mathcal{K}$-factor.

The two-particle unresolved factors, on the other hand, are unknown at this stage of the dissertation, but from the discussion of the pole structure of the single unresolved factors, we note the following. With each pair of collinear particles one can associate a $1/\epsilon$ pole, while one expects a $1/\epsilon^2$ singularity when a particle becomes soft. As a consequence, for the two-particle unresolved factors, we expect the most singular pole generated in the calculation, to be in $1/\epsilon^3$. These leading singularities will be generated in two different contributions, in the *soft/collinear* contribution from the $\gamma^\star \to q\bar{q}g\gamma$ process and in the virtual contributions associated with the one loop process $\gamma^\star \to q\bar{q}\gamma$ process where a collinear photon is emitted in the final state. However, when these two contributions are considered together, the $1/\epsilon^3$ poles must cancel leaving at most $1/\epsilon^2$ poles. We also expect the two real contributions with two pairs of collinear particles to contain terms of $\mathcal{O}(1/\epsilon^2)$ at most. Each of these divergent two-particles unresolved factors multiplies the Born cross section σ_0.

For the contributions from the $\gamma^\star \to q\bar{q}g$ process, with subsequent fragmentation we can also discuss the leading singularity structure. Here, nearly all contributions can be

	$\gamma \parallel q$			
	$g \parallel q$	g soft	$g \parallel \bar{q}$	g hard
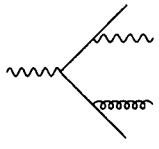	$\sigma_0 \cdot f(\frac{1}{\epsilon^2}, \frac{1}{\epsilon}, c)$	$\sigma_0 \left[\frac{A}{\epsilon^3} + g(\frac{1}{\epsilon^2}, \frac{1}{\epsilon}, c)\right]$	$\sigma_0 \cdot h(\frac{1}{\epsilon^2}, \frac{1}{\epsilon}, c)$	$\sigma_{q\bar{q}g} \cdot \check{C}_{F\gamma}$
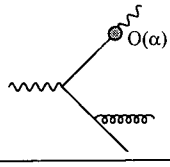	$\sigma_{q\bar{q}g} \otimes D_{q\to\gamma}(x)$	$\sigma_0 S_F \cdot D_{q\to\gamma}(z)$	$\sigma_0 C_F \cdot D_{q\to\gamma}(z)$	$\sigma_{q\bar{q}g} \cdot D_{q\to\gamma}(z)$
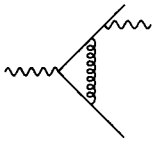	$\sigma_0 \left[-A\frac{1}{\epsilon^3} + k(\frac{1}{\epsilon^2}, \frac{1}{\epsilon}, c)\right]$			
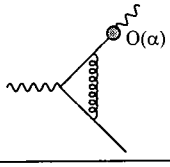	$\sigma_0 \cdot V_{q\bar{q}} \cdot D_{q\to\gamma}(z)$			
Sum	$\sigma_0 \cdot l(\frac{1}{\epsilon^2}, \frac{1}{\epsilon}) + F_a$			$\sigma_{q\bar{q}g} \cdot F_b$
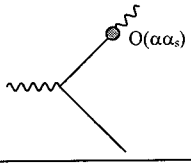	$\sigma_0 \left[D(z, \mu_F) - l(\frac{1}{\epsilon^2}, \frac{1}{\epsilon})\right]$			

Figure 3.5: Expected pole structure of contributions with a collinear photon.

written as the product of a partonic cross section and the fragmentation function. In almost all cases, if the gluon is unresolved in the final state, the partonic cross section $\sigma_{q\bar{q}g}$ factorizes further into the corresponding single unresolved factors C_F and S_F defined

	γ hard	
	g unres.	g hard
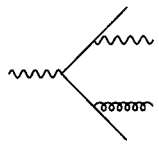	$\sigma_{q\bar{q}\gamma} \cdot R_{q\bar{q}(\gamma)}$	$\sigma_{q\bar{q}\gamma g}$
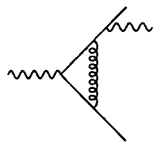	$\sigma_{q\bar{q}\gamma} \left[V_{q\bar{q}(\gamma)} + F_c\right]$	
Sum	$\sigma_{q\bar{q}\gamma} \left[K_{q\bar{q}(\gamma)} + F_c\right]$	$\sigma_{q\bar{q}\gamma g}$

Figure 3.6: Expected pole structure of all contributions with a resolved photon.

before and the two-particle tree level cross section σ_0.

However, when the gluon is collinear to the fragmenting quark, the cross section is a *convolution* of the partonic cross section and the fragmentation function as we shall see in Chapter 7. The structure of all the contributions involving the fragmentation function is summarized in Fig. 3.5.

In addition to the unresolved gluon singularities, the fragmentation function itself also contains divergences. In fact, in Section 2.4.2 we saw that the collinear quark-photon singularity contained in $C_{\gamma F}$ is factorized into the *bare* $\mathcal{O}(\alpha)$ quark-to-photon fragmentation function. For our analysis of the expected pole structure in each contribution, we can therefore also consider a single factor of $1/\epsilon$ to be associated with the *bare* $\mathcal{O}(\alpha)$ counter term present in the fragmentation function. Consequently, when the gluon in the process $\gamma^* \to q\bar{q}g$ followed by fragmentation is soft, we expect a singularity of order

$1/\epsilon^2 \times 1/\epsilon = 1/\epsilon^3$. Similarly, the one-loop $\gamma^* \to q\bar{q}$ process followed by fragmentation also generates a $1/\epsilon^3$ singularity. Because the soft gluon responsible for these poles does not probe the fragmentation region, these singularities must precisely cancel. On the other hand, when the gluon is collinear to the quark or to the antiquark we expect poles of order $1/\epsilon \times 1/\epsilon = 1/\epsilon^2$ to be generated. However, as the quark-gluon singularity does probe the fragmentation region these $1/\epsilon^2$ singularities are not completely compensated by the one-loop graphs. Any remaining singularities must be cancelled by the $\mathcal{O}(\alpha\alpha_s)$ counter term in the fragmentation function. This counter term, although it is so far unknown, will have the necessary pole structure to absorb all the left-over singularities and to ensure that the $\mathcal{O}(\alpha\alpha_s)$ $\gamma^* \to \gamma + 1$ jet cross section is finite.

Finally, the two-particle unresolved factors, along with the single unresolved factors and the resolved tree level cross sections $\sigma_{q\bar{q}g}$, $\sigma_{q\bar{q}\gamma}$ and $\sigma_{q\bar{q}\gamma g}$ will all depend on the theoretical parameter $s_{\min}$, or more precisely on $\ln(y_{\min})$. However, since the fragmentation function is process independent at any order, it must be $s_{\min}$ independent. The left-over singularities from the sum of all unresolved contributions should therefore also be independent of $s_{\min}$. We will explicitly show that this is the case in Chapter 8.

Furthermore, when the finite results from the analytic calculation, denoted by F_a, F_b, F_c in Figs. 3.5–3.6, are combined in the numerical program with the result for the resolved contributions, the final result for the $\gamma^* \to \gamma + 1$ jet cross section at $\mathcal{O}(\alpha\alpha_s)$ becomes $s_{\min}$-independent. The cancellation of the $s_{\min}$ dependence shall be explicitly proven when describing the numerical part of the calculation in Chapter 9.

3.6 Summary and Outlook

To summarize, in this chapter, we have outlined the calculation of the photon + 1 jet rate at $\mathcal{O}(\alpha\alpha_s)$. At this order, five different subprocesses are relevant. These were presented in Section 3.1. Each subprocess can further be structured into contributions from different phase space regions. A detailed phase space decomposition of all contributions is given in Sections 3.2–3.4. Finally, we have sketched the expected pole structure of all contri-

butions in Section 3.5. In the following chapters, we shall now calculate these individual contributions.

The resolved and single unresolved contributions from the tree level four parton process $\gamma^* \to q\bar{q}\gamma g$ will be presented in Chapter 4, the double unresolved contributions from this process follow in Chapter 5. Chapter 6 contains the calculation of the virtual gluon corrections in the process $\gamma^* \to q\bar{q}\gamma$. Real and virtual gluon corrections to $\gamma^* \to q\bar{q}$ with subsequent quark-to-photon fragmentation will be derived in Chapter 7. Finally, Chapter 8 summarizes the results of the analytic part of the calculation of all divergent contributions to the photon + 1 jet rate at $\mathcal{O}(\alpha\alpha_s)$. After cancellation of all divergences, this process can be evaluated numerically. The numerical calculation will be outlined in Chapter 9, while a comparison between these results and the experimental data on the photon +1 jet rate will be presented in Chapter 10.

Chapter 4

The resolved and single unresolved real contributions

In the next two chapters we will present the calculation of the contributions to the γ +1 jet rate at $\mathcal{O}(\alpha\alpha_s)$ relevant to the process $\gamma^* \to q\bar{q}\gamma$ with real gluon bremsstrahlung. The Feynman diagrams relevant to the amplitude for $\gamma^* \to q\bar{q}\gamma g$ are shown in Fig. 4.1. This process contributes to the γ +1 jet differential cross section if the final state configuration is such that only the photon jet and a single associated jet are observed. The possible topologies were illustrated in Fig. 3.2.

In the previous chapter, we have discussed how the real contributions can be theoretically resolved or unresolved depending whether the final state particles are theoretically "seen" or "unseen". A final state particle may be theoretically "unseen" if it is collinear or soft. We claimed that the real contributions associated to $\gamma^* \to q\bar{q}\gamma g$ can be separated into three categories; the theoretically resolved, single unresolved and double unresolved contributions. We will present the calculation of the double unresolved contributions in Chapter 5. The theoretically resolved and single unresolved contributions will be discussed in this chapter which is organized as follows.

In Section 4.1, we give the expressions of matrix element squared and phase space in d dimensions which are necessary for the calculation of the resolved and unresolved

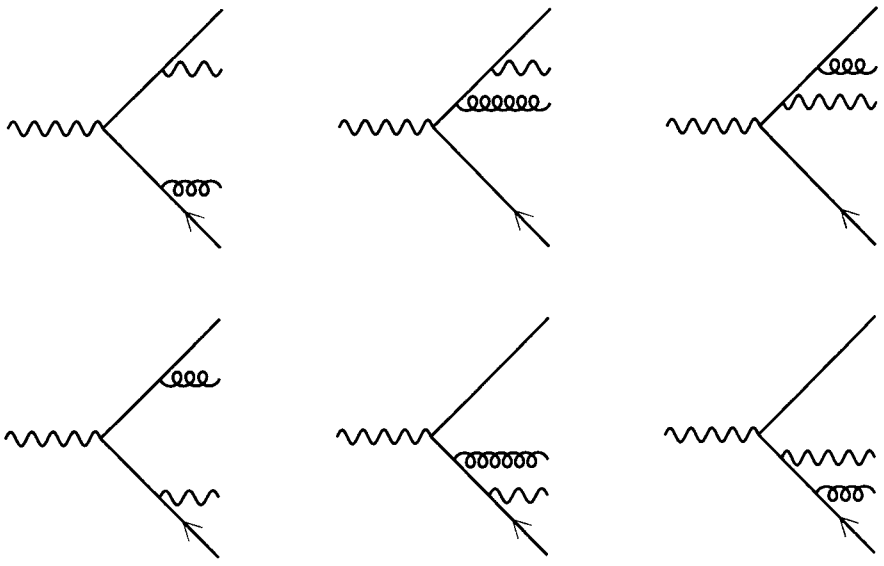

Figure 4.1: Tree level $\gamma^* \to q\bar{q}\gamma g$ amplitudes

contributions.

The different expressions for the various single unresolved matrix element squared and phase spaces will be presented in Section 4.2. In the evaluation of the associated differential cross sections, we note that "*more than two*" particles are theoretically seen (i.e. clearly distinguishable) in the final state. A γ +1 jet event can then only occur if some final state particles are clustered together according to a jet algorithm. Hence the evaluation of the phase space integrals will ultimately be performed numerically.

In Section 4.2, we shall see however that when one particle is unresolved, the fully differential four-particle differential cross section may be written as the product of a single unresolved factor which contain the divergences and a finite three particle differential cross section. Only the three particle diffential cross section will be evaluated numerically.

4.1 Resolved contributions

We introduce the following labels for the four final state particles,

$$q \equiv 1, \quad \bar{q} \equiv 2, \quad \gamma \equiv 3, \quad g \equiv 4,$$

such that the invariants containing $p_\gamma \equiv p_3$ for example become

$$s_{q\gamma} \equiv s_{13}, \quad s_{\bar{q}\gamma} \equiv s_{23} \quad \text{and} \quad s_{\gamma g} \equiv s_{34}.$$

Following this notation the matrix element squared for the scattering of a quark-antiquark pair with a photon and a gluon $|\mathcal{M}_{q\bar{q}\gamma g}|^2 \equiv |\mathcal{M}_{1234}|^2$ may be written in $d = 4-2\epsilon$ dimensions as [1],

$$\begin{aligned}
|\mathcal{M}_{1234}|^2 \;=\; & \epsilon^3 \frac{1}{y_{13}y_{14}y_{23}y_{24}} \Big(16y_{12}^3 + 16y_{12}^2y_{13} + 16y_{12}^2y_{14} + 16y_{12}^2y_{23} + 16y_{12}^2y_{24} - 32y_{12}^2 + 16y_{12}y_{13}y_{14} \\
& + 32y_{12}y_{13}y_{24} - 16y_{12}y_{13} + 32y_{12}y_{14}y_{23} - 16y_{12}y_{14} + 16y_{12}y_{23}y_{24} - 16y_{12}y_{23} - 16y_{12}y_{24} \\
& + 16y_{12} + 16y_{13}^2y_{24} - 16y_{13}y_{14}y_{23} - 16y_{13}y_{14}y_{24} - 16y_{13}y_{23}y_{24} + 16y_{13}y_{24}^2 - 32y_{13}y_{24} \\
& + 16y_{14}^2y_{23} + 16y_{14}y_{23}^2 - 16y_{14}y_{23}y_{24} - 32y_{14}y_{23} \Big) \\
& + \epsilon^3 \frac{1}{y_{13}y_{14}y_{134}^2} \Big(32y_{12}y_{13}y_{14} + 32y_{13}y_{14}y_{23} + 32y_{13}y_{14}y_{24} \Big) \\
& + \epsilon^3 \frac{1}{y_{13}y_{23}y_{134}y_{234}} \Big(-16y_{12}^3 - 32y_{12}^2y_{13} - 16y_{12}^2y_{14} - 32y_{12}^2y_{23} - 16y_{12}^2y_{24} + 32y_{12}^2 - 16y_{12}y_{13}^2 \\
& - 48y_{12}y_{13}y_{24} + 32y_{12}y_{13} - 48y_{12}y_{14}y_{23} + 16y_{12}y_{14} - 16y_{12}y_{23}^2 + 32y_{12}y_{23} + 16y_{12}y_{24} - 16y_{12} \\
& - 16y_{13}^2y_{23} - 16y_{13}^2 + 16y_{13}y_{14}y_{24} - 16y_{13}y_{14} - 16y_{13}y_{23}^2 + 64y_{13}y_{23} - 32y_{13}y_{24}^2 + 48y_{13}y_{24} \\
& - 32y_{14}^2y_{23} + 16y_{14}y_{23}y_{24} + 48y_{14}y_{23} - 16y_{23}^2 - 16y_{23}y_{24} \Big) \\
& + \epsilon^3 \frac{1}{y_{13}y_{24}y_{134}y_{234}} \Big(-32y_{12}^3 - 48y_{12}^2y_{14} - 48y_{12}^2y_{23} + 64y_{12}^2 - 16y_{12}y_{14}^2 - 64y_{12}y_{14}y_{23} \\
& + 48y_{12}y_{14} - 16y_{12}y_{23}^2 + 48y_{12}y_{23} - 32y_{12} - 16y_{14}^2y_{23} - 16y_{14}y_{23}^2 + 32y_{14}y_{23} \Big) \\
& + \epsilon^3 \frac{1}{y_{13}y_{134}^2} \Big(16y_{12}y_{14} + 16y_{14}y_{23} + 16y_{14}y_{24} \Big) \\
& + \epsilon^3 \frac{1}{y_{14}y_{23}y_{134}y_{234}} \Big(-32y_{12}^3 - 48y_{12}^2y_{13} - 48y_{12}^2y_{24} + 64y_{12}^2 - 16y_{12}y_{13}^2 - 64y_{12}y_{13}y_{24} \\
& + 48y_{12}y_{13} - 16y_{12}y_{24}^2 + 48y_{12}y_{24} - 32y_{12} - 16y_{13}^2y_{24} - 16y_{13}y_{24}^2 + 32y_{13}y_{24} \Big)
\end{aligned}$$

[1] This matrix element squared has be evaluated using the algebraic program FORM, [63]

$$+\epsilon^3\frac{1}{y_{14}y_{24}y_{134}y_{234}}\Big(-16y_{12}^3-16y_{12}^2y_{13}-32y_{12}^2y_{14}-16y_{12}^2y_{23}-32y_{12}^2y_{24}+32y_{12}^2$$
$$-48y_{12}y_{13}y_{24}+16y_{12}y_{13}-16y_{12}y_{14}^2-48y_{12}y_{14}y_{23}-64y_{12}y_{14}y_{24}+32y_{12}y_{14}+16y_{12}y_{23}$$
$$-16y_{12}y_{24}^2+32y_{12}y_{24}-16y_{12}-32y_{13}^2y_{24}+16y_{13}y_{14}y_{23}-16y_{13}y_{14}y_{24}-16y_{13}y_{14}$$
$$+16y_{13}y_{23}y_{24}+48y_{13}y_{24}-32y_{14}^2y_{24}-16y_{14}^2-32y_{14}y_{23}^2-16y_{14}y_{23}y_{24}+48y_{14}y_{23}$$
$$-32y_{14}y_{24}^2+64y_{14}y_{24}-16y_{23}y_{24}-16y_{24}^2\Big)$$
$$+\epsilon^3\frac{1}{y_{14}y_{134}^2}\Big(16y_{12}y_{13}+16y_{13}y_{23}+16y_{13}y_{24}\Big)$$
$$+\epsilon^3\frac{1}{y_{23}y_{24}y_{234}^2}\Big(32y_{12}y_{23}y_{24}+32y_{13}y_{23}y_{24}+32y_{14}y_{23}y_{24}\Big)$$
$$+\epsilon^3\frac{1}{y_{23}y_{234}^2}\Big(16y_{12}y_{24}+16y_{13}y_{24}+16y_{14}y_{24}\Big)$$
$$+\epsilon^3\frac{1}{y_{24}y_{234}^2}\Big(16y_{12}y_{23}+16y_{13}y_{23}+16y_{14}y_{23}\Big)$$
$$+\epsilon^2\frac{1}{y_{13}y_{14}y_{23}y_{24}}\Big(48y_{12}^3+48y_{12}^2y_{13}+48y_{12}^2y_{14}+48y_{12}^2y_{23}+48y_{12}^2y_{24}-96y_{12}^2+16y_{12}y_{13}^2$$
$$+64y_{12}y_{13}y_{23}+96y_{12}y_{13}y_{24}-48y_{12}y_{13}+16y_{12}y_{14}^2+96y_{12}y_{14}y_{23}+64y_{12}y_{14}y_{24}$$
$$-48y_{12}y_{14}+16y_{12}y_{23}^2-48y_{12}y_{23}+16y_{12}y_{24}^2-48y_{12}y_{24}+48y_{12}-16y_{13}^2y_{24}+16y_{13}y_{14}y_{23}$$
$$+16y_{13}y_{14}y_{24}+16y_{13}y_{23}y_{24}-16y_{13}y_{24}^2-16y_{14}^2y_{23}-16y_{14}y_{23}^2+16y_{14}y_{23}y_{24}\Big)$$
$$+\epsilon^2\frac{1}{y_{13}y_{14}y_{134}^2}\Big(-64y_{12}y_{13}y_{14}-64y_{13}y_{14}y_{23}-64y_{13}y_{14}y_{24}\Big)$$
$$+\epsilon^2\frac{1}{y_{13}y_{23}y_{134}y_{234}}\Big(-16y_{12}^3-80y_{12}^2y_{13}-16y_{12}^2y_{14}-80y_{12}^2y_{23}-16y_{12}^2y_{24}+32y_{12}^2$$
$$+32y_{12}y_{13}^2+16y_{12}y_{13}y_{14}-48y_{12}y_{13}y_{24}+80y_{12}y_{13}+16y_{12}y_{14}^2-48y_{12}y_{14}y_{23}+16y_{12}y_{14}$$
$$+32y_{12}y_{23}^2+16y_{12}y_{23}y_{24}+80y_{12}y_{23}+16y_{12}y_{24}^2+16y_{12}y_{24}-16y_{12}+32y_{13}^2y_{23}+32y_{13}^2$$
$$+48y_{13}y_{14}y_{23}-16y_{13}y_{14}y_{24}+32y_{13}y_{14}+32y_{13}y_{23}^2+48y_{13}y_{23}y_{24}-64y_{13}y_{23}+64y_{13}y_{24}^2$$
$$-48y_{13}y_{24}+64y_{14}^2y_{23}-16y_{14}y_{23}y_{24}-48y_{14}y_{23}+32y_{23}^2+32y_{23}y_{24}\Big)$$
$$+\epsilon^2\frac{1}{y_{13}y_{24}y_{134}y_{234}}\Big(-48y_{12}^3-32y_{12}^2y_{14}-32y_{12}^2y_{23}+96y_{12}^2+16y_{12}y_{14}^2-16y_{12}y_{14}y_{23}$$
$$+32y_{12}y_{14}+16y_{12}y_{23}^2+32y_{12}y_{23}-48y_{12}+16y_{14}^2y_{23}+16y_{14}^2+16y_{14}y_{23}^2-48y_{14}y_{23}+16y_{23}^2\Big)$$
$$+\epsilon^2\frac{1}{y_{13}y_{134}^2}\Big(-48y_{12}y_{14}-48y_{14}y_{23}-48y_{14}y_{24}\Big)$$
$$+\epsilon^2\frac{1}{y_{14}y_{23}y_{134}y_{234}}\Big(-48y_{12}^3-32y_{12}^2y_{13}-32y_{12}^2y_{24}+96y_{12}^2+16y_{12}y_{13}^2-16y_{12}y_{13}y_{24}$$

$$+32y_{12}y_{13}+16y_{12}y_{24}^2+32y_{12}y_{24}-48y_{12}+16y_{13}^2y_{24}+16y_{13}^2+16y_{13}y_{24}^2-48y_{13}y_{24}+16y_{24}^2\Big)$$

$$+\epsilon^2\frac{1}{y_{14}y_{24}y_{134}y_{234}}\Big(-16y_{12}^3-16y_{12}^2y_{13}-80y_{12}^2y_{14}-16y_{12}^2y_{23}-80y_{12}^2y_{24}+32y_{12}^2+16y_{12}y_{13}^2$$
$$+16y_{12}y_{13}y_{14}-48y_{12}y_{13}y_{24}+16y_{12}y_{13}+32y_{12}y_{14}^2-48y_{12}y_{14}y_{23}-160y_{12}y_{14}y_{24}+80y_{12}y_{14}$$
$$+16y_{12}y_{23}^2+16y_{12}y_{23}y_{24}+16y_{12}y_{23}+32y_{12}y_{24}^2+80y_{12}y_{24}-16y_{12}+64y_{13}^2y_{24}-16y_{13}y_{14}y_{23}$$
$$+64y_{13}y_{14}y_{24}+32y_{13}y_{14}-16y_{13}y_{23}y_{24}-48y_{13}y_{24}+48y_{14}^2y_{24}+32y_{14}^2+64y_{14}y_{23}^2$$
$$+64y_{14}y_{23}y_{24}-48y_{14}y_{23}+48y_{14}y_{24}^2+32y_{14}y_{24}+32y_{23}y_{24}+32y_{24}^2\Big)$$

$$+\epsilon^2\frac{1}{y_{14}y_{134}^2}\Big(-48y_{12}y_{13}-48y_{13}y_{23}-48y_{13}y_{24}\Big)$$

$$+\epsilon^2\frac{1}{y_{23}y_{24}y_{234}^2}\Big(-64y_{12}y_{23}y_{24}-64y_{13}y_{23}y_{24}-64y_{14}y_{23}y_{24}\Big)$$

$$+\epsilon^2\frac{1}{y_{23}y_{234}^2}\Big(-48y_{12}y_{24}-48y_{13}y_{24}-48y_{14}y_{24}\Big)$$

$$+\epsilon^2\frac{1}{y_{24}y_{234}^2}\Big(-48y_{12}y_{23}-48y_{13}y_{23}-48y_{14}y_{23}\Big)$$

$$+\epsilon\frac{1}{y_{13}y_{14}y_{23}y_{24}}\Big(-32y_{12}^3-32y_{12}^2y_{13}-32y_{12}^2y_{14}-32y_{12}^2y_{23}-32y_{12}^2y_{24}+32y_{12}^2-32y_{12}y_{13}^2$$
$$-48y_{12}y_{13}y_{14}-96y_{12}y_{13}y_{23}-16y_{12}y_{13}y_{24}+32y_{12}y_{13}-32y_{12}y_{14}^2-16y_{12}y_{14}y_{23}$$
$$-96y_{12}y_{14}y_{24}+32y_{12}y_{14}-32y_{12}y_{23}^2-48y_{12}y_{23}y_{24}+32y_{12}y_{23}-32y_{12}y_{24}^2+32y_{12}y_{24}$$
$$-32y_{12}-16y_{13}^2y_{24}+16y_{13}y_{14}y_{23}+16y_{13}y_{14}y_{24}+16y_{13}y_{23}y_{24}-16y_{13}y_{24}^2-16y_{13}y_{24}$$
$$-16y_{14}^2y_{23}-16y_{14}y_{23}^2+16y_{14}y_{23}y_{24}-16y_{14}y_{23}\Big)$$

$$+\epsilon\frac{1}{y_{13}y_{14}y_{134}^2}\Big(32y_{12}y_{13}y_{14}+32y_{13}y_{14}y_{23}+32y_{13}y_{14}y_{24}\Big)$$

$$+\epsilon\frac{1}{y_{13}y_{23}y_{134}y_{234}}\Big(16y_{12}^2y_{13}+16y_{12}^2y_{23}-32y_{12}^2-16y_{12}y_{13}^2-32y_{12}y_{13}y_{14}-48y_{12}y_{13}$$
$$-32y_{12}y_{14}^2+32y_{12}y_{14}y_{24}-16y_{12}y_{23}^2-32y_{12}y_{23}y_{24}-48y_{12}y_{23}-32y_{12}y_{24}^2-32y_{13}^2y_{23}$$
$$-16y_{13}^2-32y_{13}y_{14}y_{23}-16y_{13}y_{14}y_{24}-16y_{13}y_{14}-32y_{13}y_{23}^2-32y_{13}y_{23}y_{24}-32y_{13}y_{24}^2$$
$$+64y_{13}y_{24}-32y_{14}^2y_{23}-16y_{14}y_{23}y_{24}+64y_{14}y_{23}-16y_{23}^2-16y_{23}y_{24}\Big)$$

$$+\epsilon\frac{1}{y_{13}y_{24}y_{134}y_{234}}\Big(32y_{12}^3+48y_{12}^2y_{14}+48y_{12}^2y_{23}-96y_{12}^2+16y_{12}y_{14}^2+64y_{12}y_{14}y_{23}$$
$$-80y_{12}y_{14}+16y_{12}y_{23}^2-80y_{12}y_{23}+32y_{12}+16y_{14}^2y_{23}-32y_{14}^2+16y_{14}y_{23}^2-32y_{14}y_{23}-32y_{23}^2\Big)$$

$$+\epsilon\frac{1}{y_{13}y_{134}^2}\Big(48y_{12}y_{14}+48y_{14}y_{23}+48y_{14}y_{24}\Big)$$

$$+\epsilon\frac{1}{y_{14}y_{23}y_{134}y_{234}}\Big(32y_{12}^3+48y_{12}^2y_{13}+48y_{12}^2y_{24}-96y_{12}^2+16y_{12}y_{13}^2+64y_{12}y_{13}y_{24}$$
$$-80y_{12}y_{13}+16y_{12}y_{24}^2-80y_{12}y_{24}+32y_{12}+16y_{13}^2y_{24}-32y_{13}^2+16y_{13}y_{24}^2-32y_{13}y_{24}-32y_{24}^2\Big)$$
$$+\epsilon\frac{1}{y_{14}y_{24}y_{134}y_{234}}\Big(16y_{12}^2y_{14}+16y_{12}^2y_{24}-32y_{12}^2-32y_{12}y_{13}^2-32y_{12}y_{13}y_{14}+32y_{12}y_{13}y_{23}$$
$$-16y_{12}y_{14}^2-128y_{12}y_{14}y_{24}-48y_{12}y_{14}-32y_{12}y_{23}^2-32y_{12}y_{23}y_{24}-16y_{12}y_{24}^2-48y_{12}y_{24}$$
$$-32y_{13}^2y_{24}-16y_{13}y_{14}y_{23}-64y_{13}y_{14}y_{24}-16y_{13}y_{14}-16y_{13}y_{23}y_{24}+64y_{13}y_{24}-64y_{14}^2y_{24}$$
$$-16y_{14}^2-32y_{14}y_{23}^2-64y_{14}y_{23}y_{24}+64y_{14}y_{23}-64y_{14}y_{24}^2+128y_{14}y_{24}-16y_{23}y_{24}-16y_{24}^2\Big)$$
$$+\epsilon\frac{1}{y_{14}y_{134}}\Big(48y_{12}y_{13}+48y_{13}y_{23}+48y_{13}y_{24}\Big)$$
$$+\epsilon\frac{1}{y_{23}y_{24}y_{234}^2}\Big(32y_{12}y_{23}y_{24}+32y_{13}y_{23}y_{24}+32y_{14}y_{23}y_{24}\Big)$$
$$+\epsilon\frac{1}{y_{23}y_{234}^2}\Big(48y_{12}y_{24}+48y_{13}y_{24}+48y_{14}y_{24}\Big)$$
$$+\epsilon\frac{1}{y_{24}y_{234}^2}\Big(48y_{12}y_{23}+48y_{13}y_{23}+48y_{14}y_{23}\Big)$$
$$+\frac{1}{y_{13}y_{14}y_{23}y_{24}}\Big(32y_{12}^3+32y_{12}^2y_{13}+32y_{12}^2y_{14}+32y_{12}^2y_{23}+32y_{12}^2y_{24}+16y_{12}y_{13}^2+32y_{12}y_{13}y_{14}$$
$$+32y_{12}y_{13}y_{23}+16y_{12}y_{13}y_{24}+16y_{12}y_{14}^2+16y_{12}y_{14}y_{23}+32y_{12}y_{14}y_{24}+16y_{12}y_{23}^2+32y_{12}y_{23}y_{24}$$
$$+16y_{12}y_{24}^2+16y_{13}^2y_{24}-16y_{13}y_{14}y_{23}-16y_{13}y_{14}y_{24}-16y_{13}y_{23}y_{24}+16y_{13}y_{24}^2+16y_{13}y_{24}$$
$$+16y_{14}^2y_{23}+16y_{14}y_{23}^2-16y_{14}y_{23}y_{24}+16y_{14}y_{23}\Big)$$
$$+\frac{1}{y_{13}y_{23}y_{134}y_{234}}\Big(-32y_{12}^3-32y_{12}^2y_{13}-32y_{12}^2y_{14}-32y_{12}^2y_{23}-32y_{12}^2y_{24}+64y_{12}^2+16y_{12}y_{13}y_{14}$$
$$-64y_{12}y_{13}y_{23}-32y_{12}y_{13}y_{24}+16y_{12}y_{14}^2-32y_{12}y_{14}y_{23}-32y_{12}y_{14}y_{24}+16y_{12}y_{23}y_{24}+16y_{12}y_{24}^2$$
$$+16y_{13}^2y_{23}+16y_{13}y_{14}y_{23}+16y_{13}y_{14}y_{24}+16y_{13}y_{23}^2+16y_{13}y_{23}y_{24}-32y_{13}y_{24}+16y_{14}y_{23}y_{24}$$
$$-32y_{14}y_{23}\Big)$$
$$+\frac{1}{y_{13}y_{24}y_{134}y_{234}}\Big(-16y_{12}^3-32y_{12}^2y_{14}-32y_{12}^2y_{23}+32y_{12}^2-16y_{12}y_{14}^2-48y_{12}y_{14}y_{23}$$
$$+32y_{12}y_{14}-16y_{12}y_{23}^2+32y_{12}y_{23}+16y_{12}-16y_{14}^2y_{23}+16y_{14}^2-16y_{14}y_{23}^2+16y_{14}y_{23}+16y_{23}^2\Big)$$
$$+\frac{1}{y_{13}y_{134}^2}\Big(-16y_{12}y_{14}-16y_{14}y_{23}-16y_{14}y_{24}\Big)$$
$$+\frac{1}{y_{14}y_{23}y_{134}y_{234}}\Big(-16y_{12}^3-32y_{12}^2y_{13}-32y_{12}^2y_{24}+32y_{12}^2-16y_{12}y_{13}^2-48y_{12}y_{13}y_{24}$$
$$+32y_{12}y_{13}-16y_{12}y_{24}^2+32y_{12}y_{24}+16y_{12}-16y_{13}^2y_{24}+16y_{13}^2-16y_{13}y_{24}^2+16y_{13}y_{24}+16y_{24}^2\Big)$$

$$
\begin{aligned}
&+\frac{1}{y_{14}y_{24}y_{134}y_{234}}\Big(-32y_{12}^3-32y_{12}^2y_{13}-32y_{12}^2y_{14}-32y_{12}^2y_{23}-32y_{12}^2y_{24}+64y_{12}^2\\
&+16y_{12}y_{13}^2+16y_{12}y_{13}y_{14}-32y_{12}y_{13}y_{23}-32y_{12}y_{13}y_{24}-32y_{12}y_{14}y_{23}+32y_{12}y_{14}y_{24}\\
&+16y_{12}y_{23}^2+16y_{12}y_{23}y_{24}+16y_{13}y_{14}y_{23}+16y_{13}y_{14}y_{24}+16y_{13}y_{23}y_{24}-32y_{13}y_{24}\\
&+16y_{14}^2y_{24}+16y_{14}y_{23}y_{24}-32y_{14}y_{23}+16y_{14}y_{24}^2-32y_{14}y_{24}\Big)\\
&+\frac{1}{y_{14}y_{134}^2}\Big(-16y_{12}y_{13}-16y_{13}y_{23}-16y_{13}y_{24}\Big)\\
&+\frac{1}{y_{23}y_{234}^2}\Big(-16y_{12}y_{24}-16y_{13}y_{24}-16y_{14}y_{24}\Big)\\
&+\frac{1}{y_{24}y_{234}^2}\Big(-16y_{12}y_{23}-16y_{13}y_{23}-16y_{14}y_{23}\Big),
\end{aligned}
\tag{4.1}
$$

where we have kept terms up to $\mathcal{O}(\epsilon^3)$ and where the finite term can be found at the end of eq.(4.1). Although this expression is rather long, for the most part, we shall use it to obtain approximations in the single and double unresolved limits.

The d-dimensional phase space derived in (B.6) is given by,

$$
\begin{aligned}
\mathrm{d}R_4^{(d)}(M,p_1,p_2,p_3,p_4) &= \frac{(-\Delta_4)^{-1/2}}{M^2\,2^9}\int \mathrm{d}\Omega_{d-1}\,\mathrm{d}\Omega_{d-2}\,\mathrm{d}\Omega_{d-3}\,\mathrm{d}s_{12}\,\mathrm{d}s_{13}\mathrm{d}s_{14}\mathrm{d}s_{23}\mathrm{d}s_{24}\mathrm{d}s_{34}\\
&\quad\times\left(\frac{-\Delta_4}{M^2}\right)^{\frac{d-4}{2}}\delta(s_{12}+s_{13}+s_{14}+s_{23}+s_{24}+s_{34}-M^2),
\end{aligned}
\tag{4.2}
$$

with,

$$
\begin{aligned}
\Delta_4 &= \frac{1}{16}\Big[{s_{12}}^2{s_{34}}^2+{s_{13}}^2{s_{24}}^2+{s_{14}}^2{s_{23}}^2\\
&\quad-2\Big(s_{12}s_{23}s_{34}s_{14}+s_{13}s_{23}s_{24}s_{14}+s_{12}s_{24}s_{34}s_{13}\Big)\Big].
\end{aligned}
\tag{4.3}
$$

In the resolved phase space region which is the region of the four-particle phase space left over when all unresolved regions are excluded, the matrix element squared is finite. Thus for the evaluation of the resolved contributions, we only need to consider the 4-dimensional analogue of the matrix element squared given above by eq.(4.1) and integrate it over the 4-dimensional phase space restricted to this resolved region. The four dimensional analogues for the four particle matrix element squared and phase space can be obtained by setting $\epsilon=0$ in both eq.(4.1) and eq.(4.2). Including the overall coupling factors, we have,

$$
\mathrm{d}\sigma_4^{(R)}=\left(\frac{N^2-1}{2N}\right)\left(\frac{\alpha_s}{2\pi}\right)\left(\frac{\alpha e_q^2}{2\pi}\right)4(2\pi)^4\int|\mathcal{M}_{1234}|^2\mathrm{d}P_4^4(M,p_1,p_2,p_3,p_4),
\tag{4.4}
$$

where the 4-dimensional phase space given by,

$$\mathrm{d}P_4^4(M, p_1, p_2, p_3, p_4) = (2\pi)^{-8}\mathrm{d}R_4^4(M, p_1, p_2, p_3, p_4), \tag{4.5}$$

is understood to be restricted to non-singular regions.

4.2 Single unresolved contributions

We distinguish two classes of single unresolved real contributions depending on whether the photon or the gluon is unresolved. If the photon is unresolved, it is collinear to the quark[2]. If the gluon is unresolved it can be collinear to the quark, collinear to the antiquark or it can be soft. The possible final state configurations of simple unresolved contributions yielding a γ +1 jet event were displayed in Fig.3.2.(b).

In Sections 1.5.3 and 2.4 we have discussed the simple collinear $q - \gamma$ behaviour of the cross section $\sigma_{q\bar{q}\gamma}$ and the simple $q - g$ collinear and soft gluon behaviour of $\sigma_{q\bar{q}g}$. In both cases we found that the three-particle differential cross sections could be written as the product of the two particle cross section for the scattering of a quark-antiquark pair, σ_0 and one universal *one-particle unresolved* factor. These were $C_{F\gamma}\mathrm{d}z$, in the $q - \gamma$ limit, C_F in the $q - g$ limit and S_F in the soft gluon limit. It can be shown [25] that this behaviour of the three-particle differential cross section can be extended to cross sections with more than three particles in the final state. In the various single unresolved regions of the four-particle phase space we therefore expect to be able to write the differential cross section for the scattering of a quark-antiquark pair with a photon and a gluon as the product of *one particle unresolved* factors and a three-particle cross section. However as the cuts defining the single unresolved regions in the 4-parton phase space differ from those defining the single unresolved regions in the 3-parton phase space, the one-parton unresolved factors will be slightly modified.

[2]Recall that we only consider contributions where the photon is collinear to the quark and obtain the contribution where the photon is collinear with the antiquark by multiplying it by two.

Ultimately the γ +1 jet rate will be evaluated numerically using the hybrid subtraction method. Within this method, in a given singular region only the matrix element squared is approximated. Consequently we will choose the boundaries of the single unresolved regions according to the following criteria.

(a) Within those boundaries the known single unresolved approximations of the matrix element squared are accurate approximations of the "full" 4-particle matrix element squared.

(b) No singular region is omitted or double counted.

The resulting contributions to the γ +1 jet rate in each single unresolved region of the four-particle phase space are given below.

4.2.1 The unresolved gluon contributions

The collinear quark-gluon contribution

In the region where the quark and the gluon are collinear we have[3]:

$$s_{qg} \equiv s_{14} < s_{\min}\frac{s_{124}}{M^2}, \qquad s_{\bar{q}g} \equiv s_{24} > s_{\min}\frac{s_{124}}{M^2}, \qquad s_{q\gamma g} \equiv s_{134} > s_{\min}, \qquad s_{\bar{q}\gamma} \equiv s_{23} > s_{\min}, \tag{4.6}$$

or in terms of the scaled invariants y_{ij},

$$y_{qg} \equiv y_{14} < y_{\min}y_{124}, \qquad y_{\bar{q}g} \equiv y_{24} > y_{\min}y_{124}, \qquad y_{q\gamma g} \equiv y_{134} > y_{\min}, \qquad y_{\bar{q}\gamma} \equiv y_{23} > y_{\min}. \tag{4.7}$$

The quark and the gluon cluster to form a new parton Q such that,

$$p_1 + p_4 = p_Q,$$

where particles 4 and 1 carry respectively a fraction y and $1-y$ of the parent parton momentum p_Q,

$$p_1 = (1-y)\,p_Q, \qquad p_4 = y\,p_Q. \tag{4.8}$$

[3]As usual, M is the mass of the final state.

In this limit, the invariants s_{12}, s_{24} and s_{124} become,

$$s_{12} = (1-y)\, s_{Q2}, \qquad s_{24} = y\, s_{Q2}, \qquad s_{124} = s_{Q2} \tag{4.9}$$

while the invariants containing $p_\gamma \equiv p_3$ become,

$$s_{13} = (1-y)\, s_{Q3}, \qquad s_{34} = y\, s_{Q3}.$$

The matrix elements and phase space exhibit an overall factorization in this collinear limit. We have,

$$|\mathcal{M}_{1234}|^2 \to P_{14\to Q}(y, s_{24})|\mathcal{M}_{Q23}|^2, \tag{4.10}$$

with, $|\mathcal{M}_{Q23}|^2$ the three-particle matrix element squared for the scattering of a quark-antiquark pair with a photon and $P_{14\to Q}(y, s_{14})$ given by eq.(1.30) the simple collinear factor which is the product of the inverse of the small invariant and the Altarelli-Parisi splitting function,

$$P_{14\to Q}(z, s_{14}) = \frac{1}{s_{14}} P_{14\to Q}(y).$$

The four particle phase space becomes,

$$\mathrm{d}P_4^{(d)}(M, p_1, p_2, p_3, p_4) \to \mathrm{d}P_3^{(d)}(M, p_Q, p_2, p_3)\, \mathrm{d}P_{col}^{(d)}(p_1, p_4, y) \tag{4.11}$$

where $\mathrm{d}R_3^{(d)}(M, p_Q, p_2, p_3)$ is the three-particle phase space in d-dimensions given in Appendix B by eq.(B.5). The collinear phase space factor $\mathrm{d}P_{col}^{(d)}(p_1, p_4, y)$ given in eq.(1.33) reads,

$$\mathrm{d}P_{col}^{(d)}(p_1, p_4, y) = \frac{(4\pi)^\epsilon}{16\pi^2\Gamma(1-\epsilon)} \mathrm{d}s_{14}\, \mathrm{d}z \Big[s_{14} y(1-y) \Big]^{-\epsilon}. \tag{4.12}$$

To evaluate the quark-gluon collinear factor, we need to integrate the collinear matrix element squared over all unresolved variables defined in this simple collinear region,

$$s_{14} \qquad \text{and} \qquad y. \tag{4.13}$$

The fractional momentum y is defined with respect to the momenta carried by the colour connected particles: the quark, the antiquark and the gluon. In particular y is defined as the following ratio,

$$y \equiv \frac{y_{\bar{q}g}}{y_{q\bar{q}g}} = \frac{y_{24}}{y_{124}}. \tag{4.14}$$

Since $y_{24} > y_{\min} y_{124}$, the lower boundary of the y integral is $y_{\min}$ exactly as in the simple quark-gluon collinear region of the 3-parton phase space. Consequently the simple collinear factors C_F in the 3-parton process (1.35) and $\tilde{C}_F$ in the 4-parton process will be similar. Indeed we have,

$$\begin{aligned}
\tilde{C}_F &= \int g_s^2 \left(\frac{N^2-1}{2N}\right) P_{14\to Q}(z, s_{14}) \mathrm{d}P_{col}^{(d)}(p_1, p_4, y) \\
&= \frac{\alpha_s}{2\pi}\left(\frac{N^2-1}{2N}\right)\left(\frac{4\pi\mu^2}{M^2}\right)^{\epsilon} \frac{1}{\Gamma(1-\epsilon)} \int_0^{y_{\min} y_{124}} \mathrm{d}y_{14}\, y_{14}^{-\epsilon-1} \left[\int_{y_{\min}}^1 \mathrm{d}y\, [y(1-y)]^{-\epsilon} P_{14\to Q}(y)\right] \\
&= C_F (y_{124})^{-\epsilon} = C_F (y_{Q\bar{q}})^{-\epsilon}. \qquad (4.15)
\end{aligned}$$

Putting all the factors together, we find that in the single unresolved $quark - gluon$ limit the four particle differential cross section $\mathrm{d}\sigma_4$ factorizes,

$$\begin{aligned}
\mathrm{d}\sigma_4 &\equiv \left(\frac{N^2-1}{2N}\right)\left(\frac{\alpha_s}{2\pi}\right)\left(\frac{\alpha e_q^2}{2\pi}\right) 4(2\pi)^4 \left(\mu^2\right)^{2\epsilon} \int |\mathcal{M}_{1234}|^2 \, \mathrm{d}P_4^{(d)}(M, p_1, p_2, p_3, p_4) \\
&\to \tilde{C}_F \times \int (2\pi)^{3-2d} |\mathcal{M}_{Q23}|^2 \mathrm{d}R_3^{(d)}(M, p_Q, p_2, p_3) = \tilde{C}_F \times \sigma_{Q\bar{q}\gamma}, \qquad (4.16)
\end{aligned}$$

where $\sigma_{Q\bar{q}\gamma}$ is the three-particle cross section for the scattering of a quark-antiquark with an additional hard photon.

The collinear antiquark-gluon contribution

In the region where the antiquark and the gluon are collinear we have,

$$s_{\bar{q}g} \equiv s_{24} < s_{\min}\frac{s_{124}}{M^2}, \qquad s_{qg} \equiv s_{14} > s_{\min}\frac{s_{124}}{M^2}, \qquad s_{q\gamma} \equiv s_{13} > s_{\min}, \qquad s_{\bar{q}\gamma g} \equiv s_{234} > s_{\min}. \qquad (4.17)$$

The resulting contribution in this region of the four particle phase space to the γ +1 jet rate is similar to that in the $q - g$ collinear region. It is obtained exchanging the role of the quark and antiquark and therefore yields,

$$\mathrm{d}\sigma_4 \to \tilde{C}_F \, \sigma_{q\bar{Q}\gamma}. \qquad (4.18)$$

The soft gluon contribution

In order to match onto the simple collinear quark-gluon regions, the soft gluon region is defined as follows,

$$s_{qg} \equiv s_{14} < s_{\min}\frac{s_{124}}{M^2} \quad \text{and} \quad s_{\bar{q}g} \equiv s_{24} < s_{\min}\frac{s_{124}}{M^2}, \quad s_{q\gamma} \equiv s_{13} > s_{\min}, \quad s_{\bar{q}\gamma} \equiv s_{23} > s_{\min}. \tag{4.19}$$

The four particle matrix element squared and phase space factorize in the soft gluon limit,

$$|\mathcal{M}_{1234}|^2 \to |\mathcal{M}_{123}|^2 f_{12}(4), \tag{4.20}$$

where $f_{12}(4)$ is the *eikonal factor* defined in eq.(1.20),

$$f_{12}(4) = \frac{4s_{12}}{s_{14}s_{24}}.$$

In this limit, the four particle phase space divides into a phase space for the three hard (resolved) particles $\mathrm{d}P_3^{(d)}(M, p_1, p_2, p_3)$ and a soft phase space factor $\mathrm{d}P_{soft}^{(d)}(p_1, p_2, p_4)$,

$$\mathrm{d}P_4^{(d)}(M, p_1, p_2, p_3, p_4) \to \mathrm{d}P_3^{(d)}(M, p_1, p_2, p_3)\,\mathrm{d}P_{soft}^{(d)}(p_1, p_2, p_4), \tag{4.21}$$

where the soft phase space factor reads,

$$\mathrm{d}P_{soft}^{(d)}(p_1, p_2, p_4) = \frac{(4\pi)^\epsilon}{16\pi^2\Gamma(1-\epsilon)}\frac{\mathrm{d}s_{14}\mathrm{d}s_{24}}{s_{12}}\left[\frac{s_{14}s_{24}}{s_{12}}\right]^{-\epsilon}$$

As before, all of the dependence on the unresolved variables is collected into the soft approximations to the matrix elements and the phase space. We find,

$$\begin{aligned}\tilde{S}_F &= \int g_s^2 \left(\frac{N^2-1}{2N}\right) f_{12}(4)\mathrm{d}P_{soft}^d(p_1, p_2, p_4) \\ &= (y_{12})^{-2\epsilon}\, S_F = (y_{q\bar{q}})^{-2\epsilon}\, S_F,\end{aligned} \tag{4.22}$$

where S_F is the soft gluon factor in the 3-parton process given in eq.(1.25). The modification of this soft factor in the 4-parton process is due entirely to the changed boundaries.

As usual, the contribution to the cross section from the single soft singular region factorizes, as follows (c.f. eq.1.24),

$$\mathrm{d}\sigma_4 \to \tilde{S}_F \times \sigma_{q\bar{q}g}. \tag{4.23}$$

The sum of the unresolved gluon contributions

The sum of the single unresolved gluon contributions is then given by,

$$\left[2\tilde{C}_F + \tilde{S}_F\right] \sigma_{q\bar{q}\gamma} \equiv R_{q\bar{q}(\gamma)} \sigma_{q\bar{q}\gamma} \,,$$

where the real unresolved factor $R_{q\bar{q}(\gamma)}$ depends on the invariant mass of the quark-antiquark pair and is given by,

$$\begin{aligned} R_{q\bar{q}(\gamma)} &= \frac{\alpha_s}{2\pi}\left(\frac{N^2-1}{2N}\right)\frac{1}{\Gamma(1-\epsilon)}\left(\frac{4\pi\mu^2}{M^2}\right)^{\epsilon} \\ &\quad \times \left[\frac{2(y_{q\bar{q}})^{-\epsilon}}{\epsilon^2} + \frac{3}{\epsilon} - 2\ln^2(y_{\min}) - 3\ln(y_{q\bar{q}} y_{\min}) + 7 - \frac{2\pi^2}{3}\right]. \end{aligned} \tag{4.24}$$

4.2.2 The collinear quark-photon contribution

In the region where the quark and the photon are collinear we have,

$$s_{q\gamma} \equiv s_{13} < s_{\min}\frac{s_{123}}{M^2}, \qquad s_{\bar{q}\gamma} \equiv s_{23} > s_{\min}\frac{s_{123}}{M^2}, \qquad s_{q\gamma g} \equiv s_{134} > s_{\min}, \qquad s_{\bar{q}g} \equiv s_{24} > s_{\min}, \tag{4.25}$$

so that the quark ($\equiv 1$) and photon ($\equiv 3$), cluster to form a new parent parton Q such that,

$$p_1 + p_3 = p_Q.$$

Each carries respectively a fraction z and $1-z$ of the parent parton momentum p_Q,

$$p_1 = (1-z)\,p_Q, \qquad p_3 = z\,p_Q.$$

In this limit ($s_{13} < s_{\min}\frac{s_{123}}{M^2}$) the invariants s_{12} and s_{23} are given by,

$$s_{12} = (1-z)\,s_{Q2}, \qquad s_{23} = z\,s_{Q2}, \tag{4.26}$$

while the invariants containing p_4 become,

$$s_{14} = (1-z)\,s_{Q3}, \qquad s_{34} = z\,s_{Q3}.$$

The four-particle matrix element squared and phase space factorize in exactly the same way as in the quark-gluon collinear limit with the role of $\gamma \equiv 3$ and $g \equiv 4$ being interchanged and y replaced by z. Unlike the quark-gluon case however, the photon is observed in the final state and hence only s_{13} is an unresolved variable. z which is the fractional momentum carried by the photon inside the quark-photon cluster is defined with respect to the momenta carried by the electromagnetically connected particles,

$$z = \frac{y_{\bar{q}\gamma}}{y_{q\bar{q}\gamma}} \equiv \frac{y_{23}}{y_{123}}. \tag{4.27}$$

In this limit, the four particle differential cross section factorizes,

$$\mathrm{d}\sigma_4 \to \tilde{C}_{F\gamma}\mathrm{d}z \times \underbrace{\int (2\pi)^{3-2d} |\mathcal{M}_{Q24}|^2 \mathrm{d}R_3^{(d)}(M, p_Q, p_2, p_4)}_{\equiv \sigma_{Q\bar{q}g}}, \tag{4.28}$$

where $\sigma_{Q\bar{q}g}$ is the three-particle cross section for the scattering of a quark-antiquark pair and a gluon. And $\tilde{C}_{F\gamma}\mathrm{d}z$ is the simple quark-photon collinear factor of the 4-parton process. As in the quark-gluon collinear case, this factor is related to the known 3-parton collinear factor, $C_{F\gamma}\mathrm{d}z$ given by eq.(1.35) by,

$$\tilde{C}_{F\gamma}\mathrm{d}z = C_{F\gamma}\mathrm{d}z (y_{Q\bar{q}})^{-\epsilon}. \tag{4.29}$$

Concerning the boundaries of the single collinear regions of the 4-parton phase space it is worth noting the following. In both, $q-g$ and $q-\gamma$ collinear regions we have required $y_{134} > y_{\min}$ in order to guarantee that these regions match onto the triple collinear region defined by $y_{134} < y_{\min}$. However, when both invariants y_{13} and y_{14} are small these two simple collinear regions overlap. The contribution to the total cross section in this overlapping region is however of $\mathcal{O}(y_{\min})$ and therefore negligible. Nevertheless, as we shall ultimately evaluate the differential cross section within the hybrid subtraction method, it is important to ensure that the matrix element squared is correctly approximated within this region too. Indeed, by requiring that $y_{134} > y_{\min}$, we can be sure that in the overlapping region the matrix element squared is correctly described by the sum of the simple collinear $q-\gamma$ and $q-g$ approximations.

To conclude, in this chapter we have given the explicit forms for the matrix element squared and phase space relevant to the resolved and single unresolved real contributions. The contributions to the $\gamma + 1$ jet rate arising from the four particle process (when all the final state particles are resolved) and from the three particle processes as in eq.(4.16) and eq.(4.23) will be evaluated numerically. This will be discussed in detail in Chapter 9.

Chapter 5

The two-particle unresolved real contributions

In the previous chapter we have discussed the calculation of the theoretically resolved and single unresolved real contributions relevant to the tree level process $\gamma^* \to q\bar{q}\gamma g$. Each of these two classes of real contributions corresponds to final state configurations where *more than two* particles are theoretically "seen". In each case, we gave the analytic expressions for matrix elements squared and phase spaces. We also saw that a γ +1 jet event can only arise if some final state particles are clustered together by the jet algorithm, and that the finite differential cross sections will ultimately be evaluated numerically. The evaluation of the *two-particle unresolved* real contributions, on the other hand can be performed analytically and is the subject of the coming chapter.

For the two-particle unresolved contributions, which can arise when the photon and the gluon are theoretically "unseen", the final state configuration already corresponds to a γ +1 jet event. Hence the final state particles will not be clustered further by the jet algorithm. As mentioned in Chapter 3, these double unresolved real contributions are of three types [1]: the *triple collinear*, the *double single collinear* and the *soft/collinear*

[1] Recall that for the evaluation of all these contributions we will always only consider contributions corresponding to the configurations where the photon is collinear to the quark. The contributions corre-

contributions.

This chapter contains the calculation of these two-particle unresolved real contributions to the total γ +1 jet differential cross section at $\mathcal{O}(\alpha\alpha_s)$ and is organized as follows. In Section 5.1 we demonstrate the factorization properties of phase spaces, squared matrix elements and fully differential cross section in the triple collinear limit. In Section 5.2 we present the calculation of the phase space integrals over the triple collinear region. The evaluation of the soft/collinear and double single collinear contributions is discussed in Sections 5.3 and 5.4 respectively. In Section 5.5 we present the result for the sum of these contributions. Finally, Section 5.6 is dedicated to a study of these contributions in different strongly ordered limits.

5.1 The triple collinear contributions

As we saw in Chapter 3, the triple collinear configuration arises when the gluon and the photon are collinear to the quark. The triple collinear configuration is illustrated in Fig.3.2.(c). In order to evaluate the triple collinear contributions to the photon +1 jet rate we need to determine the appropriate approximations for the matrix element squared and phase space in the *triple collinear* limit and perform the phase space integrals over the unresolved variables.

The *triple collinear* region of phase space is defined by,

$$s_{q\gamma g} \equiv s_{134} < s_{\min} \quad \text{and} \quad s_{\bar{q}g} \equiv s_{24} > s_{\min}. \tag{5.1}$$

Hence the triple collinear limit is obtained considering $s_{q\gamma g} \equiv s_{134} < s_{\min}$. In this limit, the photon, gluon and quark cluster to form a new parent parton Q such that,

$$p_q + p_\gamma + p_g = p_Q. \tag{5.2}$$

sponding to configurations where the photon is collinear to the antiquark are identical. When summing all the contributions, we will therefore multiply the result obtained considering the photon associated with the quark leg by two.

The photon, the gluon and the quark carry respectively a fraction z, y and $(1-y-z)$ of the parent parton momentum p_Q,

$$p_\gamma = z\, p_Q, \qquad p_g = y\, p_Q, \qquad p_q = (1-z-y)\, p_Q. \tag{5.3}$$

The invariants $s_{q\bar{q}} \equiv s_{12}$,$s_{\bar{q}\gamma} \equiv s_{23}$ and $s_{\bar{q}g} \equiv s_{24}$ are given by the following,

$$\begin{aligned} s_{12} &= (1-y-z)\, s_{Q2} \equiv (1-y-z)\, M^2, \\ s_{23} &= z\, s_{Q2} \equiv z\, M^2, \\ s_{24} &= y\, s_{Q2} \equiv y\, M^2, \end{aligned} \tag{5.4}$$

where M is the invariant mass of the final state.

The algebraic structure of these double unresolved contributions is unique to the triple collinear limit of the matrix element squared, and when analytically integrated over the singular regions of phase space will form the *triple collinear factor*. These contributions are expected to arise in *analytic* calculations of *exclusive* quantities at the second order in perturbation theory. Such calculations have, to the best of our knowledge, not been performed before in the literature. Hence, in Section 5.2 we will present the evaluation of the triple collinear contributions to the γ +1 jet rate in some detail.

5.1.1 The triple collinear limit of the matrix element squared

As usual to simplify the notations, we choose to label the final state particles as follows,

$$q \equiv 1, \qquad \bar{q} \equiv 2, \qquad p \equiv 3, \qquad g \equiv 4.$$

We are interested in the *triple collinear* limit of the matrix element squared for the scattering of a quark-antiquark pair with a photon and a gluon. In this limit, $1 \parallel 3 \parallel 4$ and the d-dimensional four-particle matrix element squared given by eq.(4.1) factorizes,

$$|\mathcal{M}_{1234}|^2 \to P_{134\to Q}(z, y, s_{13}, s_{14}, s_{134})\; |\mathcal{M}_{Q2}|^2.$$

$|\mathcal{M}_{Q2}|^2$ is the two-particle matrix element squared and $P_{134\to Q}(z, y, s_{13}, s_{14}, s_{134})$ defines the *triple collinear* matrix element squared. This triple collinear matrix element squared is obtained by keeping only the terms which contain any pair of the invariants,

$$s_{q\gamma} \equiv s_{13}, \qquad s_{qg} \equiv s_{14} \qquad \text{and} \qquad s_{q\gamma g} \equiv s_{134},$$

in the "full" four particle squared matrix elements (given by eq.(4.1)). It reads,

$$\begin{aligned}
&P_{134\to Q}(z, y, s_{13}, s_{14}, s_{134}) = \\
&+ \frac{4}{s_{13}s_{14}} \frac{(1-z-y)(1+(1-z-y)^2 - \epsilon(z^2+zy+y^2) - \epsilon^2 zy)}{zy} \\
&+ \frac{4}{s_{13}s_{134}} \frac{(1-z-y)(1-z+\epsilon^2 zy) + (1-y)^3 - \epsilon(1-y)(z^2+zy+y^2) + \epsilon^2 zy}{zy} \\
&+ \frac{4}{s_{14}s_{134}} \frac{(1-z-y)(1-y+\epsilon^2 zy) + (1-z)^3 - \epsilon(1-z)(z^2+zy+y^2) + \epsilon^2 zy}{zy} \\
&- \frac{4(1-\epsilon)}{s_{134}^2} \left((1-\epsilon)\frac{s_{13}}{s_{14}} + (1-\epsilon)\frac{s_{14}}{s_{13}} - 2\epsilon \right).
\end{aligned} \tag{5.5}$$

The same factor is appropriate for the collinear $q\gamma g$ limit of the $Z \to q\bar{q}\gamma g$, $Z \to q\bar{q}\gamma\gamma g$ and $Z \to q\bar{q}\gamma g g$ squared matrix elements. We expect this triple collinear factor to be the generalization of the simple collinear factor with three collinear particles instead of two and to be as universal as the single soft and single collinear matrix element squared encountered in Chapter 1 and 2.

In terms of the scaling variables $y_{ij} \equiv \frac{s_{ij}}{M^2}$,

$$P_{134\to Q}(z, y, s_{13}, s_{14}, s_{134}) = \frac{1}{M^4} P_{134\to Q}(z, y, y_{13}, y_{14}, y_{134}). \tag{5.6}$$

5.1.2 The triple collinear limit of the phase space

The 4-particle phase space in d-dimensions derived in (B.6) is given by,

$$\int \mathrm{d}P_4^{(d)} = (2\pi)^{4-3d} \int \mathrm{d}R_4^{(d)},$$

where,

$$\int \mathrm{d}R_4^{(d)} = \frac{(-\Delta_4)^{-1/2}}{M^2\, 2^9} \int \mathrm{d}\Omega_{d-1}\, \mathrm{d}\Omega_{d-2}\, \mathrm{d}\Omega_{d-3} \mathrm{d}s_{12}\, \mathrm{d}s_{13} \mathrm{d}s_{14} \mathrm{d}s_{23} \mathrm{d}s_{24} \mathrm{d}s_{34} \times \left(\frac{-\Delta_4}{M^2}\right)^{\frac{d-4}{2}} \delta(s_{12}+s_{13}+s_{14}+s_{23}+s_{24}+s_{34}-M^2), \tag{5.7}$$

with,

$$\Delta_4 = \frac{1}{16}\Big[{s_{12}}^2{s_{34}}^2 + {s_{13}}^2{s_{24}}^2 + {s_{14}}^2{s_{23}}^2 - 2\Big(s_{12}s_{23}s_{34}s_{14} + s_{13}s_{23}s_{24}s_{14} + s_{12}s_{24}s_{34}s_{13}\Big)\Big]. \tag{5.8}$$

In the triple collinear limit of the four-particle phase space, as the triple invariant s_{134}, which is constrained in the triple collinear region to be less than $s_{\min}$, does not appear as an integration variable in the expression of the four-particle phase space, $\mathrm{d}P_4^{(d)}$ we need to insert it using,

$$\int \mathrm{d}s_{134}\, \delta(s_{13}+s_{14}+s_{34}-s_{134}) = 1.$$

Using the definitions of s_{12}, s_{23}, s_{24} in the triple collinear limit, given in eq.(5.5), the product of the integration variables $\mathrm{d}s_{ij}$ in the 4-particle phase space given above yields,

$$\underbrace{\mathrm{d}s_{134}\, \mathrm{d}s_{13}\, \mathrm{d}s_{14}\, \mathrm{d}s_{34}}\, \mathrm{d}s_{12}\, \mathrm{d}s_{23}\, \mathrm{d}s_{24} \rightarrow \underbrace{\mathrm{d}s_{134}\, \mathrm{d}s_{13}\, \mathrm{d}s_{14}\, \mathrm{d}s_{34}}\, \mathrm{d}s_{Q2}\, \mathrm{d}z\, \mathrm{d}y\, (s_{Q2})^2.$$

The Gram determinant becomes,

$$[-\Delta_4] \rightarrow \frac{M^4}{16}\Big[-((1-y-z)\, s_{34} - y\, s_{13} - z\, s_{14})^2 + 4zy\, s_{13}\, s_{14}\Big] \equiv \frac{M^4}{16}\,[-\Delta_4'].$$

In the triple collinear limit, $s_{134} = s_{13}+s_{14}+s_{34}$ is less then $s_{\min}$ and the invariants s_{13}, s_{14} and s_{34} are of $\mathcal{O}(s_{\min})$. Consequently, all the terms in Δ_4' are of the same order, namely of $\mathcal{O}(s_{\min}^2)$ and none of them can *a priori* be neglected. This differs from the single soft or collinear phase space where the approximation simplified the phase space.

A particular feature of the triple collinear limit is the factorization of the four-particle phase space, $\mathrm{d}R_4^{(d)}$ into the 2-particle phase space $\mathrm{d}R_2^{(d)}(M, p_Q, p_2)$ and a triple collinear phase space factor,

$$\mathrm{d}R_4^{(d)}(M, p_1, p_3, p_4, p_2) \rightarrow \mathrm{d}R_2^{(d)}(M, p_Q, p_2)\, \mathrm{d}R_{col}^{(d)}(p_Q, p_1, p_3, p_4)\, \mathrm{d}s_{134},$$

and equivalently,

$$\underbrace{(2\pi)^{4-3d}\mathrm{d}R_4^{(d)}}_{\mathrm{d}P_4^{(d)}} \;\to\; \underbrace{(2\pi)^{2-d}\mathrm{d}R_2^{(d)}}_{\mathrm{d}P_2^{(d)}} \times \underbrace{(2\pi)^{2-2d}\mathrm{d}R_{col}^{(d)}}_{\equiv \mathrm{d}P_{col}^{(d)}}\,\mathrm{d}s_{134}.$$

$\mathrm{d}R_2^{(d)}(M, p_Q, p_2)$ is the two particle phase space given according to (B.3) by,

$$\mathrm{d}R^{(d)}(M, p_Q, p_2) \;=\; (s_{Q2})^{\frac{d-4}{2}}\,\frac{\mathrm{d}\Omega_{d-1}}{2^{d-1}}\,\mathrm{d}s_{Q2}\,\delta(s_{Q2}-M^2)\,,$$

while the triple collinear phase space factor reads,

$$\begin{aligned}\mathrm{d}R_{col}^{(d)}(p_Q,p_1,p_3,p_4)\,\mathrm{d}s_{134} \;&=\; \left[\frac{1}{16}\right]^{\frac{d-4}{2}}\left[\frac{1}{16}\right]^{-\frac{1}{2}}\left[-\Delta_4'\right]^{\frac{d-4}{2}}\left[-\Delta_4'\right]^{-\frac{1}{2}}\\ &\times\; \frac{2^{d-1}}{2^9}\,\delta(s_{13}+s_{14}+s_{34}-s_{134})\,\mathrm{d}\Omega_{d-2}\,\mathrm{d}\Omega_{d-3}\\ &\times\; \mathrm{d}s_{134}\,\mathrm{d}s_{13}\,\mathrm{d}s_{14}\,\mathrm{d}s_{34}\,\mathrm{d}z\,\mathrm{d}y\,, \end{aligned} \tag{5.9}$$

or in terms of the dimensionless invariants $y_{ij} \equiv \frac{s_{ij}}{M^2}$,

$$\begin{aligned}\mathrm{d}R_{col}^{(d)}(p_Q,p_1,p_3,p_4)\,\mathrm{d}s_{134} \;&=\; F\,\mathrm{d}y_{134}\,\mathrm{d}y_{13}\,\mathrm{d}y_{14}\,\mathrm{d}y_{34}\,\mathrm{d}z\,\mathrm{d}y\left[-\Delta_4''\right]^{\frac{d-4}{2}}\left[-\Delta_4''\right]^{-\frac{1}{2}}\\ &\times\; \delta(y_{13}+y_{14}+y_{34}-y_{134}) \end{aligned} \tag{5.10}$$

where $\Delta' \equiv M^4\Delta''$ and the overall factor F is given by,

$$F \;=\; 2^{-d}\,\mathrm{d}\Omega_{d-2}\,\mathrm{d}\Omega_{d-3}\,M^4\,[M^2]^{d-4}\,. \tag{5.11}$$

The angular integration terms in eq.(5.11) can be intuitively understood as follows: While the remaining invariants $\{y_{ij}\}$ in the problem are fixed, a rotation of the $qg\gamma$-system around the $\bar{q}$ axis is still possible ($\mathrm{d}\Omega_{d-2}$) and the parity of the $qg\gamma$-system allows two combinations ($\mathrm{d}\Omega_{d-3}$). Performing these angular integrations and setting $d = 4-2\epsilon$, we find,

$$F \;=\; \frac{1}{\Gamma(1-2\epsilon)}\frac{\pi}{4}\pi^{-2\epsilon}M^4\,[M^2]^{-2\epsilon}. \tag{5.12}$$

5.1.3 The triple collinear limit of the differential cross section

As for the matrix elements and phase space, the four particle differential cross section for the scattering of a quark-antiquark pair with a photon and a gluon, factorizes in the triple collinear limit,

$$\begin{aligned} \mathrm{d}\sigma_4 &\equiv \left(\frac{N^2-1}{2N}\right)\left(\frac{\alpha_s}{2\pi}\right)\left(\frac{\alpha e_q^2}{2\pi}\right) 4(2\pi)^4\left(\mu^2\right)^{2\epsilon}\int |\mathcal{M}_{1234}|^2\,\mathrm{d}P_4^{(d)}(M;p_1,p_2,p_3,p_4), \\ &\to TC_{F\gamma}\mathrm{d}z \times \underbrace{\int |\mathcal{M}_{Q2}|^2 \mathrm{d}P_2^{(d)}(M,p_Q,p_2)}_{\equiv\sigma_0}. \end{aligned} \tag{5.13}$$

As usual, σ_0 is the two-particle cross section while the dimensionless factor $TC_{F\gamma}\mathrm{d}z$ containing all the singularities, is formally given by,

$$TC_{F\gamma}\mathrm{d}z \equiv \left(\frac{N^2-1}{2N}\right)\left(\frac{\alpha_s}{2\pi}\right)\left(\frac{\alpha e_q^2}{2\pi}\right) 4(2\pi)^4\left(\mu^2\right)^{2\epsilon}\int \mathrm{d}s_{134}\mathrm{d}P_{col}^{(d)}|\mathcal{M}_{col}|^2,$$

where

$$|\mathcal{M}_{col}|^2 \equiv \frac{1}{M^4}P_{134\to Q}(z,y,y_{13},y_{14},y_{134}), \qquad \mathrm{d}P_{col}^{(d)} \equiv (2\pi)^{2-2d}\mathrm{d}R_{col}^{(d)}(p_Q;p_1,p_3,p_4).$$

The triple collinear contribution to the differential cross section is then obtained as the product of σ_0 and $TC_{F\gamma}\mathrm{d}z$. To evaluate $TC_{F\gamma}\mathrm{d}z$ we need to integrate the triple collinear factor $P_{134\to Q}$ for the emission of a photon and a gluon off a quark over all "unresolved" variables defined in the triple collinear phase space region. These unresolved variables appear in the denominator of $|M_{col}|^2$, and are given by,

$$y_{134}, \qquad y_{14}, \qquad y_{13} \qquad \text{and} \qquad y.$$

In the next section we shall evaluate these four phase space integrals. Before doing so, we shall briefly outline how one can organize the calculation. In fact, the large number of terms in this contribution can be conveniently managed if $TC_{F\gamma}\mathrm{d}z$ is decomposed according to the scaled invariants $\{y_{ij}\}$ present in the denominator of the triple collinear matrix element squared, $P_{134\to Q}(z,y,y_{13},y_{14},y_{134})$ given in eq.(5.5). We consider,

$$TC_{F\gamma}\mathrm{d}z = H\mathrm{d}z \times \left\{TC_{F\gamma}^{(a)}\left[\frac{1}{y_{13}y_{14}}\right] + TC_{F\gamma}^{(b)}\left[\frac{1}{y_{13}y_{134}}\right] + TC_{F\gamma}^{(c)}\left[\frac{1}{y_{14}y_{134}}\right]\right.$$

$$+TC_{F\gamma}^{(d)}\left[\frac{y_{13}}{y_{14}y_{134}^2}\right]+TC_{F\gamma}^{(e)}\left[\frac{y_{14}}{y_{13}y_{134}^2}\right]+TC_{F\gamma}^{(f)}\left[\frac{1}{y_{134}^2}\right]\Bigg\}.$$

H is an overall factor and is given by,

$$H \equiv \left(\frac{N^2-1}{2N}\right)\ \left(\frac{\alpha_s}{2\pi}\right)\ \left(\frac{\alpha e_q^2}{2\pi}\right)\left(\mu^2\right)^{2\epsilon}\ 4\,(2\pi)^{-2+4\epsilon}\ F$$

where F is the factor present in the triple collinear phase space factor of eq.(5.12). H then reads,

$$H = \left(\frac{N^2-1}{2N}\right)\left(\frac{4\pi\mu^2}{M^2}\right)^{2\epsilon}\left(\frac{\alpha_s}{2\pi}\right)\left(\frac{\alpha e_q^2}{2\pi}\right)\frac{1}{4\pi}\ \frac{1}{\Gamma(1-2\epsilon)}. \tag{5.14}$$

When explicitly evaluating the phase space integrals, we shall see that if these integrals can be reordered such that the first integral does not have the integration variable $\{y_{ij}\}$ in the denominator of the integrand, the integration procedure simplifies. This simplification will be achieved for all terms in $TC_{F\gamma}\mathrm{d}z$ apart from $TC_{F\gamma}^{(a)}\left[\frac{1}{y_{13}y_{14}}\right]$.

The integration variable y_{134} is already constrained by the definition of the triple collinear region, so that for all terms we will choose to do this integral last. The lower boundary of the y integral is fixed to be $y_{\min}$ to avoid overlapping with the soft/collinear region. The integration variables y_{13} and y_{14} are unconstrained and we choose to integrate over these two variables first.

As an example we consider the expression for the differential cross section $TC_{F\gamma}^{(c)}\left[\frac{1}{y_{14}y_{134}}\right]$,

$$TC_{F\gamma}^{(c)}\left[\frac{1}{y_{14}y_{134}}\right] = \int_0^{y_{\min}}\mathrm{d}y_{134}\int_{y_{\min}}^{1-z}\mathrm{d}y\int_0^{(1-z)y_{134}}\mathrm{d}y_{14}\int_{y_{13a}}^{y_{13b}}\mathrm{d}y_{13}\left[-\Delta_4''\right]^{-1/2-\epsilon}P_{134\to Q}\left[\frac{1}{y_{14}y_{134}}\right].$$

The Gram determinant is written as a quadratic in y_{13} and the boundaries of the y_{13} integral, i.e. y_{13a} and y_{13b}, are the solutions of $\Delta_4''=0$. The upper boundaries of the subsequent integrals y_{14} and y are fixed by requiring that Δ_4'' is negative. Note as well that the integration over y_{34} has been performed using the delta function $\delta(y_{13}+y_{14}+y_{34}-y_{134})$. Moreover to simplify further the notations, we have chosen to denote by $P_{134\to Q}\left[\frac{1}{y_{14}y_{134}}\right]$ the part in $P_{134\to Q}(z,y,y_{13},y_{14},y_{134})$ which contains the denominator $\{y_{14}y_{134}\}$. Similarly

we can write,

$$TC^{(b)}_{F\gamma}\left[\frac{1}{y_{13}y_{134}}\right] = \int_0^{y_{\min}} \mathrm{d}y_{134} \int_{y_{\min}}^{1-z} \mathrm{d}y \int_0^{(1-y)y_{134}} \mathrm{d}y_{13} \int_{y_{14a}}^{y_{14b}} \mathrm{d}y_{14} \left[-\Delta_4''\right]^{-1/2-\epsilon} P_{134\to Q}\left[\frac{1}{y_{13}y_{134}}\right],$$

where the order of the integrations over y_{13} and y_{14} has been swapped, since the integrand contains a factor $\{\frac{1}{y_{13}}\}$ instead of $\{\frac{1}{y_{14}}\}$. The boundaries of the second and third integral (here y_{13} and y) are obtained in a similar way as for the expression of $TC^{(c)}_{F\gamma}$: We write $-\Delta_4''$ as a quadratic in y_{14} and require that it is positive. The other contributions,

$$TC^{(d)}_{F\gamma}\left[\frac{y_{13}}{y_{14}y_{134}^2}\right],\ TC^{(e)}_{F\gamma}\left[\frac{y_{14}}{y_{13}y_{134}^2}\right] \quad \text{and} \quad TC^{(f)}_{F\gamma}\left[\frac{1}{y_{134}^2}\right],$$

can be obtained in an analogous way.

For $TC^{(a)}_{F\gamma}\left[\frac{1}{y_{13}y_{14}}\right]$ we will choose to consider,

$$TC^{(a)}_{F\gamma}\left[\frac{1}{y_{13}y_{14}}\right] = \int_0^{y_{\min}} \mathrm{d}y_{134} \int_{y_{\min}}^{1-z} \mathrm{d}y \int_0^{(1-z)y_{134}} \mathrm{d}y_{14} \int_{y_{13a}}^{y_{13b}} \mathrm{d}y_{13} \left[-\Delta_4''\right]^{-1/2-\epsilon} P_{134\to Q}\left[\frac{1}{y_{13}y_{14}}\right].$$

This contribution will be harder to calculate because the first integral over y_{13} has a factor of y_{13} in the denominator of the integrand.

For the whole triple collinear differential cross section $TC_{F\gamma}\mathrm{d}z$ we will therefore have to evaluate,

$$\begin{aligned}
TC_{F\gamma}\mathrm{d}z \;=\; & H\mathrm{d}z \times \int_0^{y_{\min}} \mathrm{d}y_{134} \int_{y_{\min}}^{1-z} \mathrm{d}y \int_0^{(1-z)y_{134}} \mathrm{d}y_{14} \int_{y_{13a}}^{y_{13b}} \mathrm{d}y_{13} \left[-\Delta_4''\right]^{-1/2-\epsilon} \\
& \times\left\{ P_{134\to Q}\left[\frac{1}{y_{13}y_{14}}\right] + P_{134\to Q}\left[\frac{1}{y_{14}y_{134}}\right] + P_{134\to Q}\left[\frac{y_{13}}{y_{14}y_{134}^2}\right] + P_{134\to Q}\left[\frac{1}{y_{134}^2}\right] \right\} \\
+ \; & H\mathrm{d}z \times \int_0^{y_{\min}} \mathrm{d}y_{134} \int_{y_{\min}}^{1-z} \mathrm{d}y \int_0^{(1-y)y_{134}} \mathrm{d}y_{13} \int_{y_{14a}}^{y_{14b}} \mathrm{d}y_{14} \left[-\Delta_4''\right]^{-1/2-\epsilon} \\
& \times\left\{ P_{134\to Q}\left[\frac{1}{y_{13}y_{134}}\right] + P_{134\to Q}\left[\frac{y_{14}}{y_{13}y_{134}^2}\right] \right\}. \qquad (5.15)
\end{aligned}$$

5.2 The triple collinear cross section

We choose to divide the calculation of $TC_{F\gamma}$ into three distinct phases corresponding to three different types of contributions to $TC_{F\gamma}$. These types are defined according

to the different double invariants $\{y_{ij}\}$ present in the denominator of $P_{134\to Q}$. We have contributions involving: $\left\{\frac{1}{y_{14}}\right\}$, $\left\{\frac{1}{y_{13}}\right\}$ and $\left\{\frac{1}{y_{13}y_{14}}\right\}$. For all these contributions, we perform the y integral in the range $[y_{\min},(1-z)]$ as the difference between integrations over the ranges, $[0,(1-z)]$ and $[0,y_{\min}]$. We label the integrals by $TC_{F\gamma}^{(j.1)}$ and $TC_{F\gamma}^{(j.2)}$ respectively for $j=a,\ldots,f$ and perform each integral separately. The full cross section is thus,

$$TC_{F\gamma}^{(j)} = TC_{F\gamma}^{(j.1)} - TC_{F\gamma}^{(j.2)}.$$

5.2.1 Contributions involving $\left\{\frac{1}{y_{14}}\right\}$

As an example, we present the calculation of $TC_{F\gamma}^{(c)}$,

$$\begin{aligned} TC_{F\gamma}^{(c)}\left[\frac{1}{y_{14}y_{134}}\right] &= 4\int_0^{y_{\min}} \mathrm{d}y_{134}\,\frac{1}{y_{134}}\int_{y_{\min}}^{1-z}\mathrm{d}y\int_0^{(1-z)y_{134}}\mathrm{d}y_{14}\,\frac{1}{y_{14}}\,P_{134\to Q}\left[\frac{1}{y_{134}y_{14}}\right] \\ &\quad\times\int_{y_{13a}}^{y_{13b}}\mathrm{d}y_{13}\left[(y_{13b}-y_{13})\,(y_{13}-y_{13a})\right]^{-1/2-\epsilon}\,(1-z)^{-1-2\epsilon}; \end{aligned}$$

explicitly.

To simplify the notations, we define,

$$P_{134\to Q}\left[\frac{1}{y_{134}y_{14}}\right] \equiv \frac{P^c(z,y)}{y_{134}\,y_{14}},$$

such that $P^c(z,y)$ is independent of y_{134} and y_{14}.

The contribution $TC_{F\gamma}^{(c.1)}$

We shall first describe the calculation of $TC_{F\gamma}^{(c.1)}$, the contribution to $TC_{F\gamma}^{(c)}$ for $0<y<(1-z)$. With the rescaling $y_{13}=\chi\,(y_{13b}-y_{13a})+y_{13a}$, the y_{13} integral becomes,

$$\int_0^1 \mathrm{d}\chi\,(y_{13b}-y_{13a})^{-2\epsilon}\left[\chi(1-\chi)\right]^{-1/2-\epsilon}.$$

The χ integral gives rise to a *Beta* function as defined in (A.6) such that,

$$\begin{aligned} \int_0^1 \mathrm{d}\chi\,(y_{13b}-y_{13a})^{-2\epsilon}\left[\chi(1-\chi)\right]^{-1/2-\epsilon} &= (y_{13b}-y_{13a})^{-2\epsilon}\,\frac{\Gamma^2(1/2-\epsilon)}{\Gamma(1-2\epsilon)} \\ &= 16^{\epsilon}\pi\,(y_{13b}-y_{13a})^{-2\epsilon}\,\frac{\Gamma(1-2\epsilon)}{\Gamma^2(1-\epsilon)}, \end{aligned}$$

where we have used the relation (A.1) between Gamma functions, $\Gamma(x)$.

The difference between the upper and lower boundary of the first phase space integral raised to the power -2ϵ, i.e. $(y_{13b} - y_{13a})^{-2\epsilon}$, gives us the phase space factor which regulates the integration over the unresolved variables. This will be the case for each of the contributions to the triple collinear differential cross section.

If we solve $-\Delta_4'' = 0$ as a polynomial in y_{13} we obtain $y_{13a,b} = [-\beta \pm \delta]/2\alpha$ with,

$$\alpha = -(1-z)^2, \quad \beta = 2(1-y-z)\,[(1-z)y_{134} - y_{14}] + 2y_{14}\,y\,z\,,$$

$$\delta^2 = 16\,y_{14}\,y\,z\,(1-y-z)\,[(1-z)y_{134} - y_{14}]\,,$$

and therefore,

$$16^{\epsilon}\,(y_{13b} - y_{13a})^{-2\epsilon} = \Big[y_{14}\,y\,z\,(1-y-z)\,[(1-z)y_{134} - y_{14}]\Big]^{-\epsilon}(1-z)^{4\epsilon}.$$

The positivity of $-\Delta_4''$ implies, $y_{14} \leq (1-z)\,y_{134}$ and $y \leq (1-z)$ which leads to the natural choice of variables,

$$y_{14} = v(1-z)\,y_{134} \qquad \text{and} \qquad y = t(1-z), \tag{5.16}$$

for which the regularizing phase space factor reads,

$$16^{\epsilon}\,(y_{13b} - y_{13a})^{-2\epsilon} = \Big[v\,(1-v)\,t\,(1-t)\,y_{134}^2\,z\Big]^{-\epsilon}.$$

The contribution, $TC_{F\gamma}^{(c.1)}$ is thus,

$$TC_{F\gamma}^{(c.1)}\left[\frac{1}{y_{14}y_{134}}\right] = 4\pi\,\frac{\Gamma(1-2\epsilon)}{\Gamma^2(1-\epsilon)}\,(1-z)^{-2\epsilon}z^{-\epsilon} \times \int_0^{y_{\min}} \mathrm{d}y_{134}\;(y_{134})^{-1-2\epsilon}\int_0^1 \mathrm{d}t\,[t(1-t)]^{-\epsilon}\int_0^1 \mathrm{d}v\,\frac{1}{v}\,[(1-v)v]^{-\epsilon}\;P^c(z,t).$$

According to (A.6), the v (or y_{14}) integral gives a *Beta* function,

$$\int_0^1 \mathrm{d}v\,\frac{1}{v}\,[(1-v)v]^{-\epsilon} = -\frac{1}{\epsilon}\,\frac{\Gamma^2(1-\epsilon)}{\Gamma(1-2\epsilon)},$$

so that,

$$TC_{F\gamma}^{(c.1)}\left[\frac{1}{y_{14}y_{134}}\right] = -\frac{4\pi}{\epsilon}\,(1-z)^{-2\epsilon}\,z^{-\epsilon}\int_0^{y_{\min}} \mathrm{d}y_{134}\,(y_{134})^{-2\epsilon-1}\int_0^1 \mathrm{d}t\,[t(1-t)]^{-\epsilon}\;P^c(z,t),$$

where,

$$P^c(z,t) = \frac{1}{tz}\Big[(1-t)\left[(1-t(1-z)) + \epsilon^2(1-z)zt\right] + (1-z)^3 - \epsilon(1-z)\left[z^2 + (1-z)zt + (1-z)^2\,t^2\right] + \epsilon^2(1-z)zt\Big].$$

The y_{134} integral is straightforward yielding,

$$\int_0^{y_{\min}} \mathrm{d}y_{134}\ (y_{134})^{-2\epsilon-1} = -\frac{(y_{\min})^{-2\epsilon}}{2\epsilon},$$

so that, after performing the t integral which yields only Γ functions, $TC_{F\gamma}^{(c.1)}$ finally reads,

$$TC_{F\gamma}^{(c.1)}\left[\frac{1}{y_{14}y_{134}}\right] = \frac{2\pi}{\epsilon^2}\,(1-z)^{-2\epsilon}\,z^{-\epsilon}\,(y_{\min})^{-2\epsilon}\,\frac{\Gamma^2(1-\epsilon)}{\Gamma(1-2\epsilon)} \times\left[-\frac{1}{\epsilon}P^\epsilon(z) - \frac{(3-z)(1-\epsilon^2 z)}{2z(1-2\epsilon)} - \epsilon\,z\,\frac{(1-z)}{z(1-2\epsilon)} - \epsilon\frac{(1-z)^2}{2\,z(1-2\epsilon)}\right],$$

where $P^\epsilon(z)$ stands for the d-dimensional Altarelli-Parisi splitting function given by $(1 + (1-z)^2 - \epsilon z^2)/z$.

The contribution $TC_{F\gamma}^{(c.2)}$

For the calculation of the contribution to $TC_{F\gamma}^{(c)}$ where $0 < y < y_{\min}$, we can neglect terms of $\mathcal{O}(y)$ in the matrix element and phase space as they become of $\mathcal{O}(y_{\min})$. In this limit,

$$P^c(z,y) \to \frac{(1-z)P^\epsilon(z)}{y},$$

and solving $-\Delta_4'' = 0$ as a quadratic in y_{13} yields,

$$(y_{13b} - y_{13a})^{-2\epsilon} = [16y_{14}yz(1-z)[(1-z)y_{134} - y_{14}]^{-\epsilon}\,(1-z)^{+4\epsilon}.$$

The integration over y_{13} is unchanged. However, in this limit and with the following redefinitions,

$$y_{14} = v(1-z)y_{134} \qquad \text{and} \qquad y = t y_{\min},$$

we find,

$$16^\epsilon(y_{13b} - y_{13a})^{-2\epsilon} = \left[v(1-v)\,t\,y_{\min}\,y_{134}^2 z\right]^{-\epsilon}(1-z)^\epsilon.$$

Therefore,

$$TC_{F\gamma}^{(c.2)}\left[\frac{1}{y_{14}y_{134}}\right] = 4\int_0^{y_{\min}} dy_{134}\,\frac{1}{y_{134}} \times \int_0^{y_{\min}} dy \int_0^{(1-z)y_{134}} dy_{14}\,\frac{1}{y_{14}}\,P^c(z,y) \times \int_{y_{13a}}^{y_{13b}} dy_{13}\,[(y_{13b}-y_{13})\,(y_{13}-y_{13a})]^{-1/2-\epsilon}\,(1-z)^{-1-2\epsilon};$$

becomes,

$$TC_{F\gamma}^{(c.2)} = 4\pi\,\frac{\Gamma(1-2\epsilon)}{\Gamma^2(1-\epsilon)}\,(1-z)^{-\epsilon}\;z^{-\epsilon}P^\epsilon(z)(y_{\min})^{-\epsilon} \times \underbrace{\int_0^1 dv\,\frac{1}{v}[v(1-v)]^{-\epsilon}}_{=-\frac{1}{\epsilon}\frac{\Gamma^2(1-\epsilon)}{\Gamma(1-2\epsilon)}} \underbrace{\int_0^{y_{\min}} dy_{134}\,(y_{134})^{-2\epsilon-1}\int_0^1 dt\,t^{-\epsilon-1}}_{=\frac{1}{2\epsilon^2}(y_{\min})^{-2\epsilon}}$$

$$= -\frac{2\pi}{\epsilon^3}(1-z)^{-\epsilon}\;z^{-\epsilon}P^\epsilon(z)(y_{\min})^{-3\epsilon}.$$

The total for $TC_{F\gamma}^{(c)}$

Combining the results of the previous two subsections and reintroducing the overall factor H, we finally obtain,

$$H\times TC_{F\gamma}^{(c)}\left[\frac{1}{y_{14}y_{134}}\right] = \left(\frac{N^2-1}{2N}\right)\left(\frac{4\pi\mu^2}{M^2}\right)^{2\epsilon}\left(\frac{\alpha_s}{2\pi}\right)\left(\frac{\alpha e_q^2}{2\pi}\right)\frac{1}{\Gamma^2(1-\epsilon)} \times z^{-\epsilon}(1-z)^{-2\epsilon}\,(y_{\min})^{-2\epsilon}\,\frac{\Gamma^4(1-\epsilon)}{\Gamma^2(1-2\epsilon)} \times\frac{1}{2\epsilon^2}\left[-\frac{1}{\epsilon}P^\epsilon(z)\left(1-(y_{\min})^{-\epsilon}(1-z)^\epsilon\frac{\Gamma(1-2\epsilon)}{\Gamma^2(1-\epsilon)}\right) -\frac{(3-z)(1-\epsilon^2 z)}{2z(1-2\epsilon)}-\epsilon\,\frac{(1-z)}{(1-2\epsilon)}-\epsilon\frac{(1-z)^2}{2\,z(1-2\epsilon)}\right]. \quad (5.17)$$

Other similar contributions

Following the same steps for the integrations over y_{13}, y_{14}, y_{134} and y we can obtain two other contributions to the triple differential cross section, namely $TC_{F\gamma}^{(d)}$ and $TC_{F\gamma}^{(f)}$. They

respectively read,

$$H \times TC_{F\gamma}^{(d)}\left[\frac{y_{13}}{y_{14}y_{134}^2}\right] = \left(\frac{N^2-1}{2N}\right)\left(\frac{4\pi\mu^2}{M^2}\right)^{2\epsilon}\left(\frac{\alpha_s}{2\pi}\right)\left(\frac{\alpha e_q^2}{2\pi}\right)\frac{1}{\Gamma^2(1-\epsilon)} \times z^{-\epsilon}(1-z)^{-2\epsilon}\left(y_{\min}\right)^{-2\epsilon}\frac{\Gamma^4(1-\epsilon)}{\Gamma^2(1-2\epsilon)} \times\frac{1}{4\epsilon}\frac{(1-\epsilon)^2}{(1-2\epsilon)^2}\left[z - \frac{1}{\epsilon}(1-\epsilon)\right], \tag{5.18}$$

$$H \times TC_{F\gamma}^{(f)}\left[\frac{1}{y_{134}^2}\right] = -\left(\frac{N^2-1}{2N}\right)\left(\frac{4\pi\mu^2}{M^2}\right)^{2\epsilon}\left(\frac{\alpha_s}{2\pi}\right)\left(\frac{\alpha e_q^2}{2\pi}\right)\frac{1}{\Gamma^2(1-\epsilon)} \times z^{-\epsilon}(1-z)^{-2\epsilon}\left(y_{\min}\right)^{-2\epsilon}\frac{\Gamma^4(1-\epsilon)}{\Gamma^2(1-2\epsilon)} \times\frac{(1-z)(1-\epsilon)}{(1-2\epsilon)^2}. \tag{5.19}$$

Notice that for these two contributions we can safely extend the $\int_{y_{\min}}^{1-z} \mathrm{d}y$ down to 0, since $\int_0^{y_{\min}} \mathrm{d}y$ gives only a contribution of $\mathcal{O}(y_{\min})$, which we can neglect.

5.2.2 Contributions involving $\left\{\frac{1}{y_{13}}\right\}$

As an example we describe the calculation of $TC_{F\gamma}^{(b)}$ formally given by,

$$TC_{F\gamma}^{(b)}\left[\frac{1}{y_{13}y_{134}}\right] = 4\int_0^{y_{\min}}\mathrm{d}y_{134}\,\frac{1}{y_{134}}\int_{y_{\min}}^{1-z}\mathrm{d}y\int_0^{(1-y)y_{134}}\mathrm{d}y_{13}\,\frac{1}{y_{13}}\,P^b(z,y) \times\int_{y_{14a}}^{y_{14b}}\mathrm{d}y_{14}\left[(y_{14b}-y_{14})\,(y_{14}-y_{14a})\right]^{-1/2-\epsilon}\,(1-y)^{-1-2\epsilon},$$

where $P^b(z,y)$ is defined in an analogous way to $P^c(z,y)$ and is independent of y_{134} and y_{13}.

As before, we divide the cross section into two pieces according to the range of the y integral; $0 < y < 1-z$ and $0 < y < y_{\min}$ denoted by $TC_{F\gamma}^{(b.1)}$ and $TC_{F\gamma}^{(b.2)}$ respectively. In both cases, the first integral – over the invariant that does not appear in the denominator

of this part of $P_{134\to Q}$ which in this case is y_{14} - gives a similar result to the first integral encountered in the evaluation of $TC_{F\gamma}^{(c.1)}$,

$$\frac{\Gamma^2(1/2-\epsilon)}{\Gamma(1-2\epsilon)}\,(y_{14b}-y_{14a})^{-2\epsilon}=\pi\frac{\Gamma(1-2\epsilon)}{\Gamma^2(1-\epsilon)}16^{\epsilon}\,(y_{14b}-y_{14a})^{-2\epsilon}\,.$$

Solving $-\Delta_4''=0$ as a polynomial in y_{14} we obtain $y_{14a,b}=\left[-\beta\pm\delta\right]/2\alpha$ with,

$$\alpha\;=\;-(1-y)^2,\quad \beta\;=\;2(1-y-z)\left[(1-y)y_{134}-y_{13}\right]\;+\;2y_{13}\,y\,z\,,$$

$$\delta^2=16\,y_{13}\,y\,z\,(1-y-z)\,\left[(1-y)y_{134}-y_{13}\right],$$

and the difference between the upper and lower boundaries raised to the power -2ϵ reads,

$$16^{\epsilon}\,(y_{14b}-y_{14a})^{-2\epsilon}\;=\;\left[y_{13}\,y\,z\,(1-y-z)\,\left[(1-y)y_{134}-y_{13}\right]\right]^{-\epsilon}(1-y)^{4\epsilon}.$$

The positivity of $-\Delta_4''$ implies $y_{13}\le(1-y)\,y_{134}$ and $y\le(1-z)$ which leads to the following natural choice of variables,

$$y_{13}=v(1-y)\;y_{134}\qquad\text{and}\qquad y=t(1-z). \tag{5.20}$$

The regularizing phase space factor is thus given by,

$$16^{\epsilon}\,(y_{14b}-y_{14a})^{-2\epsilon}\;=\;\left[v\,(1-v)\,t\,(1-t)\,y_{134}^2\,z\,\right]^{-\epsilon}(1-z)^{-2\epsilon}\,[1-t(1-z)]^{2\epsilon},$$

so that,

$$\begin{aligned}TC_{F\gamma}^{(b.1)}\;&=\;4\,\pi\frac{\Gamma(1-2\epsilon)}{\Gamma^2(1-\epsilon)}\,(1-z)^{-2\epsilon+1}\,z^{-\epsilon}\int_0^{y_{\min}}\mathrm{d}y_{134}\;(y_{134})^{-1-2\epsilon}\\&\quad\times\int_0^1\mathrm{d}v\,\frac{1}{v}\,[(1-v)v]^{-\epsilon}\int_0^1\mathrm{d}t\,[t(1-t)]^{-\epsilon}\;\frac{1}{[1-(1-z)t]}P^b(z,t),\end{aligned}$$

where,

$$\begin{aligned}P^b(z,t)\;&=\;\frac{1}{tz(1-z)}\Big[(1-z)\,(1-t)\left[(1-z)\;+\epsilon^2(1-z)zt\right]+(1-(1-z)t)^3\\&\quad-\epsilon\,[1-(1-z)t]\,\left[z^2+(1-z)zt+(1-z)^2\,t^2\right]+\epsilon^2(1-z)\,z\,t\Big].\end{aligned}$$

The integrations over v (or y_{13}) and y_{134}, give similar results to those in $\mathrm{d}\sigma_{col}^{(\mathrm{c.1})}$,

$$-\frac{1}{\epsilon}\,\frac{\Gamma^2(1-\epsilon)}{\Gamma(1-2\epsilon)} \quad \text{and} \quad -\frac{(y_{\min})^{-2\epsilon}}{2\epsilon},$$

respectively.

The t integral requires more thought. It reads,

$$\begin{aligned} I \;=\; & \int_0^1 \mathrm{d}t\, \frac{t^{-\epsilon-1}(1-t)^{-\epsilon}}{[1-t(1-z)]} \\ & \times\Big[-\epsilon[1-t(1-z)]\,\left[z^2+(1-z)zt+(1-z)^2\,t^2\right] + (1-(1-z)t)^3 \;+\epsilon^2\, z(1-z)\,t \\ & + (1-z)\,(1-t)\left[(1-z)\;+\epsilon^2(1-z)zt\right],\Big]. \end{aligned}$$

which we divide into two pieces, according to the presence of two different denominators in the integrand, $I = I_1 + I_2$, where,

$$\begin{aligned} I_1 \;=\; & -\int_0^1 \mathrm{d}t\; t^{-\epsilon-1}(1-t)^{-\epsilon} \times \epsilon\,[z^2+(1-z)zt+(1-z)^2\,t^2], \\ I_2 \;=\; & \int_0^1 \mathrm{d}t\, \frac{t^{-\epsilon-1}(1-t)^{-\epsilon}}{[1-t(1-z)]} \\ & \times\left[(1-z)\,(1-t)\,\left[(1-z)\;+\epsilon^2(1-z)zt\right] + (1-(1-z)t)^3 \;+\epsilon^2\, z(1-z)\,t\,\right]. \end{aligned}$$

The evaluation of I_1 is straightforward, yielding only *Beta* functions,

$$I_1 \;=\; \frac{\Gamma^2(1-\epsilon)}{\Gamma(2-2\epsilon)}\left[-\frac{1}{\epsilon}(1-\epsilon\,z^2)(1-2\epsilon) \;-\; (1-z)(2+\epsilon\,z) \;+\; \frac{1}{2}(1-z)^2(1-\epsilon)\right].$$

All terms in I_2 contain a factor $[1-t(1-z)]$ in the denominator such that the result of the integrations yields *hypergeometric* functions. We decompose it further according to the powers of t and $(1-t)$ present in the integrand of I_2 so that $I_2 = I_{21} + I_{22} + I_{23}$ with,

$$\begin{aligned} I_{21} \;=\; & (1-z)^2 \int_0^1 \mathrm{d}t\, \frac{t^{-\epsilon-1}(1-t)^{-\epsilon+1}}{[1-t(1-z)]} \\ =\; & -\frac{1}{\epsilon}\,\frac{\Gamma(1-\epsilon)\Gamma(2-\epsilon)}{\Gamma(2-2\epsilon)}(1-z)^2\,F_{21}(1,-\epsilon;2-2\epsilon;1-z)\,, \end{aligned}$$

$$
\begin{aligned}
I_{22} &= \epsilon^2\, z\,(1-z)^2 \int_0^1 \mathrm{d}t\, \frac{t^{-\epsilon}(1-t)^{-\epsilon+1}}{[1-t(1-z)]} \\
&= \epsilon^2\, z\,(1-z)^2\, \frac{\Gamma(1-\epsilon)\Gamma(2-\epsilon)}{\Gamma(3-2\epsilon)}\, F_{21}(1,1-\epsilon;3-2\epsilon;1-z)\,, \\
I_{23} &= \epsilon^2\, z\,(1-z) \int_0^1 \mathrm{d}t\, \frac{t^{-\epsilon}(1-t)^{-\epsilon}}{[1-t(1-z)]} \\
&= \epsilon^2\, z\,(1-z)\, \frac{\Gamma^2(1-\epsilon)}{\Gamma(2-2\epsilon)}\, F_{21}(1,1-\epsilon;2-2\epsilon;1-z).
\end{aligned}
$$

$F_{21}(a,b;c;x)$ is the *hypergeometric* function defined in (A.10). Using the identities amongst contiguous hypergeometric functions given in Appendix A by eq.(A.17), I can be considerably simplified. We find,

$$
\begin{aligned}
I &= \frac{\Gamma^2(1-\epsilon)}{\Gamma(1-2\epsilon)} \times \Bigg[-\frac{P^\epsilon(z)}{\epsilon} - \frac{(1-\epsilon^2)(1-z)^2}{(1-2\epsilon)}\, F_{21}(1,1-\epsilon;2-2\epsilon;1-z) \\
&\quad -\frac{(1-z)(2+\epsilon z)}{z(1-2\epsilon)} + \frac{(1-z)^2(1-\epsilon)}{2\,z(1-2\epsilon)} + \frac{\epsilon^2(1-z)}{(1-2\epsilon)} \Bigg].
\end{aligned} \tag{5.21}
$$

Altogether, we find that the contribution to $TC_{F\gamma}^{(b)}$ for the region of phase space where $0 < y < (1-z)$ is given by,

$$
\begin{aligned}
TC_{F\gamma}^{(b.1)}\left[\frac{1}{y_{13}y_{134}}\right] &= \frac{2\pi}{\epsilon^2}\, \frac{\Gamma^2(1-\epsilon)}{\Gamma(1-2\epsilon)} (1-z)^{-2\epsilon}\, z^{-\epsilon}\, (y_{\min})^{-2\epsilon} \\
&\quad \times \Bigg[-\frac{P^\epsilon(z)}{\epsilon} - \frac{(1-\epsilon^2)(1-z)^2}{(1-2\epsilon)}\, F_{21}(1,1-\epsilon;2-2\epsilon;1-z) \\
&\quad -\frac{(1-z)(2+\epsilon z)}{z(1-2\epsilon)} + \frac{(1-z)^2(1-\epsilon)}{2\,z(1-2\epsilon)} + \frac{\epsilon^2(1-z)}{(1-2\epsilon)} \Bigg].
\end{aligned} \tag{5.22}
$$

As in the previous section, for the contribution from the $0 < y < y_{\min}$ integral some simplifications of matrix element and phase space can be made. Terms of $\mathcal{O}(y)$ can be ignored,

$$
P^b(z,y) \to \frac{P^\epsilon(z)}{y},
$$

and with the following change of variables

$$
y_{14} = v y_{134} \qquad \text{and} \qquad y = t y_{\min},
$$

$TC_{F\gamma}^{(b.2)}$ reads,

$$TC_{F\gamma}^{(b.2)} = -\frac{2\pi}{\epsilon^3}\frac{\Gamma^2(1-\epsilon)}{\Gamma(1-2\epsilon)} z^{-\epsilon}(1-z)^{-\epsilon}(y_{\min})^{-3\epsilon}\, P^{\epsilon}(z). \tag{5.23}$$

Combining these two results and reinserting the overall factor H, we find,

$$\begin{aligned} H \times TC_{F\gamma}^{(b)}\left[\frac{1}{y_{13}y_{134}}\right] &= \left(\frac{N^2-1}{2N}\right)\left(\frac{4\pi\mu^2}{M^2}\right)^{2\epsilon}\left(\frac{\alpha_s}{2\pi}\right)\left(\frac{\alpha e_q^2}{2\pi}\right)\frac{1}{\Gamma^2(1-\epsilon)} \\ &\quad \times z^{-\epsilon}(1-z)^{-2\epsilon}\,(y_{\min})^{-2\epsilon}\,\frac{\Gamma^4(1-\epsilon)}{\Gamma^2(1-2\epsilon)} \\ &\quad \times\frac{1}{2\epsilon^2}\left[\left(-\frac{P^{\epsilon}(z)}{\epsilon}+\frac{P^{\epsilon}(z)}{\epsilon}(y_{\min})^{-\epsilon}(1-z)^{\epsilon}\,\frac{\Gamma(1-2\epsilon)}{\Gamma^2(1-\epsilon)}\right)\right. \\ &\quad -\frac{(1-\epsilon^2)(1-z)^2}{(1-2\epsilon)}\,F_{21}(1,1-\epsilon;2-2\epsilon;1-z) \\ &\quad \left.-\frac{(1-z)(2+\epsilon z)}{z(1-2\epsilon)}+\frac{(1-z)^2(1-\epsilon)}{2\,z(1-2\epsilon)}+\frac{\epsilon^2(1-z)}{(1-2\epsilon)}\right]. \end{aligned} \tag{5.24}$$

Following similar steps, one can easily also obtain $TC_{F\gamma}^{(e)}\left[\frac{y_{14}}{y_{13}y_{134}^2}\right]$. The results of the y_{13} and y_{14} integrals contain *Beta* functions, whereas the integration over y generates hypergeometric functions. We obtain,

$$\begin{aligned} H \times TC_{F\gamma}^{(e)}\left[\frac{y_{14}}{y_{13}y_{134}^2}\right] &= \left(\frac{N^2-1}{2N}\right)\left(\frac{4\pi\mu^2}{M^2}\right)^{2\epsilon}\left(\frac{\alpha_s}{2\pi}\right)\left(\frac{\alpha e_q^2}{2\pi}\right)\frac{1}{\Gamma^2(1-\epsilon)} \\ &\quad \times z^{-\epsilon}(1-z)^{-2\epsilon}\,(y_{\min})^{-2\epsilon}\,\frac{\Gamma^4(1-\epsilon)}{\Gamma^2(1-2\epsilon)} \\ &\quad \times\frac{1}{2\epsilon^2}\,\frac{(1-z)(1-\epsilon)^2}{z(1-2\epsilon)}\left[1-F_{21}(1,1-\epsilon;2-2\epsilon;1-z)\right] \end{aligned} \tag{5.25}$$

As with the contributions $TC_{F\gamma}^{(d.2)}$ and $TC_{F\gamma}^{(f.2)}$, since there is no factor of y in the denominator of the integrand, the contribution $TC_{F\gamma}^{(e.2)}$ where $0 < y < y_{\min}$ gives only a contribution of $\mathcal{O}(y_{\min})$ and can therefore be neglected.

5.2.3 Contributions involving $\left\{\frac{1}{y_{13}y_{14}}\right\}$

As this part of the calculation of the triple collinear contribution to the γ +1 jet rate at $\mathcal{O}(\alpha\alpha_s)$ presents some additional calculational difficulties, we will describe it in great detail, although the proofs of all identities used are given in the Appendix A. The differential cross section $TC_{F\gamma}^{(a)}\left[\frac{1}{y_{13}y_{14}}\right]$ is formally given by,

$$TC_{F\gamma}^{(a)}\left[\frac{1}{y_{13}y_{14}}\right] = 4\,(1-z)^{-1-2\epsilon}\int_0^{y_{\rm min}} {\rm d}y_{134}\int_{y_{\rm min}}^{1-z}{\rm d}y\int_0^{(1-z)y_{134}}{\rm d}y_{14}\,\frac{1}{y_{14}} \times\int_{y_{13a}}^{y_{13b}}{\rm d}y_{13}\,\frac{1}{y_{13}}\left[(y_{13b}-y_{13})\,(y_{13}-y_{13a})\right]^{-1/2-\epsilon}\,P^a(z,y),$$

where $P^a(z,y)$ is defined in an analogous way to $P^b(z,y)$ and $P^c(z,y)$. As usual we divide the y integration into two pieces and first present the calculation of $TC_{F\gamma}^{(a.1)}$, the contribution to $TC_{F\gamma}^{(a)}$ for the region of phase space where $0<y<(1-z)$.

Denoting the y_{13} integral as I, and making the substitution, $y_{13}=(y_{13b}-y_{13a})\chi+y_{13a}$ we obtain,

$$I = (y_{13b}-y_{13a})^{-2\epsilon}\int_0^1\left[\chi(1-\chi)\right]^{-1/2-\epsilon}\underbrace{\left[(y_{13b}-y_{13a})\,\chi+y_{13a}\right]^{-1}}_{\frac{1}{y_{13a}}\left[1-\frac{(y_{13a}-y_{13b})\chi}{y_{13a}}\right]^{-1}}$$

$$= (y_{13b}-y_{13a})^{-2\epsilon}\,\frac{1}{y_{13a}}\,\frac{\Gamma^2(1/2-\epsilon)}{\Gamma(1-2\epsilon)}\,F_{21}\left(1,1/2-\epsilon,1-2\epsilon,\frac{(y_{13a}-y_{13b})}{y_{13a}}\right) \quad (5.26)$$

We wish to bring I into a form which allows us to perform the y_{14} and y integrals. Hence we consider the following redefinitions,

$$y_{14}=v(1-z)\,y_{134} \qquad \text{and} \qquad y=t(1-z), \quad (5.27)$$

so that, $y_{13a,b}=y_{134}\,(A\pm B)^2$ where, $A=\sqrt{(1-t)(1-v)}$, $B=\sqrt{zvt}$ and,

$$\frac{(y_{13a}-y_{13b})}{y_{13a}} = -\frac{4AB}{(A-B)^2} \equiv \frac{4Z}{(1+Z)^2}, \quad (5.28)$$

with $Z=-\frac{B}{A}$. the integration boundary y_{13a} is then related to Z, A and B in the following way,

$$(1+Z)^2 = \left(\frac{A-B}{A}\right)^2 = \frac{1}{y_{134}}\,\frac{y_{13a}}{A^2}. \quad (5.29)$$

With these definitions (5.28) and (5.29) for the argument of the hypergeometric function and the lower boundary y_{13a}, both appearing in eq.(5.26), we apply the following relation between two hypergeometric series of argument $\{\frac{4Z}{(1+Z)^2}\}$ and $\{Z^2\}$,

$$F_{21}\left(1, b, 2b, \frac{4Z}{(1+Z)^2}\right) = (1+Z)^2\, F_{21}(1, 3/2-b, b+1/2, Z^2) \tag{5.30}$$

which is explicitly proven to hold for all values of z in Appendix A .

With the help of this relation (5.30), I can be rewritten as follows,

$$\begin{aligned} I &= (y_{13b}-y_{13a})^{-2\epsilon}\ \frac{1}{y_{134}}\ \frac{1}{(1-v)(1-t)}\ \frac{\Gamma^2(1/2-\epsilon)}{\Gamma(1-2\epsilon)}\ F_{21}\Big(1, 1+\epsilon; 1-\epsilon; \frac{z\,v\,t}{(1-t)(1-v)}\Big), \\ &= 16^{\epsilon}\,(y_{13b}-y_{13a})^{-2\epsilon}\ \frac{\pi}{y_{134}}\ \frac{1}{(1-v)(1-t)}\ \frac{\Gamma(1-2\epsilon)}{\Gamma^2(1-\epsilon)}\ F_{21}\Big(1, 1+\epsilon; 1-\epsilon; \frac{z\,v\,t}{(1-t)(1-v)}\Big), \end{aligned} \tag{5.31}$$

where,

$$16^{\epsilon}\,(y_{13b}-y_{13a})^{-2\epsilon} \;=\; \Big[t(1-t)v(1-v)\,z\,y_{134}^2\Big]^{-\epsilon}.$$

$TC_{F\gamma}^{(a.1)}\left[\frac{1}{y_{13}y_{14}}\right]$ then yields,

$$\begin{aligned} TC_{F\gamma}^{(a.1)} \;=\; & 4\pi(1-z)^{-2\epsilon-1}z^{-\epsilon}\frac{\Gamma(1-2\epsilon)}{\Gamma^2(1-\epsilon)}\int_0^{y_{\min}}(y_{134})^{-1-2\epsilon}dy_{134}\int_0^1 dt\; t^{-\epsilon}(1-t)^{-1-\epsilon}\; P^a(z,t) \\ & \times \underbrace{\int_0^1 dv\; v^{-\epsilon-1}(1-v)^{-\epsilon-1}F_{21}\Big(1, 1+\epsilon; 1-\epsilon; \frac{z\,v\,t}{(1-t)(1-v)}\Big)}_{\equiv\, I'} \end{aligned} \tag{5.32}$$

For the calculation of I', defining $\alpha \equiv \frac{zt}{1-t}$ and using the definition of $F_{21}(a,b,c;z)$ in terms of infinite series given by (A.8) we obtain [2],

$$I' = \sum_{n=1}^{\infty}\frac{\Gamma(n+1+\epsilon)\Gamma(1-\epsilon)}{\Gamma(n+1-\epsilon)\Gamma(1+\epsilon)} \times \alpha^n \underbrace{\int_0^1 dv\; v^{-\epsilon-1+n}(1-v)^{-\epsilon-1-n}}_{=\,\frac{\Gamma(n-\epsilon)\Gamma(-n-\epsilon)}{\Gamma(-2\epsilon)}}. \tag{5.33}$$

[2]It shall be noted that this series diverges for $Z=1$. However this divergence is integrable and does not affect the validity of eq.(5.33) as is proven in the Appendix A.

where the last equality is explicitly proven in Appendix A. According to eq.(A.2) we also have,

$$\Gamma(-n-\epsilon) = (-1)^{n+1}\frac{\Gamma(1+\epsilon)\Gamma(1-\epsilon)}{\epsilon\Gamma(n+1+\epsilon)},$$

and I' yields,

$$I' = -\frac{2}{\epsilon}\frac{\Gamma(1-\epsilon)^2}{\Gamma(1-2\epsilon)}\,F_{21}\left(1,-\epsilon;1-\epsilon;\frac{-zt}{(1-t)}\right). \tag{5.34}$$

Inserting I' back into eq.(5.32) and performing the trivial integral over y_{134}, we find that,

$$TC_{F\gamma}^{(a.1)} = \frac{2\pi}{\epsilon^2}(1-z)^{-2\epsilon}z^{-\epsilon}(y_{\min})^{-2\epsilon}\int_0^1 \mathrm{d}t\; t^{-\epsilon}(1-t)^{-\epsilon}\frac{1}{(1-z)(1-t)}\,P^a(z,t) \times F_{21}\left(1,-\epsilon;1-\epsilon;\frac{-zt}{(1-t)}\right), \tag{5.35}$$

where $P^a(z,t)$ is given by,

$$P^a(z,t) = \frac{(1-t)(1-z)}{zt}\times\Big[1 + (1-z)^2(1-t)^2 -\epsilon\left(z^2 + z(1-z)t + (1-z)^2t^2\right) -\epsilon^2\, z(1-z)t\Big].$$

Rewriting $P^a(z,t)$ as a polynomial in t,

$$\frac{1}{(1-z)(1-t)}P^a(z,t) = \left[\frac{1}{t}A_{-1}(z) + A_0(z) + t\,A_1(z)\right], \tag{5.36}$$

where the index denotes the associated power of t,

$$A_{-1}(z) = P^e(z), \qquad A_0(z) = -\frac{(1-z)}{z}[2(1-z) + \epsilon\, z(1+\epsilon)], \tag{5.37}$$

$$A_1(z) = \frac{(1-z)^2}{z}(1-\epsilon), \tag{5.38}$$

we can write,

$$TC_{F\gamma}^{(a.1)} = 2\pi(1-z)^{-2\epsilon}z^{-\epsilon}(y_{\min})^{-2\epsilon}\sum_{\alpha=-1}^{1}A_\alpha(z)\underbrace{\frac{1}{\epsilon^2}\int_0^1 \mathrm{d}t\; t^{-\epsilon+\alpha}(1-t)^{-\epsilon}\,F_{21}\left(1,-\epsilon;1-\epsilon;\frac{-zt}{(1-t)}\right)}_{\equiv B_\alpha}. \tag{5.39}$$

To evaluate B_α, we rewrite the hypergeometric function present in B_α in its integral form,

$$F_{21}\left(1,-\epsilon;1-\epsilon;\frac{-zt}{1-t}\right) = -\epsilon\int_0^1 \mathrm{d}u\, u^{-\epsilon-1}\left[1+\frac{uzt}{1-t}\right]^{-1},$$

and then split B_α into I_{α_1} and I_{α_2} with integrands respectively proportional to $\frac{1}{u}$ and $\left[1+\frac{uzt}{1-t}\right]^{-1}$. Partial fractioning, we have,

$$\begin{aligned}
B_\alpha &= -\frac{1}{\epsilon}\int_0^1 \mathrm{d}t(1-t)^{-\epsilon}t^{-\epsilon+\alpha} \\
&\quad \times\int_0^1 \mathrm{d}u\, u^{-\epsilon}\left[u^{-1} - \left[1+\frac{uzt}{1-t}\right]^{-1}\frac{zt}{1-t}\right] \\
&= \frac{1}{\epsilon^2}\int_0^1 \mathrm{d}t\, t^{-\epsilon+\alpha}\,(1-t)^{-\epsilon} \\
&\quad +\frac{z}{\epsilon}\int_0^1 \mathrm{d}t(1-t)^{-\epsilon-1}t^{-\epsilon+\alpha+1}\int_0^1 \mathrm{d}u\, u^{-\epsilon}\left[1+\frac{uzt}{1-t}\right]^{-1} \\
&= I_{\alpha_1} + I_{\alpha_2}
\end{aligned}$$

For I_{α_1} it is straightforward to perform the u and t integrations,

$$I_{\alpha_1} = \frac{1}{\epsilon^2}\frac{\Gamma(1-\epsilon)\Gamma(1+\alpha-\epsilon)}{\Gamma(2+\alpha-2\epsilon)}. \tag{5.40}$$

The second integral, $I_{\alpha 2}$ on the other hand requires more effort,

$$\begin{aligned}
I_{\alpha 2} &= \frac{z}{\epsilon}\int_0^1 \mathrm{d}t\, t^{-\epsilon+1+\alpha}(1-t)^{-\epsilon-1}\int_0^1 \mathrm{d}u\, u^{-\epsilon}\left[1+\frac{uzt}{1-t}\right]^{-1} \\
&\equiv \frac{z}{\epsilon}\int_0^1 \mathrm{d}t\, t^{-\epsilon+1+\alpha}(1-t)^{-\epsilon-1}\times J.
\end{aligned}$$

We note that $I_{\alpha 2}$ is only multiplied by $\frac{1}{\epsilon}$ and it is therefore sufficient to expand J at most up to the order of ϵ,

$$\begin{aligned}
J &= \int_0^1 \mathrm{d}u\,\left[1+\frac{uzt}{1-t}\right]^{-1} - \epsilon\int_0^1 \mathrm{d}u\,\ln u\,\left[1+\frac{uzt}{1-t}\right]^{-1} + \mathcal{O}(\epsilon^2) \\
&= J_1 - \epsilon J_2.
\end{aligned}$$

Performing the u integral in J_1, we obtain,

$$J_1 = \frac{1-t}{zt}\ln\left(\frac{1-t(1-z)}{1-t}\right),$$

such that $I_{\alpha 2}$ becomes,

$$
\begin{aligned}
I_{\alpha 2} &= \frac{1}{\epsilon}\int_0^1 \mathrm{d}t\, t^{-\epsilon+\alpha}(1-t)^{-\epsilon}\,\ln\left(\frac{1-t(1-z)}{1-t}\right) \\
&\quad -z\int_0^1 \mathrm{d}u \ln u \int_0^1 \mathrm{d}t\,(1-t)^{-\epsilon}t^{-\epsilon+\alpha+1}\left[(1-t(1-uz)\right]^{-1}. \qquad (5.41)
\end{aligned}
$$

In the last line neither of the integrations u or t has been performed yet, however, the order of integration has been swapped. For specific choices of α, we expand $I_{\alpha 2}$ as a series in ϵ. The integrals contain generally polylogarithms. For example, for $\alpha = -1$, we find,

$$
\begin{aligned}
I_{(\alpha=-1)2} &= \frac{1}{\epsilon}\times\left[-\int_0^1 \mathrm{d}t\,\frac{\ln(1-t)}{t}+\int_0^1 \mathrm{d}t\,\frac{\ln\left(1-t(1-z)\right)}{t}\right. \\
&\quad +\epsilon\int_0^1 \mathrm{d}t\,\frac{\ln^2(1-t)}{t}+\epsilon\int_0^1 \mathrm{d}t\,\frac{\ln t\ln(1-t)}{t} \\
&\quad -\epsilon\int_0^1 \mathrm{d}t\,\frac{\ln t\ln\left(1-t(1-z)\right)}{t}-\epsilon\int_0^1 \mathrm{d}t\,\frac{\ln(1-t)\ln\left(1-t(1-z)\right)}{t} \\
&\quad \left.+z\epsilon\int_0^1 \mathrm{d}u\,\frac{\ln^2 u}{(1-uz)}+z\epsilon\int_0^1 \mathrm{d}u\,\ln z\,\frac{\ln u}{(1-uz)}\right].
\end{aligned}
$$

Replacing the definite integrals by the di-and trilogarithm functions Li_2 and Li_3, S_{12}, defined in the Appendix A, we find,

$$
\begin{aligned}
I_{(\alpha=-1)2} &= \frac{1}{\epsilon}\left[\left(\frac{\pi^2}{6}-\mathrm{Li}_2(1-z)\right)\right. \\
&\quad \left.+\epsilon\Big(3\,\zeta_3-2\,\mathrm{Li}_3(1-z)-S_{12}(1-z)+2\,\mathrm{Li}_3(z)-\ln(z)\mathrm{Li}_2(z)\Big)\right]. \qquad (5.42)
\end{aligned}
$$

Following similar steps we can easily obtain $I_{(\alpha=0)2}$ and $I_{(\alpha=1)2}$,

$$
I_{(\alpha=0)2} = -\frac{1}{\epsilon}\left[-z\ln z+\epsilon\Big(-2z\ln z-z\mathrm{Li}_2\left(-\frac{(1-z)}{z}\right)+z\mathrm{Li}_2(1-z)\Big)\right], \qquad (5.43)
$$

$$
\begin{aligned}
I_{(\alpha=1)2} &= \frac{1}{\epsilon}\times\left[\frac{3}{4}(1-z)^2+\epsilon\left\{\left(\frac{11}{4}-\frac{1}{12}\pi^2\right)(1-z)^2-\frac{1}{8}\left[8z^2-6z^2\ln(z)\right.\right.\right. \\
&\quad \left.\left.\left.+14-22z+8z\ln(z)-4z(z-2)\,\mathrm{Li}_2\left(-\frac{(1-z)}{z}\right)\right]\right. \\
&\quad \left.+\frac{1}{4}\Big(-4+5z-2z\ln z-z^2+2\mathrm{Li}_2(1-z)+z^2\ln(z)\Big)\right.
\end{aligned}
$$

$$+\frac{1}{2}(1-z)^2\Big(\mathrm{Li}_2(z)+\ln(z)\ln(1-z)\Big)-\frac{1}{2}(1-z)z\ln(z)\Bigg\}\Bigg]. \quad (5.44)$$

The final result for $TC_{F\gamma}^{(a.1)}$ is thus,

$$\begin{aligned} H\times TC_{F\gamma}^{(a.1)}\left[\frac{1}{y_{13}y_{14}}\right] &= \left(\frac{N^2-1}{2N}\right)\left(\frac{4\pi\mu^2}{M^2}\right)^{2\epsilon}\left(\frac{\alpha_s}{2\pi}\right)\left(\frac{\alpha e_q^2}{2\pi}\right)\frac{1}{\Gamma^2(1-\epsilon)} \\ &\quad\times(1-z)^{-2\epsilon}z^{-\epsilon}(y_{\min})^{-2\epsilon}\frac{\Gamma^2(1-\epsilon)}{\Gamma(1-2\epsilon)} \\ &\quad\times\frac{1}{2}\sum_{\alpha=-1}^{1}A_\alpha(z)\left(I_{\alpha 1}+I_{\alpha 2}\right). \end{aligned} \quad (5.45)$$

Turning to the contribution from the region of phase space where $0<y<y_{\min}$, $TC_{F\gamma}^{(a.2)}$, we note that, as before, some simplifications of the integrand can be made. First,

$$P^a(z,y)\to\frac{P^\epsilon(z)(1-z)}{y},$$

such that $TC_{F\gamma}^{(a.2)}$ is given by,

$$\begin{aligned} TC_{F\gamma}^{(a.2)}\left[\frac{1}{y_{13}y_{14}}\right] &= 4\,P^\epsilon(z)(1-z)^{-2\epsilon}\int_0^{y_{\min}}\mathrm{d}y_{134}\int_0^{y_{\min}}\frac{\mathrm{d}y}{y}\int_0^{(1-z)y_{134}}\mathrm{d}y_{14}\,\frac{1}{y_{14}} \\ &\quad\times\int_{y_{13a}}^{y_{13b}}\mathrm{d}y_{13}\,\frac{1}{y_{13}}\left[(y_{13b}-y_{13})\,(y_{13}-y_{13a})\right]^{-1/2-\epsilon}. \end{aligned}$$

Integrating out y_{13} gives the same factor as before,

$$\pi 16^\epsilon(y_{13b}-y_{13a})^{-2\epsilon}\,\frac{1}{y_{13a}}\frac{\Gamma(1-2\epsilon)}{\Gamma^2(1-\epsilon)}\,F_{21}\left(1,1/2-\epsilon;1-2\epsilon;\frac{y_{13a}-y_{13b}}{y_{13a}}\right).$$

Making the obvious change of variables,

$$y_{14}=v(1-z)\,y_{134},\qquad y=ty_{\min},$$

the regularising phase space factor yields,

$$16^\epsilon(y_{13b}-y_{13a})^{-2\epsilon}=\left[y_{134}^2\,y_{\min}\,zt\,v(1-v)\right]^{-\epsilon}(1-z)^{+\epsilon},$$

where, $y_{13a,b}=\frac{y_{134}}{1-z}(A\pm B)^2$ with,

$$A=\sqrt{(1-z)(1-v)},\qquad B=\sqrt{zvty_{\min}}.$$

Using the relation (5.30) between two hypergeometric functions of argument $\frac{4z}{(1+z)^2}$ and z^2 as we did for the evaluation of $TC_{F\gamma}^{(a.1)}$ we finally obtain a hypergeometric function of the form,

$$F_{21}\left(1, 1+\epsilon; 1-\epsilon; \frac{zvty_{\min}}{(1-z)(1-v)}\right) = 1 + \mathcal{O}(y_{\min}).$$

The remaining integrals are trivial, and putting all the factors back, we find,

$$\begin{aligned} H \times TC_{F\gamma}^{(a.2)}\left[\frac{1}{y_{13}y_{14}}\right] &= \left(\frac{N^2-1}{2N}\right)\left(\frac{4\pi\mu^2}{M^2}\right)^{2\epsilon}\left(\frac{\alpha_s}{2\pi}\right)\left(\frac{\alpha e_q^2}{2\pi}\right)\frac{1}{\Gamma^2(1-\epsilon)} \\ &\times\frac{\Gamma^2(1-\epsilon)}{\Gamma(1-2\epsilon)}\left\{-\frac{1}{\epsilon^3}(y_{\min})^{-3\epsilon}z^{-\epsilon}(1-z)^{-\epsilon}P^{\epsilon}(z)\right\}. \end{aligned} \quad (5.46)$$

Finally, the complete result for this contribution is obtained as the difference of eqs.(5.45) and (5.46), it reads,

$$\begin{aligned} H \times TC_{F\gamma}^{(a)}\left[\frac{1}{y_{13}y_{14}}\right] &= \left(\frac{N^2-1}{2N}\right)\left(\frac{4\pi\mu^2}{M^2}\right)^{2\epsilon}\left(\frac{\alpha_s}{2\pi}\right)\left(\frac{\alpha e_q^2}{2\pi}\right)\frac{1}{\Gamma^2(1-\epsilon)} \\ &\times(1-z)^{-2\epsilon}z^{-\epsilon}(y_{\min})^{-2\epsilon}\frac{\Gamma^2(1-\epsilon)}{\Gamma(1-2\epsilon)} \\ &\times\left\{\frac{1}{2}\sum_{\alpha=-1}^{1}A_\alpha(z)\left(I_{\alpha 1}+I_{\alpha 2}\right)+\frac{1}{\epsilon^3}(y_{\min})^{-\epsilon}(1-z)^{\epsilon}\,P^{\epsilon}(z)\right\}, \end{aligned} \quad (5.47)$$

where the I_α are defined in eqs.(5.40) and (5.41) and the A_α are given by eqs.(5.37) and (5.38).

Summary

In this section we have completed the calculation of all terms contributing to the singular factor from the triple collinear region of phase space. For some of these terms we have here only given the unexpanded form. In Section 5.5, we will develop the remaining unexpanded hypergeometric function in ϵ series up to $\mathcal{O}(\epsilon^3)$ and, after some rearrangements of terms, we will give the final result for the triple collinear contributions to the γ +1 jet rate at $\mathcal{O}(\alpha\alpha_s)$.

5.3 The soft/collinear contribution

The soft/collinear configuration arises when the photon is collinear to the quark and the gluon is soft as illustrated in Fig.3.2.(c). In order to evaluate these contributions, we need first to determine the relevant approximations for the squared matrix elements and phase space in the *soft/collinear* limit and then integrate the unresolved variables over the soft/collinear phase space region.

The soft/collinear region of phase space is defined by,

$$s_{q\gamma} \equiv s_{13} < s_{\min} \quad \text{and} \quad s_{qg} \equiv s_{14} < s_{\min}, \quad s_{\bar{q}g} \equiv s_{24} < s_{\min}, \tag{5.48}$$

as one could have expected. In this region we require $s_{q\gamma} \equiv s_{13} < s_{\min}$ since the photon and the quark are collinear and $s_{qg} \equiv s_{14} < s_{\min}$, $s_{\bar{q}g} \equiv s_{24} < s_{\min}$ as the gluon is soft. Unlike in the triple collinear region of phase space, s_{134} is unconstrained and may also be less than $s_{\min}$ in the soft/collinear region. There is however no overlapping between these two regions because in the triple collinear region we require $s_{24} > s_{\min}$.

In the soft/collinear limit, the photon and the quark cluster to form a new parton, the parent parton Q such that,

$$p_1 + p_3 = p_Q, \tag{5.49}$$

and the energy of the gluon tends to 0 such that $p_4 \to 0$. The photon and the quark carry respectively a fraction z and $(1-z)$ of the parent parton momentum p_Q,

$$p_3 = z\, p_Q, \quad p_1 = (1-z)\, p_Q. \tag{5.50}$$

The invariants $s_{q\bar{q}} \equiv s_{12}$, $s_{\bar{q}\gamma} \equiv s_{23}$ are given by the following,

$$s_{12} = (1-z)\, s_{Q2} \equiv (1-z)\, M^2 \qquad \text{and} \qquad s_{23} = z\, s_{Q2} \equiv z\, M^2, \tag{5.51}$$

where M is the invariant mass of the final state.

In this section we will present the factorization of matrix element squared and phase space in the soft/collinear limit defined above and evaluate the soft/collinear contribution to the differential γ +1 jet differential cross section.

5.3.1 The soft/collinear limit of the $|\mathcal{M}|^2$

In the soft/collinear limit defined above, the matrix element squared for the scattering of a quark-antiquark pair with a photon and a gluon factorizes,

$$|\mathcal{M}_{1234}|^2 \to P^{soft/col}_{134\to Q}(z, s_{24}, s_{13}, s_{14}, s_{134})\ |\mathcal{M}_{Q\bar{q}}|^2.$$

As usual, $|\mathcal{M}_{Q\bar{q}}|^2$ is the two-particle matrix element squared, $P^{soft/col}_{134\to Q}(z, s_{24}, s_{13}, s_{14}, s_{134})$ defines the soft/collinear approximation to the squared matrix elements. This soft/collinear factor is obtained by setting $y = 0$ in the triple collinear matrix element squared, $P_{134\to Q}$, given in eq.(5.5) and is therefore,

$$P^{soft/col}_{134\to Q}(z, s_{24}, s_{13}, s_{14}, s_{134}) \equiv \frac{4}{s_{13}s_{14}s_{24}}\left((1-z) + \frac{s_{14} + (1-z)s_{13}}{s_{134}}\right) P^{\epsilon}(z). \qquad (5.52)$$

In terms of the scaled invariants,

$$P^{soft/col}_{134\to Q}(z, y_{24}, y_{13}, y_{14}, y_{134}) \equiv \frac{4}{M^6 y_{13}y_{14}y_{24}}\left((1-z) + \frac{y_{14} + (1-z)y_{13}}{y_{134}}\right) P^{\epsilon}(z). \qquad (5.53)$$

5.3.2 The soft/collinear limit of the phase space

We would like to determine the soft/collinear limit of the four-particle phase space as given by eq.(B.6). In this limit the 4-particle phase space is expected to factorize into a soft/collinear factor $\mathrm{d}R^{(d)}_{soft}$ and the known 2-particle phase space $\mathrm{d}R^{(d)}_2$. Using the definitions of s_{12}, s_{23}, s_{24} in the soft/collinear limit, given in eq.(5.51), the product of the integration variables $\{\mathrm{s_{ij}}\}$ in the 4-particle phase space can be rewritten,

$$\underbrace{\mathrm{d}s_{13}\ \mathrm{d}s_{24}\ \mathrm{d}s_{14}}\ \mathrm{d}s_{12}\ \mathrm{d}s_{23}\ \mathrm{d}s_{34}\ \delta\left(s_{12} + s_{13} + s_{14} + s_{23} + s_{24} + s_{34} - M^2\right)$$
$$\to\ \underbrace{\mathrm{d}y_{13}\ \mathrm{d}y_{24}\ \mathrm{d}y_{14}}\ \mathrm{d}z\ \mathrm{d}y_{34}\ \mathrm{d}y_{134}\delta(y_{134} - y_{13} - y_{14} - y_{34})\mathrm{d}s_{Q2}\ \delta(s_{Q2} - M^2)M^{10}\ ,$$

where we introduced the integration variable y_{134} via a δ-function, just as we did in the calculation of the triple collinear contribution in the previous section. Replacing the

factors of 2π, we find that,

$$(2\pi)^{4-3d}\mathrm{d}R_4^{(d)}(M,p_2,p_2,p_3,p_4) \to (2\pi)^{2-d}\mathrm{d}R_2^{(d)}(M,p_Q,p_2)\times\underbrace{(2\pi)^{2-2d}\mathrm{d}R_{soft/col}^{(d)}(p_1,p_2,p_3,p_4)}_{\mathrm{d}P_{soft/col}^{(d)}(p_1,p_2,p_3,p_4)}, \tag{5.54}$$

where,

$$\begin{aligned}\mathrm{d}R_{soft/col}^{(d)}(p_1,p_2,p_3,p_4) &= 2^{-d}\,\mathrm{d}\Omega_{d-2}\,\mathrm{d}\Omega_{d-3}\,M^6\,[M^2]^{d-4}\\ &\times \mathrm{d}y_{134}\,\mathrm{d}y_{13}\,\mathrm{d}y_{14}\,\mathrm{d}y_{34}\,\mathrm{d}z\,\mathrm{d}y_{24}\,\delta(y_{134}-y_{13}-y_{14}-y_{34})\\ &\times\Big[-\Delta_4''\Big]^{\frac{d-4}{2}}\Big[-\Delta_4''\Big]^{-\frac{1}{2}}.\end{aligned} \tag{5.55}$$

This is similar to the triple collinear factor given by eq.(5.5) with y replaced by y_{24}.

As y_{134} is unconstrained in this region of phase space, we choose to rewrite Δ_4'' as a quadratic in y_{134}. In other words when performing the phase space integrals we will first integrate over y_{134}. With the definitions of the invariants y_{12} and y_{23} in the soft/collinear region of phase space,

$$-\Delta_4'' = \frac{1}{16}\Big((1-z)^2(y_{134b}-y_{134})(y_{134}-y_{134a})\Big),$$

with $y_{134a,b}$ given by,

$$y_{134a,b} = \frac{1}{1-z}\Big(y_{13}(1-z)+y_{14}+y_{13}y_{14}\pm 2\sqrt{y_{13}y_{14}y_{24}z}\Big).$$

5.3.3 The soft/collinear limit of the differential cross section

As in the triple collinear limit, the differential cross section factorizes in the soft/collinear limit. It can be written as the product of σ_0, the two-particle cross section and a singular soft/collinear factor, $SC_{F\gamma}\mathrm{d}z$,

$$\mathrm{d}\sigma_4 \to SC_{F\gamma}\mathrm{d}z\times\sigma_0, \tag{5.56}$$

where,

$$SC_{F\gamma}\mathrm{d}z \equiv \left(\frac{N^2-1}{2N}\right)\left(\frac{\alpha_s}{2\pi}\right)\left(\frac{\alpha e_q^2}{2\pi}\right)4(2\pi)^4\left(\mu^2\right)^{2\epsilon}\int \mathrm{d}P_{soft/col}^{(d)}|\mathcal{M}_{soft/col}|^2,$$

where,

$$|\mathcal{M}_{soft/col}|^2 \equiv P^{soft/col}_{134\to Q}(z, s_{24}, s_{13}, s_{14}, s_{134}),$$

and,

$$\mathrm{d}P^{(d)}_{soft/col} = (2\pi)^{2-2d}\mathrm{d}R^{(d)}_{soft/col}(p_1, p_2, p_3, p_4). \tag{5.57}$$

To evaluate the soft/collinear differential factor $SC_{F\gamma}\mathrm{d}z$ we need to integrate $|\mathcal{M}_{soft/col}|^2$, given by eq.(5.52) over the soft/collinear phase space given by eq.(5.55).

As in the previous section, it is useful to organize the calculation in terms of the behaviour of the matrix elements with respect to the invariants. We therefore decompose $SC_{F\gamma}\mathrm{d}z$ as follows,

$$SC_{F\gamma}\mathrm{d}z = H\mathrm{d}z \times \left(SC^{(a)}_{F\gamma}\left[\frac{1}{y_{13}y_{14}y_{24}}\right] + SC^{(b)}_{F\gamma}\left[\frac{1}{y_{13}y_{14}y_{24}y_{134}}\right]\right), \tag{5.58}$$

where, $SC^{(a)}_{F\gamma}\left[\frac{1}{y_{13}y_{14}y_{24}}\right]$ and $SC^{(b)}_{F\gamma}\left[\frac{1}{y_{13}y_{14}y_{24}y_{134}}\right]$ are respectively obtained by integrating the first and second term of $P^{soft/col}_{134\to Q}$ as given in eq.(5.52) over the soft/collinear phase space.

Before we present the calculation of each of these two contributions to $SC_{F\gamma}$ let us note the following. As we mentioned before we will write the Gram determinant as a quadratic in y_{134} and carry out the y_{134} integration first. The integrations over the other unresolved variables y_{13}, y_{14} and y_{24} will be performed subsequently. Unlike for the triple collinear phase space region, the positivity requirement of $-\Delta''_4$ only fixes the boundaries on the y_{134} integral and does not constrain the other integrations which are therefore bounded by the slicing parameter $y_{\min}$.

Returning to our derivation of the soft/collinear cross section, we find that the contribution $SC^{(a)}_{F\gamma}\left[\frac{1}{y_{13}y_{14}y_{24}}\right]$ reads,

$$\begin{aligned} SC^{(a)}_{F\gamma}\left[\frac{1}{y_{13}y_{14}y_{24}}\right] &= 4\int_0^{y_{\min}}\frac{\mathrm{d}y_{13}}{y_{13}}\int_0^{y_{\min}}\frac{\mathrm{d}y_{24}}{y_{24}}\int_0^{y_{\min}}\frac{\mathrm{d}y_{14}}{y_{14}}P^{\epsilon}(z)(1-z) \\ &\quad\times\int_{y_{134a}}^{y_{134b}}\mathrm{d}y_{134}\left[(1-z)^2(y_{134b}-y_{134})(y_{134}-y_{134a})\right]^{-1/2-\epsilon}. \end{aligned}$$

Performing the y_{134} integration, and using the usual identity for Γ functions, we obtain the regularising phase space factor,

$$\frac{\Gamma^2(1/2-\epsilon)}{\Gamma(1-2\epsilon)}\left(y_{134b}-y_{134a}\right)^{-2\epsilon}(1-z)^{-2\epsilon-1} = \pi\left[z y_{13}y_{14}y_{24}\right]^{-\epsilon}(1-z)^{-1}\frac{\Gamma(1-2\epsilon)}{\Gamma^2(1-\epsilon)}.$$

The other integrations are now trivial, such that,

$$\begin{aligned} H\times SC^{(a)}_{F\gamma}\left[\frac{1}{y_{13}y_{14}y_{24}}\right] &= -\left(\frac{N^2-1}{2N}\right)\left(\frac{4\pi\mu^2}{M^2}\right)^{2\epsilon}\left(\frac{\alpha_s}{2\pi}\right)\left(\frac{\alpha e_q^2}{2\pi}\right)\frac{1}{\Gamma^2(1-\epsilon)} \\ &\quad\times\frac{1}{\epsilon^3}\left(y_{\min}\right)^{-3\epsilon}P^{\epsilon}(z)\,z^{-\epsilon}. \end{aligned} \tag{5.59}$$

For $SC^{(b)}_{F\gamma}\left[\frac{1}{y_{13}y_{14}y_{24}y_{134}}\right]$ on the other hand we have to evaluate,

$$\begin{aligned} SC^{(b)}_{F\gamma}\left[\frac{1}{y_{13}y_{14}y_{24}y_{134}}\right] &= 4\int_0^{y_{\min}}\frac{\mathrm{d}y_{13}}{y_{13}}\int_0^{y_{\min}}\frac{\mathrm{d}y_{24}}{y_{24}}\int_0^{y_{\min}}\frac{\mathrm{d}y_{14}}{y_{14}}\times P^{\epsilon}(z)\left[y_{14}+y_{13}(1-z)\right] \\ &\quad\int_{y_{134a}}^{y_{134b}}\frac{\mathrm{d}y_{134}}{y_{134}}\left[(1-z)^2(y_{134b}-y_{134})(y_{134}-y_{134a})\right]^{-1/2-\epsilon}. \end{aligned}$$

Because of the factor of $\{\frac{1}{y_{134}}\}$, this integral is rather more tricky to evaluate.

As in the case of the evaluation of $TC^{(a)}_{F\gamma}$ in the previous section, the first phase space integration gives rise to a hypergeometric function,

$$\begin{aligned} I_{134} &\equiv \int_{y_{134a}}^{y_{134b}}\frac{\mathrm{d}y_{134}}{y_{134}}\left[(y_{134b}-y_{134})(y_{134}-y_{134a})\right]^{-1/2-\epsilon} \\ &= \pi\frac{\Gamma(1-2\epsilon)}{\Gamma^2(1-\epsilon)}16^{\epsilon}\left(y_{134b}-y_{134a}\right)^{-2\epsilon}\frac{1}{y_{134a}}F_{21}\left(1,1/2-\epsilon,1-2\epsilon;\frac{y_{134a}-y_{134b}}{y_{134a}}\right). \end{aligned}$$

With the change of variables, $y_{24}=t y_{\min}$, the argument of the hypergeometric function reads,

$$\frac{y_{134a}-y_{134b}}{y_{134a}} = \frac{-4\sqrt{z y_{13}y_{14}t y_{\min}}}{y_{14}+y_{13}(1-z)+y_{13}t y_{\min}-2\sqrt{z y_{13}y_{14}t y_{\min}}},$$

while,

$$\frac{1}{y_{134a}} = \frac{(1-z)}{y_{14}+y_{13}(1-z)+y_{13}t y_{\min}-2\sqrt{z y_{13}y_{14}t y_{\min}}}.$$

To simplify the notations we temporarily make the identifications $A\equiv y_{14}+y_{13}(1-z)$ and $\alpha\equiv z y_{13}y_{14}t$. Neglecting all terms of $\mathcal{O}(y_{\min})$,

$$I_{134}\times 4\left[y_{14}+y_{13}(1-z)\right] = \left(z y_{14}y_{13}t y_{\min}\right)^{-\epsilon}P^{\epsilon}(z)\,4\pi\frac{\Gamma(1-2\epsilon)}{\Gamma^2(1-\epsilon)}$$

$$\times \frac{A}{A-2\sqrt{y_{\min}\alpha}}\, F_{21}\left(1,1/2-\epsilon,1-2\epsilon;\frac{-4\sqrt{y_{\min}\alpha}}{A-2\sqrt{y_{\min}\alpha}}\right)$$

$$\equiv\ 4\pi(z\,y_{14}\,y_{13}\,t\,y_{\min})^{-\epsilon}\,P^{\epsilon}(z)\,\frac{\Gamma(1-2\epsilon)}{\Gamma^2(1-\epsilon)}\times I'_{134}.$$

A priori it seems that I'_{134} contains terms of $\mathcal{O}(\sqrt{y_{\min}})$ which we have not encountered anywhere else in this calculation. In fact, one could argue whether it is "allowed" to neglect terms of this type at all. Fortunately it turns out that I'_{134} does not contain explicit terms of $\mathcal{O}(\sqrt{y_{\min}})$ but $I'_{134}=1+\mathcal{O}(y_{\min})$ as we show below.

By definition of the hypergeometric function we have,

$$F_{21}\left(1,1/2-\epsilon,1-2\epsilon;\frac{-4\sqrt{y_{\min}\alpha}}{A-2\sqrt{y_{\min}\alpha}}\right) = \sum_{n=0}^{1}\left[\frac{-4\sqrt{y_{\min}\alpha}}{A-2\sqrt{y_{\min}\alpha}}\right]^n \frac{\Gamma(n+1/2-\epsilon)\Gamma(1-2\epsilon)}{\Gamma(1/2-\epsilon)\Gamma(n+1-2\epsilon)}$$

$$= 1-4\frac{\sqrt{y_{\min}\alpha}C}{A}+\mathcal{O}(y_{\min}),$$

where we have truncated the sum at $n=1$ since for larger values of n the terms are of $\mathcal{O}(y_{\min})$. The coefficient C is easily evaluated,

$$C = \frac{\Gamma(3/2-\epsilon)\Gamma(1-2\epsilon)}{\Gamma(1/2-\epsilon)\Gamma(2-2\epsilon)}=\frac{1}{2}$$

such that inserting the expanded hypergeometric function back into I'_{134} we have,

$$I'_{134} = \left(1-2\frac{\sqrt{y_{\min}\alpha}}{A}\right)^{-1}\left(1-2\frac{\sqrt{y_{\min}\alpha}}{A}\right)=1+\mathcal{O}(y_{\min}).$$

Setting I'_{134} to 1, the evaluation of the remaining integrals is immediate and we obtain,

$$H\times SC^{(b)}_{F\gamma}\left[\frac{1}{y_{13}y_{14}y_{24}y_{134}}\right] = -\left(\frac{N^2-1}{2N}\right)\left(\frac{4\pi\mu^2}{M^2}\right)^{2\epsilon}\left(\frac{\alpha_s}{2\pi}\right)\left(\frac{\alpha e_q^2}{2\pi}\right)\frac{1}{\Gamma^2(1-\epsilon)}$$

$$\times\frac{1}{\epsilon^3}\,(y_{\min})^{-3\epsilon}P^{\epsilon}(z)z^{-\epsilon}. \qquad (5.60)$$

Summary

Collecting the two terms, the full contribution to the $\gamma+1$ jet differential cross section arising when the photon is collinear to the quark and the gluon is soft reads,

$$SC_{F\gamma}\mathrm{d}z = \left(\frac{N^2-1}{2N}\right)\left(\frac{4\pi\mu^2}{M^2}\right)^{2\epsilon}\left(\frac{\alpha_s}{2\pi}\right)\left(\frac{\alpha e_q^2}{2\pi}\right)\frac{1}{\Gamma^2(1-\epsilon)}\mathrm{d}z$$

$$\times \left[-\frac{2}{\epsilon^3} \left(y_{\min}\right)^{-3\epsilon} z^{-\epsilon} P^{\epsilon}(z) \right]. \tag{5.61}$$

5.4 The double single collinear contribution

The double single collinear region of phase space is defined by the following constraints on the invariants,

$$s_{q\gamma} \equiv s_{13} < s_{\min}, \qquad s_{\bar{q}g} \equiv s_{24} < s_{\min}, \tag{5.62}$$

with the additional requirement,

$$s_{qg} \equiv s_{14} > s_{\min}, \tag{5.63}$$

as the gluon is collinear to the antiquark but is *not* soft. This configuration occurs when simultaneously, the photon and the quark form a collinear pair while the gluon and the antiquark are also collinear. This is illustrated in Fig.3.2.(c).

In order to evaluate these contributions we need first to determine the relevant approximations for the squared matrix elements and phase space in the *double single collinear* limit and then integrate the unresolved variables over the double single collinear phase space region.

In this limit, the photon and the quark cluster to form a new parent parton Q such that,

$$p_1 + p_3 = p_Q, \tag{5.64}$$

while the gluon and the antiquark cluster to form a new parent parton, $\bar{Q}$ with,

$$p_2 + p_4 = p_{\bar{Q}}, \tag{5.65}$$

The photon and the quark carry respectively a fraction z and $(1-z)$ of the parent parton momentum p_Q,

$$p_3 = z\ p_Q, \qquad p_1 = (1-z)\ p_Q. \tag{5.66}$$

whereas the gluon and the antiquark each carry a fraction y and $1-y$ of the parent momentum $p_{\bar{Q}}$ such that,

$$p_4 = y\ p_{\bar{Q}}, \qquad p_2 = (1-y)\ p_{\bar{Q}}. \tag{5.67}$$

In this section we will present the factorization properties of the four-particle final state matrix elements and phase space in the double collinear limit and evaluate the corresponding differential cross section. We will however see that the factorization procedure is slightly different than in the previous cases (triple collinear, soft/collinear contributions). In particular, we will see that the invariants which are not less than $s_{\min}$ need to be defined slightly differently when evaluating the matrix elements and the phase space in the double single collinear limit.

5.4.1 The double single collinear limit of the $|\mathcal{M}|^2$

In the double single collinear limit defined by eqs.(5.66, 5.67), the invariants $s_{q\bar{q}} \equiv s_{12}$, $s_{qg} \equiv s_{14}$, $s_{\bar{q}\gamma} \equiv s_{23}$ and $s_{\gamma g} = s_{34}$ can be redefined as follows,

$$\begin{aligned} s_{12} &= (1-y)(1-z)\, s_{Q\bar{Q}} \equiv (1-y)(1-z)\, M^2 \\ s_{14} &= y(1-z)\, s_{Q\bar{Q}} \equiv y(1-z)\, M^2 \\ s_{23} &= z(1-y)\, s_{Q\bar{Q}} \equiv z(1-y)\, M^2 \\ s_{34} &= yz\, s_{Q\bar{Q}} \equiv yz\, M^2, \end{aligned} \tag{5.68}$$

where M is the invariant mass of the final state.

Note that unlike in the soft/collinear region, s_{34} is here precisely defined. Consequently the triple invariant s_{134} is also fixed, $s_{134} = s_{13} + s_{14} + s_{34} = yM^2$. This appears to reduce the number of independent variables by one, however, we will show that, correctly integrating out y_{134} yields the same result than considering it equal to y.

Using the redefinitions of the invariants given by eq.(5.68), the four particle matrix element squared factorizes in the double single collinear limit as follows,

$$|\mathcal{M}_{1234}|^2 \to P_{13\to Q;24\to\bar{Q}}(z, y, s_{13}, s_{24}))|\mathcal{M}_{Q\bar{Q}}|^2 \tag{5.69}$$

with,

$$\begin{aligned} P_{13\to Q;24\to\bar{Q}}(z, y, s_{13}, s_{24})) &= 4P_{13\to Q}(z, s_{13})P_{24\to\bar{Q}}(y, s_{24}) \\ &= \frac{4}{M^4}\frac{1}{y_{13}}P^{\epsilon}(z)\frac{1}{y_{24}}P^{\epsilon}(y). \end{aligned} \tag{5.70}$$

In other words, the double single collinear factor is the product of two simple collinear factors multiplying the two-particle squared matrix element $|\mathcal{M}_{Q\bar{Q}}|^2$.

5.4.2 The double single collinear limit of the phase space

In the double single collinear limit $s_{13},\ s_{24} \leq s_{\min}$, and $s_{14} > s_{\min}$, the four-particle phase space factorizes into a double collinear phase space factor: $\mathrm{d}R^{(d)}_{double}(p_1, p_3, p_2, p_4)$ and the two-particle phase space, $\mathrm{d}R^{(d)}_2(M, p_Q, p_{\bar{Q}})$. However to write the four-particle phase space as the product of $\mathrm{d}R^{(d)}(M, p_Q, p_{\bar{Q}})$ and $\mathrm{d}R^{(d)}_{double}$ one needs to be careful.

In fact, if one uses the redefinitions of the invariants $\mathrm{s_{ij}}$ given by eq.(5.68), there are too many integration variables present in the four particle phase space to define $\mathrm{d}z$ and $\mathrm{d}y$. To show the factorization property of the four-particle phase space in the double single collinear limit we proceed therefore as follows:

We first insert $\int \mathrm{d}s_{Q\bar{Q}}\ \delta\left(s_{Q\bar{Q}} - M^2\right)$ in the four-particle phase space (B.6) in order to obtain the necessary δ-function to build $\mathrm{d}R^d_2(M, p_Q, p_{\bar{Q}})$. We then consider the following redefinitions of the invariants,

$$\begin{aligned} y_{12} &= 1 - y_{13} - y_{14} - y_{23} - y_{24} - y_{34}, \\ y_{23} &= y_{234} - y_{34} - y_{24}, \\ y_{34} &= y_{134} - y_{13} - y_{14}, \\ y_{14} &= y(1-z), \\ y_{234} &= z. \end{aligned} \tag{5.71}$$

The integration variables are thus, z, y, y_{13}, y_{24} and y_{134}. We then write $(-\Delta''_4)$ as a quadratic in y_{134} and integrate over y_{134}. When discussing the factorization of the matrix elements, we saw that y_{34} and hence y_{134} were fixed and replaced them respectively by zy and y. However, in order to see the factorization of the phase space we are forced to integrate over y_{134}. A priori there seems to be an inconsistency in the procedure used to obtain the factorization properties of matrix elements and phase space.

A closer look enables us to assert that there is no inconsistency in this procedure. In fact, the boundaries of the y_{134} integration turn out to be $y_{134a,b} = y \pm \mathcal{O}(y_{\min})$. Hence by replacing y_{134} by y in order to obtain the double single collinear matrix elements we make an error of $\mathcal{O}(y_{\min})$, which we do throughout this calculation and it is therefore a consistent approximation to make.

With the definitions of the invariants given by eq.(5.71),

$$-\Delta_4'' = \frac{1}{16}\left[(1-z)^2(y_{134}-y_{134a})(y_{134b}-y_{134})\right],$$

where, up to $\mathcal{O}(y_{\min})$,

$$y_{134a,b} = y \pm 2\sqrt{\frac{y_{13}y_{24}zy(1-y)}{(1-z)}}.$$

Furthermore, with the same redefinitions of the variables y_{ij} the measure of the four-particle phase space becomes,

$$\begin{aligned}
&\int \underbrace{\mathrm{d}s_{13}\,\mathrm{d}s_{24}}\ \mathrm{d}s_{14}\,\mathrm{d}s_{12}\,\mathrm{d}s_{23}\,\mathrm{d}s_{34}\,\delta\left(s_{12}+s_{13}+s_{14}+s_{23}+s_{24}+s_{34}-M^2\right)\\
&\quad\to \underbrace{\mathrm{d}s_{13}\,\mathrm{d}s_{24}}\int \mathrm{d}s_{134}\,\mathrm{d}z\,\mathrm{d}y\int \mathrm{d}s_{Q\bar{Q}}\delta(s_{Q\bar{Q}}-M^2)\,M^4\,,\\
&\quad\to \underbrace{\mathrm{d}y_{13}\,\mathrm{d}y_{24}}\int \mathrm{d}y_{134}\,\mathrm{d}z\,\mathrm{d}y\int \mathrm{d}s_{Q\bar{Q}}\delta(s_{Q\bar{Q}}-M^2)\,M^{10}\,.
\end{aligned}$$

Changing variables once more, considering $y_{134} = (1-z)(x(y_{134b}-y_{134a})+y_{134a})$, in this limit the four-particle phase space reads,

$$\mathrm{d}R_4^{(d)}(M,p_2,p_2,p_3,p_4) \to \mathrm{d}R_2^{(d)}(M,p_Q,p_{\bar{Q}}) \times \mathrm{d}R_{double}^{(d)}(p_1,p_2,p_3,p_4), \tag{5.72}$$

where,

$$\begin{aligned}
\mathrm{d}R_{double}^{(d)}(p_1,p_2,p_3,p_4) &= 2^{-d}\mathrm{d}\Omega_{d-2}\,\mathrm{d}\Omega_{d-3}\ \mathrm{d}y_{13}\,\mathrm{d}y_{24}\,\mathrm{d}z\mathrm{d}yM^4\,[M^2]^{d-4}\\
&\quad\times\left[16z(1-z)(y(1-y)\,y_{13}y_{24}\right]^{-\epsilon}\underbrace{\int_0^1 \mathrm{d}x\,[x(1-x)]^{-1/2-\epsilon}}_{=16^{\epsilon}\pi\frac{\Gamma(1-2\epsilon)}{\Gamma^2(1-\epsilon)}},\\
&= \pi 2^{-d}\,\mathrm{d}\Omega_{d-2}\,\mathrm{d}\Omega_{d-3}\ \mathrm{d}y_{13}\,\mathrm{d}y_{24}\,\mathrm{d}z\mathrm{d}yM^4\,[M^2]^{d-4}\\
&\quad\times\left[z(1-z)(y(1-y)\,y_{13}y_{24}\right]^{-\epsilon}\frac{\Gamma(1-2\epsilon)}{\Gamma^2(1-\epsilon)}.
\end{aligned}$$

This x integration plays the role of an angular integral over the polar angle between the $(q-\gamma)$ and $(\bar{q}-g)$ planes. Replacing the factors of 2π and integrating out the unresolved angular variables, we find that,

$$\begin{aligned} \mathrm{d}P^{(d)}_{double}(p_1,p_3,p_2,p_4) &= (2\pi)^{2-2d}\mathrm{d}R^{(d)}_{double}(p_1,p_3,p_2,p_4) \\ &= \frac{(4\pi)^{2\epsilon}M^4}{M^{4\epsilon}(16\pi^2)^2\Gamma^2(1-\epsilon)}\Big(\mathrm{d}y_{13}\,\mathrm{d}z\Big[z(1-z)y_{13}\Big]^{-\epsilon}\Big) \\ &\quad\times\Big(\mathrm{d}y_{24}\,\mathrm{d}y\Big[y(1-y)y_{24}\Big]^{-\epsilon}\Big), \end{aligned} \tag{5.73}$$

which is exactly the product of two single collinear phase space factors as one could have expected.

5.4.3 The double single collinear limit of the differential cross section

As with the previous double unresolved contributions, the integration of the resolved two particle matrix elements over the two particle phase space yields a factor of σ_0. This is multiplied by the integral of the approximation of the unresolved matrix elements over the unresolved phase space. Explicitly, we have,

$$\mathrm{d}\sigma_4 \to DC_{F\gamma}\mathrm{d}z \times \sigma_0, \tag{5.74}$$

where,

$$DC_{F\gamma}\mathrm{d}z = \left(\frac{N^2-1}{2N}\right)\left(\frac{\alpha_s}{2\pi}\right)\left(\frac{\alpha e_q^2}{2\pi}\right)4(2\pi)^4\left(\mu^2\right)^{2\epsilon}\int \mathrm{d}P^{(d)}_{double}|\mathcal{M}_{double}|^2, \tag{5.75}$$

with,

$$|\mathcal{M}_{double}|^2 = P_{13\to Q;24\to\bar{Q}}(z,y,s_{13},s_{24}). \tag{5.76}$$

Identifying terms, we find,

$$\begin{aligned} DC_{F\gamma} &= \left(\frac{N^2-1}{2N}\right)\left(\frac{4\pi\mu^2}{M^2}\right)^{2\epsilon}\left(\frac{\alpha_s}{2\pi}\right)\left(\frac{\alpha e_q^2}{2\pi}\right)z^{-\epsilon}(1-z)^{-\epsilon}P^{\epsilon}(z)\frac{1}{\Gamma^2(1-\epsilon)} \\ &\quad\times\underbrace{\int_0^{y_{\min}}\mathrm{d}y_{13}\,y_{13}^{-\epsilon-1}\int_0^{y_{\min}}\mathrm{d}y_{24}\,y_{24}^{-\epsilon-1}\int_{\frac{y_{\min}}{1-z}}^{1}\mathrm{d}y\;[y(1-y)]^{-\epsilon}\;P^{\epsilon}(y)}_{\equiv I_{col}}. \end{aligned}$$

The constraint $y_{14} > y_{\min}$ fixes the lower boundary of the y integral to be $\frac{y_{\min}}{1-z}$ since in the double single collinear region $y_{14} = y(1-z)$. I_{col} is straightforward to calculate and is given by,

$$I_{col} = \frac{(y_{\min})^{-2\epsilon}}{\epsilon^3}\left[2(y_{\min})^{-\epsilon}(1-z)^{\epsilon} - \frac{(1-\epsilon)(4-\epsilon)}{2(1-2\epsilon)}\frac{\Gamma^2(1-\epsilon)}{\Gamma(1-2\epsilon)}\right].$$

The double single collinear contribution to the differential cross section then finally reads,

$$DC_{F\gamma} = \left(\frac{N^2-1}{2N}\right)\left(\frac{4\pi\mu^2}{M^2}\right)^{2\epsilon}\left(\frac{\alpha_s}{2\pi}\right)\left(\frac{\alpha e_q^2}{2\pi}\right)\frac{1}{\Gamma^2(1-\epsilon)}z^{-\epsilon}(1-z)^{-\epsilon}P^{\epsilon}(z)$$
$$\times\frac{(y_{\min})^{-2\epsilon}}{\epsilon^3}\left[2(y_{\min})^{-\epsilon}(1-z)^{\epsilon} - \frac{(1-\epsilon)(4-\epsilon)}{2(1-2\epsilon)}\frac{\Gamma^2(1-\epsilon)}{\Gamma(1-2\epsilon)}\right]. \quad (5.77)$$

With the evaluation of the double single collinear contributions we have completed the evaluation of all two-particle unresolved real contributions to the $\gamma + 1$ jet rate at $\mathcal{O}(\alpha\alpha_s)$. In the next section, we will present a compact answer for the sum of these three contributions.

5.5 Sum of the real contributions

In this forthcoming section we present the results obtained for the ϵ expansions of the three double unresolved real contributions to the differential cross section; the *triple collinear*, the *soft/collinear* and the *double single collinear* contributions.

We first note that the ϵ expansion up to $\mathcal{O}(\epsilon^2)$ of $F_{21}(1, 1-\epsilon; 2-2\epsilon; 1-z)$ is given by,

$$\begin{aligned} F_{21}(1,1-\epsilon;2-2\epsilon;1-z) &= \frac{\Gamma(2-2\epsilon)}{\Gamma^2(1-\epsilon)}\int_0^1 \mathrm{d}t\, t^{-\epsilon}(1-t)^{-\epsilon}[1-t(1-z)]^{-1} \\ &= \frac{\Gamma(1-2\epsilon)}{\Gamma^2(1-\epsilon)}\frac{(1-2\epsilon)}{(1-z)}\Bigg[-\ln z \\ &\quad +\epsilon\left(2\mathrm{Li}_2(1-z)+\frac{1}{2}\ln^2(z)\right) \\ &\quad +\epsilon^2\left(4\mathrm{Li}_3(1-z)-2\mathrm{S}_{12}(1-z)-\frac{1}{6}\ln^3(z)\right. \end{aligned}$$

$$-2\mathrm{Li}_2(1-z)\ln(z)+\frac{\pi^2}{6}\ln(z)\Big)\Big]. \tag{5.78}$$

This is needed for some terms of the triple collinear contributions.

Collecting together the results for the triple collinear contribution to the differential cross section (equations (5.17), (5.18), (5.24), (5.19) and (5.47)) and expanding the expressions as series in ϵ where we have not done it so far, we find,

$$\begin{aligned}
\frac{1}{\sigma_0}\frac{\mathrm{d}\sigma_{triple}}{\mathrm{d}z} &= TC_{F\gamma} \\
&= \frac{1}{\Gamma^2(1-\epsilon)}\left(\frac{N^2-1}{2N}\right)\left(\frac{4\pi\mu^2}{M^2}\right)^{2\epsilon}\left(\frac{\alpha_s}{2\pi}\right)\left(\frac{\alpha e_q^2}{2\pi}\right) \\
&\times\Bigg\{\frac{1}{\epsilon^2}\Bigg[\ln(z)\left(1-\frac{z}{2}\right)+1-\frac{z}{4}-\frac{3\,P(z)}{2}+2\,\ln(1-z)P(z)-2\,\ln(y_{\min})P^{\epsilon}(z)\Bigg] \\
&+\frac{1}{\epsilon}\Bigg[\ln(z)\ln(1-z)\,(-2+z-2\,P(z))+\ln(z)\left(-1-\frac{5\,z}{4}+\frac{3\,P^{\epsilon}(z)}{2}\right) \\
&\quad+\ln^2(z)\left(-\frac{3}{2}+\frac{3\,z}{4}\right)-3\,\ln^2(1-z)P(z)-\frac{1}{4}+\frac{11\,z}{4}-\frac{7\,P(z)}{2} \\
&\quad+\ln(1-z)\left(-2-\frac{3\,z}{2}+3\,P(z)\right)+\mathrm{Li}_2(1-z)\,(-2+z-P(z))+\frac{\pi^2P(z)}{2} \\
&\quad+\ln(y_{\min})\Big(-2+\frac{5\,z}{2}+3\,P(z)+\ln(z)\,(-2+z+2\,P(z)) \\
&\quad-2\,\ln(1-z)P(z)\Big)+\ln^2(y_{\min})\,5P(z)\Bigg] \\
&-1+\pi^2\left(-\frac{1}{3}-\frac{5\,z}{12}+\frac{P(z)}{2}\right)+\ln(z)\left(\frac{13}{4}-\frac{17\,z}{4}+\frac{7\,P(z)}{2}\right) \\
&+\ln(z)\pi^2\left(-\frac{1}{3}+\frac{z}{6}-\frac{P(z)}{3}\right)+\ln^2(z)\left(\frac{1}{2}+\frac{17\,z}{8}-\frac{3\,P(z)}{4}\right) \\
&+\ln(z)\ln(1-z)\left(2+\frac{9\,z}{2}-3\,P(z)\right)+\ln(z)\mathrm{Li}_2(1-z)\,(4-2\,z) \\
&+\ln^2(1-z)\left(2+\frac{5\,z}{2}-3\,P(z)\right)+\ln(1-z)\mathrm{Li}_2(1-z)\,(4-2\,z+2\,P(z)) \\
&+\frac{25\,z}{4}-7\,P(z)+\ln^3(z)\left(\frac{7}{6}-\frac{7\,z}{12}\right)+\ln^2(z)\ln(1-z)\left(3-\frac{3\,z}{2}+P(z)\right)
\end{aligned}$$

$$
\begin{aligned}
&+\ln(z)\ln^2(1-z)\,(2-z+3\,P(z))+\ln(1-z)\left(\frac{1}{2}-\frac{11\,z}{2}+7\,P(z)\right)\\
&+\mathrm{Li}_3(1-z)\,(-4+2\,z-2\,P(z))+S_{12}(1-z)\,(2-z-3\,P(z))\\
&+\frac{7\,\ln^3(1-z)P(z)}{3}+4z\,\mathrm{Li}_2(1-z)+9\,P(z)\zeta(3)-\frac{4\,\ln(1-z)\pi^2P(z)}{3}\\
&+\ln(y_{\min})\Bigg(\mathrm{Li}_2(1-z)\,(4-2\,z+2\,P(z))+\ln(z)\ln(1-z)\,(4-2\,z+2\,P(z))\\
&\qquad+\ln^2(z)\left(3-\frac{3\,z}{2}-P(z)\right)-\frac{2\,\pi^2P(z)}{3}+\ln(1-z)\,(4+z-6\,P(z))\\
&\qquad+\ln(z)\left(2+\frac{z}{2}-3\,P(z)\right)+5\,(\ln(1-z))^2\,P(z)+\frac{1}{2}-\frac{11\,z}{2}+7\,P(z)\Bigg)\\
&+\ln^2(y_{\min})\left(\ln(z)\,(2-z-5\,P(z))+2-\frac{11\,z}{2}-3\,P(z)-\ln(1-z)P(z)\right)\\
&-\frac{19\,\ln^3(y_{\min})P(z)}{3},
\end{aligned}
\tag{5.79}
$$

where $P(z)$ is the 4-dimensional splitting function, it is equal to $[1+(1-z)^2]/z$.

Similarly, collecting together the results for the soft/collinear contributions (equations (5.59) and (5.60)), and making similar expansions in ϵ, we find,

$$
\begin{aligned}
\frac{1}{\sigma_0}\frac{\mathrm{d}\sigma_{soft/col}}{\mathrm{d}z} &= SC_{F\gamma}\\
&= \frac{1}{\Gamma^2(1-\epsilon)}\left(\frac{N^2-1}{2N}\right)\left(\frac{4\pi\mu^2}{M^2}\right)^{2\epsilon}\left(\frac{\alpha_s}{2\pi}\right)\left(\frac{\alpha e_q^2}{2\pi}\right)\\
&\quad\times\Bigg\{\frac{1}{\epsilon^3}\left[-2P(z)\right]+\frac{1}{\epsilon^2}\left[2z+2P(z)\,\ln(z)+6\,\ln(y_{\min})\,P(z)\right]\\
&\qquad+\frac{1}{\epsilon}\Big[-2z\,\ln(z)-P(z)\ln^2(z)+\ln(y_{\min})\,(-6z-6P(z)\ln(z))\\
&\qquad\quad-9\,\ln^2(y_{\min})\,P(z)\Big]\\
&\qquad+z\,\ln^2(z)+\frac{P(z)\,\ln^3(z)}{3}+\ln(y_{\min})\left(6z\ln(z)+3P(z)\,\ln^2(z)\right)\\
&\qquad+\ln^2(y_{\min})\,(9z+9P(z)\,\ln(z))+9\ln^3(y_{\min})P(z)\Bigg\}.
\end{aligned}
\tag{5.80}
$$

The intermediate results for the double single collinear contribution are given by equation

(5.77), which after expansion in the $\epsilon \to 0$ limit yield,

$$
\begin{aligned}
\frac{1}{\sigma_0}\frac{\mathrm{d}\sigma_{double}}{\mathrm{d}z} &= DC_{F\gamma} \\
&= \frac{1}{\Gamma^2(1-\epsilon)}\left(\frac{N^2-1}{2N}\right)\left(\frac{4\pi\mu^2}{M^2}\right)^{2\epsilon}\left(\frac{\alpha_s}{2\pi}\right)\left(\frac{\alpha e_q^2}{2\pi}\right) \\
&\times\Bigg\{\frac{1}{\epsilon^2}\left[2\,\ln(1-z)P(z) - \frac{3\,P(z)}{2} - 2\,\ln(y_{\min})P(z)\right] \\
&+\frac{1}{\epsilon}\Bigg[-2\,\ln(z)\ln(1-z)P(z) + \frac{3\,z}{2} - \frac{7\,P(z)}{2} + \ln(1-z)\left(-2\,z + \frac{3\,P(z)}{2}\right) \\
&\quad + \frac{3\,\ln(z)P(z)}{2} - \ln^2(1-z)P(z) + \frac{\pi^2 P(z)}{3} \\
&\quad + \ln(y_{\min})\left(2\,z + 3\,P(z) + 2\,\ln(z)P(z) - 4\,\ln(1-z)P(z)\right) \\
&\quad + 5\,\ln^2(y_{\min})P(z)\Bigg] \\
&+\frac{7\,z}{2} + \ln^2(1-z)\left(z - \frac{3\,P(z)}{4}\right) + \ln(z)\left(-\frac{3\,z}{2} + \frac{7\,P(z)}{2}\right) \\
&+\pi^2\left(-\frac{z}{3} + \frac{P(z)}{4}\right) + \ln^2(z)\ln(1-z)P(z) + \ln(z)\ln^2(1-z)P(z) \\
&+\ln(z)\ln(1-z)\left(2\,z - \frac{3\,P(z)}{2}\right) - \frac{\ln(1-z)\pi^2 P(z)}{3} - 7\,P(z) - \frac{3\,\ln^2(z)P(z)}{4} \\
&+\frac{\ln^3(1-z)P(z)}{3} + \ln(1-z)\left(-\frac{3\,z}{2} + \frac{7\,P(z)}{2}\right) - \frac{\ln(z)\pi^2 P(z)}{3} + 4\,P(z)\zeta(3) \\
&+\ln(y_{\min})\Bigg(-3\,z + 7\,P(z) + \ln(z)\,(-2\,z - 3\,P(z)) - \frac{2\,\pi^2 P(z)}{3} - \ln^2(z)P(z) \\
&+\ln(1-z)\,(4\,z - 3\,P(z)) + 2\,\ln^2(1-z)P(z) + 4\,\ln(z)\ln(1-z)P(z)\Bigg) \\
&+\ln^2(y_{\min})\,(-5\,z - 3\,P(z) - 5\,\ln(z)P(z) + 4\,\ln(1-z)P(z)) \\
&-\frac{19\,\ln^3(y_{\min})P(z)}{3}\Bigg\}. \qquad (5.81)
\end{aligned}
$$

The sum of all three two-particle unresolved real contributions therefore reads,

$$
\begin{aligned}
\frac{1}{\sigma_0}\frac{\mathrm{d}\sigma_R^{(U)}}{\mathrm{d}z} &= TC_{F\gamma} + SC_{F\gamma} + DC_{F\gamma} \\
&= \frac{1}{\Gamma^2(1-\epsilon)}\left(\frac{N^2-1}{2N}\right)\left(\frac{4\pi\mu^2}{M^2}\right)^{2\epsilon}\left(\frac{\alpha_s}{2\pi}\right)\left(\frac{\alpha e_q^2}{2\pi}\right) \\
&\times\Bigg\{ \frac{1}{\epsilon^3}\left[-2\,P(z)\right] \\
&+\frac{1}{\epsilon^2}\Bigg[4\,\ln(1-z)P(z) + \ln(z)\left(1-\frac{z}{2}+2\,P(z)\right) + 1 + \frac{7\,z}{4} - 3\,P(z) \\
&\quad +2\,\ln(y_{\min})P(z)\Bigg] \\
&+\frac{1}{\epsilon}\Bigg[-\frac{1}{4}+\frac{17\,z}{4} - 7\,P(z) + \mathrm{Li}_2(1-z)\,(-2+z-P(z)) \\
&\quad +\ln(1-z)\left(-2-\frac{7\,z}{2}+\frac{9\,P(z)}{2}\right) + \ln(z)\ln(1-z)\,(-2+z-4\,P(z)) \\
&\quad +\ln(z)\left(-1-\frac{13\,z}{4}+3\,P(z)\right) + \ln^2(z)\left(-\frac{3}{2}+\frac{3\,z}{4}-P(z)\right) \\
&\quad -4\,\ln^2(1-z)P(z) + \frac{5\,\pi^2 P(z)}{6} \\
&\quad +\ln(y_{\min})\left(\ln(z)\,(-2+z-2\,P(z)) - 6\,\ln(1-z)P(z) - 2 - \frac{3\,z}{2} + 6\,P(z)\right) \\
&\quad +\ln^2(y_{\min})\,P(z)\Bigg] \\
&-1+\pi^2\left(-\frac{1}{3}-\frac{3\,z}{4}+\frac{3\,P(z)}{4}\right) + \ln(z)\left(\frac{13}{4}-\frac{23\,z}{4}+7\,P(z)\right) \\
&+\ln(z)\pi^2\left(-\frac{1}{3}+\frac{z}{6}-\frac{2\,P(z)}{3}\right) + \ln^2(z)\left(\frac{1}{2}+\frac{25\,z}{8}-\frac{3\,P(z)}{2}\right) \\
&+\ln(z)\ln(1-z)\left(2+\frac{13\,z}{2}-\frac{9\,P(z)}{2}\right) + \ln(z)\mathrm{Li}_2(1-z)\,(4-2\,z) \\
&+\ln^2(1-z)\left(2+\frac{7\,z}{2}-\frac{15\,P(z)}{4}\right) + \ln(1-z)\mathrm{Li}_2(1-z)\,(4-2\,z+2\,P(z))
\end{aligned}
$$

$$
\begin{aligned}
&+\frac{39\,z}{4} - 14\,P(z) + \ln^3(z)\left(\frac{7}{6} - \frac{7\,z}{12} + \frac{P(z)}{3}\right) + \ln(1-z)\left(\frac{1}{2} - 7\,z + \frac{21\,P(z)}{2}\right) \\
&+\ln^2(z)\ln(1-z)\left(3 - \frac{3\,z}{2} + 2\,P(z)\right) + \ln(z)\ln^2(1-z)\,(2 - z + 4\,P(z)) \\
&+\mathrm{Li}_3(1-z)\,(-4 + 2\,z - 2\,P(z)) + \mathrm{S}_{12}(1-z)\,(2 - z - 3\,P(z)) \\
&+\frac{8\,\ln^3(1-z)P(z)}{3} + 4\,\mathrm{Li}_2(1-z)z + 13\,P(z)\zeta(3) - \frac{5\,\ln(1-z)\pi^2 P(z)}{3} \\
&+\ln(y_{\min})\Bigg(\mathrm{Li}_2(1-z)\,(4 - 2\,z + 2\,P(z)) + \ln(z)\ln(1-z)\,(4 - 2\,z + 6\,P(z)) \\
&\quad +\ln(1-z)\,(4 + 5\,z - 9\,P(z)) - \frac{4\,\pi^2 P(z)}{3} + 7\,\ln^2(1-z)P(z) + \frac{1}{2} - \frac{17\,z}{2} \\
&\quad +14\,P(z) + \ln(z)\left(2 + \frac{9\,z}{2} - 6\,P(z)\right) + \ln^2(z)\left(3 - \frac{3\,z}{2} + P(z)\right)\Bigg) \\
&+\ln^2(y_{\min})\left(3\,\ln(1-z)P(z) + \ln(z)\,(2 - z - P(z)) + 2 - \frac{3\,z}{2} - 6\,P(z)\right) \\
&-\frac{11\,\ln^3(y_{\min})P(z)}{3}\Bigg\}. \qquad (5.82)
\end{aligned}
$$

5.6 The approach with "strong ordering"

As a check of our calculation of the real two particle unresolved contributions to the differential cross section, we rederived it in two strongly ordered limits. Instead of considering particle 1 and particle 2 to be collinear *at the same time* to particle 3, we consider the two different contributions; **either** particle 1 is collinear to particle 3 *followed* by particle 2 collinear to the cluster of particles 1 and 3, (denoted by (13)), so that ($s_{13} \ll s_{23}$), **or** particle 2 is collinear to particle 3 *followed* by particle 1 being collinear to particle (23) where we have ($s_{23} \ll s_{13}$). In general, in the strongly ordered approximation, each of the unresolved real contributions (*triple collinear*, *soft/collinear* and *double single collinear*), gets "replaced" by the sum of two *strongly ordered* contributions. Each strongly ordered contribution is obtained by considering a different strongly ordered limit for each singular region.

As a result of this calculation we will find that the strongly ordered approximation correctly reproduces the *leading divergences* –those proportional to $\mathcal{O}(\frac{1}{\epsilon^3})$ or $\mathcal{O}(\frac{1}{\epsilon^2})$ which are associated with the leading and next-to-leading logarithms – but does not generate the correct *subleading divergences* proportional to $\mathcal{O}(\frac{1}{\epsilon})$ (corresponding to the next-to-next-to-leading logarithms) or the non-logarithmic terms of $\mathcal{O}(1)$.

5.6.1 The strongly ordered limits of the triple collinear differential cross section

In this section we will determine the two strongly ordered limits of the triple collinear matrix element squared, phase space and differential cross section.

The strongly ordered limits of the triple collinear matrix element squared

In the *strongly ordered collinear* limit, $s_{13} \ll s_{14}$, so that first 1 and 3 become collinear to form a cluster (13) followed by (13) and 4 becoming collinear, i.e.,

$$1 + 3 + 4 \to (13) + 4 \to Q.$$

The momenta can be expressed as,

$$p_1 = (1-a)\, p_{(13)}, \qquad p_3 = a\, p_{(13)}, \qquad p_4 = b\, p_Q, \qquad p_{(13)} = (1-b)\, p_Q, \tag{5.83}$$

such that $b = y$ and $a = z/(1-y)$.

In this strongly ordered limit, the triple collinear factor $P_{134\to Q}(x, y, s_{13}, s_{14}, s_{134})$ given by eq.(5.5) factorizes into the product of two simple collinear factors of consecutive Altarelli-Parisi splitting functions divided by the small invariants in this limit. More precisely, the Altarelli-Parisi splitting functions are functions of the momentum fraction a and b or equivalently $\frac{z}{1-y}$ and y, while the small invariants are s_{13} and $s_{(13)4}$, so that,

$$P_{134\to Q}(z, y, s_{13}, s_{14}, s_{134}) \to P_{13\to(13)}\left(\frac{z}{(1-y)}, s_{13}\right)\, P_{(13)4\to Q}(y, s_{(13)4}), \tag{5.84}$$

where $P_{ab\to c}(z, s_{ab})$ is given by eq.(1.30). In this limit, $s_{(13)4} \sim s_{134}$ while $s_{14} = (1-z-y)/(1-y)s_{134}$.

Alternatively if we let 1 and 4 become collinear and form the cluster (14), followed by (14) and 3 becoming collinear, i.e. in the strongly ordered limit where $s_{14} \ll s_{13}$, then we have the following two-stage process,

$$1+3+4 \to (14)+3 \to Q.$$

Introducing the momentum fractions a and b as before,

$$p_1 = (1-a)\, p_{(14)}, \qquad p_4 = a\, p_{(14)}, \qquad 3 = b\, p_Q, \qquad p_{(14)} = (1-b)\, p_Q, \tag{5.85}$$

such that $a = y/(1-z)$ and $b = z$. In this limit, the triple collinear factor again factorizes into a product of two consecutive Altarelli-Parisi splitting functions divided by the small invariants namely,

$$P_{134\to Q}(x, y, s_{13}, s_{14}, s_{134}) \to P_{14\to(14)}\left(\frac{y}{(1-z)}, s_{14}\right)\, P_{(14)3\to Q}(z, s_{(14)3}). \tag{5.86}$$

The two small invariants are s_{14} and $s_{(14)3} \sim s_{134}$ while $s_{13} = (1-y-z)/(1-z)s_{134}$.

At this stage, before we determine the strongly ordered limits of the triple collinear phase space and differential cross section, we would like to be able to decide when one or the other of the strongly ordered approximations is a "good" approximation to the triple collinear matrix element squared $P_{134\to Q}$. As an example let us consider the strongly ordered collinear limit of $P_{134\to Q}$ when $y_{13} \ll y_{14}$. We define the ratio $r \equiv \frac{y_{13}}{y_{14}}$ and the ratio of the triple collinear factor and its strongly ordered limit

$$R(r) \equiv \frac{P_{134\to Q}}{P_{13\to(13)}\, P_{(13)4\to Q}}.$$

Figure (5.1) displaying $R(r)$, will help us to determine the quality of the approximation. Here we have fixed $z = 2/3$, $y = 1/6$, $y_{14} = 1/100$ and select various values of y_{134}. In the strongly ordered limit, y_{134} is fixed, $y_{134} = (1-y)/(1-z-y)y_{14} = 5y_{14}$, shown as a solid line in figure 5.1. As r approaches 0, the ratio $R(r)$ approaches 1, indicating that the strongly

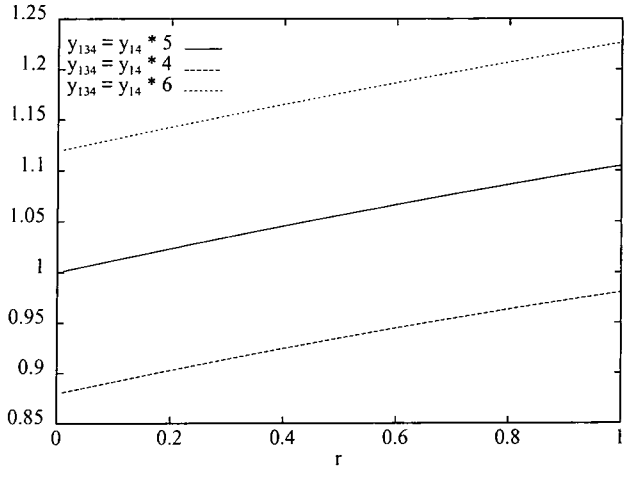

Figure 5.1: The ratio $R(r)$ (for $y_{13} \ll y_{14}$) as defined in the text. We choose, $z = 2/3$, $y = 1/6$, $y_{14} = 1/100$ for convenience and different values for y_{134} as a function of y_{14}.

ordered limit is indeed a good approximation when $y_{13} \ll y_{14}$. When r increases, the ratio $R(r)$ increases as the strongly ordered approximation becomes significantly smaller than the "full" approximation $P_{134\to Q}$. However, as soon as we allow y_{134} to deviate from its strongly ordered limit value, the approximation breaks down over the whole range of r. This is shown by the dashed and dotted lines. In practice, however, y_{134} is constrained by the Gram determinant, so that the deviations are still relatively small.

In summary, the strongly ordered limit of the matrix element squared given by eq.(5.84) is a good approximation of the "full" matrix element squared $P_{134\to Q}$ only if the requirements $y_{13} \ll y_{14}$ and $y_{134} = \frac{(1-y)}{(1-y-z)} y_{14}$ are both satisfied.

The strongly ordered limits of the triple collinear phase space and differential cross section

In the two strongly ordered limits the phase space also factorizes and becomes the product of two simple collinear phase space factors.

In the first strongly ordered limit, defined in eq.(5.83), $s_{13} \ll s_{14}$, we find that the phase space factor takes the form,

$$\begin{aligned} \mathrm{d}P_{triple}^{(d)(a)} &\sim \mathrm{d}y_{(13)4}\mathrm{d}y_{13}\mathrm{d}a\mathrm{d}b \times [a(1-a)]^{-\epsilon}[b(1-b)]^{-\epsilon}(y_{(13)4})^{-\epsilon}(y_{13})^{-\epsilon} \\ &\sim z^{-\epsilon}(1-z-y)^{-\epsilon}(1-y)^{-1+\epsilon}y^{-\epsilon}(y_{(13)4})^{-\epsilon}(y_{13})^{-\epsilon}\mathrm{d}z\ \mathrm{d}y\ \mathrm{d}y_{(13)4}\ \mathrm{d}y_{13}, \end{aligned}$$

such that in this strongly ordered limit, the contribution to the differential cross section reads,

$$\begin{aligned} TC_{F\gamma}^{strong(a)} &\equiv \left(\frac{N^2-1}{2N}\right)\left(\frac{4\pi\mu^2}{M^2}\right)^{2\epsilon}\left(\frac{\alpha_s}{2\pi}\right)\left(\frac{\alpha e_q^2}{2\pi}\right)\frac{1}{\Gamma^2(1-\epsilon)} \\ &\times \int_0^{y_{\min}} \mathrm{d}y_{(13)4}\,(y_{(13)4})^{-\epsilon-1}\int_0^{(1-y)y_{(13)4}} \mathrm{d}y_{13}\,(y_{13})^{-\epsilon-1} \\ &\times \int_{y_{\min}}^{1-z} \mathrm{d}y\ z^{-\epsilon}[1-y-z]^{-\epsilon}y^{-\epsilon}\,(1-y)^{-1+\epsilon}\,P^{\epsilon}\left(\frac{z}{1-y}\right)P^{\epsilon}(y) \\ &= \left(\frac{N^2-1}{2N}\right)\left(\frac{4\pi\mu^2}{M^2}\right)^{2\epsilon}\left(\frac{\alpha_s}{2\pi}\right)\left(\frac{\alpha e_q^2}{2\pi}\right)\frac{1}{\Gamma^2(1-\epsilon)}\,\frac{1}{2\epsilon^2}(y_{\min})^{-2\epsilon}\,z^{-\epsilon} \\ &\times \int_{y_{\min}}^{1-z} \mathrm{d}y(1-y-z)^{-\epsilon}\,y^{-\epsilon}\,P^{\epsilon}\left(\frac{z}{1-y}\right)P^{\epsilon}(y)\,\frac{1}{1-y}. \end{aligned} \tag{5.87}$$

Since $0 \leq a \leq 1$ and $a = \frac{z}{1-y}$ the y integral is bounded by $1-z$. Furthermore $s_{13} \ll s_{14}$ implies that the y_{13} integral is bounded by $(1-y)y_{(13)4}$.

On the other hand, if $s_{14} \ll s_{13}$, in the strongly ordered limit defined by eq.(5.85) the phase space factor takes the following form:

$$\begin{aligned} \mathrm{d}P_{triple}^{(d)(b)} &\sim \mathrm{d}y_{(14)3}\mathrm{d}y_{14}\mathrm{d}a\mathrm{d}b \times [a(1-a)]^{-\epsilon}[b(1-b)]^{-\epsilon}(y_{(14)3})^{-\epsilon}(y_{14})^{-\epsilon} \\ &\sim y^{-\epsilon}(1-z-y)^{-\epsilon}(1-z)^{-1+\epsilon}z^{-\epsilon}(y_{(14)3})^{-\epsilon}(y_{14})^{-\epsilon}\mathrm{d}z\mathrm{d}y\mathrm{d}y_{(14)3}\mathrm{d}y_{14}. \end{aligned}$$

In this limit z, y and y_{13}, y_{14} are interchanged with respect to the previous strongly ordered differential cross section, so that,

$$TC_{F\gamma}^{strong(b)} \equiv \left(\frac{N^2-1}{2N}\right)\left(\frac{4\pi\mu^2}{M^2}\right)^{2\epsilon}\left(\frac{\alpha_s}{2\pi}\right)\left(\frac{\alpha e_q^2}{2\pi}\right)\frac{1}{\Gamma^2(1-\epsilon)}$$

$$\times \int_0^{y_{\min}} \mathrm{d}y_{(14)3}\,(y_{(14)3})^{-\epsilon-1} \int_0^{(1-z)y_{(14)3}} \mathrm{d}y_{14}\,(y_{14})^{-\epsilon-1}$$

$$\times \int_{y_{\min}}^{1-z} \mathrm{d}y\; y^{-\epsilon}[1-y-z]^{-\epsilon} z^{-\epsilon}(1-z)^{-1+\epsilon}\; P^{\epsilon}\left(\frac{y}{1-z}\right) P^{\epsilon}(z)$$

$$= \left(\frac{N^2-1}{2N}\right)\left(\frac{4\pi\mu^2}{M^2}\right)^{2\epsilon}\left(\frac{\alpha_s}{2\pi}\right)\left(\frac{\alpha e_q^2}{2\pi}\right)\frac{1}{\Gamma^2(1-\epsilon)}\,\frac{1}{2\epsilon^2}(y_{\min})^{-2\epsilon}\, z^{-\epsilon}$$

$$\times \int_{y_{\min}}^{1-z} (1-y-z)^{-\epsilon}\, y^{-\epsilon}\, P^{\epsilon}\left(\frac{y}{1-z}\right) P^{\epsilon}(z)\,\frac{1}{1-z}, \tag{5.88}$$

where the y integral is bounded by $1-z$ as $b = \frac{y}{1-z} \leq 1$ and the y_{14} integral is bounded by $(1-z)y_{(14)3}$ since $s_{14} \ll s_{13}$ in this strongly ordered limit.

5.6.2 The strongly ordered limits of the soft/collinear differential cross section

The strongly ordered limits of the soft/collinear matrix element squared

In the limit where the gluon (parton 4) first becomes soft with the quark and photon (partons 1 and 3) subsequently becoming collinear, $s_{14},\ s_{24} \ll s_{13}$, i.e.,

$$1+3+4 \to 1+3 \to Q,$$

such that,

$$p_1 = (1-z)\,p_Q, \qquad p_3 = z\,p_Q,$$

the soft/collinear approximation to the matrix element squared, $P^{soft/col}_{134\to Q}$ given by equation (5.52) also factorizes. We obtain a product of a soft and a simple collinear factor,

$$P^{soft/col}_{134\to Q}(z, y_{24}, s_{13}, s_{14}, s_{134}) \to \frac{1}{2} f_{12}(4)\; P_{13\to Q}(z, s_{13}),$$

where the eikonal factor $f_{ab}(c)$ is defined in eq.(1.20). To obtain this form we made the identifications,

$$\begin{aligned} s_{134} &\to s_{13}, \\ \frac{1}{y_{24}} &\to \frac{s_{Q2}}{s_{24}} = \frac{s_{12}}{(1-z)s_{24}}. \end{aligned}$$

Alternatively, if we let 1 and 3 become collinear before the gluon becomes soft, $s_{13} \ll s_{Q4},\ s_{24}$, then,

$$1 + 3 + 4 \to Q + 4 \to Q,$$

such that,

$$p_1 = (1 - z)\, p_Q, \qquad p_3 = z\, p_Q,$$

then,

$$P^{soft/col}_{134\to Q}(z, y_{24}, s_{13}, s_{14}, s_{134}) \to \frac{1}{2} f_{Q2}(4)\ P_{13\to Q}(z, s_{13}),$$

where we have used the replacements,

$$\begin{aligned} s_{134} &\to s_{Q4} \\ s_{14} &\to (1 - z) s_{Q4} \\ \frac{1}{y_{24}} &\to \frac{s_{Q2}}{s_{24}}. \end{aligned}$$

As in the previous section, the strongly ordered limits of the soft/collinear matrix element squared depends only on four of the unresolved variables, while the full soft/collinear matrix elements squared (given by $P^{soft/col}_{134\to Q}$ in eq.(5.53)) depends on all five. As a result, when the fifth variable deviates from the strict strongly ordered limit, the strongly ordered approximation is not reliable.

The strongly ordered soft/collinear phase space and differential cross section

In both strongly ordered limits the soft/collinear phase space factorizes. It becomes a product of a simple collinear phase space and a simple soft phase space factor.

In the strongly ordered limit, where parton 4 first becomes soft followed by 1 and 3 becoming collinear, $s_{14},\ s_{24} \ll s_{13}$, the phase space factor becomes:

$$\mathrm{d}P^{(d)(a)}_{soft} \sim \left[\frac{s_{14} s_{24}}{s_{12}}\right]^{-\epsilon} (s_{13})^{-\epsilon} [z(1 - z)]^{-\epsilon} \mathrm{d}s_{13} \mathrm{d}s_{24} \mathrm{d}s_{14} \mathrm{d}z,$$

whereas if parton 1 and 3 become collinear before 4 becomes soft, $s_{13} \ll s_{Q4},\ s_{24}$, the phase space factor becomes,

$$\mathrm{d}P^{(d)(b)}_{soft} \sim \left[\frac{s_{Q4} s_{24}}{s_{Q2}}\right]^{-\epsilon} (s_{13})^{-\epsilon} [z(1 - z)]^{-\epsilon} \mathrm{d}s_{13} \mathrm{d}s_{24} \mathrm{d}s_{Q4} \mathrm{d}z.$$

For the differential cross section we then obtain,

$$
\begin{aligned}
SC_{F\gamma}^{strong(a)} &\equiv \left(\frac{N^2-1}{2N}\right)\left(\frac{4\pi\mu^2}{M^2}\right)^{2\epsilon}\left(\frac{\alpha_s}{2\pi}\right)\left(\frac{\alpha e_q^2}{2\pi}\right)\frac{1}{\Gamma^2(1-\epsilon)}P^\epsilon(z)[(1-z)z]^{-\epsilon} \\
&\quad\times\int_0^{y_{\min}} \mathrm{d}y_{13}\,(y_{13})^{-1-\epsilon}\int_0^{y_{13}}\mathrm{d}y_{14}\int_0^{y_{\min}}\mathrm{d}y_{24}\left[\frac{y_{14}y_{24}}{y_{12}}\right]^{-1-\epsilon}\frac{1}{y_{12}} \\
&= -\frac{1}{2\epsilon^3}\left(\frac{N^2-1}{2N}\right)\left(\frac{4\pi\mu^2}{M^2}\right)^{2\epsilon}\left(\frac{\alpha_s}{2\pi}\right)\left(\frac{\alpha e_q^2}{2\pi}\right)\frac{1}{\Gamma^2(1-\epsilon)} \\
&\quad\times(y_{\min})^{-3\epsilon}\,z^{-\epsilon}P^\epsilon(z), \qquad (5.89)
\end{aligned}
$$

for $s_{14},\ s_{24} \ll s_{13}$, while, if $s_{13} \ll s_{14},\ s_{24}$, we have,

$$
\begin{aligned}
SC_{F\gamma}^{strong(b)} &\equiv \left(\frac{N^2-1}{2N}\right)\left(\frac{4\pi\mu^2}{M^2}\right)^{2\epsilon}\left(\frac{\alpha_s}{2\pi}\right)\left(\frac{\alpha e_q^2}{2\pi}\right)\frac{1}{\Gamma^2(1-\epsilon)}P^\epsilon(z)[(1-z)z]^{-\epsilon} \\
&\quad\times\int_0^{y_{\min}}\mathrm{d}y_{24}\int_0^{y_{\min}}\mathrm{d}y_{13}\,\frac{1}{y_{13}}(y_{13})^{-\epsilon}\int_{y_{13}}^{y_{\min}}\mathrm{d}y_{Q4}\,\frac{1}{y_{Q2}}\left[\frac{y_{Q4}y_{24}}{y_{Q2}}\right]^{-1-\epsilon} \\
&= -\frac{1}{2\epsilon^3}\left(\frac{N^2-1}{2N}\right)\left(\frac{4\pi\mu^2}{M^2}\right)^{2\epsilon}\left(\frac{\alpha_s}{2\pi}\right)\left(\frac{\alpha e_q^2}{2\pi}\right)\frac{1}{\Gamma^2(1-\epsilon)} \\
&\quad\times(y_{\min})^{-3\epsilon}(1-z)^{-\epsilon}z^{-\epsilon}P^\epsilon(z). \qquad (5.90)
\end{aligned}
$$

This contribution differs from the expression given by eq.(5.89) only by a factor of $(1-z)^{-\epsilon}$.

5.6.3 The strongly ordered limits of the double single collinear differential cross section

Firstly, the double single collinear $|\mathcal{M}|^2$ given in eq.(5.69) and the double single collinear phase space given by eq.(5.73) are already in a strongly ordered form. They are given by the product of two simple collinear matrix element squared and phase spaces. Furthermore, in the two strongly ordered double single collinear limits the invariants are defined as in eq.(5.68). In particular, we have $y_{14} = y(1-z)$ in both strongly ordered limits.

Nevertheless, for the evaluation of the strongly ordered double single collinear differential cross section we need to distinguish two limits; either $y_{13} \ll y_{24}$ **or** $y_{24} \ll y_{13}$. In these limits the boundaries of the phase space integral change.

In order to determine the double single collinear contribution to the cross section, we have integrated the double single collinear matrix element squared over the double single collinear region of phase space. Furthermore, we made sure that this double single collinear region precisely matches onto the soft/collinear region. This was achieved by requiring that,

$$y_{13} < y_{\min} \qquad \text{and} \qquad y_{24} < y_{\min},$$

in both regions of phase space, and $y_{14} < y_{\min}$ in the soft/collinear region whereas $y_{14} > y_{\min}$ in the double single collinear region. Similarly, when the two strongly ordered limits are considered we must ensure that each strongly ordered soft/collinear region matches onto the corresponding strongly ordered double single collinear region.

Again, in both strongly ordered soft/collinear and double single collinear regions we will have,

$$y_{13} < y_{\min} \qquad \text{and} \qquad y_{24} < y_{\min}.$$

The invariant y_{14}, however is not constrained in the same manner in both different strongly ordered soft/collinear regions of the phase space as we can infer from eq.(5.59) and eq.(5.60). Therefore y_{14} will also be constrained differently in both strongly ordered double single collinear regions.

More precisely, in the strongly ordered soft/collinear limit where $y_{14}, y_{24} \ll y_{13}$, inspection of eq.(5.89) shows that y_{14} is constrained to be less than $y_{\min}$. Consequently, in the strongly ordered double single collinear region where ($y_{24} \ll y_{13}$), to guarantee that the matching between this region and the corresponding strongly ordered soft/collinear is realized we require that $y_{14} > y_{\min}$. As $y_{14} = y(1-z)$, the lower boundary of the y integral for this strongly ordered region is then $\frac{y_{\min}}{1-z}$.

On the other hand, in the strongly ordered soft/collinear region where $y_{13} \ll y_{14}, y_{24}$, from eq.(5.90), we see that in this case y_{Q4} is bounded to be less than $y_{\min}$ and as $y_{Q4} = \frac{y_{14}}{1-z}$ we have $y_{14} < y_{\min}(1-z)$. In order for the corresponding strongly ordered double single collinear region ($y_{13} \ll y_{24}$) to match onto this strongly ordered soft/collinear region, we will require $y_{14} > y_{\min}(1-z)$ which corresponds to a lower bound on y of $y > y_{\min}$.

Following this remark, the sum of these two strongly ordered approximations of the double single collinear contribution yields,

$$
\begin{aligned}
DC_{F\gamma}^{strong} \equiv & \left(\frac{N^2-1}{2N}\right)\left(\frac{4\pi\mu^2}{M^2}\right)^{2\epsilon}\left(\frac{\alpha_s}{2\pi}\right)\left(\frac{\alpha e_q^2}{2\pi}\right)\frac{1}{\Gamma^2(1-\epsilon)}P^\epsilon(z)[(1-z)z]^{-\epsilon} \\
& \times\Bigg\{\int_0^{s_{\min}} \mathrm{d}s_{13}(s_{13})^{-\epsilon-1}\int_0^{s_{13}}\mathrm{d}s_{24}(s_{24})^{-\epsilon-1}\int_{\frac{y_{\min}}{1-z}}^1 \mathrm{d}y \\
& +\int_0^{s_{\min}} \mathrm{d}s_{24}(s_{24})^{-\epsilon-1}\int_0^{s_{24}}\mathrm{d}s_{13}(s_{13})^{-\epsilon-1}\int_{y_{\min}}^1 \mathrm{d}y\Bigg\}[(1-y)y]^{-\epsilon}\,P^\epsilon(y) \\
= & \left(\frac{N^2-1}{2N}\right)\left(\frac{4\pi\mu^2}{M^2}\right)^{2\epsilon}\left(\frac{\alpha_s}{2\pi}\right)\left(\frac{\alpha e_q^2}{2\pi}\right)\frac{1}{\Gamma^2(1-\epsilon)}P^\epsilon(z)[(1-z)z]^{-\epsilon} \\
& \times\frac{1}{\epsilon^2}\left[\frac{1}{\epsilon}(y_{\min})^{-\epsilon}[1+(1-z)^\epsilon]-\frac{(1-\epsilon)(4-\epsilon)}{2\epsilon(1-2\epsilon)}\frac{\Gamma^2(1-\epsilon)}{\Gamma(1-2\epsilon)}\right]. \qquad (5.91)
\end{aligned}
$$

Comparing this expression with the expression of the double single collinear contribution without any strongly ordering given by eq.(5.77) we see that the strongly ordered result is obtained by the replacement,

$$\frac{2}{\epsilon}(1-z)^\epsilon \;\rightarrow \frac{1}{\epsilon}[1+(1-z)^\epsilon].$$

5.6.4 The sum of all strongly ordered contributions

The sum of all strongly ordered real contributions is obtained as follows. Each singular contribution (triple collinear, soft/collinear and double single collinear), is replaced by the sum of its two corresponding strongly ordered limits. Evaluating the resulting integrals for the sum of all real strongly ordered contributions, the pole part yields,

$$
\begin{aligned}
\frac{1}{\sigma_0}\frac{\mathrm{d}\sigma_R^{(U)strong}}{\mathrm{d}z} = & \; TC_{F\gamma}^{strong(a)}+TC_{F\gamma}^{strong(b)}+SC_{F\gamma}^{strong(a)}+SC_{F\gamma}^{strong(b)}+DC_{F\gamma}^{strong} \\
= & \left(\frac{N^2-1}{2N}\right)\left(\frac{4\pi\mu^2}{M^2}\right)^{2\epsilon}\left(\frac{\alpha_s}{2\pi}\right)\left(\frac{\alpha e_q^2}{2\pi}\right)\frac{1}{\Gamma^2(1-\epsilon)} \\
& \times\Bigg\{-\frac{2}{\epsilon^3}P(z)+\frac{1}{\epsilon^2}\Big[2P(z)\ln(y_{\min})+\Big(1+\frac{7}{4}z-3P(z)\Big)\Big]
\end{aligned}
$$

$$
\begin{aligned}
&+\ln(z)\left(1-\frac{1}{2}z+2P(z)\right)+4P(z)\ln(1-z)\Big] \\
+\ &\frac{1}{\epsilon}\Big\{\Big(-\frac{1}{2}+\frac{9}{2}z-7P(z)+\frac{2}{3}P(z)\pi^2\Big)+\ln^2(y_{\min})P(z) \\
&+\ln(y_{\min})\Big[\Big(-2-\frac{3}{2}z+6P(z)\Big)+\ln(z)(-2+z+P(z)) \\
&-6P(z)\ln(1-z)\Big] \\
&+\ln(1-z)\ln(z)[-2+z-4P(z)]-4P(z)\ln^2(1-z) \\
&+\ln^2(z)\Big[-\frac{3}{2}+\frac{3}{4}z-P(z)\Big]+\mathrm{Li}_2(1-z)[-2+z] \\
&+\ln(1-z)\Big[-2-\frac{7}{2}z+\frac{9}{2}P(z)\Big]+\ln(z)\Big[-\frac{5}{2}-\frac{9}{4}z+3P(z)\Big]\Big\} \\
+\ &\mathcal{O}(1)\Big\}. \qquad (5.92)
\end{aligned}
$$

If we compare this result with the result obtained for the sum of the three two-particle unresolved real contributions without taking the strongly ordered approximation (as in eq.(5.82)) we see that, the strongly ordered approximation correctly reproduces the *leading divergences* - those proportional to $\mathcal{O}(\frac{1}{\epsilon^3})$ and $\mathcal{O}(\frac{1}{\epsilon^2})$ - but does not generate the correct *subleading divergences* proportional to $\mathcal{O}(\frac{1}{\epsilon})$. The finite terms of $\mathcal{O}(1)$ are also incorrectly reproduced. The leading and next-to-leading logarithms generated by expanding the most singular poles are correctly reproduced, but single logarithms and non-logarithmic terms are not. We understand this as follows: The poles in $\frac{1}{\epsilon^2}, \frac{1}{\epsilon^3}$ arise from the evaluation of successive phase space integrals at the lower boundaries where the strongly ordered approximation is very close to "full" approximation of the matrix elements. On the other hand, terms proportional to $\frac{1}{\epsilon}$ arise when evaluating only one of the phase space integrals at its lower boundary while the other phase space integrals contain significant contributions close to their upper boundaries. At these upper boundaries, the ratio r between the two invariants defining the strongly ordered limit is no longer small and the strongly ordered approximation to the matrix elements is no longer accurate.

In summary, in this section we have performed a cross check of our calculation by

evaluating the real contributions in different strongly ordered limits. We have found agreement for the most singular terms, while less singular terms appear to be different. This disagreement can be explained as due to an insufficient approximation of the differential cross section in the strongly ordered limits. Therefore, since the results obtained applying "strong ordering" only reproduce the leading divergent terms correctly, they will not be taken into account in any further part of this dissertation.

Chapter 6

Virtual contributions

In the previous two chapters we have decomposed the four-particle phase space and extracted the divergences present in the $\mathcal{O}(\alpha\alpha_s)$ four-parton process $\gamma^* \to q\bar{q}\gamma g$ where one or two particles are theoretically unresolved. In other words, only two or three particles are *theoretically* identified in the final state. If three particles are theoretically well separated, the experimental cuts will combine these particles further to select photon +1 jet events.

In this chapter we will take into account the exchange of a virtual gluon in the $\gamma^* \to q\bar{q}\gamma$ process, which when interfered with the tree level process also gives rise to contributions of $\mathcal{O}(\alpha\alpha_s)$. More precisely, the matrix element "squared" $|\mathcal{M}|_V^2$ associated with the loop diagrams is obtained by interfering the lowest order real amplitude $\mathcal{T}$ with the loop amplitude $\mathcal{L}$,

$$|\mathcal{M}|_V^2 \equiv 2\,\mathrm{Re}(\mathcal{L}\mathcal{T}^*).$$

The Feynman diagrams related to the real and virtual amplitudes for $\gamma^* \to q\bar{q}\gamma$ are shown in Fig. 6.1 and Fig. 6.2.

As discussed in Section 3.1, the calculation naturally divides into two parts, depending on whether or not the three particles are resolved. Both resolved and unresolved contributions are divergent and need to be combined with the appropriate real contributions described earlier. In the *resolved* virtual contribution both quarks and the photon are

clearly distinguishable and we expect the divergences to cancel when combined with the real contribution if the gluon is either collinear with one of the quarks or is soft (c.f. Section 3.3). On the other hand, in the *unresolved* part, the quark and photon are considered to be collinear and form a single pseudo particle, Q the parent quark. The expected leading singularity is proportional to $(P(z)/\epsilon^3)$. In fact, the most singular divergences from this piece arises from the possibility of a soft gluon being internally exchanged, which gives rise to a term proportional to $(\mathcal{O}(1/\epsilon^2))$, occurring simultaneously with the collinear emission of the photon from a quark – which is related to a contribution proportional to $(P(z)/\epsilon)$. These most singular poles should cancel with those present in the soft/collinear contributions calculated in the previous chapter.

This chapter is organized as follows. First, we consider the well known forms for the virtual matrix elements and specify over which region of phase space these will be used in our further study. The known published forms are not suitable for extracting the collinear limit, so in Section 6.2, we reformulate the matrix elements in order to be able to take the limit $s_{q\gamma} \to 0$. As Bern, Dixon, Dunbar and Kosower have studied the helicity amplitudes for the collinear limits of one-loop amplitudes we compare their results with ours for the collinear virtual matrix elements in Section 6.2.2. Finally, the collinear matrix elements are integrated over the simple collinear phase space in Section 6.2.3.

6.1 The resolved contribution

The squared matrix elements for the $\gamma^* \to q\bar{q}g$ process at one loop have been calculated many times in the literature [25, 31, 34]. The calculation of this process is part of the $\mathcal{O}(\alpha_s^2)$ corrections to the three-jet rate in e^+e^- annihilation, which was originally derived by Ellis, Ross and Terrano in [31].

As we are interested in the virtual contributions with an outgoing photon instead of an outgoing gluon, we need to replace the colour factors in eq.(2.20) of [31] as follows,

$$C_A \to 0, \qquad N_F \to 0, \qquad C_F^2 \to C_F,$$

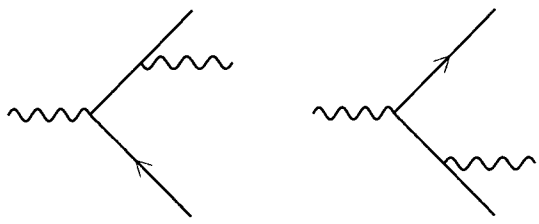

Figure 6.1: Tree level $\gamma^\star \to q\bar{q}\gamma$ amplitudes.

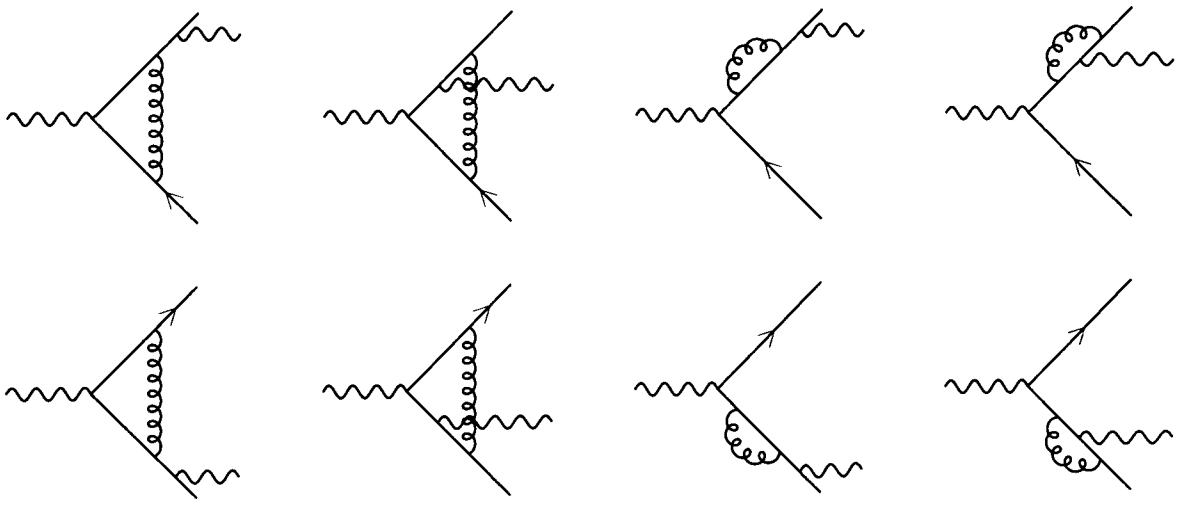

Figure 6.2: Virtual gluon corrections to the $\gamma^\star \to q\bar{q}\gamma$ amplitude.

furthermore we need to consider,

$$\alpha_s^2 \to \alpha_s \alpha e_q^2,$$

when the quark has charge e_q. After these replacements, eq.(2.20) of [31] reads,

$$|\mathcal{M}|_V^2 = \left(|\mathcal{M}_{q\bar{q}\gamma}|^2 \times V_{q\bar{q}(\gamma)} + F(y_{12}, y_{13}, y_{23})\right), \tag{6.1}$$

where,

$$V_{q\bar{q}(\gamma)} = \frac{\alpha_s}{2\pi}\left(\frac{N^2-1}{2N}\right)\frac{\Gamma^2(1-\epsilon)\Gamma(1+\epsilon)}{\Gamma(1-2\epsilon)}\left(\frac{4\pi\mu^2}{M^2}\right)^\epsilon\left[-\frac{2(y_{q\bar{q}})^{-\epsilon}}{\epsilon^2} - \frac{3}{\epsilon} + \pi^2 - 8\right], \tag{6.2}$$

and,

$$
\begin{aligned}
F(y_{12},y_{13},y_{23}) &= \frac{\alpha_s}{2\pi}\left(\frac{N^2-1}{2N}\right) \\
&\times \left\{ \frac{y_{12}}{y_{12}+y_{13}} + \frac{y_{12}}{y_{12}+y_{23}} + \frac{y_{12}+y_{23}}{y_{13}} + \frac{y_{12}+y_{13}}{y_{23}} \right. \\
&\quad + \ln y_{13}\left[\frac{4y_{12}^2+2y_{12}y_{13}+4y_{12}y_{23}+y_{13}y_{23}}{(y_{12}+y_{23})^2}\right] \\
&\quad + \ln y_{23}\left[\frac{4y_{12}^2+2y_{12}y_{23}+4y_{12}y_{13}+y_{13}y_{23}}{(y_{12}+y_{13})^2}\right] \\
&\quad -2\left[\frac{y_{12}^2+(y_{12}+y_{13})^2}{y_{13}y_{23}}R(y_{12},y_{23}) + \frac{y_{12}^2+(y_{12}+y_{23})^2}{y_{13}y_{23}}R(y_{12},y_{13})\right. \\
&\quad \left.\left. + \frac{y_{13}^2+y_{23}^2}{y_{13}y_{23}(y_{13}+y_{23})} - 2\ln y_{12}\left(\frac{y_{12}^2}{(y_{13}+y_{23})^2}+\frac{2y_{12}}{y_{13}+y_{23}}\right)\right]\right\}. \qquad (6.3)
\end{aligned}
$$

The function R is defined as,

$$
R(x,y) = \Big[\ln x \ln y - \ln x \ln(1-x) - \ln y \ln(1-y) + \frac{1}{6}\pi^2 - \mathrm{Li}_2(x) - \mathrm{Li}_2(y)\Big]. \qquad (6.4)
$$

As usual we made the identifications of $q \equiv 1$, $\bar{q} \equiv 2$ and $\gamma \equiv 3$ in addition to the invariant masses $s_{ij} = (p_i + p_j)^2$ and the scaled variables $y_{ij} = s_{ij}/M^2$ where $M^2 = s_{123}$ is the (mass)^2 of the off-shell photon. We see that in eq.(6.1) the divergent terms coming from the emission of a soft or collinear gluon have precisely the necessary form to cancel the singularities present in the single unresolved soft or collinear contributions to the tree level process $\gamma^* \to q\bar{q}\gamma g$, i.e. those present in $R_{q\bar{q}(\gamma)}$ defined in eq.(4.24). The cancellation of singularities between these two classes of contributions will be presented in Chapter 8.

To ensure that the photon is resolved from the quark and antiquark, we define the *resolved* three parton phase space to be,

$$
s_{q\gamma} > s_{\min}, \qquad\qquad s_{\bar{q}\gamma} > s_{\min}.
$$

In this region the resolved virtual cross section can be written as

$$
\mathrm{d}\sigma_V^{(R)} = V_{q\bar{q}(\gamma)}\mathrm{d}\sigma_{q\bar{q}\gamma} + F_c \qquad (6.5)
$$

$V_{q\bar{q}(\gamma)}$ is the virtual factor defined in eq.(6.2) while F_c will be evaluated numerically using the finite expression of Ellis, Ross and Terrano in eq.(6.3) and the experimental jet algorithm to select a photon +1 jet final state events. $\sigma_{q\bar{q}\gamma}$ will also be evaluated numerically. The more interesting problem lies in the *unresolved* region as we shall see in the next section.

6.2 The unresolved contribution

In the *unresolved* region of phase space, the quark becomes collinear with the photon so that, defining a new parent quark, Q, with momentum p_Q we have,

$$p_Q = p_q + p_\gamma = p_1 + p_3.$$

As usual, we introduce the variable z,

$$p_1 = (1-z)p_Q, \qquad p_3 = zp_Q. \tag{6.6}$$

The photon carries then a fraction z of the composite quark momentum. In this simple collinear limit the three particle phase space factorizes into a simple collinear phase space factor, as we saw in Chapter 2,

$$\mathrm{d}P_3^{(d)}(M, p_q, p_{\bar{q}}, p_\gamma) \to \mathrm{d}P_2^{(d)}(M, p_Q, p_{\bar{q}})\,\mathrm{d}P_{col}^{(d)}(p_q, p_\gamma, z). \tag{6.7}$$

$\mathrm{d}P_2^{(d)}(M, p_Q, p_{\bar{q}})$ is the known two-particle phase space in d dimensions given in the Appendix B by eq.(B.3) and the collinear phase space factor $\mathrm{d}P_{col}^{(d)}(p_q, p_\gamma, z)$,

$$\mathrm{d}P_{col}^{(d)}(p_q, p_\gamma, z) = \frac{(4\pi)^\epsilon}{16\pi^2\Gamma(1-\epsilon)}\mathrm{d}s_{q\gamma}\,\mathrm{d}z\Big[s_{q\gamma}z(1-z)\Big]^{-\epsilon}. \tag{6.8}$$

At this stage we would like to take the corresponding limit of the virtual matrix elements. However, we note that the form given in eq.(6.3) is unsuitable for taking the collinear limit, since as s_{13} (or equivalently y_{13}) $\to 0$, terms of the form,

$$\frac{\log(s_{13})}{s_{13}},$$

are generated. Such terms are problematic and are generated by taking the $s_{13} \to 0$ limit **after** an expansion of the virtual matrix elements as a series in ϵ. The correct procedure would be to take the collinear limit first and then expand the matrix elements as power series in ϵ. For example, consider the term,

$$\frac{s^{-\epsilon}}{\epsilon}.$$

Expanding as a series in ϵ yields,

$$\frac{1}{\epsilon} - \log(s) + \mathcal{O}(\epsilon),$$

which, as $s \to 0$, is ill-defined. Dimensional regularization solves this problem with the prescription,

$$\frac{s^{-\epsilon}}{\epsilon} \equiv 0,$$

in the limit $s = 0$. In the unresolved region, s_{13} lies in the range $[0, s_{\min}]$ and the unexpanded form must be used.

6.2.1 The collinear limit of the virtual contribution

With the help of the scalar loop integrals B_0, C_0 and D_0, we can bring the matrix element squared of eq.(6.1) into an "unexpanded form" [64] and then take the collinear limit. Explicit calculation yields a dimensionless *virtual collinear* factor $VC_{F\gamma}\mathrm{d}z$ multiplying the lowest order two particle cross section[1],

$$\mathrm{d}\sigma_V \to VC_{F\gamma}\mathrm{d}z \times \sigma_0, \tag{6.9}$$

where,

$$\begin{aligned} VC_{F\gamma}\mathrm{d}z \;\equiv\; & (-1)^{-\epsilon}\left(\frac{N^2-1}{2N}\right)\left(\frac{4\pi\mu^2}{M^2}\right)^{2\epsilon}\left(\frac{\alpha_s}{2\pi}\right)\left(\frac{\alpha e_q^2}{2\pi}\right)\frac{\Gamma(1+\epsilon)\Gamma^2(1-\epsilon)}{\Gamma(1-2\epsilon)} \\ & \mathrm{d}z\,[z(1-z)]^{-\epsilon} \times \int_0^{y_{min}} \mathrm{d}y_{13}\,(y_{13})^{-\epsilon}\,V_{col}, \end{aligned} \tag{6.10}$$

[1]Recall that we only consider the contribution where the photon is on the quark leg. We shall multiply the result by two at the end.

where the function V_{col} contains the scalar integrals. Explicitly,

$$V_{col} = V_{col}^1 + V_{col}^2 + V_{col}^3,$$

where we have divided the contributions into parts with different z dependences. V_{col}^1, V_{col}^2, V_{col}^3 are respectively given by,

$$\begin{aligned}
V_{col}^1 &= \frac{P^\epsilon(z)}{y_{13}} \times \Big\{ -\hat{D}_0(p_2,p_1,p_3) - \hat{D}_0(p_1,p_2,p_3) + \hat{C}_0(p_1,p_3) - \hat{C}_0(p_{13},p_2) \\
&\quad + \hat{C}_0(p_2,p_3) - 2\hat{C}_0(p_{12},p_3) - \hat{C}_0(p_{23},p_1) - 5\hat{B}_0(p_{123}) + 2(1-\epsilon)\hat{B}_0(p_{123}) \Big\}, \\
V_{col}^2 &= \frac{1}{y_{13}} \times \left[-z(1-\epsilon)^2 + 5(1-\epsilon)z + \frac{4z}{1-\epsilon} - \frac{2}{1-\epsilon} - 7z \right] \\
&\quad \times \Big\{ -\hat{D}_0(p_1,p_2,p_3) + \hat{C}_0(p_1,p_2) + \hat{C}_0(p_2,p_3) - \hat{C}_0(p_{12},p_3) - \hat{C}_0(p_{23},p_1) \Big\}, \\
V_{col}^3 &= -\frac{1}{y_{13}} \hat{B}_0(p_{13}) \epsilon(1-\epsilon z).
\end{aligned} \tag{6.11}$$

The $\hat{C}_0$ and $\hat{D}_0$ integrals contain double poles in ϵ while the integral over y_{13} will generate an additional pole in ϵ. We therefore expect that the leading contribution comes from V_{col}^1, while the scalar integrals in V_{col}^2 must conspire to give zero.

The scalar integrals $\hat{I}$ appearing in the above expression are related to the usual loop integrals I as described below. It is useful to define the constant,

$$C_\Gamma = i \left(\frac{4\pi}{M^2} \right)^\epsilon (-1)^\epsilon \frac{\Gamma(1+\epsilon)\Gamma^2(1-\epsilon)}{\Gamma(1-2\epsilon)}. \tag{6.12}$$

The above loop integrals are derived in their most general form in [65]. Only four integrals are necessary for this computation; the bubble integral, the triangle integral with one and two external masses equal to zero and the box integral with three massless external lines. We here quote the general results for the scalar integrals prior to taking the collinear limit.

First, the bubble integral for momentum p_a, $B_0(p_a)$, is given by,

$B_0(p_a) \equiv$ 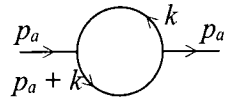

$$\begin{aligned}
&= \int \frac{\mathrm{d}^d k}{(2\pi)^d} \frac{1}{k^2(k+p_a)^2} \\
&= \frac{i}{(4\pi)^{2-\epsilon}} \frac{\Gamma(1+\epsilon)}{\epsilon} \frac{\Gamma^2(1-\epsilon)}{\Gamma(2-2\epsilon)} (-p_a^2)^{-\epsilon}
\end{aligned}$$

$$= \frac{C_\Gamma}{(4\pi)^2}\frac{1}{1-2\epsilon}\frac{1}{\epsilon}\left(\frac{p_a^2}{M^2}\right)^{-\epsilon}.$$
$$= \frac{C_\Gamma}{(4\pi)^2}\hat{B}_0(p_a).$$

For the triangle integral, it is useful to first give the result for two off-shell legs. If momentum $p_c = p_a + p_b$ enters and momenta p_a and p_b exit then if $p_c^2, p_a^2 \neq 0$, and $p_b^2 = 0$, the scalar triangle loop integral $C_0(p_a, p_b)$ reads,

$C_0(p_a,p_b) \equiv$ 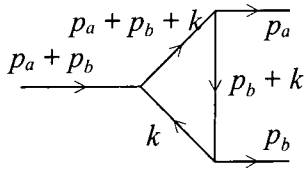

$$= \int \frac{\mathrm{d}^d k}{(2\pi)^d}\frac{1}{k^2(k+p_b)^2(k+p_a+p_b)^2}$$
$$= \frac{i}{(4\pi)^{2-\epsilon}}\frac{\Gamma(1+\epsilon)}{\epsilon^2}\frac{\Gamma^2(1-\epsilon)}{\Gamma(1-2\epsilon)}\frac{(-p_c^2)^{-\epsilon}-(-p_a^2)^{-\epsilon}}{p_c^2-p_a^2}$$
$$= \frac{C_\Gamma}{(4\pi)^2}\frac{1}{\epsilon^2}\left(\left(\frac{p_c^2}{M^2}\right)^{-\epsilon}-\left(\frac{p_a^2}{M^2}\right)^{-\epsilon}\right)\frac{1}{(p_c^2-p_a^2)}$$
$$= \frac{C_\Gamma}{(4\pi)^2}\frac{1}{(p_c^2-p_a^2)}\hat{C}_0(p_a,p_b).$$

This is a suitable form for taking the $p_a^2 \to 0$ limit, so that the triangle integral with $p_c^2 = s_{ab} \neq 0$ and $p_a^2 = p_b^2 = 0$, is given by,

$$C_0(p_a,p_b) = \frac{i}{(4\pi)^{2-\epsilon}}\frac{\Gamma(1+\epsilon)}{\epsilon^2}\frac{\Gamma^2(1-\epsilon)}{\Gamma(1-2\epsilon)}\frac{(-p_c^2)^{-\epsilon}}{p_c^2}$$
$$= \frac{C_\Gamma}{(4\pi)^2}\frac{1}{\epsilon^2}\,(y_{ab})^{-\epsilon}\frac{1}{s_{ab}}$$
$$= \frac{C_\Gamma}{(4\pi)^2}\frac{1}{s_{ab}}\hat{C}_0(p_a,p_b).$$

The box diagram $D_0(p_a, p_b, p_c)$ needs only to be considered in the limit where, $p_a^2 = p_b^2 = p_c^2 = 0$,

$D_0(p_a,p_b,p_c) \equiv$ 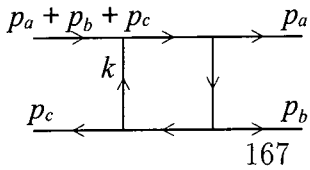

$$
\begin{aligned}
&= \frac{C_\Gamma}{(4\pi)^2}\,\frac{2}{\epsilon^2}\,\frac{1}{s_{ab}s_{bc}}(y_{ab})^{-\epsilon}(y_{bc})^{-\epsilon} \\
&\quad \times\Bigg[(1-y_{ab})^{-\epsilon}\,F_{21}\left(-\epsilon,-\epsilon;1-\epsilon;\frac{y_{ac}}{1-y_{ac}}\right) \\
&\qquad +(1-y_{bc})^{\epsilon}\,F_{21}\left(-\epsilon,-\epsilon;1-\epsilon;\frac{y_{ac}}{1-y_{bc}}\right) \\
&\qquad -(1-y_{ab})^{\epsilon}(1-y_{bc})^{\epsilon}\,F_{21}\left(-\epsilon,-\epsilon;1-\epsilon;\frac{y_{ac}}{(1-y_{bc})(1-y_{ab})}\right)\Bigg] \\
&= \frac{C_\Gamma}{(4\pi)^2}\,\frac{1}{s_{ab}s_{bc}}\hat{D}_0(p_a,p_b,p_c),
\end{aligned}
$$

where $F_{21}(-\epsilon,-\epsilon;1-\epsilon;z)$ can be expanded as a series in ϵ,

$$F_{21}(-\epsilon,-\epsilon;1-\epsilon;z) \;=\; 1+\epsilon^2\,\mathrm{Li}_2(z)+\epsilon^3\,[\mathrm{Li}_3(z)-\mathrm{S}_{12}(z)]+\mathcal{O}(\epsilon^4).$$

It is necessary to consider these scalar integrals for the specific momentum configurations appearing in eq.(6.11) and take the collinear limit. This corresponds to the replacements,

$$y_{12}\to(1-z),\qquad y_{23}\to z,$$

while selecting y_{13} to be small. In this limit, and using the notations $p_{ij}=p_i+p_j$, $p_{ijk}=p_i+p_j+p_k$ we find,

$$
\begin{aligned}
\hat{B}_0(p_{123}) &\to \frac{1}{\epsilon(1-2\epsilon)}, \\
\hat{B}_0(p_{13}) &\to \frac{y_{13}^{-\epsilon}}{\epsilon(1-2\epsilon)}, \\
\hat{C}_0(p_1,p_3) &\to \frac{y_{13}^{-\epsilon}}{\epsilon^2}, \\
\hat{C}_0(p_2,p_3) &\to \frac{z^{-\epsilon}}{\epsilon^2}, \\
\hat{C}_0(p_1,p_2) &\to \frac{(1-z)^{-\epsilon}}{\epsilon^2}, \\
\hat{C}_0(p_{23},p_1) &\to \left[1-(z)^{-\epsilon}\right]\frac{1}{\epsilon^2},
\end{aligned}
$$

$$
\begin{aligned}
\hat{C}_0(p_{12},p_3) &\rightarrow \left[1-(1-z)^{-\epsilon}\right]\frac{1}{\epsilon^2},\\
\hat{C}_0(p_{13},p_2) &\rightarrow \frac{1}{\epsilon^2},\\
\hat{D}_0(p_2,p_1,p_3) &\rightarrow \frac{2}{\epsilon^2}(1-z)^{-\epsilon}y_{13}^{-\epsilon}\,F_{21}\left(-\epsilon,-\epsilon;1-\epsilon;z\right),\\
\hat{D}_0(p_1,p_2,p_3) &\rightarrow \frac{2}{\epsilon^2}\left[(1-z)^{-\epsilon}+(z)^{-\epsilon}-1\right],
\end{aligned}
\tag{6.13}
$$

so that,

$$
\begin{aligned}
V^1_{col} &= \frac{P^\epsilon(z)}{y_{13}}\left[-\frac{2}{\epsilon^2}+\frac{2}{\epsilon^2}\,y_{13}^{-\epsilon}-\frac{2}{\epsilon^2}\,y_{13}^{-\epsilon}\,(1-z)^{-\epsilon}\,F_{21}\left(-\epsilon,-\epsilon;1-\epsilon;z\right)\right.\\
&\qquad\left.-\frac{1}{\epsilon}\frac{(3+2\epsilon)}{(1-2\epsilon)}\right],\\
V^2_{col} &= 0,\\
V^3_{col} &= \frac{1}{y_{13}}\frac{(\epsilon z-1)}{(1-2\epsilon)}.
\end{aligned}
$$

As expected, the leading pole contribution not proportional to the quark-photon splitting function $P^\epsilon(z)$ vanishes. V^3_{col} is not required to vanish because of the extra power of ϵ which makes it a sub-leading term.

6.2.2 Check of the collinear limit of $|\mathcal{M}|^2_V$

The collinear behaviour of one-loop amplitudes has been studied by Bern, Dixon, Dunbar and Kosower [66] using helicity amplitudes. In this subsection we wish to use their work to check our result for the collinear limit of the squared matrix element $|\mathcal{M}|^2_V \equiv 2\,\mathrm{Re}(\mathcal{L}\mathcal{T}^*)$.

Given an arbitrary helicity configuration, in [66] the quark-photon collinear limit of the tree amplitude $\mathcal{M}_{q\bar{q}\gamma}$, associated with the real process $\gamma^* \rightarrow q\bar{q}\gamma$ is given by,

$$
\mathcal{M}_{q\bar{q}\gamma} \xrightarrow{q\|\gamma} \sum_{\lambda=\pm} Split^{tree}_{-\lambda}(p_q^{\lambda_a},p_\gamma^{\lambda_b})\,\mathcal{M}_{Q\bar{q}},
\tag{6.14}
$$

whereas the collinear limit of the one loop helicity amplitude $\mathcal{M}^{loop}_{q\bar{q}\gamma}$ yields,

$$
\mathcal{M}^{loop}_{q\bar{q}\gamma} \xrightarrow{q\|\gamma} \sum_{\lambda=\pm}\left(Split^{tree}_{-\lambda}(p_q^{\lambda_a},p_\gamma^{\lambda_b})\,\mathcal{M}^{loop}_{Q,\bar{q}} + Split^{loop}_{-\lambda}(p_q^{\lambda_a},p_\gamma^{\lambda_b})\,\mathcal{M}_{Q\bar{q}}\right),
\tag{6.15}
$$

with λ the helicity of the parent quark Q.

The splitting amplitudes $Split^{tree}_{-\lambda}(p_q^{\lambda_a}, p_\gamma^{\lambda_b})$ and $Split^{loop}_{-\lambda}(p_q^{\lambda_a}, p_\gamma^{\lambda_b})$ are expected to be universal and to depend only on the two external legs becoming collinear. Furthermore, the tree splitting amplitudes $Split^{tree}_{-\lambda}$ are such that, when one takes the sum of all squared amplitudes of definite helicity one obtains the usual four dimensional simple collinear limit of the $\gamma^* \to q\bar{q}\gamma$ matrix element squared encountered before [2] in Section 1.5.3,

$$\sum_\lambda |\mathcal{M}_{q\gamma\bar{q}}|^2 \xrightarrow{q\|\gamma} \frac{1}{s_{q\gamma}} P(z)|\mathcal{M}_{Q\bar{q}}|^2. \tag{6.16}$$

The relevant tree splitting amplitudes squared are in fact given by,

$$|Split^{tree}_{-}(p_q^+, p_\gamma^+)|^2 = |Split^{tree}_{+}(p_q^-, p_\gamma^-)|^2 = \frac{1}{s_{q\gamma}} \frac{(1-z)^2}{z}, \tag{6.17}$$

$$|Split^{tree}_{-}(p_q^+, p_\gamma^-)|^2 = |Split^{tree}_{+}(p_q^-, p_\gamma^+)|^2 = \frac{1}{s_{q\gamma}} \frac{1}{z}. \tag{6.18}$$

The one-loop splitting functions $Split^{loop}_{-\lambda}(p_q^{\lambda_a}, p_\gamma^{\lambda_b})$ arising in eq.(6.15) are,

$$Split^{loop}_{-\lambda}(p_q^{\lambda_a}, p_\gamma^{\lambda_b}) = Split^{tree}_{-\lambda}(p_q^{\lambda_a}, p_\gamma^{\lambda_b}) \times r_S(p_q^{\lambda_a}, p_\gamma^{\lambda_b}), \tag{6.19}$$

with the relevant $r_S(p_q^{\lambda_a}, p_\gamma^{\lambda_b})$ given by,

$$\begin{aligned} r_S(p_q^-, p_\gamma^+) &= r_S(p_q^+, p_\gamma^-) = \frac{1}{2} f(z, s_{q\gamma}), \\ r_S(p_q^-, p_\gamma^-) &= r_S(p_q^+, p_\gamma^+) = \frac{1}{2}\left(f(z, s_{q\gamma}) - \frac{z}{2}\right), \end{aligned} \tag{6.20}$$

and where the function $f(z, s_{q\gamma})$ is,

$$f(z, s_{q\gamma}) = \left[-\frac{2}{\epsilon^2}(1-z)^{-\epsilon}(y_{q\gamma})^{-\epsilon} + \frac{2}{\epsilon^2}(y_{q\gamma})^{-\epsilon} - 2\mathrm{Li}_2(z)\right] \tag{6.21}$$

We also have that for all helicity amplitudes,

$$|\mathcal{M}^{loop}_{q\bar{q}}|^2 = \frac{1}{2} V_{q\bar{q}} |\mathcal{M}_{q\bar{q}}|^2, \tag{6.22}$$

[2] Recall that $P(z)$ is the four dimensional splitting function.

where $V_{q\bar{q}}$ is the virtual factor associated with the loop diagram related to the process $\gamma^* \to q\bar{q}$ encountered in eq.(1.38).

For an arbitrary helicity configuration, let us denote twice the product of the loop and tree amplitude by $|\mathcal{M}^{\lambda}|^2_V$. In the collinear limit it becomes (for a single helicity),

$$|\mathcal{M}^{\lambda}_V|^2 \xrightarrow{q||\gamma} \frac{1}{s_{q\gamma}} |Split^{tree}_{-\lambda|}|^2 \times \Big[V_{q\bar{q}} + 2\, r_S\Big] \times |\mathcal{M}^{tree}_{\lambda}|^2. \tag{6.23}$$

Summing over all possible helicity configurations and using the results in [66], the collinear limit of $|\mathcal{M}|^2_V$ reads,

$$|\mathcal{M}|^2_V \xrightarrow{q||\gamma} \frac{1}{s_{q\gamma}} |\mathcal{M}_{q\bar{q}}|^2 \times \Big[P(z)\Big(V_{q\bar{q}} + f(z, s_{q\gamma})\Big) + r(z)\Big], \tag{6.24}$$

with $r(z) = -1$. In this equation (6.24) all terms are proportional to,

$$\frac{1}{s_{q\gamma}} |\mathcal{M}_{q\bar{q}}|^2, \tag{6.25}$$

as one could have expected. The term which is not proportional to $P(z)$, $r(z)$ arises from terms proportional to z present only for some of the helicity configurations as can be seen from eq.(6.20).

Finally, we find that the expression (6.24) can also be represented diagrammatically,

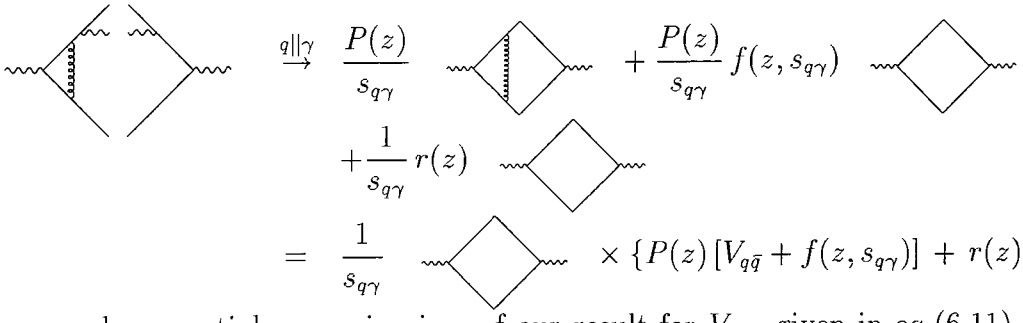

If we now make a partial expansion in ϵ of our result for V_{col}, given in eq.(6.11) we see that

$$\begin{aligned} V_{col} \;=\; & \frac{1}{s_{q\gamma}}\Bigg\{P(z)\Bigg(\Big[-\frac{2}{\epsilon^2} - \frac{3}{\epsilon} - 8 + \pi^2\Big] \\ & + \Big[-\frac{2}{\epsilon^2}(1-z)^{-\epsilon}(y_{13})^{-\epsilon} + \frac{2}{\epsilon^2}(y_{13})^{-\epsilon} - 2\mathrm{Li}_2(z)\Big]\Bigg) - 1\Bigg\}, \end{aligned} \tag{6.26}$$

which is of the form of (6.24) and therefore agrees with the collinear limit of the virtual one-loop amplitudes given by Bern, Dixon, Dunbar and Kosower.

6.2.3 Integration over the unresolved phase space region

Let us now return to our derivation of the singular virtual collinear contributions to the total differential cross section $\gamma^* \to \gamma + 1$ jet, $VC_{F\gamma}$. The integration of y_{13} over the unresolved region generates an overall $1/\epsilon$ factor. In order to calculate the virtual contributions up to $\mathcal{O}(1)$ in ϵ we need therefore to keep terms of $\mathcal{O}(\epsilon)$ in V_{col}. In other words, we need to expand V_{col} one order further in ϵ than it was necessary for the comparison of our result with the one of Bern, Dixon, Dunbar and Kosower (as in eq.(6.26)). Performing furthermore the y_{13} integration, the unresolved quark-photon collinear virtual factor is given by,

$$\begin{aligned} VC_{F\gamma} &= \left(\frac{N^2-1}{2N}\right)\left(\frac{4\pi\mu^2}{Q^2}\right)^{2\epsilon}(-1)^{\epsilon}\left(\frac{\alpha_s}{2\pi}\right)\left(\frac{\alpha e_q^2}{2\pi}\right)\frac{\Gamma(1+\epsilon)\Gamma^2(1-\epsilon)}{\Gamma(1-2\epsilon)} \\ &\times (y_{\min})^{-2\epsilon}\ [z(1-z)]^{-\epsilon} \\ &\times \left(P^{\epsilon}(z)\left[\frac{2}{\epsilon^3}\,y_{\min}^{\epsilon} - \frac{1}{\epsilon^3} + \frac{1}{\epsilon^2}\,y_{\min}^{\epsilon}\left(\frac{3+2\epsilon}{1-2\epsilon}\right) + \frac{1}{\epsilon^3}\,(1-z)^{-\epsilon}\,F_{21}(-\epsilon,-\epsilon;1-\epsilon;z)\right]\right. \\ &\qquad \left. + \frac{(1-\epsilon z)}{2\epsilon(1-2\epsilon)}\right). \end{aligned}$$

As expected, the most divergent part of this expression is proportional to $P^{\epsilon}(z)$ and precisely cancels the leading singularity present in the two-particle unresolved contributions to the four parton process discussed in the previous chapter, namely the leading singularity in the soft/collinear contribution $SC_{F\gamma}$ (c.f. Section 5.3.3). The subleading poles do not cancel; they are ultimately factorized into the $\mathcal{O}(\alpha\alpha_s)$ fragmentation function, as will be presented in Chapter 8.

In conclusion, in this chapter we have determined the divergences present in the resolved and unresolved virtual contributions from the one-loop process, $\gamma^* \to q\bar{q}\gamma(g)$. We saw that the resolved contributions possess divergences which have the right form to cancel those present in the real single unresolved contributions. For the unresolved virtual contributions on the other hand, only the leading singularity part has a similar form to the leading singularity part of the double unresolved contributions. The remaining singular terms will need to be absorbed in the $\mathcal{O}(\alpha\alpha_s)$ counter term of the quark-to-photon frag-

mentation. The cancellation of these singularities together with the construction of the fragmentation counter term will be performed in Chapter 8. The evaluation of all finite contributions arising in this chapter, such as F_c and $\sigma_{q\bar{q}\gamma}$ will be dealt with numerically and presented in Chapter 9.

Chapter 7

Contributions involving $D^B_{q\to\gamma}(x)$

In addition to the real and virtual contributions derived in the three previous chapters, we need to consider a further process contributing to the $\gamma^* \to \gamma$ +1 jet rate at $\mathcal{O}(\alpha\alpha_s)$: the production of a quark-antiquark pair associated with a real or virtual gluon, followed by the fragmentation of a quark into a photon. The contribution of this process to the differential cross section is given by the convolution of the tree level $\gamma^* \to q\bar{q}g$ or one-loop $\gamma^* \to q\bar{q}$ cross section with the *bare* quark-to-photon fragmentation function, $D^B_{q\to\gamma}(x)$, which we introduced in Section 1.5.3.

The Feynman diagrams associated with this process are shown in Fig. 7.1. As usual, charge conjugation invariance implies $D^B_{q\to\gamma} = D^B_{\bar{q}\to\gamma}$ Therefore, to simplify the discussion, we only consider the contribution where the quark fragments into a photon, and account for the antiquark fragmentation contribution by multiplying the result by two. The general structure of this contribution is,

$$\mathrm{d}\sigma_D^{q\bar{q}(g)} \;=\; \mathrm{d}\sigma^{q\bar{q}(g)}\, D^B_{q\to\gamma}(x)\,\mathrm{d}x, \tag{7.1}$$

$\mathrm{d}\sigma_D^{q\bar{q}(g)}$, and $\mathrm{d}\sigma^{q\bar{q}(g)}$ are the fully differential cross sections and x is the ratio between the photon and the *parent quark* momenta.

The *bare* quark-to-photon fragmentation function, $D^B_{q\to\gamma}(x)$ is the sum of a *non perturbative* part, $D_{q\to\gamma}(x,\mu_F)$ which depends on the factorization scale μ_F and can only be determined by experiment, and a *perturbative* counter term. Since the underlying

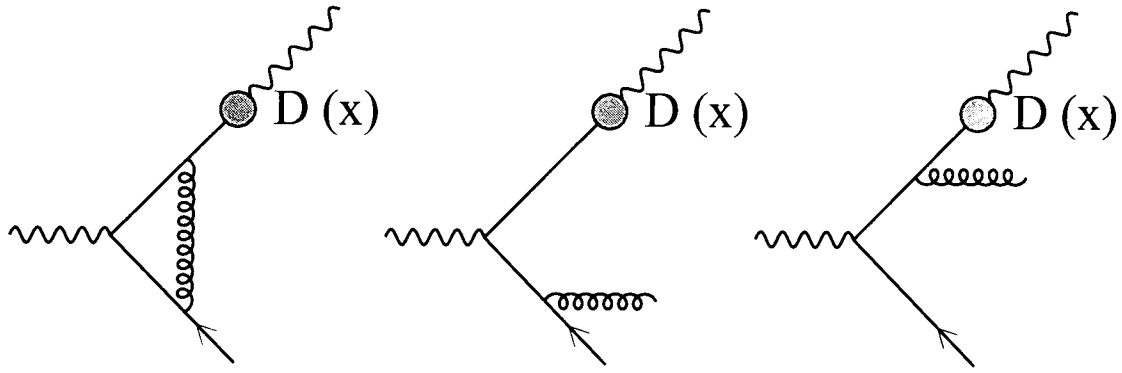

Figure 7.1: Contributions involving the bare fragmentation function $D^B_{q\to\gamma}(x)$.

$\gamma^* \to q\bar{q}(g)$ process is already of $\mathcal{O}(\alpha_s)$, only the $\mathcal{O}(\alpha)$ counter term needs to be considered. The contribution from the convolution of the tree-level $\gamma^* \to q\bar{q}$ process with the $\mathcal{O}(\alpha\alpha_s)$ counter term is discussed in the next chapter. To the order α, the fragmentation function can be decomposed,

$$D^B_{q\to\gamma}(x) = D_{q\to\gamma}(x,\mu_F) + \frac{1}{\epsilon}\frac{\alpha e_q^2}{2\pi}\left(\frac{4\pi\mu^2}{\mu_F^2}\right)^{\epsilon}\frac{1}{\Gamma(1-\epsilon)}\left(\frac{1+(1-x)^2}{x}\right). \qquad (7.2)$$

As usual, this separation introduces a dependence on the fragmentation scale μ_F to the physical fragmentation function $D_{q\to\gamma}(x,\mu_F)$.

As discussed in Section 3.1, the fragmentation contributions separate into three categories, depending whether the gluon is resolved, unresolved or virtual. If the gluon is identified in the final state, we will find that the singularities present in this resolved contribution are exactly cancelled by the real *collinear photon/resolved gluon* contribution from the $\gamma^* \to q\bar{q}g\gamma$ process. This precisely parallels the cancellation of the quark-photon collinear singularity in the $\gamma^* \to q\bar{q}\gamma$ process with the $\mathcal{O}(\alpha)$ fragmentation counterterm multiplying the $\gamma^* \to q\bar{q}$ process present at lowest order discussed in Chapter 2.

If, on the other hand, the gluon is unresolved, it can be combined with the quark or with the antiquark or it can be soft. In the absence of the quark-to-photon fragmentation function, the infrared singularities from the $\gamma^* \to q\bar{q}g$ process exactly cancel against those

from the one-loop $\gamma^* \to q\bar{q}$ process as we saw in Section 1.5.3 . Due to the presence of the fragmentation function, this is no longer the case. When the gluon is collinear to the quark which subsequently fragments into a photon, the parent quark momentum is shared between the quark and the gluon and the fractional momenta carried by the photon and the gluon are related to each other. The consequence is that a convolution between fragmentation function and parton level cross section arises. As we shall see in Section 7.4, a large part of the divergences present in this contribution cancels against the divergences present in the double unresolved contributions discussed in Chapter 5.

The organization of this chapter is as follows. In Section 7.1 we shall give the form of the resolved contributions. The general structure of the unresolved contributions with associated fragmentation will be presented in 7.2, while the calculation of these contributions will be described in some detail in the remainder of this chapter. As a check on our intermediate results, in Section 7.6 we compare our expression for the sum of the contributions with the result of Kunszt and Trócsányi in [47]. As they do not specifically consider the $\gamma^* \to \gamma + 1$ jet rate, but rather the cross section for the process $\gamma^* \to \gamma + X$ we shall find that both results only agree in the most singular piece.

7.1 Resolved contributions

We saw in Section 3.1 that the tree level process $\gamma^* \to q\bar{q}g$ with a theoretically well separated gluon accompanied by fragmentation of the quark contributes to the $\gamma + 1$ jet differential cross section in the following two cases:

(i) The gluon is clustered together with the quark which fragments into a photon.

(ii) The gluon is clustered to the antiquark or it is isolated while the antiquark is clustered with the photon jet.

In both cases the cross section has the form given by (7.1) with x, the fractional momentum carried by the photon inside the *quark-photon* collinear cluster,

$$\mathrm{d}\sigma_D^{q\bar{q}g} \;=\; \mathrm{d}\sigma^{q\bar{q}g}\, D^B_{q\to\gamma}(x)\, \mathrm{d}x. \tag{7.3}$$

It is worth noting that x is a *theoretical* parameter which is only related to the momenta of quark and photon. It does not necessarily coincide with the fractional momenta carried by the photon inside the photon jet z, which is reconstructed by the jet algorithm. In particular $x = z$ only holds if the photon jet only contains the quark and photon, while the antiquark and gluon are combined to form the second jet. If on the other hand, the antiquark or the gluon are clustered by the jet algorithm into the photon jet, one will generally find $z < x$. Ultimately, it is the *experimental* z, which is compared with the experimental cut z_{cut} and required to be greater than z_{cut}.

We note that the singularity structure from the $q\bar{q}g\gamma$ final state in the limit where the quark and photon are collinear (discussed in Section 2.4.2) is proportional to $P(x)$ and depends only on the theoretical x value. In fact, when the gluon is resolved, the cancellation of the singularities between the $q\bar{q}g$ final state with fragmentation counter term and those generated in the $q\bar{q}g\gamma$ final state when the quark and photon are collinear is unaffected by the possible discrepancy between x and z. This explicit cancellation will be demonstrated in Chapter 8.

7.2 The structure of the unresolved contributions

In the previous section, the precise value of z was determined by the jet algorithm and is not necessarily the same as x. Similarly, when the gluon is unresolved, z and x do not necessarily coincide.

If the gluon is soft or collinear to the antiquark, we can identify the ratio between the photon and the quark momenta x by z, since only quark and photon form the "photon" jet, and,

$$\mathrm{d}\sigma_D^{q\bar{q}g} = \mathrm{d}\sigma^{q\bar{q}g} D^B_{q\to\gamma}(z)\mathrm{d}z.$$

Explicit expressions for the individual contributions will be given in Section 7.3. On the other hand, if the gluon is collinear to the quark, so that the gluon carries a fraction y of the quark/gluon cluster momentum, z is no longer equal to x. In fact, z is given by the product of the momentum fraction carried by the quark, $1-y$ and the ratio between

photon and quark momenta x, so that,

$$z = x(1-y).$$

We therefore introduce the constraint, $\int_0^1 \mathrm{d}z\delta\left(x(1-y)-z\right)$ and integrate over x so that, $\mathrm{d}\sigma_D^{q\bar{q}g}$ yields,

$$\mathrm{d}\sigma_D^{q\bar{q}g} \;=\; \mathrm{d}\sigma^{q\bar{q}g}\, D^B_{q\to\gamma}\left(\frac{z}{1-y}\right)\frac{\mathrm{d}z}{1-y}. \tag{7.4}$$

This "unresolved variable" y will be integrated out with the constraint $y < 1-z$. A detailed presentation of the calculation of this particular contribution is given in Section 7.4.

7.3 Contributions with $D^B_{q\to\gamma}(z)$

In this section, we shall list the contributions obtained when the gluon is virtual, collinear to the antiquark or it is soft. In these cases, as we mentioned in Section 7.2, since the fragmenting quark carries all of the photon jet momentum, $x = z$ and the cross section has the following form

$$\mathrm{d}\sigma_D^{q\bar{q}(g)} \;=\; \mathrm{d}\sigma^{q\bar{q}(g)}\, D^B_{q\to\gamma}(z)\mathrm{d}z.$$

Furthermore we have seen in Section 1.5.3 that in the unresolved regions of the three-particle phase space, the partonic cross section $\mathrm{d}\sigma^{q\bar{q}g}$ factorizes into a single unresolved factor multiplying the tree level cross section σ_0. These single unresolved factors were, C_F (given in eq. (1.35)) if the gluon is collinear and S_F (given by eq. (1.25)) if it is soft.

A similar feature also occurs when the gluon is virtual; the cross section factorizes into a known virtual factor $V_{q\bar{q}}$ (eq.(1.38)) and the tree level cross section σ_0. As these factors have already been derived before, we will merely quote their unintegrated form before performing the integrations over the unresolved variables. This should lead us to the result for the contributions with associated fragmentation. The different contributions with $D^B_{q\to\gamma}(z)$ are given as follows.

If a gluon is exchanged internally, the contribution to the $\gamma^* \to \gamma + 1$ jet reads,

$$\mathrm{d}\sigma_D^V \;=\; \sigma_0\, V_{q\bar{q}} D^B(z)\mathrm{d}z$$

$$= \sigma_0 \frac{\alpha_s}{2\pi}\left(\frac{4\pi\mu^2}{M^2}\right)^{\epsilon}\left(\frac{N^2-1}{2N}\right)\frac{\Gamma(1+\epsilon)\Gamma^2(1-\epsilon)}{\Gamma(1-2\epsilon)}$$
$$D^B(z)\mathrm{d}z \times \left[-\frac{2}{\epsilon^2} - \frac{3}{\epsilon} - 8 + \pi^2 - 16\epsilon + \frac{3}{2}\pi^2\epsilon + \mathcal{O}(\epsilon^2)\right]. \qquad (7.5)$$

When the gluon is real but soft, the invariants s_{qg} and $s_{\bar{q}g}$ are both less than the theoretical cut $s_{\min}$ we find,

$$\begin{aligned}
\mathrm{d}\sigma_D^S &= \sigma_0\, S_F D^B(z)\mathrm{d}z \\
&= \sigma_0 \frac{\alpha_s}{2\pi}\left(\frac{4\pi\mu^2}{M^2}\right)^{\epsilon}\left(\frac{N^2-1}{2N}\right)\frac{1}{\Gamma(1-\epsilon)} \\
&\quad \times \int_0^{y_{\min}} \mathrm{d}y_{\bar{q}g}(y_{\bar{q}g})^{-\epsilon-1}\int_0^{y_{\min}} \mathrm{d}y_{qg}\,(y_{qg})^{-\epsilon-1} \times D^B(z)\mathrm{d}z \\
&= \sigma_0 \frac{\alpha_s}{2\pi}\left(\frac{4\pi\mu^2}{M^2}\right)^{\epsilon}\left(\frac{N^2-1}{2N}\right)\frac{1}{\Gamma(1-\epsilon)} D^B(z)\mathrm{d}z\left[-\frac{2}{\epsilon^2}\,(y_{\min})^{-2\epsilon}\right]. \qquad (7.6)
\end{aligned}$$

When the gluon is collinear to the antiquark, $s_{\bar{q}g} < s_{\min}$ but $s_{qg} > s_{\min}$. As usual, y is the fractional momentum carried by the gluon, $s_{qg} = yM^2$ and the differential cross section reads[1],

$$\begin{aligned}
\mathrm{d}\sigma_D^{C(\bar{q})} &= \sigma_0\, C_F D^B(z)\mathrm{d}z \\
&= \sigma_0 \frac{\alpha_s}{2\pi}\left(\frac{4\pi\mu^2}{M^2}\right)^{\epsilon}\left(\frac{N^2-1}{2N}\right)\frac{1}{\Gamma(1-\epsilon)} \\
&\quad \times \int_0^{y_{\min}} \mathrm{d}y_{\bar{q}g}(y_{\bar{q}g})^{-\epsilon-1}\int_{y_{\min}}^{1} \mathrm{d}y\,[y(1-y)]^{-\epsilon} P_{\bar{q}g\to\bar{Q}}(y) \times D^B(z)\mathrm{d}z \\
&= \sigma_0 \frac{\alpha_s}{2\pi}\left(\frac{4\pi\mu^2}{M^2}\right)^{\epsilon}\left(\frac{N^2-1}{2N}\right)\frac{1}{\Gamma(1-\epsilon)} D^B(z)\mathrm{d}z(y_{\min})^{-\epsilon} \\
&\quad \times \left[-\frac{2}{\epsilon^2}(y_{\min})^{-\epsilon} + \frac{(1-\epsilon)(4-\epsilon)}{2\epsilon^2(1-2\epsilon)}\,\frac{\Gamma^2(1-\epsilon)}{\Gamma(1-2\epsilon)}\right]. \qquad (7.7)
\end{aligned}$$

Note that to simplify the notation, inside the equations we have denoted the bare quark-to-photon fragmentation function by $D^B(z)$ instead of $D^B_{q\to\gamma}(z)$. We will use the same simplified notation in the next section as well.

[1] $P_{\bar{q}g\to\bar{Q}}$ is the usual n-dimensional Altarelli-Parisi splitting function defined in 1.5.3.

7.4 Contributions with the gluon collinear to the quark

As discussed in Section 7.2, when the gluon, which carries a fraction y of the parent quark momentum p_Q, is collinear to the fragmenting quark, we can make the identification $z = x(1-y)$. The fragmentation function is thus a function of $z/(1-y)$ and the general form for the cross section is given by eq.(7.1). Moreover, in the quark-gluon collinear limit, the partonic cross section $\sigma_{q\bar{q}g}$ takes a similar form as in eq.(7.7), but with y limited by $1-z$ instead of 1. The contribution to the differential cross section denoted by $\mathrm{d}\sigma_D^{C(q)}$ reads,

$$\begin{aligned}
\mathrm{d}\sigma_D^{C(q)} &= \mathrm{d}\sigma^{q\bar{q}g}\, D^B\left(\frac{z}{1-y}\right)\frac{\mathrm{d}z}{1-y} \\
&= \sigma_0\,\frac{\alpha_s}{2\pi}\left(\frac{4\pi\mu^2}{M^2}\right)^{\epsilon}\left(\frac{N^2-1}{2N}\right)\frac{1}{\Gamma(1-\epsilon)} \\
&\quad\times\int_0^{y_{\min}}\mathrm{d}y_{\bar{q}g}(y_{\bar{q}g})^{-\epsilon-1}\int_{y_{\min}}^{1-z}\frac{\mathrm{d}y}{1-y}\,[y(1-y)]^{-\epsilon}P_{qg\to Q}(y)\times D^B\left(\frac{z}{1-y}\right)\mathrm{d}z \\
&= -\frac{1}{\epsilon}\frac{\alpha_s}{2\pi}\left(\frac{4\pi\mu^2}{M^2}\right)^{\epsilon}\left(\frac{N^2-1}{2N}\right)\sigma_0\,\frac{1}{\Gamma(1-\epsilon)}(y_{\min})^{-\epsilon} \\
&\quad\times\int_{y_{\min}}^{1-z}\frac{\mathrm{d}y}{1-y}\,[y(1-y)]^{-\epsilon}P(y)\times D^B\left(\frac{z}{1-y}\right)\mathrm{d}z
\end{aligned} \tag{7.8}$$

The y integral now involves the fragmentation function and requires some work to evaluate. The resulting expression will involve a convolution of the splitting function with the fragmentation function. However, the convolution integral present in eq.(7.8) appears to have an explicit $y_{\min}$ dependence coming from the lower boundary of the y integral. However, we know that since $y_{\min}$ is an artificial parameter which cannot influence the physical cross section for any choice of fragmentation function, the $y_{\min}$ dependence must merely act multiplicatively on the fragmentation function D^B.

To see that this is indeed the case, we add and subtract the contribution where a gluon is collinear to a quark multiplied by $D^B(z)$. We can thus rewrite this convolution integral

in the following way,

$$\begin{aligned}
\mathrm{d}\sigma_D^{C(q)} &= \mathrm{d}\sigma_D^{C(q)} + \frac{1}{\epsilon}\frac{\alpha_s}{2\pi}\left(\frac{4\pi\mu^2}{M^2}\right)^{\epsilon}\left(\frac{N^2-1}{2N}\right)\frac{1}{\Gamma(1-\epsilon)}(y_{\min})^{-\epsilon}\, D^B(z)\mathrm{d}z\sigma_0 \\
&\quad \times\left\{\int_{y_{\min}}^{1}\mathrm{d}y\,[y(1-y)]^{-\epsilon}P_{qg\to Q}(y)\right. \\
&\quad \left.-\left[\frac{2}{\epsilon}(y_{\min})^{-\epsilon} - \frac{(1-\epsilon)(4-\epsilon)}{2\epsilon(1-2\epsilon)}\,\frac{\Gamma^2(1-\epsilon)}{\Gamma(1-2\epsilon)}\right]\right\} \\
&= \mathrm{d}\sigma_D^{C(q)'} + \sigma_0\, C_F\, D^B(z)\mathrm{d}z, \qquad (7.9)
\end{aligned}$$

with $\mathrm{d}\sigma_D^{C(q)'}$ given by,

$$\begin{aligned}
\mathrm{d}\sigma_D^{C(q)'} &= -\frac{1}{\epsilon}\sigma_0\frac{\alpha_s}{2\pi}\left(\frac{4\pi\mu^2}{M^2}\right)^{\epsilon}\left(\frac{N^2-1}{2N}\right)\frac{1}{\Gamma(1-\epsilon)}(y_{\min})^{-\epsilon}\mathrm{d}z \\
&\quad \times\left\{\int_{y_{\min}}^{1-z}\mathrm{d}y\,[y(1-y)]^{-\epsilon}P_{qg\to Q}(y)\times\left[\frac{D^B\left(\frac{z}{1-y}\right)}{1-y} - D^B(z)\right]\right. \\
&\quad \left.-\int_{1-z}^{1}\mathrm{d}y\,[y(1-y)]^{-\epsilon}P_{qg\to Q}(y)D^B(z)\right\}.
\end{aligned}$$

In the first integral of the expression for $\mathrm{d}\sigma_D^{C(q)'}$, the integrand vanishes when $y \to 0$, and we can safely extend the range of integration to 0. By doing so, the convolution contribution itself becomes $y_{\min}$ independent as we wanted. Using the definition,

$$P_{qg\to Q}(y) = \frac{1+(1-y)^2-\epsilon y^2}{y},$$

and the change of variable $y = 1-t$, $\mathrm{d}\sigma_D^{C(q)'}$ can be rewritten in a more familiar form,

$$\begin{aligned}
\mathrm{d}\sigma_D^{C(q)'} &= -\frac{1}{\epsilon}\sigma_0\mathrm{d}z\frac{\alpha_s}{2\pi}\left(\frac{4\pi\mu^2}{M^2}\right)^{\epsilon}\left(\frac{N^2-1}{2N}\right)\frac{1}{\Gamma(1-\epsilon)}(y_{\min})^{-\epsilon} \\
&\quad \times\left\{\int_{z}^{1}\mathrm{d}t\,[t(1-t)]^{-\epsilon}\left(\frac{1+t^2-\epsilon(1-t)^2}{1-t}\right)\left[\frac{D^B\left(\frac{z}{t}\right)}{t} - D^B(z)\right]\right. \\
&\quad \left.-\int_{0}^{z}\mathrm{d}t\,[t(1-t)]^{-\epsilon}\left(\frac{1+t^2-\epsilon(1-t)^2}{1-t}\right)D^B(z)\right\}.
\end{aligned}$$

This can be rearranged using the definition of the "+" prescription defined in Appendix A.5,

$$\int_z^1 \mathrm{d}t \, \frac{h(t)}{((1-t)^{1+\epsilon})_+} \equiv \int_z^1 \mathrm{d}t \, \frac{h(t)-h(1)}{(1-t)^{1+\epsilon}} - \int_0^z \mathrm{d}t \, \frac{h(1)}{(1-t)^{1+\epsilon}},$$

with,

$$h(t) = \frac{(1+t^2)t^{-\epsilon} D^B\left(\frac{z}{t}\right)}{t} \qquad \text{and} \qquad h(1) = 2\, D^B(z),$$

so that,

$$\begin{aligned}
\mathrm{d}\sigma_D^{C(q)'} &= -\frac{1}{\epsilon}\sigma_0 \mathrm{d}z \frac{\alpha_s}{2\pi}\left(\frac{4\pi\mu^2}{M^2}\right)^{\epsilon}\left(\frac{N^2-1}{2N}\right)\frac{1}{\Gamma(1-\epsilon)}(y_{\min})^{-\epsilon} \\
&\times\left\{\int_z^1 \frac{\mathrm{d}t}{t}\,\frac{(1+t^2)t^{-\epsilon}}{((1-t)^{1+\epsilon})_+} D^B\left(\frac{z}{t}\right) + D^B(z)\int_0^1 \mathrm{d}t\,\frac{2-(1+t^2)t^{-\epsilon}}{(1-t)^{1+\epsilon}}\right. \\
&\left. -\epsilon\left[\int_z^1 \frac{\mathrm{d}t}{t}(1-t)^{1-\epsilon}t^{-\epsilon} D^B\left(\frac{z}{t}\right) - D^B(z)\int_0^1 \mathrm{d}t\, t^{-\epsilon}(1-t)^{1-\epsilon}\right]\right\} \quad (7.10)
\end{aligned}$$

It is convenient to divide $\mathrm{d}\sigma_D^{C(q)'}$ into two parts: $\mathrm{d}\sigma_D^{C(q.1)'}$, which is proportional to $D^B(z)$, and $\mathrm{d}\sigma_D^{C(q.2)'}$ involving $D^B(z/t)$. Each of these contributions turns out to be of $\mathcal{O}(1/\epsilon^2)$. Indeed each term is explicitly of $\mathcal{O}(1/\epsilon)$ while the $\mathcal{O}(\alpha)$ counter term present in $D^B_{q\to\gamma}$ as given in eq.(7.2) is proportional to $1/\epsilon$. We must therefore expand each term up to $\mathcal{O}(\epsilon^2)$. By doing so we obtain the following expressions,

$$\begin{aligned}
\mathrm{d}\sigma_D^{C(q.1)'} &= -\frac{1}{\epsilon}\sigma_0 \mathrm{d}z \frac{\alpha_s}{2\pi}\left(\frac{4\pi\mu^2}{M^2}\right)^{\epsilon}\left(\frac{N^2-1}{2N}\right)\frac{1}{\Gamma(1-\epsilon)}(y_{\min})^{-\epsilon} D^B(z) \\
&\times\left\{-\frac{2}{\epsilon} + \frac{\Gamma^2(1-\epsilon)}{\Gamma(1-2\epsilon)}\left[\frac{2}{\epsilon} + \frac{3}{2(1-2\epsilon)} + \frac{\epsilon}{2(1-2\epsilon)}\right]\right\} \\
&= -\frac{1}{\epsilon}\sigma_0 \mathrm{d}z \frac{\alpha_s}{2\pi}\left(\frac{4\pi\mu^2}{M^2}\right)^{\epsilon}\left(\frac{N^2-1}{2N}\right)\frac{1}{\Gamma(1-\epsilon)}(y_{\min})^{-\epsilon} D^B(z) \\
&\times\left\{\frac{3}{2} + \epsilon\left(3 - \frac{\pi^2}{3}\right) + \epsilon^2\left(-4\zeta(3) - \frac{1}{4}\pi^2 + 7\right)\right\},
\end{aligned}$$

$$\mathrm{d}\sigma_D^{C(q.2)'} = -\frac{1}{\epsilon}\sigma_0 \mathrm{d}z \frac{\alpha_s}{2\pi}\left(\frac{4\pi\mu^2}{M^2}\right)^{\epsilon}\left(\frac{N^2-1}{2N}\right)\frac{1}{\Gamma(1-\epsilon)}(y_{\min})^{-\epsilon}$$

$$
\begin{aligned}
&\times \int_z^1 \frac{\mathrm{d}t}{t} D\left(\frac{z}{t}\right) \left\{ \frac{(1+t^2)t^{-\epsilon}}{((1-t)^{1+\epsilon})_+} - \epsilon(1-t)^{1-\epsilon} t^{-\epsilon} \right\} \\
= \; & -\frac{1}{\epsilon} \mathrm{d}\sigma_0 \mathrm{d}z \frac{\alpha_s}{2\pi} \left(\frac{4\pi\mu^2}{M^2}\right)^{\epsilon} \left(\frac{N^2-1}{2N}\right) \frac{1}{\Gamma(1-\epsilon)} (y_{\min})^{-\epsilon} \\
&\times \int_z^1 \frac{\mathrm{d}t}{t} D\left(\frac{z}{t}\right) \left\{ \left[\frac{(1+t^2)}{(1-t)_+} \right] \right. \\
&-\epsilon \left[\left(\frac{\ln(1-t)}{1-t} \right)_+ (1+t^2) + \frac{\ln(t)}{1-t}(1+t^2) + (1-t) \right] \\
&+\epsilon^2 \left[\frac{1}{2} \left(\frac{\ln^2(1-t)}{1-t} \right)_+ (1+t^2) + \frac{1}{2} \frac{\ln^2(t)}{1-t} (1+t^2) \right. \\
&\left. \left. + \frac{\ln(t)\ln(1-t)}{1-t} (1+t^2) + (1-t)\left[\ln(t) + \ln(1-t)\right] \right] \right\}.
\end{aligned}
$$

7.5 Sum of all unresolved contributions

In combining the different terms from the previous sections, we notice that the unresolved gluon contributions discussed in Section (7.3) ($\mathrm{d}\sigma_D^{C(\bar{q})}$, $\mathrm{d}\sigma_D^S$ and $\mathrm{d}\sigma_D^V$) which are all proportional to $D^B(z)$ can be combined with the collinear quark-gluon contribution, also proportional to $D^B(z)$, that is present in $\mathrm{d}\sigma_D^{C(q)}$, c.f. eq.(7.9), to give,

$$
\begin{aligned}
\mathrm{d}\sigma_D^K &= \left[2C_F + S_F + V_{q\bar{q}}\right] \sigma_0 D^B(z)\mathrm{d}z \\
&= \mathcal{K}_{q\bar{q}} \sigma_0 D^B(z)\mathrm{d}z,
\end{aligned}
$$

where $\mathcal{K}_{q\bar{q}}$ is the finite two quark $\mathcal{K}$-factor introduced in Section 1.5.3. Expanding up to $\mathcal{O}(\epsilon)$, we find,

$$
\begin{aligned}
\mathrm{d}\sigma_D^K &= \sigma_0 \frac{1}{\Gamma(1-\epsilon)} \frac{\alpha_s}{2\pi} \left(\frac{4\pi\mu^2}{M^2}\right)^{\epsilon} \left(\frac{N^2-1}{2N}\right) \times D^B(z)\mathrm{d}z \\
&\times \left[\left(-2\ln^2(y_{\min}) - 3\ln(y_{\min}) + \frac{\pi^2}{3} - 1 \right) + \epsilon \left(2\ln^3(y_{\min}) + \frac{3}{2}\ln^2(y_{\min}) \right. \right. \\
&\left. \left. + \left(\frac{2\pi^2}{3} - 7 \right) \ln(y_{\min}) - 2 + \pi^2 - 4\zeta(3) \right) \right]. \qquad (7.11)
\end{aligned}
$$

Finally, the sum of all the contributions involving $D^B_{q\to\gamma}$ reads,

$$
\begin{aligned}
\mathrm{d}\sigma_D^{q\bar{q}(g)} &= \mathrm{d}\sigma_D^K + \mathrm{d}\sigma_D^{C(q)'} \\
&= -\frac{1}{\epsilon}\sigma_0 \frac{1}{\Gamma(1-\epsilon)}\frac{\alpha_s}{2\pi}\left(\frac{4\pi\mu^2}{M^2}\right)^{\epsilon}\left(\frac{N^2-1}{2N}\right)\int_z^1 \frac{\mathrm{d}t}{t}\, D\left(\frac{z}{t}\right)\mathrm{d}z \\
&\quad \times\left\{\left[\frac{(1+t^2)}{(1-t)_+}+\frac{3}{2}\delta(1-t)\right]\right. \\
&\quad +\epsilon\left[\left(-2\ln^2(y_{\min})-\frac{3}{2}\ln(y_{\min})+\left(\frac{2\pi^2}{3}-\frac{9}{2}\right)\right)\delta(1-t)\right. \\
&\quad \left.+\frac{(1+t^2)}{(1-t)_+}\ln(y_{\min})+\left(\frac{\ln(1-t)}{1-t}\right)_+(1+t^2)+\frac{\ln(t)}{1-t}(1+t^2)+(1-t)\right] \\
&\quad +\epsilon^2\left[\left(2\ln^3(y_{\min})+\frac{3}{2}\ln^2(y_{\min})+\left(\frac{2\pi^2}{3}-7\right)\ln(y_{\min})\right.\right. \\
&\qquad \left.+5+\frac{3}{4}\pi^2-8\zeta(3)\right)\delta(1-t) \\
&\qquad +\frac{1}{2}\left(\frac{\ln^2(1-t)}{1-t}\right)_+(1+t^2)+\frac{1}{2}\frac{\ln^2(t)}{1-t}(1+t^2) \\
&\qquad \left.\left.+\frac{\ln(t)\ln(1-t)}{1-t}(1+t^2)+(1-t)\ln(t)+(1-t)\ln(1-t)\right]\right\},
\end{aligned}
\tag{7.12}
$$

which can be written in the following form

$$
\begin{aligned}
\mathrm{d}\sigma_D^{q\bar{q}(g)} &\equiv \sigma_0 \frac{1}{\Gamma(1-\epsilon)}\frac{\alpha_s}{2\pi}\left(\frac{4\pi\mu^2}{M^2}\right)^{\epsilon}\left(\frac{N^2-1}{2N}\right)\int_z^1 \frac{\mathrm{d}t}{t}\, D\left(\frac{z}{t}\right)\mathrm{d}z \\
&\quad \times\left[-\frac{1}{\epsilon}P_{qq}^{(0)}+c_q^{(1)}+\epsilon c_q^{(2)}\right].
\end{aligned}
\tag{7.13}
$$

The coefficient of the leading pole term represents the universal lowest order Altarelli-Parisi [40] quark-to-quark splitting function in four dimensions, $P_{qq}^{(0)}$, which is given by,

$$
P_{qq}^{(0)} = \left[\frac{(1+t^2)}{(1-t)_+}+\frac{3}{2}\delta(1-t)\right]. \tag{7.14}
$$

7.6 Check of our result

As a check of our result given in eq. (7.13), we compare this expression for $\mathrm{d}\sigma_D^{q\bar{q}(g)}$ which represents the unresolved contribution to the γ +1 jet rate involving $D^B_{q\to\gamma}$, with the result obtained by Kunszt and Trocsanyi in [47] for the corresponding contribution to the *inclusive* differential cross section.

The fragmentation contribution to the cross section for $\gamma^* \to \gamma + X$ given in [47] reads,

$$\begin{aligned}
\mathrm{d}\sigma_{Incl.}^{q\bar{q}(g)} &= -\frac{1}{\epsilon}\sigma_0 \frac{1}{\Gamma(1-\epsilon)}\frac{\alpha_s}{2\pi}\left(\frac{4\pi\mu^2}{M^2}\right)^{\epsilon}\left(\frac{N^2-1}{2N}\right)\int_{x_\gamma}^1 \frac{\mathrm{d}t}{t}\, D^B\left(\frac{x_\gamma}{t}\right)\mathrm{d}x_\gamma \\
&\times\Bigg\{\left[\frac{(1+t^2)}{(1-t)_+}+\frac{3}{2}\delta(1-t)\right] \\
&+\epsilon\times\left[\left(\frac{\ln(1-t)}{1-t}\right)_+(1+t^2)\ -\frac{3}{2}\left(\frac{1}{1-t}\right)_+\right. \\
&\left.+\frac{2\ln(t)}{1-t}(1+t^2)\ +\left(\frac{2\pi^2}{3}-\frac{9}{2}\right)\delta(1-t)-\frac{3}{2}t\ +\frac{5}{2}\right]+\mathcal{O}(\epsilon^2)\Bigg\}, \quad (7.15)
\end{aligned}$$

where $x_\gamma = \frac{2E_\gamma}{\sqrt{s}}$. $\mathrm{d}\sigma_{Incl.}^{q\bar{q}(g)}$ is the sum of the virtual contributions involving $D^B(x_\gamma)$ given by

$$\begin{aligned}
\mathrm{d}\sigma_{Incl}^{V} &= \sigma_0\, V_{q\bar{q}} D^B(x_\gamma)\mathrm{d}x_\gamma \\
&= \sigma_0\,\frac{\alpha_s}{2\pi}\left(\frac{4\pi\mu^2}{M^2}\right)^{\epsilon}\left(\frac{N^2-1}{2N}\right)\frac{\Gamma(1+\epsilon)\Gamma^2(1-\epsilon)}{\Gamma(1-2\epsilon)} \\
&\quad D^B(x_\gamma)\mathrm{d}x_\gamma\times\left[-\frac{2}{\epsilon^2}-\frac{3}{\epsilon}-8+\pi^2+\mathcal{O}(\epsilon)\right],
\end{aligned}$$

and the real contributions, $\mathrm{d}\sigma_{Incl}^{R}$ involving $D^B\left(\frac{x_\gamma}{x_q}\right)$. These real contributions, in contrast to our case, are obtained by integrating the three particle matrix element squared over the *whole* three particle phase space,

$$\begin{aligned}
\mathrm{d}\sigma_{Incl}^{R} &= \sigma_0\,\frac{\alpha_s}{2\pi}\left(\frac{4\pi\mu^2}{M^2}\right)^{\epsilon}\left(\frac{N^2-1}{2N}\right)\int_{x_\gamma}^1\frac{\mathrm{d}x_q}{x_q}\,D^B\left(\frac{x_\gamma}{x_q}\right) \\
&\times\frac{1}{\Gamma(1-\epsilon)}\int \mathrm{d}y_{12}\,\mathrm{d}y_{13}\,\mathrm{d}y_{23}\,\Theta(1-y_{13}-y_{23})\,(y_{12}y_{13}y_{23})^{-\epsilon} \\
&\times\left[(1-\epsilon)\left(\frac{y_{23}}{y_{13}}+\frac{y_{13}}{y_{23}}\right)+\frac{2y_{12}-\epsilon y_{13}y_{23}}{y_{13}y_{23}}\right]
\end{aligned}$$

$$\times\delta\left(1-y_{12}-y_{13}-y_{23}\right)\,\delta\left(1-y_{23}-\frac{2E_q}{\sqrt{s}}\right).$$

Identifying $x_q \equiv \frac{2E_q}{\sqrt{s}}$ by t as we did in eq.(7.13) one obtains,

$$\begin{aligned}\mathrm{d}\sigma^R_{Incl} &= \sigma_0\,\frac{\alpha_s}{2\pi}\left(\frac{4\pi\mu^2}{M^2}\right)^{\epsilon}\left(\frac{N^2-1}{2N}\right)\frac{1}{\Gamma(1-\epsilon)}\int_{x_\gamma}^1\frac{\mathrm{d}t}{t}\,D\left(\frac{x_\gamma}{t}\right)\\ &\quad\times\left\{-\frac{1}{\epsilon}\frac{(1+t^2)}{1-t}-\frac{3}{2}\left(\frac{1}{1-t}\right)-\frac{3}{2}t+\frac{5}{2}+\frac{7}{2}\delta(1-t)\right\},\end{aligned}$$

which, after utilizing the + -prescription and combining with $\mathrm{d}\sigma^V_{Incl}$ gives eq.(7.15).

The virtual contributions involving the fragmentation function are identical in both approaches. However, the contributions from the real emission are different. Indeed, to calculate the real contributions, we have not integrated over the whole of phase space, but limited ourselves to the unresolved collinear and soft regions of the three particle phase space. As a consequence, $\mathrm{d}\sigma_D^{q\bar{q}(g)}$ and $\mathrm{d}\sigma_{Incl}^{q\bar{q}(g)}$ are the contributions involving $D_{q\to\gamma}$ for two different process: the *exclusive* $\gamma+1$ jet rate in our case (eq.(7.13)) compared to the *inclusive* $\gamma+X$ differential cross section in the other case (eq.(7.15)). Hence we should not expect these two contributions to be identical.

However, at the edges of the phase space, in the so called "unresolved region" x_γ and $z=E_\gamma/(E_\gamma+E_q)$ are equal to each other and we therefore find that the most singular contribution,

$$\sigma_0\,\frac{\alpha_s}{2\pi}\left(\frac{4\pi\mu^2}{M^2}\right)^{\epsilon}\left(\frac{N^2-1}{2N}\right)\frac{1}{\Gamma(1-\epsilon)}\int_{x_\gamma}^1\frac{\mathrm{d}t}{t}\,D\left(\frac{x_\gamma}{t}\right)\times\left\{-\frac{1}{\epsilon}\left[\frac{(1+t^2)}{(1-t)_+}+\frac{3}{2}\delta(1-t)\right]\right\},$$

is the same in both expressions $\mathrm{d}\sigma_D^{q\bar{q}(g)}$ and $\mathrm{d}\sigma_{Incl}^{q\bar{q}(g)}$. Note that this term can be written in a more compact form as follows,

$$\sigma_0\,\frac{\alpha_s}{2\pi}\left(\frac{4\pi\mu^2}{M^2}\right)^{\epsilon}\left(\frac{N^2-1}{2N}\right)\frac{1}{\Gamma(1-\epsilon)}\times\left[-\frac{1}{\epsilon}P_{qq}^{(0)}\otimes D\right] \tag{7.16}$$

where the *convolution* symbol $\otimes$ is defined by,

$$\begin{aligned}(f\otimes g)(x) &= \int_0^1\mathrm{d}x_1\int_0^1\mathrm{d}x_2\,\delta(x-x_1x_2)f(x_1)g(x_2)\\ &= \int_x^1\frac{\mathrm{d}x_1}{x_1}\,f(x_1)g\left(\frac{x}{x_1}\right),\end{aligned} \tag{7.17}$$

and $P_{qq}^{(0)}$ is the universal lowest order Altarelli-Parisi quark-to-quark splitting function encountered in eq.(7.13).

7.7 Integration of the fragmentation counter term

The final step is to insert the decomposition of the bare fragmentation function given in eq.(7.2) into the sum of all fragmentation contributions given in eq.(7.13). In doing so, we will obtain the *fragmentation collinear* factor, $FC_{F\gamma}\mathrm{d}z$ which is made up with two different contributions, $\mathrm{d}\sigma_{\mathrm{np}}^{q\bar{q}(g)}$ and $\mathrm{d}\sigma_{\mathrm{p}}^{q\bar{q}(g)}$, containing the non-perturbative and perturbative terms of the fragmentation function respectively. The precise form of the non-perturbative part of the fragmentation function, $D(z,\mu_F)$ must be fixed by experiment and it is our goal to try to determine it by comparing our final results with the actual data from LEP. For $\mathrm{d}\sigma_{\mathrm{np}}^{q\bar{q}(g)}$, we therefore cannot perform the integrations analytically and rely on numerical methods to compute the relevant convolutions. Neglecting terms of $\mathcal{O}(\epsilon)$, we find,

$$
\begin{aligned}
\mathrm{d}\sigma_{\mathrm{np}}^{q\bar{q}(g)} &= \sigma_0 \frac{1}{\Gamma(1-\epsilon)} \frac{\alpha_s}{2\pi} \left(\frac{4\pi\mu^2}{M^2}\right)^{\epsilon} \left(\frac{N^2-1}{2N}\right) \int_z^1 \frac{\mathrm{d}t}{t}\, D\left(\frac{z}{t},\mu_F\right) \mathrm{d}z \\
&\quad \times \left\{ -\frac{1}{\epsilon}\left[\frac{(1+t^2)}{(1-t)_+} + \frac{3}{2}\delta(1-t)\right] \right. \\
&\quad - \left[\left(-2\ln^2(y_{\min}) - 3\ln(y_{\min}) + \left(\frac{2\pi^2}{3} - \frac{9}{2}\right)\right)\delta(1-t) \right. \\
&\quad \left.\left. + \frac{(1+t^2)}{(1-t)_+}\ln(y_{\min}) + \left(\frac{\ln(1-t)}{1-t}\right)_+ (1+t^2) + \frac{\ln(t)}{1-t}(1+t^2) + (1-t)\right]\right\} \\
&= \sigma_0 \frac{1}{\Gamma(1-\epsilon)} \frac{\alpha_s}{2\pi} \left(\frac{4\pi\mu^2}{M^2}\right)^{\epsilon} \left(\frac{N^2-1}{2N}\right) \mathrm{d}z \left[-\frac{1}{\epsilon}P_{qq}^{(0)} + c_q^{(1)}\right] \otimes D(z,\mu_F) \\
&\equiv \sigma_0\, \mathrm{d}z \hat{F}_q \otimes D(z,\mu_F). \qquad (7.18)
\end{aligned}
$$

A divergence remains $\left[-\frac{1}{\epsilon}P_{qq}^{(0)}\right]$, which will ultimately be cancelled by the $\mathcal{O}(\alpha\alpha_s)$ counterterm part of the bare fragmentation function multiplied by the lowest order $\gamma^* \to q\bar{q}$ cross section.

On the other hand, the t integration over the perturbative counter term in (7.12) can

be analytically carried through. We find,

$$
\begin{aligned}
\mathrm{d}\sigma_{\mathrm{P}}^{q\bar{q}(g)} \;=\; & \sigma_0 \frac{1}{\Gamma^2(1-\epsilon)} \left(\frac{N^2-1}{2N}\right) \left(\frac{\alpha_s}{2\pi}\right) \left(\frac{\alpha e_q^2}{2\pi}\right) \left(\frac{4\pi\mu^2}{M^2}\right)^{2\epsilon} \mathrm{d}z \\
& \times \Bigg\{ \frac{1}{\epsilon^2}\Bigg[-2 + \frac{z}{2} + \ln(z)\,(-2+z) - 2\,\ln(1-z) P(z) \Bigg] \\
& + \frac{1}{\epsilon}\Bigg[+ \ln^2(1-z) P(z) + \ln^2(z)\left(1-\frac{z}{2}\right) - \frac{7\,z}{2} - P(z) + \ln(z)\,(5+z) \\
& \quad + \ln(1-z)\left(2 - \frac{z}{2} - \frac{3\,P(z)}{2}\right) + \ln(z)\ln(1-z)\,(2-z) \\
& \quad + \mathrm{Li}_2(1-z)\,(2-z-2\,P(z)) + \frac{2\,\pi^2 P(z)}{3} \\
& \quad + \ln(y_{\min})\left(2 - \frac{z}{2} - 3\,P(z) + \ln(z)\,(2-z) + 2\,\ln(1-z) P(z)\right) \\
& \quad + \ln(\mu_F^2/M^2)\left(2 - \frac{z}{2} + \ln(z)\,(2-z) + 2\,\ln(1-z) P(z)\right) \\
& \quad + \ln^2(y_{\min})\,(-2P(z)) \Bigg] \\
& -6 - z - 2\,P(z) + \ln^2(z)\left(-\frac{5}{2} - \frac{z}{2}\right) + \ln(z)\ln(1-z)\,(-5-z) \\
& + \ln^2(1-z)\left(-1 + \frac{z}{4} + \frac{3\,P(z)}{4}\right) + \ln(1-z)\mathrm{Li}_2(1-z)\,(-2+z+2\,P(z)) \\
& + \ln^3(z)\left(-\frac{1}{3} + \frac{z}{6}\right) + \ln^2(z)\ln(1-z)\left(-1+\frac{z}{2}\right) + \ln(z)\,(5-4\,z) \\
& + \ln(z)\ln^2(1-z)\left(-1+\frac{z}{2}\right) + \ln(1-z)\left(\frac{7\,z}{2} - \frac{7\,P(z)}{2}\right) \\
& + \mathrm{Li}_2(1-z)\left(-3 - \frac{3\,z}{2} - \frac{3\,P(z)}{2}\right) + \mathrm{Li}_3(1-z)\,(2-z-2\,P(z)) \\
& + \mathrm{S}_{12}(1-z)\,(2-z-2\,P(z)) + \frac{5\,\pi^2 P(z)}{4} - \frac{1}{3}\ln^3(1-z) P(z) \\
& + \ln^3(y_{\min})\,2P(z) \\
& + \ln^2(y_{\min})\left(\ln(z)\left(-1+\frac{z}{2}\right) - \ln(1-z) P(z) - 1 + \frac{z}{4} + \frac{3\,P(z)}{2}\right)
\end{aligned}
$$

$$
\begin{aligned}
&+\ln(y_{\min})\Bigg(\ln(z)\,(-5-z)+\ln^2(z)\left(-1+\frac{z}{2}\right)+\mathrm{Li}_2(1-z)\,(-2+z+2\,P(z))\\
&\quad+\frac{\pi^2 P(z)}{3}+\ln(z)\ln(1-z)\,(-2+z)+\ln(1-z)\left(-2+\frac{z}{2}+\frac{3\,P(z)}{2}\right)\\
&\quad-\ln^2(1-z)P(z)+\frac{7\,z}{2}-7\,P(z)\Bigg)\\
&+\ln(\mu_F^2/M^2)\Bigg(\ln^2(z)\left(-1+\frac{z}{2}\right)+\ln(z)\,(-5-z)-\ln^2(1-z)P(z)\\
&\quad+\mathrm{Li}_2(1-z)\,(-2+z+2\,P(z))+\ln(1-z)\left(-2+\frac{z}{2}+\frac{3\,P(z)}{2}\right)\\
&\quad+\ln(z)\ln(1-z)\,(-2+z)-\frac{2\,\pi^2 P(z)}{3}+\frac{7\,z}{2}+P(z)\Bigg)\\
&+\ln^2(\mu_F^2/M^2)\left(-1+\frac{z}{4}-\ln(1-z)P(z)+\ln(z)\left(-1+\frac{z}{2}\right)\right)\\
&+\ln^2(y_{\min})\ln(\mu_F^2/M^2)\;2P(z)\\
&+\ln(y_{\min})\ln(\mu_F^2/M^2)\left(-2+\frac{z}{2}+3\,P(z)-2\,\ln(1-z)P(z)+\ln(z)\,(-2+z)\right)\Bigg\}.
\end{aligned}
\tag{7.19}
$$

Analysing the structure of the answer we find that it can be written in the following compact form,

$$
\begin{aligned}
\mathrm{d}\sigma_{\mathrm{p}}^{q\bar{q}(g)} &= \sigma_0\,\frac{1}{\Gamma^2(1-\epsilon)}\left(\frac{\alpha e_q^2}{2\pi}\right)\left(\frac{\alpha_s}{2\pi}\right)\left(\frac{4\pi\mu^2}{M^2}\right)^{2\epsilon}\left(\frac{N^2-1}{2N}\right)\mathrm{d}z\\
&\quad\times\left\{-\frac{1}{\epsilon}\left[1-\epsilon\ln\left(\frac{\mu_F^2}{M^2}\right)\right]\;P_{qq}^{(0)}+c_q^{(1)}+\epsilon c_q^{(2)}\right\}\otimes\frac{1}{\epsilon}P_{q\gamma}^{(0)},
\end{aligned}
\tag{7.20}
$$

where $c_q^{(1)}$ and $c_q^{(2)}$ are both given in eq.(7.12).

The *fragmentation collinear* factor $FC_{F\gamma}$ is then finally given by

$$
FC_{F\gamma}=\frac{1}{\sigma_0\,\mathrm{d}z}\left(\sigma_{np}^{q\bar{q}(g)}+\mathrm{d}\sigma_{np}^{q\bar{q}(g)}\right).
\tag{7.21}
$$

To summarize, in this chapter we have presented the calculation of the contributions to the $\gamma^*\to\gamma+1$ jet cross section from the $\mathcal{O}(\alpha_s)$ $\gamma^*\to q\bar{q}(g)$ processes followed by

quark-to-photon fragmentation through to order $\mathcal{O}(\alpha\alpha_s)$. We found that the contributions where the gluon is theoretically resolved contain at most $1/\epsilon$ poles (from the fragmentation counter term) which exactly cancel with the $1/\epsilon$ singularity present in the single unresolved real contributions related to $\gamma^* \to q\bar{q}\gamma g$ where the quark and the photon are collinear. The result for the unresolved contributions, on the other hand, contains $1/\epsilon^2$ poles as leading singularities. In the next chapter, these contributions will be combined with the virtual and the double unresolved contributions presented in Chapters 5 and 6.

This concludes not only Chapter 7, but also our presentation of the calculation of all contributions to the $\gamma + 1$ jet rate at $\mathcal{O}(\alpha\alpha_s)$ which we started to describe in Chapter 4. In the next chapter we shall collect our results together and absorb the "left-over singularity" in the $\mathcal{O}(\alpha\alpha_s)$ quark-to-photon fragmentation function. Once this is achieved, we shall be able to evaluate numerically the $\gamma + 1$ jet rate at $\mathcal{O}(\alpha\alpha_s)$ in Chapter 9 and compare our results with the existing experimental data of the ALEPH Collaboration in Chapter 10.

Chapter 8

Factorization of the collinear singularities

Our ultimate goal is to determine the non perturbative quark-to-photon fragmentation function. This will be achieved by comparing the *measured* photon +1 jet rate and the perturbatively calculated up to $\mathcal{O}(\alpha\alpha_s)$ photon +1 jet differential cross section.

So far we have determined all different contributions to the γ +1 jet rate and calculated analytically all theoretically unresolved and hence divergent contributions to it. What is left to do in order to obtain a finite photon + 1 jet rate is the following. We need to evaluate the finite cross sections in the different resolved regions of the phase space. This shall be dealt with numerically in Chapter 9. Furthermore, we need to regroup all divergent contributions together and absorb the "left-over" singularities into the *bare* quark-to-photon fragmentation counter term. We shall fulfill this task in this chapter.

In Section 8.1 we present an outline of the results obtained so far, and regroup the different unresolved contributions in such a way that cancellation of singularities become feasible. In Section 8.2 we give the final result of the analytic calculation and *factorize* the left-over singularities, essentially due to the emission of a collinear photon in the final state, into the $\mathcal{O}(\alpha\alpha_s)$ counterterm of the bare quark-to-photon fragmentation function, rendering the differential cross section finite.

So far, when performing the calculation of the γ +1 jet rate, we have determined the perturbative counterterm in the quark-to-photon fragmentation function order by order. We have ensured that the physical cross section is finite at $\mathcal{O}(\alpha)$ in Section 2.4 and shall ensure that it is finite at $\mathcal{O}(\alpha\alpha_s)$ in Section 8.2. An alternative and equivalent way used in the literature to obtain the finite cross section is to construct the $\mathcal{O}(\alpha)$ and the $\mathcal{O}(\alpha\alpha_s)$ counterterms simultaneously. In Section 8.3 we shall present our results following this more widely used approach.

Finally requiring that the bare fragmentation function is independent of the choice of the factorization scale μ_F will yield the next-to-leading order evolution equation for the non-perturbative fragmentation function $D_{q\to\gamma}(z,\mu_F)$. We shall derive this evolution equation and an exact solution of it in Section 8.4.

8.1 The sum of all contributions to the γ +1 jet rate at $\mathcal{O}(\alpha\alpha_s)$

As the coupling α_s is small at high energy, we can express the γ + 1 jet differential cross section as a perturbative series in the strong coupling α_s. In this thesis we limited ourselves to consider the first two terms of this perturbative series. In Section 2.4 we saw that the first order term in this series, the lowest order contribution to the the γ + 1 jet rate was proportional to the electromagnetic coupling constant α, that it was dependent on the factorization scale μ_F but independent of the slicing parameter $y_{\min}$ as it should be. At next-to-leading order, i.e. at $\mathcal{O}(\alpha\alpha_s)$, an outline of the results obtained so far is given below.

The sum of all real and virtual contributions participating to the γ + 1 jet rate at $\mathcal{O}(\alpha\alpha_s)$ is formally given by the following,

$$\frac{1}{\sigma_0}\frac{\mathrm{d}\sigma^{NLO}(\gamma+1\text{ jet})}{\mathrm{d}z} = \Theta\Big\{\frac{1}{\sigma_0}\frac{\mathrm{d}\sigma_R(3\text{ partons}+\gamma)}{\mathrm{d}z} + \frac{1}{\sigma_0}\frac{\mathrm{d}\sigma_V(2\text{ partons}+\gamma)}{\mathrm{d}z}$$

$$
\begin{aligned}
&+\sum_a \frac{1}{\sigma_0}\frac{\mathrm{d}\sigma_R}{\mathrm{d}E_a}(3 \text{ partons})\,\mathrm{d}E_a\,\mathrm{d}E_\gamma\delta(E_\gamma - zE_a)\,D^B_{a\to\gamma}(z) \\
&+\sum_a \frac{1}{\sigma_0}\frac{\mathrm{d}\sigma_V}{\mathrm{d}E_a}(2 \text{ partons})\,\mathrm{d}E_a\,\mathrm{d}E_\gamma\,\delta(E_\gamma - zE_a)\,D^B_{a\to\gamma}(z)\Big\} \\
&+\sum_a \frac{1}{\sigma_0}\frac{\mathrm{d}\sigma_R}{\mathrm{d}E_a}(2 \text{ partons})\,\mathrm{d}E_a\,\mathrm{d}E_\gamma\,\delta(E_\gamma - zE_a)\,D^B_{a\to\gamma}(z) \\
\equiv\ & \frac{1}{\sigma_0}\frac{\mathrm{d}\sigma_R}{\mathrm{d}z} + \frac{1}{\sigma_0}\frac{\mathrm{d}\sigma_V}{\mathrm{d}z} + \frac{\mathrm{d}\sigma_D^{q\bar{q}(g)}}{\sigma_0} + \frac{\mathrm{d}\sigma_D^{q\bar{q}}}{\sigma_0}. \qquad (8.1)
\end{aligned}
$$

The symbol Θ represents the projection of the three and four particle phase space onto the experimental definition of a $\gamma + 1$ jet final state. Each type of parton a contributes to the *bare* parton-to-photon fragmentation function $D^B_{a\to\gamma}$ and the sum runs over all partons. Note that at this order, the gluon-to-photon fragmentation function does not contribute to the γ +1 jet rate, only quark and antiquark can fragment into a photon. Furthermore, due to charge invariance, as usual we can assume that the quark-to-photon and the antiquark-to-photon fragmentation functions are equal.

As discussed in the previous chapter, in the contributions involving the bare fragmentation function, denoted by $\sigma_D^{q\bar{q}(g)}$, the underlying $\gamma^* \to q\bar{q}(g)$ process is already of order α_s, and only the $\mathcal{O}(\alpha)$ counterterm present in the quark-to-photon fragmentation function needs to be considered. On the other hand, for the contributions denoted by $\sigma_D^{q\bar{q}}$, the underlying $\gamma^* \to q\bar{q}$ process is of $\mathcal{O}(1)$, therefore perturbative counterterms of $\mathcal{O}(\alpha)$ *and* of $\mathcal{O}(\alpha\alpha_s)$ need to be taken into account. The fragmentation contribution from the two parton final state is simply,

$$
\mathrm{d}\sigma_D^{q\bar{q}} = \sum_a D^B_{a\to\gamma}(z)\,\sigma_0 \mathrm{d}z = 2D^B_{q\to\gamma}(z)\sigma_0 \mathrm{d}z. \qquad (8.2)
$$

In the previous four chapters we have seen that the real contributions, the virtual contributions and the contributions involving the bare quark-to-photon fragmentation function could be divided according to whether or not the final state particles are resolved or unresolved,

$$
\frac{1}{\sigma_0}\frac{\mathrm{d}\sigma_R}{\mathrm{d}z} = \frac{1}{\sigma_0}\frac{\mathrm{d}\sigma_R^{(R)}}{\mathrm{d}z} + \frac{2}{\sigma_0}\frac{\mathrm{d}\sigma_R^{(U)}}{\mathrm{d}z} + R_{q\bar{q}(\gamma)}\frac{1}{\sigma_0}\frac{\sigma_{q\bar{q}\gamma}}{\mathrm{d}z} + 2\check{C}_{F\gamma}\frac{\sigma_{q\bar{q}g}}{\sigma_0} \qquad (8.3)
$$

$$\frac{1}{\sigma_0}\frac{\mathrm{d}\sigma_V}{\mathrm{d}z} = \frac{2}{\sigma_0}\frac{\mathrm{d}\sigma_V^{(U)}}{\mathrm{d}z} + [V_{q\bar{q}(\gamma)} + F_c]\frac{1}{\sigma_0}\frac{\sigma_{q\bar{q}\gamma}}{\mathrm{d}z} \tag{8.4}$$

$$\frac{\mathrm{d}\sigma_D^{q\bar{q}(g)}}{\sigma_0} = 2\frac{\mathrm{d}\sigma_D^{(U)}}{\sigma_0} + 2D^B_{q\to\gamma}(z)\mathrm{d}z\frac{\sigma_{q\bar{q}g}}{\sigma_0}. \tag{8.5}$$

The fully resolved contributions $\mathrm{d}\sigma^{(R)}$ are finite, while the unresolved contributions $\mathrm{d}\sigma_j^{(U)}$ contain all infinities and are proportional to σ_0. Furthermore, all contributions corresponding to the presence of a collinear photon or associated with the quark-to-photon fragmentation function have been multiplied by a factor of **two** as identical contributions are obtained considering either the photon collinear to the antiquark or associated with the antiquark-to-photon fragmentation function. Contributions associated with a hard photon are not multiplied by this factor.

Regrouping the terms in eq.(8.1) according to the cross section they are proportional to, we obtain,

$$\begin{aligned}\frac{1}{\sigma_0}\frac{\mathrm{d}\sigma^{NLO}(\gamma+1\text{ jet})}{\mathrm{d}z} = {} & \frac{2}{\sigma_0}\frac{\mathrm{d}\sigma_R^{(U)}}{\mathrm{d}z} + \frac{2}{\sigma_0}\frac{\mathrm{d}\sigma_V^{(U)}}{\mathrm{d}z} + 2\frac{\mathrm{d}\sigma_D^{(U)}}{\sigma_0} + 2D^B_{q\to\gamma}(z) \\ & + \left[\mathcal{K}_{q\bar{q}(\gamma)} + F_c\right]\frac{1}{\sigma_0}\frac{\sigma_{q\bar{q}\gamma}}{\mathrm{d}z} + 2\underbrace{\left[\tilde{C}_{F\gamma} + D^B_{q\to\gamma}\right]}_{\equiv F_b + D(z,\mu_F)}\frac{\sigma_{q\bar{q}g}}{\sigma_0} \\ & + \frac{1}{\sigma_0}\frac{\mathrm{d}\sigma_R^{(R)}}{\mathrm{d}z}.\end{aligned} \tag{8.6}$$

Recalling that $\tilde{C}_{F\gamma} = (y_{12})^{-\epsilon}C_{F\gamma}$, F_b is given by

$$F_b = \left(\frac{\alpha e_q^2}{2\pi}\right) \times \left[P^{(0)}_{q\gamma}\ln\left(\frac{s_{\min}y_{12}\,z(1-z)}{\mu_F^2}\right) + z\right], \tag{8.7}$$

while $\mathcal{K}_{q\bar{q}(\gamma)}$ is obtained as the sum of the unresolved gluon factor $R_{q\bar{q}(\gamma)}$ given in eq.(4.24) and the virtual factor $V_{q\bar{q}(\gamma)}$ defined by eq.(6.1),

$$\mathcal{K}_{q\bar{q}(\gamma)} = -2\log^2(y_{\min}) - 3\log(y_{\min}y_{12}) + \frac{\pi^2}{3} - 1. \tag{8.8}$$

These, and the other contributions given in the last two lines of eq.(8.6) are finite and will be evaluated numerically later in this thesis.

Here we focus only on the first line of eq.(8.6) which contains the only remaining divergences. The sum of all unresolved contributions yields,

$$\frac{1}{\sigma_0}\frac{\left[\mathrm{d}\sigma_R^{(U)}+\mathrm{d}\sigma_V^{(U)}+\sigma_D^{(U)}\right]}{\mathrm{d}z} = TC_{F\gamma}+SC_{F\gamma}+DC_{F\gamma}+VC_{F\gamma}+FC_{F\gamma}$$

$$\begin{aligned}
= \;& \frac{1}{\Gamma^2(1-\epsilon)}\left(\frac{N^2-1}{2N}\right)\left(\frac{\alpha_s}{2\pi}\right)\left(\frac{\alpha e_q^2}{2\pi}\right)\left(\frac{4\pi\mu^2}{M^2}\right)^{2\epsilon} \\
& \times\Bigg\{ \frac{1}{\epsilon^2}\left[-1+\frac{z}{4}-\ln(1-z)P(z)+\ln(z)\left(-1+\frac{z}{2}\right)\right] \\
& +\frac{1}{\epsilon}\Bigg[-4\,\mathrm{Li}_2(1-z)P(z)+\ln(z)\left(4-\frac{z}{4}\right)-\frac{\ln^2(1-z)P(z)}{2}+\frac{1}{4}-\frac{9\,z}{4} \\
& \quad +\ln^2(z)\left(-\frac{1}{2}+\frac{z}{4}\right)-\ln(1-z)z+\frac{2\,\pi^2P(z)}{3}-2\,\ln(z)\ln(1-z)P(z) \\
& \quad +\left(\ln(z)\,(2-z)+2\,\ln(1-z)P(z)+2-\frac{z}{2}\right)\ln\left(\frac{\mu_F^2}{M^2}\right)\Bigg] \\
& +F_a\left(z,\ln\left(\frac{\mu_F^2}{M^2}\right),y_{\min}\right)\Bigg\} \\
+ \;& \frac{1}{\Gamma(1-\epsilon)}\left(\frac{N^2-1}{2N}\right)\frac{\alpha_s}{2\pi}\left(\frac{4\pi\mu^2}{M^2}\right)^{\epsilon}\left[\left(-\frac{1}{\epsilon}P_{qq}^{(0)}+c_q^{(1)}\right)\otimes D_{q\to\gamma}(z,\mu_F)\right]. \qquad (8.9)
\end{aligned}$$

Note that, we give here explicitly only the pole part of the sum of the unresolved contributions. At this point of the dissertation, we are principally interested to know what are the left-over singularities which need to be absorbed in the perturbative counterterm of the bare fragmentation function. The knowledge of the finite part is not relevant for this purpose and we denote it by,

$$F_a\left(z,\ln\left(\frac{\mu_F^2}{M^2}\right),y_{\min}\right). \qquad (8.10)$$

The sum of all unresolved contributions can be written in a more suggestive and concise form as,

$$\frac{1}{\sigma_0}\frac{\left[\mathrm{d}\sigma_R^{(U)}+\mathrm{d}\sigma_V^{(U)}+\sigma_D^{(U)}\right]}{\mathrm{d}z} =$$

$$
\begin{aligned}
&\frac{1}{\Gamma^2(1-\epsilon)}\left(\frac{N^2-1}{2N}\right)\ \left(\frac{\alpha_s}{2\pi}\right)\left(\frac{\alpha e_q^2}{2\pi}\right)\left(\frac{4\pi\mu^2}{M^2}\right)^{2\epsilon} \\
&\times\left[-\frac{1}{2\epsilon^2}P_{qq}^{(0)}\otimes P_{q\gamma}^{(0)}-\frac{1}{2\epsilon}P_{q\gamma}^{(1)}+\frac{1}{\epsilon}\ln\left(\frac{\mu_F^2}{M^2}\right)P_{qq}^{(0)}\otimes P_{q\gamma}^{(0)}+F_a\right] \\
+\ &\frac{1}{\Gamma(1-\epsilon)}\left(\frac{N^2-1}{2N}\right)\ \frac{\alpha_s}{2\pi}\left(\frac{4\pi\mu^2}{M^2}\right)^{\epsilon}\left[\left(-\frac{1}{\epsilon}P_{qq}^{(0)}+c_q^{(1)}\right)\otimes D_{q\to\gamma}(z,\mu_F)\right],
\end{aligned}
\tag{8.11}
$$

where we have introduced the next-to-leading order quark-to-photon Altarelli-Parisi splitting function $P_{q\gamma}^{(1)}$.

An important check on the above result is the agreement between the next-to-leading order quark-to-photon Altarelli-Parisi splitting function $P_{q\gamma}^{(1)}$ with results previously obtained in the literature. Although $P_{q\gamma}^{(1)}$ has *as such* never been directly calculated before, it can be inferred from the known timelike next-to-leading order quark-to-gluon splitting function $P_{qg}^{(1)}$ [51, 67] by considering the following replacements of colour factors,

$$
C_A \to 0, \qquad N_F \to 0, \qquad C_F^2 \to C_F,
$$

The next-to-leading order quark-to-photon splitting function reads [1],

$$
\begin{aligned}
P_{q\gamma}^{(1)}(z) \ = \ &\left\{-\frac{1}{2}+\frac{9}{2}z+\left(-8+\frac{1}{2}z\right)\ln z+2z\ln(1-z)+\left(1-\frac{1}{2}z\right)\ln^2 z\right. \\
&\left.+\left[\ln^2(1-z)+4\ln z\ln(1-z)+8\mathrm{Li}_2(1-z)-\frac{4}{3}\pi^2\right]P_{q\gamma}^{(0)}(z)\right\}. \qquad (8.12)
\end{aligned}
$$

The calculation of $P_{qg}^{(1)}$ was originally performed by Curci, Furmanski and Petronzio [51], as part of the derivation of the $\mathcal{O}(\alpha_s^2)$ corrections to the spacelike and timelike Altarelli-Parisi evolution equations. The method of their calculation – an explicit projection of the splitting functions out of the corresponding parton level subprocesses – is however mostly undocumented. Very recently, Rijken and van Neerven [67] have rederived $P_{qg}^{(1)}$ in the calculation of the $\mathcal{O}(\alpha_s^2)$ corrections to the inclusive fragmentation of hadrons

[1] Note that in our calculation we have taken the colour factor C_F and the electric charge of the quark e_q outside of the splitting function.

in e^+e^- annihilation. In their calculation $P_{qg}^{(1)}$ appears as the residue of the simple pole of the $\mathcal{O}(\alpha_s^2)$ bare cross section. Similarly, $P_{q\gamma}^{(1)}$ is the residue of the simple pole in the bare $\mathcal{O}(\alpha\alpha_s)$ exclusive γ +1 jet rate. The Altarelli-Parisi splitting functions are in fact universal and are expected to arise in any next-to-leading order perturbative calculation where initial or final state partons can be collinear. The collinear singularities occurring in these potentially substantially different calculations are precisely given in terms of Altarelli-Parisi splitting functions.

8.2 Factorization of the collinear singularities in the fragmentation counter term

The left-hand side of eq.(8.6) is an observable and finite quantity. The explicit divergences present on the right hand side of eq.(8.6) need therefore to be compensated by similar divergences in the bare quark-to-photon fragmentation function. Hence, in the bare fragmentation function we need to add the following $\mathcal{O}(\alpha\alpha_s)$ perturbative counterterm,

$$
\begin{aligned}
D_p^{(\alpha\alpha_s)} &= \frac{1}{\Gamma^2(1-\epsilon)}\left(\frac{N^2-1}{2N}\right)\left(\frac{\alpha_s}{2\pi}\right)\left(\frac{\alpha e_q^2}{2\pi}\right)\left(\frac{4\pi\mu^2}{\mu_F^2}\right)^{2\epsilon}\left[\frac{1}{2\epsilon^2}P_{qq}^{(0)}\otimes P_{q\gamma}^{(0)}+\frac{1}{2\epsilon}P_{q\gamma}^{(1)}\right] \\
&+\frac{1}{\Gamma(1-\epsilon)}\left(\frac{N^2-1}{2N}\right)\left(\frac{\alpha_s}{2\pi}\right)\left(\frac{4\pi\mu^2}{\mu_F^2}\right)^{\epsilon}\left[\frac{1}{\epsilon}P_{qq}^{(0)}\otimes D_{q\to\gamma}(z,\mu_F)\right].
\end{aligned}
$$

The *bare* quark-to-photon fragmentation function up to $\mathcal{O}(\alpha\alpha_s)$ is therefore given by,

$$
\begin{aligned}
D_{q\to\gamma}^B(z) &= D_{q\to\gamma}(z,\mu_F)+\frac{\alpha e_q^2}{2\pi}S_\epsilon\left(\frac{\mu^2}{\mu_F^2}\right)^{\epsilon}\left[\frac{1}{\epsilon}P_{q\gamma}^{(0)}\right] \\
&+\left(\frac{N^2-1}{2N}\right)\left(\frac{\alpha_s}{2\pi}\right)\left(\frac{\alpha e_q^2}{2\pi}\right)S_\epsilon^2\left(\frac{\mu^2}{\mu_F^2}\right)^{2\epsilon}\left[\frac{1}{2\epsilon^2}P_{qq}^{(0)}\otimes P_{q\gamma}^{(0)}+\frac{1}{2\epsilon}P_{q\gamma}^{(1)}\right] \\
&+\left(\frac{N^2-1}{2N}\right)\left(\frac{\alpha_s}{2\pi}\right)S_\epsilon\left(\frac{\mu^2}{\mu_F^2}\right)^{\epsilon}\left[\frac{1}{\epsilon}P_{qq}^{(0)}\otimes D_{q\to\gamma}(z,\mu_F)\right], \qquad (8.13)
\end{aligned}
$$

where S_ϵ stands for $\frac{(4\pi)^\epsilon}{\Gamma(1-\epsilon)}$.

The unresolved contributions to the $\mathcal{O}(\alpha\alpha_s)$ cross section added to the NLO counterterm in the quark-to-photon fragmentation function therefore read,

$$
\begin{aligned}
&\frac{1}{\sigma_0}\frac{\left[\mathrm{d}\sigma_R^{(U)}+\mathrm{d}\sigma_V^{(U)}+\sigma_D^{(U)}\right]}{\mathrm{d}z}+D_p^{(\alpha\alpha_s)}= \\
&\frac{1}{\Gamma^2(1-\epsilon)}\left(\frac{N^2-1}{2N}\right)\left(\frac{4\pi\mu^2}{M^2}\right)^{2\epsilon}\frac{\alpha e_q^2}{2\pi}\frac{\alpha_s}{2\pi} \\
&\times\Bigg\{-6+\frac{z}{4}+\pi^2\left(-\frac{1}{3}+\frac{z}{12}+\frac{P(z)}{2}\right)+\ln(z)\left(\frac{31}{4}-\frac{27\,z}{4}-P(z)\right) \\
&\quad+\ln(z)\pi^2\left(-\frac{1}{3}+\frac{z}{6}+\frac{P(z)}{3}\right)+\ln^2(z)\left(-2+\frac{13\,z}{8}\right) \\
&\quad+\ln(z)\ln(1-z)\left(-3+\frac{7\,z}{2}-\frac{3\,P(z)}{2}\right)+\ln(z)\mathrm{Li}_2(1-z)\,(4-2\,z) \\
&\quad+\ln^2(1-z)\left(1+\frac{5\,z}{4}-\frac{3\,P(z)}{2}\right)+\ln(1-z)\mathrm{Li}_2(1-z)\,(2-z+5\,P(z)) \\
&\quad+\ln^3(z)\left(\frac{5}{6}-\frac{5\,z}{12}\right)+\ln^2(z)\ln(1-z)\,(2-z+P(z))-\frac{\ln(1-z)\pi^2P(z)}{2} \\
&\quad+\ln(z)\ln^2(1-z)\left(1-\frac{z}{2}+3\,P(z)\right)+\ln(1-z)\left(-\frac{z}{2}-P(z)\right) \\
&\quad+\mathrm{Li}_2(1-z)\left(-3+\frac{7\,z}{2}-\frac{3\,P(z)}{2}\right)+\mathrm{Li}_3(1-z)\,(-2+z-3\,P(z)) \\
&\quad+\mathrm{S}_{12}(1-z)\,(4-2\,z-6\,P(z))+\frac{5\,\ln^3(1-z)P(z)}{6}+9\,P(z)\zeta(3) \\
&\quad+\ln\left(\frac{\mu_F^2}{M^2}\right)\Bigg[-2\,\ln^2(1-z)P(z)+\ln(1-z)\left(-2-\frac{3\,z}{2}+\frac{3\,P(z)}{2}\right) \\
&\qquad+\mathrm{Li}_2(1-z)\,(-2+z-6\,P(z))+\ln(z)\left(3-\frac{3\,z}{2}\right)+\frac{1}{2}-z+P(z) \\
&\qquad+\ln^2(z)\,(-2+z)+\ln(z)\ln(1-z)\,(-2+z-4\,P(z))+\frac{2\,\pi^2P(z)}{3}\Bigg] \\
&\quad+\ln^2\left(\frac{\mu_F^2}{M^2}\right)\left[\ln(1-z)P(z)+1-\frac{z}{4}+\ln(z)\left(1-\frac{z}{2}\right)\right] \\
&\quad+\ln(y_{\min})\Bigg[-\frac{1}{2}-2\,z-P(z)+2\,\ln^2(1-z)P(z)-\frac{\pi^2P(z)}{3}+\ln^2(z)\,(2-z)
\end{aligned}
$$

$$
\begin{aligned}
&+\ln(z)\ln(1-z)\,(2-z+4\,P(z))+\ln(1-z)\left(2+\frac{3\,z}{2}-\frac{9\,P(z)}{2}\right)\\
&+\mathrm{Li}_2(1-z)\,(2-z+6\,P(z))+\ln(z)\left(-3+\frac{3\,z}{2}-3\,P(z)\right)\Bigg]\\
&+\ln^2(y_{\min})\left[\ln(z)\left(1-\frac{z}{2}-2\,P(z)\right)+1-\frac{9\,z}{4}-3\,P(z)-\ln(1-z)P(z)\right]\\
&-2\,\ln^3(y_{\min})P(z)\\
&+\ln\left(\frac{\mu_F^2}{M^2}\right)\ln(y_{\min})\left[-2+\frac{z}{2}+3\,P(z)+\ln(z)\,(-2+z)-2\,\ln(1-z)P(z)\right]\\
&+2\,\ln\left(\frac{\mu_F^2}{M^2}\right)\ln^2(y_{\min})P(z)\Bigg\}. \qquad (8.14)
\end{aligned}
$$

This result obtained for the sum of all unresolved contributions added to the NLO counterterm in the bare quark-to-photon fragmentation function is independent of μ but depends on the factorization scale μ_F and on the theoretical slicing parameter $y_{\min}$. When it is combined with the resolved contributions to the differential cross section present formally in eq.(8.6), this $y_{\min}$ dependence will cancel as we will explicitly show in the next chapter. Furthermore, note that to the finite contributions at $\mathcal{O}(\alpha\alpha_s)$ we also need to add the finite contributions involving the renormalized non-perturbative quark-to-photon fragmentation function, $D_{q\to\gamma}(z,\mu_F)$. It originates from the combination of eq.(8.9) and eq.(8.13) and reads,

$$
\frac{1}{\sigma_0}\frac{\mathrm{d}\sigma_{D(np)}}{\mathrm{d}z}\equiv\frac{\alpha_s}{2\pi}S_\epsilon\left(\frac{N^2-1}{2N}\right)\left[P_{qq}^{(0)}\ln\left(\frac{M^2}{\mu_F^2}\right)+c_q^{(1)}\right]\otimes D_{q\to\gamma}(z,\mu_F). \qquad (8.15)
$$

8.3 Structure of the NLO result in terms of convolutions

In this section we shall present an alternative way of constructing the finite $\mathcal{O}(\alpha\alpha_s)$ cross section. It is an equivalent procedure of absorbing the collinear singularities in the perturbative fragmentation counter term.

In this formalism, which is widely used in the literature [68, 69] the collinear divergences present in the bare *lowest order* and in the bare *next-to-leading order* cross section are factorized *simultaneously* in the bare quark-to-photon fragmentation function, $D^B_{q\to\gamma}(z)$. For this purpose, the finite differential cross section (up to $\mathcal{O}(\alpha\alpha_s)$) is written as a sum of convolutions between so-called finite *coefficient* functions C_{ij} and infinite *transition* functions Γ_{ij}. Both functions depend on the factorization scale μ_F. More precisely in our case, the finite cross section up to $\mathcal{O}(\alpha\alpha_s)$ is given by,

$$\frac{1}{\sigma_0}\frac{\mathrm{d}\sigma(\gamma+1\mathrm{jet})}{\mathrm{d}z} \equiv A = 2\hat{F}_\gamma + 2\hat{F}_q \otimes \hat{D}_q, \tag{8.16}$$

where $\hat{D}_q$ represents the bare quark-to-photon fragmentation function $D^B_{q\to\gamma}(z)$ and the bare cross sections are given by,

$$\hat{F}_\gamma = F_\gamma + C_{qq} \otimes \Gamma_{q\gamma}, \tag{8.17}$$

$$\hat{F}_q = C_{qq} \otimes \Gamma_{qq}. \tag{8.18}$$

$\hat{F}_q$ which is given in eq.(7.18) by,

$$\hat{F}_q = \frac{\alpha_s}{2\pi} S_\epsilon \left(\frac{\mu^2}{M^2}\right)^\epsilon \left(\frac{N^2-1}{2N}\right)\left[-\frac{1}{\epsilon}P^{(0)}_{qq} + c^{(1)}_q\right]. \tag{8.19}$$

can be rewritten as the convolution of a coefficient function and a transition function as follows,

$$\hat{F}_q = C_{qq} \otimes \Gamma_{qq}, \tag{8.20}$$

with,

$$\Gamma_{qq} = 1 - \frac{\alpha_s}{2\pi} S_\epsilon \left(\frac{\mu^2}{\mu_F^2}\right)^\epsilon \left(\frac{N^2-1}{2N}\right)\left[\frac{1}{\epsilon}P^{(0)}_{qq}\right], \tag{8.21}$$

where the 1 denotes the distribution $\delta(1-z)$. The finite coefficient function C_{qq} reads[2],

$$C_{qq} = \frac{\alpha_s}{2\pi} S_\epsilon \left(\frac{N^2-1}{2N}\right)\left[\ln\left(\frac{M^2}{\mu_F^2}\right) P^{(0)}_{qq} + c^{(1)}_q\right]. \tag{8.22}$$

[2] $c^{(1)}_q$ is given in the previous chapter by eq.(7.12).

The *bare* cross section $\hat{F}_\gamma$ on the other hand, corresponds in our calculation to the sum of the bare lowest order cross section and the next-to-leading order sum of the real and virtual contributions. It is given by,

$$\hat{F}_\gamma = F_\gamma^{(0)}(z, y_{\min}) + \frac{\alpha e_q^2}{2\pi} S_\epsilon \left(\frac{\mu^2}{M^2}\right)^\epsilon \left[-\frac{1}{\epsilon} P_{q\gamma}^{(0)}\right] + \frac{1}{\sigma_0} \frac{\left[\mathrm{d}\sigma_R^{(U)} + \mathrm{d}\sigma_V^{(U)}\right]}{\mathrm{d}z}, \tag{8.23}$$

where $F_\gamma^{(0)}(z, y_{\min})$ is the finite part of the bare lowest order cross section. The sum of real and virtual contributions at next-to-leading order is given by,

$$\begin{aligned}
&\frac{1}{\sigma_0} \frac{\left[\mathrm{d}\sigma_R^{(U)} + \mathrm{d}\sigma_V^{(U)}\right]}{\mathrm{d}z} = TC_{F\gamma} + SC_{F\gamma} + DC_{F\gamma} + VC_{F\gamma} \\
&\frac{1}{\Gamma^2(1-\epsilon)} \left(\frac{N^2-1}{2N}\right) \left(\frac{4\pi\mu^2}{M^2}\right)^{2\epsilon} \frac{\alpha e_q^2}{2\pi} \frac{\alpha_s}{2\pi} \\
&\times \Bigg\{ \frac{1}{\epsilon^2}\left[1 - \frac{1}{4}z + \ln(z)\left(1 - \frac{1}{2}z\right) + \ln(1-z)\,P(z)\right] \\
&\quad + \frac{1}{\epsilon}\Bigg[\frac{1}{4} + \frac{5}{4}z + P(z) + \ln(z)\left(-1 - \frac{5}{4}z\right) + \ln^2(z)\left(-\frac{3}{2} + \frac{3}{4}z\right) \\
&\qquad - \frac{3\ln^2(1-z)\,P(z)}{2} + \ln(z)\ln(1-z)\,(-2 + z - 2P(z)) \\
&\qquad + \ln(1-z)\left(-2 - \frac{1}{2}z + \frac{3}{2}P(z)\right) + \mathrm{Li}_2(1-z)\,(-2 + z - 2P(z)) \\
&\qquad + \ln(y_{\min})\left(-2 + \frac{1}{2}z + 3P(z) + \ln(z)\,(-2+z) - 2\ln(1-z)\,P(z)\right) \\
&\qquad + \ln^2(y_{\min}) 2P(z)\Bigg] \\
&\quad + F_\gamma^{(1)}(z, y_{\min})\Bigg\}.
\end{aligned} \tag{8.24}$$

Note that here too, we only explicitly give the pole part of the sum of the real and virtual contributions as the knowledge of its finite part, denoted by $F_\gamma^{(1)}$ is not necessary to see how the factorization of collinear singularities occurs in this formalism.

The infinite part of $\hat{F}_\gamma$ can also be written as the convolution of a coefficient function and a transition function, as $C_{qq} \otimes \Gamma_{q\gamma}$. The coefficient function C_{qq} is given in eq.(8.22)

and $\Gamma_{q\gamma}$ contains all infinities. All terms present in $\Gamma_{q\gamma}$ appear then to be proportional to universal Altarelli-Parisi splitting functions or convolutions of two of them. We have,

$$\begin{aligned}\hat{F}_\gamma &= F_\gamma + \frac{\alpha e_q^2}{2\pi} S_\epsilon \left(\frac{\mu^2}{M^2}\right)^\epsilon \left[-\frac{1}{\epsilon} P_{q\gamma}^{(0)}\right] \\ &+ \frac{\alpha e_q^2}{2\pi}\frac{\alpha_s}{2\pi} S_\epsilon^2 \left(\frac{N^2-1}{2N}\right)\left\{\left(\frac{\mu^2}{M^2}\right)^{2\epsilon}\left[\frac{1}{2\epsilon^2} P_{q\gamma}^{(0)} \otimes P_{qq}^{(0)} - \frac{1}{2\epsilon} P_{q\gamma}^{(1)}\right]\right. \\ &\left. + \left(\frac{\mu^2}{M^2}\right)^\epsilon \left[-\frac{1}{\epsilon} c_q^{(1)} \otimes P_{q\gamma}^{(0)}\right]\right\}. \end{aligned} \tag{8.25}$$

F_γ is the sum of the finite lowest order and next-to-leading order terms occuring in the corresponding bare differential cross sections. More precisely, it is given by $F_\gamma = F_\gamma^{(0)} + F_\gamma^{(1)} + \frac{1}{2\sigma_0} F_R$ where F_R stands for the finite terms resulting from the sum of all resolved contributions not proportional to σ_0, c.f. eq.(8.6). Moreover, F_γ is a function of z and $y_{\min}$. The infinite transition function $\Gamma_{q\gamma}$ is defined on the other hand by,

$$\begin{aligned}\Gamma_{q\gamma} &= \frac{\alpha e_q^2}{2\pi} S_\epsilon \left(\frac{\mu^2}{\mu_F^2}\right)^\epsilon \left[-\frac{1}{\epsilon} P_{q\gamma}^{(0)}\right] \\ &+ \frac{\alpha e_q^2}{2\pi}\frac{\alpha_s}{2\pi} S_\epsilon^2 \left(\frac{\mu^2}{\mu_F^2}\right)^{2\epsilon}\left(\frac{N^2-1}{2N}\right)\left[\frac{1}{2\epsilon^2} P_{q\gamma}^{(0)} \otimes P_{qq}^{(0)} - \frac{1}{2\epsilon} P_{q\gamma}^{(1)}\right]. \end{aligned} \tag{8.26}$$

Using the above definition of transition functions and coefficient functions, the $\gamma + 1$ jet differential cross section (up to order $\alpha\alpha_s$) denoted by A, can then formally be written as,

$$A = 2\hat{F}_\gamma + 2\hat{F}_q \otimes \hat{D}_q = 2F_\gamma + 2C_{qq} \otimes \left[\Gamma_{q\gamma} + \Gamma_{qq} \otimes \hat{D}_q\right]. \tag{8.27}$$

As A is finite, it can also be written only in terms of finite quantities,

$$A = 2F_\gamma + 2C_{qq} \otimes D_q, \tag{8.28}$$

where D_q stands for the renormalized fragmentation function $D_{q\to\gamma}(z, \mu_F)$. From this equation, it is possible to deduce the form of the NLO *bare* quark-to-photon fragmentation function, yielding,

$$\hat{D}_q \equiv D_{q\to\gamma}^B(z) = \Gamma_{qq}^{-1} \otimes D_q - \Gamma_{qq}^{-1} \otimes \Gamma_{q\gamma}$$

$$
\begin{aligned}
&= D_{q\to\gamma}(z,\mu_F) + \frac{\alpha e_q^2}{2\pi} S_\epsilon \left(\frac{\mu^2}{\mu_F^2}\right)^\epsilon \frac{1}{\epsilon} P_{q\gamma}^{(0)} \\
&+ \frac{\alpha_s}{2\pi} S_\epsilon \left(\frac{N^2-1}{2N}\right) \left(\frac{\mu^2}{\mu_F^2}\right)^\epsilon \frac{1}{\epsilon} P_{qq}^{(0)} \otimes D_{q\to\gamma}(z,\mu_F) \\
&+ \frac{\alpha e_q^2}{2\pi}\frac{\alpha_s}{2\pi} S_\epsilon^2 \left(\frac{N^2-1}{2N}\right) \left(\frac{\mu^2}{\mu_F^2}\right)^{2\epsilon} \left[\frac{1}{2\epsilon^2} P_{qq}^{(0)} \otimes P_{q\gamma}^{(0)} + \frac{1}{2\epsilon} P_{q\gamma}^{(1)}\right].
\end{aligned}
\tag{8.29}
$$

It has exactly the same form as the one we obtained in eq.(8.13) summing the results obtained *separately* after the factorization of the collinear singularities at $\mathcal{O}(\alpha)$ and $\mathcal{O}(\alpha\alpha_s)$.

Furthermore, as a particular case of this symbolic way of presenting the finite cross section as in eq.(8.27, 8.28) we can rederive the result obtained for the lowest order cross section only. Omitting all terms proportional to α_s in the original coefficient and transition functions these become,

$$
C_{qq}^{(\alpha)} = 1, \qquad \Gamma_{qq}^{(\alpha)} = 1,
$$

$$
\Gamma_{q\gamma}^{(\alpha)} = -\frac{\alpha e_q^2}{2\pi} S_\epsilon \left(\frac{\mu^2}{\mu_F^2}\right)^\epsilon \frac{1}{\epsilon} P_{q\gamma}^{(0)}, \tag{8.30}
$$

so that,

$$
\begin{aligned}
A^{(\alpha)} &= 2\hat{F}_\gamma^{(\alpha)} + 2\hat{F}_q^{(\alpha)} \otimes \hat{D}_q^{(\alpha)} \\
&= 2F_\gamma^{(\alpha)} + 2C_{qq}^{(\alpha)} \otimes \left[\Gamma_{q\gamma}^{(\alpha)} + \Gamma_{qq}^{(\alpha)} \otimes \hat{D}_q^{(\alpha)}\right] \\
&= 2F_\gamma^{(\alpha)} + 2\Gamma_{q\gamma}^{(\alpha)} + 2\hat{D}_q^{(\alpha)} \\
&= 2F_\gamma^{(\alpha)} + 2D_q^{(\alpha)}.
\end{aligned}
\tag{8.31}
$$

Equating the terms in the last two lines, we find,

$$
D_q^{(\alpha)} = \Gamma_{q\gamma}^{(\alpha)} + \hat{D}_q^{(\alpha)}. \tag{8.32}
$$

The lowest order expression for the bare fragmentation function as found in Section 2.4 is then restored,

$$\begin{aligned}\hat{D}_q^\alpha \equiv D_{q\to\gamma}^\alpha(z) &= D_{q\to\gamma}(z,\mu_F) - \Gamma_{q\gamma}^{(\alpha)} \\ &= D_{q\to\gamma}(z,\mu_F) + \frac{\alpha e_q^2}{2\pi} S_\epsilon \left(\frac{\mu^2}{\mu_F^2}\right)^\epsilon \frac{1}{\epsilon} P_{q\gamma}^{(0)}.\end{aligned}$$

To conclude this section, we would like to comment on the utility of this formalism. From equation (8.27), it might seem at first sight that within this framework where the renormalization procedure occurs only once, the bare cross sections $\hat{F}_\gamma$ and $\hat{F}_q$ only, need to be evaluated explicitly in order to obtain a finite cross section. It might appear that one does not need to insert the explicit lowest order fragmentation counter term to evaluate some contributions to the cross section – as we needed to in our calculation. However this is not the case. In order to know how to define the transition function $\Gamma_{q\gamma}$ and to know which poles need to be absorbed in the $\mathcal{O}(\alpha\alpha_s)$ fragmentation counter term, one needs to perform the calculation as we did, factorizing the collinear singularities order by order. In particular, in order to know that the residue of the simple pole in $\Gamma_{q\gamma}$ is given by $\left[-\frac{1}{2}P_{q\gamma}^{(1)}\right]$ one needs to have previously calculated $\hat{F}_\gamma$ and $\hat{F}_q \otimes \frac{1}{\epsilon}P_{q\gamma}^{(0)}$. Nevertheless this formalism enables us to present our results in a compact and elegant form, in terms of universal splitting functions or convolutions of them.

8.4 The NLO evolution equation for $D_{q\to\gamma}(z,\mu_F)$

In order to obtain a finite differential cross section we have factorized the collinear singularities in the perturbative counterterm of the bare quark-to-photon fragmentation function at some factorization scale μ_F. The bare quark-to-photon fragmentation function should however not depend on the scale at which the factorization procedure takes place. Requiring in fact that it is independent of the factorization scale μ_F yields the NLO evolution equation for the renormalized non-perturbative fragmentation function $D_{q\to\gamma}(z,\mu_F)$. In the following, we shall first derive this evolution equation and then present an exact (up to $\mathcal{O}(\alpha\alpha_s)$) solution of it.

8.4.1 The derivation of the evolution equation for $D_{q\to\gamma}(z,\mu_F)$

Requiring that the bare quark-to-photon fragmentation function defined in eq.(8.13) does not depend on the scale at which the factorization procedure takes place implies,

$$\begin{aligned}\frac{\mathrm{d}D^B_{q\to\gamma}(z)}{\mathrm{d}\ln(\mu_F^2)}=0 \iff \frac{\partial D_{q\to\gamma}(z,\mu_F)}{\partial\ln(\mu_F^2)} &= \frac{\alpha e_q^2}{2\pi}S_\epsilon P^{(0)}_{q\gamma}+\frac{\alpha e_q^2}{2\pi}\frac{\alpha_s}{2\pi}S_\epsilon^2\left(\frac{N^2-1}{2N}\right)P^{(1)}_{q\gamma}\\ &-\frac{\alpha e_q^2}{2\pi}\frac{\alpha_s}{2\pi}S_\epsilon^2\left(\frac{N^2-1}{2N}\right)P^{(0)}_{qq}\otimes P^{(0)}_{q\gamma}\left[-\frac{1}{\epsilon}+2\ln\left(\frac{\mu_F^2}{M^2}\right)\right]\\ &+\frac{\alpha_s}{2\pi}S_\epsilon\left(\frac{N^2-1}{2N}\right)P^{(0)}_{qq}\otimes\frac{\partial D_{q\to\gamma}(z,\mu_F)}{\partial\ln(\mu_F^2)}\left[-\frac{1}{\epsilon}+\ln\left(\frac{\mu_F^2}{M^2}\right)\right]\\ &+\frac{\alpha_s}{2\pi}S_\epsilon\left(\frac{N^2-1}{2N}\right)P^{(0)}_{qq}\otimes D_{q\to\gamma}(z,\mu_F). \qquad (8.33)\end{aligned}$$

For terms in the third line of this equation, which are proportional to α_s, the variation of the non-perturbative fragmentation function with respect to μ_F, $\frac{\partial D_{q\to\gamma}(z,\mu_F)}{\partial\ln(\mu_F^2)}$ is given by the lowest order evolution equation for $D_{q\to\gamma}(z,\mu_F)$. To be more precise, at $\mathcal{O}(\alpha)$, we have,

$$D^{(\alpha)}_{q\to\gamma}(z)=D_{q\to\gamma}(z,\mu_F)+\frac{1}{\epsilon}\frac{\alpha e_q^2}{2\pi}S_\epsilon\left(\frac{\mu^2}{\mu_F^2}\right)^\epsilon P^{(0)}_{q\gamma}, \qquad (8.34)$$

so that,

$$\frac{\mathrm{d}D^{(\alpha)}_{q\to\gamma}(z)}{\mathrm{d}\ln(\mu_F^2)}=0 \iff \frac{\partial D_{q\to\gamma}(z,\mu_F)}{\partial\ln(\mu_F^2)}=+\frac{\alpha e_q^2}{2\pi}S_\epsilon P^{(0)}_{q\gamma}-\epsilon\frac{\alpha e_q^2}{2\pi}S_\epsilon\ln\left(\frac{\mu_F^2}{M^2}\right)P^{(0)}_{q\gamma}. \qquad (8.35)$$

Note that, in this lowest order evolution equation we have kept terms up to $\mathcal{O}(\epsilon)$. We need to do so in order to keep all terms up to $\mathcal{O}(1)$ in the next-to-leading order evolution equation (eq.(8.33)) since $\frac{\partial D_{q\to\gamma}(z,\mu_F)}{\partial\ln(\mu_F^2)}$ is multiplied by $\{\frac{1}{\epsilon}\}$.

Inserting the lowest order evolution equation given by eq.(8.35) instead of $\frac{\partial D_{q\to\gamma}(z,\mu_F)}{\partial\ln(\mu_F^2)}$ in the next-to-leading order evolution equation (eq.(8.33)), we find the following result,

$$\frac{\partial D(z,\mu_F)}{\partial\ln(\mu_F^2)}=\frac{\alpha e_q^2}{2\pi}P^{(0)}_{q\gamma}+\frac{\alpha e_q^2}{2\pi}\frac{\alpha_s}{2\pi}\left(\frac{N^2-1}{2N}\right)P^{(1)}_{q\gamma}+\frac{\alpha_s}{2\pi}\left(\frac{N^2-1}{2N}\right)P^{(0)}_{qq}\otimes D(z,\mu_F) \qquad (8.36)$$

The structure of this evolution equation is specific to the quark-to-photon fragmentation function. This equation is made up with two type of terms: The lowest and next-to-

leading order *inhomogeneous* terms,

$$\frac{\alpha e_q^2}{2\pi} P_{q\gamma}^{(0)} + \frac{\alpha e_q^2}{2\pi}\frac{\alpha_s}{2\pi}\left(\frac{N^2-1}{2N}\right) P_{q\gamma}^{(1)}$$

and a *convolution* term,

$$\frac{\alpha_s}{2\pi}\left(\frac{N^2-1}{2N}\right) P_{qq}^{(0)} \otimes D_{q\to\gamma}(z,\mu_F).$$

This convolution term or similar ones are expected to arise in any evolution equation of renormalized parton-to-hadron fragmentation functions. A similar term occurs also in the calculation of the inclusive hadron fragmentation process by van Neerven and Rijken [67]. This convolution term is related to the fact that the photon can be produced via the fragmentation of a secondary quark into a photon.

The existence of the inhomogeneous terms on the other hand is specific to the quark-to-photon fragmentation function. This terms appear since the photon can couple directly to the original quark via the electric charge of the quark e_q whereas other hadrons like pions or kaons cannot. More precisely, in our case, where the identified hadron is a photon, it can also be produced through the bremsstrahlung emission off a quark participating in the hard scattering.

8.4.2 A solution of the NLO evolution equation

This NLO evolution equation is insufficient to uniquely determine the non-perturbative quark-to-photon fragmentation function $D_{q\to\gamma}(z,\mu_F)$. This determination will ultimately be performed by comparing the calculated photon +1 jet rate and its experimental measurement. However it is possible to give an exact (up to $\mathcal{O}(\alpha\alpha_s)$) solution of the next-to-leading order evolution equation. This solution is a first step leading to the ultimate determination of $D_{q\to\gamma}(z,\mu_F)$. In the same way, the exact (up to $\mathcal{O}(\alpha)$) solution of the leading order evolution equation, presented in Chapter 2 (eq.(2.29)) led to a determination of the quark-to-photon fragmentation function by a comparison between the LO calculation of the photon +1 jet rate and the data.

An exact ($\mathcal{O}(\alpha\alpha_s)$) solution of the next-to-leading order evolution equation is obtained considering the following. We construct this solution by imposing that it takes the following general form,

$$D_{q\to\gamma}(z,\mu_F) = \left[1 + \left(\frac{N^2-1}{2N}\right)\frac{\alpha_s}{2\pi}A\right] \otimes D^{(LO)}(z,\mu_F) + \frac{\alpha e_q^2}{2\pi}\frac{\alpha_s}{2\pi}\left(\frac{N^2-1}{2N}\right)B, \quad (8.37)$$

where A, B are unknown functions of z, μ_F and μ_0 which is a constant of integration. $D^{(LO)}(z,\mu_F)$ is the exact solution of the lowest order evolution equation (eq.(2.27)). We saw in Section 2.4.4 that it is given by,

$$D^{(LO)}(z,\mu_F) = \frac{\alpha e_q^2}{2\pi}P_{q\gamma}^{(0)}\ln\left(\frac{\mu_F^2}{\mu_0^2}\right) + D(z,\mu_0). \quad (8.38)$$

where the non-perturbative input fragmentation function $D(z,\mu_0)$ is given (at order α) by,

$$D(z,\mu_0) = \frac{\alpha e_q^2}{2\pi}\left[-P_{q\gamma}^{(0)}\ln(1-z)^2 + C\right],$$

with C being a fitted constant as in eq.(2.41). Inserting equation (8.38) in the general form suggested for the exact solution of the next-to-leading evolution equation (eq.(8.37)) and neglecting all terms which have more than one power of α_s, we obtain,

$$A\left(z,\frac{\mu_F^2}{\mu_0^2}\right) = P_{qq}^{(0)}\ln\left(\frac{\mu_F^2}{\mu_0^2}\right), \qquad B\left(z,\frac{\mu_F^2}{\mu_0^2}\right) = P_{q\gamma}^{(1)} - \frac{1}{2}P_{qq}^{(0)}\otimes P_{q\gamma}^{(0)}\ln^2\left(\frac{\mu_F^2}{\mu_0^2}\right), \quad (8.39)$$

so that the solution of the NLO evolution equation reads,

$$\begin{aligned} D^{(NLO)}(z,\mu_F) &= D(z,\mu_0) + \frac{\alpha e_q^2}{2\pi}P_{q\gamma}^{(0)}\ln\left(\frac{\mu_F^2}{\mu_0^2}\right) + \frac{\alpha e_q^2}{2\pi}\frac{\alpha_s}{2\pi}\left(\frac{N^2-1}{2N}\right)P_{q\gamma}^{(1)}\ln\left(\frac{\mu_F^2}{\mu_0^2}\right) \\ &\quad + \frac{\alpha_s}{2\pi}\left(\frac{N^2-1}{2N}\right)\ln\left(\frac{\mu_F^2}{\mu_0^2}\right)P_{qq}^{(0)}\otimes\left[\frac{\alpha e_q^2}{2\pi}\frac{1}{2}P_{q\gamma}^{(0)}\ln\left(\frac{\mu_F^2}{\mu_0^2}\right) + D(z,\mu_0)\right]. \end{aligned} \quad (8.40)$$

The non-perturbative contribution $D(z,\mu_0)$ must still be extracted from the data. Furthermore, it is worth noting that, since this solution $D^{(NLO)}(z,\mu_F)$ is an *exact* solution of the next-to-leading order evolution equation, the factorization scale dependence of the photon +1 jet rate, is eliminated.

In conclusion, after having presented a summary of the results obtained in the previous chapters for the calculation of the γ +1 jet rate at next-to-leading order, in this chapter we have absorbed all the remaining collinear singularities in the fragmentation counterterm and obtained a finite – μ_F and $y_{\min}$ dependent – answer for the sum of the unresolved contributions. Finally, we have also determined a solution of the next-to-leading order evolution equation which shall help to determine the quark-to-photon fragmentation function. In the next chapter, we shall evaluate within a FORTRAN program the resolved contributions and calculate the photon +1 jet rate at $\mathcal{O}(\alpha\alpha_s)$. The final comparison between those results, and the experimentally measured γ +1 jet rate leading to a next-to-leading order determination of $D_{q\to\gamma}(z,\mu_F)$ will be fulfilled in Chapter 10.

Chapter 9

Numerical part of the calculation

We have now collected all necessary ingredients to evaluate the next-to-leading order γ + 1 jet differential cross section numerically. This evaluation shall be dealt with in this chapter, which is organized as follows. In Section 9.1, after having outlined the general structure of the program we shall explain how all different contributions mentioned in the previous chapters are implemented in the numerical program. Particular features of the evaluation of the fully resolved real contributions with the hybrid subtraction method will be illustrated in Section 9.2. Finally, the $y_{\min}$ dependence of the resulting cross section is studied in Section 9.3.

9.1 Structure of the program

9.1.1 Generalities

The FORTRAN program evaluates the γ +1 jet rate as the sum of four cross sections. Those are determined according to the following criteria: the number of particles present in the final state and the presence (or absence) of the quark-to-photon fragmentation function. For each contribution, the appropriate matrix element squared is integrated over the corresponding γ +1 jet phase space using Monte Carlo techniques, i.e. with VEGAS [70]. To be more precise, the cross section is obtained as follows. The events,

which are just points in the phase space, are generated randomly. To a given event, a succession of selection criteria are applied in the course of the program. As the phase space is constructed, the physical events are chosen and each event is weighted by the volume of phase space associated with it. At the same time the invariants y_{ij} are defined allowing the reconstruction of the four-momenta p_i^μ of the particles in the events. The jet algorithm is then applied to these momenta to select the γ +1 jet events. Finally, for these selected events, the matrix element squared is evaluated. As a result, each γ + 1 jet event is weighted by its corresponding phase space volume and matrix element squared. The collection of all weighted events ultimately builds the cross section.

9.1.2 The individual contributions

The four individual contributions to the photon +1 jet rate at $\mathcal{O}(\alpha\alpha_s)$ are denoted by: `sigb, sigc, sigd, sige`[1]. These four contributions are as follows:

(1) **2 partons + photon** (`sigb`).

There are two contributing processes with a hard photon in the final state.

(a) The LO process: $\gamma^* \to q\bar{q}\gamma$.

(b) The NLO process: $\gamma^* \to q\bar{q}\gamma(g)$ with an unresolved (real or virtual) gluon in the final state.

The LO contribution is obtained by integrating the 3-parton matrix element squared over the 3-parton 1-jet phase space, while the NLO contribution is obtained by integrating the product of the 3-parton matrix element squared and the unresolved factor $\mathcal{K}_{q\bar{q}(\gamma)}$ (defined in eq.(8.8)) over the 3-parton 1-jet phase space. Furthermore the NLO part also contains the result of the integration over the 3-parton 1-jet phase

[1] `siga` is omitted for historical reasons. In fact, originally the `FORTRAN` program (`EEPRAD`) [46], evaluated the next-to-leading order cross section for the production of n jets and one isolated photon. The cross section `siga` is the cross section for the production of n **jet partons** + γ. However if the number of jets produced is 1 as in our case, `siga` does not contribute to the total cross section.

space of the finite expression present in the matrix element squared associated with the resolved virtual contribution (given by eq.6.3) yielding F_c as presented in Fig.3.6.

(2) **2 partons with fragmentation** (`sigc`).

There are two contributing processes:

(a) The LO process: $\gamma^* \to q\bar{q} \otimes D_{q\to\gamma}$

(b) The NLO process: $\gamma^* \to q\bar{q} \otimes D_{q\to\gamma}$

For both contributions, the final state configuration corresponds already to a photon + 1 jet event – one parton must fragment into a recognizable photon while the other forms a jet. The LO contribution is the sum of the non-perturbative and μ_F-dependent lowest-order quark-to-photon fragmentation function and a finite contribution. This finite contribution, given in eq.(2.25), is the result of the sum of the simple quark-photon collinear contribution of the 3-parton final state process and the bare quark-to-photon fragmentation function. The non-perturbative fragmentation function is the result of the comparison between the calculated rate at lowest order and the measured photon +1 jet rate as was discussed in Section 2.6.

The NLO contribution is made of three terms: The non-perturbative next-to-leading order and μ_F–dependent quark-to-photon fragmentation function, the finite sum of all two-particle unresolved contributions (given by eq.(8.14)) and a convolution term involving the lowest order μ_F–dependent quark-to-photon fragmentation function given by eq.(8.15). The next-to-leading order μ_F–dependent fragmentation function is itself composed of two contributions, a *perturbative* part which is dictated by the solution of the NLO evolution equation (given in eq.(8.40)) and a *non-perturbative* part which is at this stage of the dissertation still unknown. It will be ultimately obtained in the next chapter from a comparison between the result of the calculated up to $\mathcal{O}(\alpha\alpha_s)$ jet differential cross section and the measured rate. Consequently, note that all plots showed in the remainder of this chapter are obtained considering the lowest order non-perturbative quark-to-photon fragmentation function given in

eq.(8.38).

(3) **3 partons + photon** (`sigd`).

This contribution is only present at $\mathcal{O}(\alpha\alpha_s)$ and describes the process $\gamma^* \to q\bar{q}\gamma g$ where both photon and gluon are theoretically resolved. This cross section is obtained by integrating the 4-parton matrix element squared over the 4-parton phase space subject to the requirement that only one jet is observed in addition to the photon. It is in order to evaluate this contribution correctly that we need to implement the hybrid subtraction method. The results of the implementation of this method will be illustrated in Section 9.2.

(4) **3 partons with fragmentation** (`sige`).

This contribution is also only present at next-to-leading order and describes the process where a hard gluon and the fragmentation function are present in the final state, $\gamma^* \to q\bar{q}g \otimes D_{q\to\gamma}$. The fragmentation function considered here is the sum of the lowest order non-perturbative quark-to-photon fragmentation function and the finite contribution[2] F_b given in eq.(8.7). Finally, the cross section `sige` is obtained as the integration of the 3-parton matrix element squared multiplied by the fragmentation function considered above over the 3-parton $\Rightarrow$ photon + 1-jet phase space. Notice that the contribution from the gluon-to-photon fragmentation function does not occur at this order.

These individual contributions and their sum as functions of $y_{\min}$ are illustrated in Figs. (9.3,9.4).

[2]This finite contribution has been obtained as the sum of the bare quark-to-photon fragmentation function and the simple collinear quark-photon contribution in the 4-parton $\Rightarrow$ photon + 1-jet phase space, (c.f. eq.(4.29)).

9.2 Consequence of the application of the hybrid subtraction method

As we already mentioned, the implementation of the hybrid subtraction method is crucial for the evaluation of the fully resolved real contributions. Within this method, inside a singular region we evaluate the difference between the full 4-parton matrix element squared and its approximation in that singular region while outside any singular region, i.e. in the resolved region, we calculate the full 4-parton matrix element squared. The approximated matrix element squared considered here is either the double unresolved matrix element squared (triple collinear, soft/collinear, double collinear) or one of the single unresolved ones (simple soft or simple collinear), all defined in Chapters 4 and 5 of this dissertation. Inside the singular regions, by choosing appropriately their boundaries, we have ensured that the approximations of the matrix element squared are accurate. At the boundaries of the double unresolved regions and the single soft gluon region the approximations of the matrix element squared are also accurate. However, at the boundaries of the single collinear regions it turns out that it is not the case. This can be seen in Fig. 9.1 which shows the cross section as a function of one of the invariants, y_{qg}, in different single unresolved regions. Clearly, in the single collinear domain, the size of the cross section at the boundary of this region or just below $y_{\min}$ is still significant, while it is completely negligible in the soft-gluon region[3].

As discussed in Section 4.2.2, (c.f. eq.(4.25)), in the $(q-\gamma)$ collinear region, the invariant y_{qg} can become less than $y_{\min}$, but is not necessarily so. In other words, we allow the $(q-\gamma)$-collinear **and** the $(q-g)$-collinear regions to overlap when $y_{qg} < y_{\min}$ and $y_{q\gamma} < y_{\min}$. The reason for this can be seen in Fig. 9.1: in the region $y_{qg} > y_{\min}$, the $(q-\gamma)$-collinear contribution grows for decreasing y_{qg}. This behaviour is due to terms proportional to $\{\frac{1}{y_{qg}}\}$ in the matrix element squared. Those terms naturally are not at all accounted for by the simple collinear $(q-\gamma)$ approximation of the matrix element squared,

[3]Note that in Fig. 9.1, the rates in the double unresolved regions are not shown as they are smaller by orders of magnitude than the rates displayed.

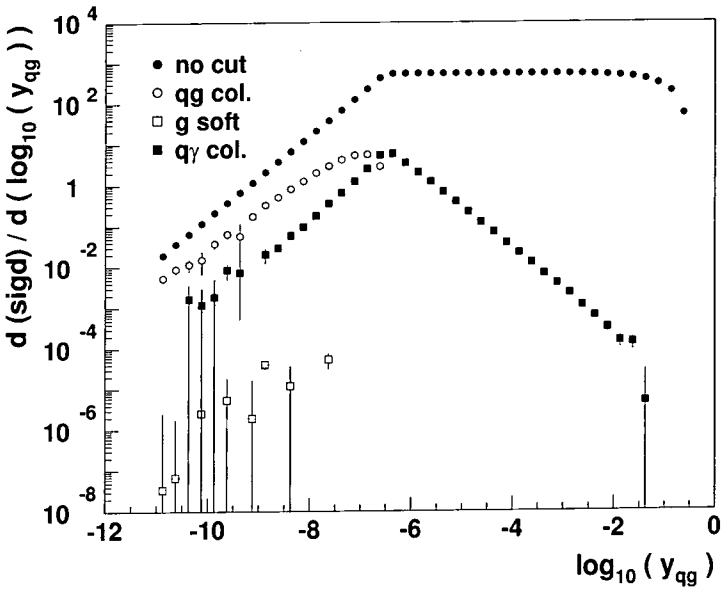

Figure 9.1: The four-parton contribution (`sigd`) to the cross section as function of $\log_{10}(y_{qg})$ for different regions of phase space. The parton resolution cut is $y_{\min} = 10^{-6}$ and $\alpha e_q^2 = \alpha_s C_F = 2\pi$, while $y_{\text{cut}} = 0.1$ and $z_{\text{cut}} = 0.7$.

used in the region $y_{q\gamma} < y_{\min}$ but with $y_{qg} > y_{\min}$. For $y_{qg} < y_{\min}$, as we allow the two collinear regions cited above to overlap, the approximation of the matrix element squared is given by the sum of the two $((q-\gamma)$ and $(q-g))$ simple collinear approximations. The terms in $\{\frac{1}{y_{qg}}\}$ are then correctly taken under consideration. As can be seen in Fig. 9.1, in the region where $y_{qg} < y_{\min}$, the divergent terms in the single collinear $q-\gamma$ collinear region are removed, the corresponding cross section decreases towards lower values of y_{qg}.

In a given single collinear region only one invariant is required to be less than $y_{\min}$, while in any other singular region at least two invariants are constrained to be less than $y_{\min}$. Due to the large particle multiplicity in the final state, at the boundaries of a given single collinear region, it can happen that an invariant which is not constrained to be less than $y_{\min}$ can approach this theoretical cut and be of the same order of magnitude than the invariant which is constrained in this singular region. The invariant which is

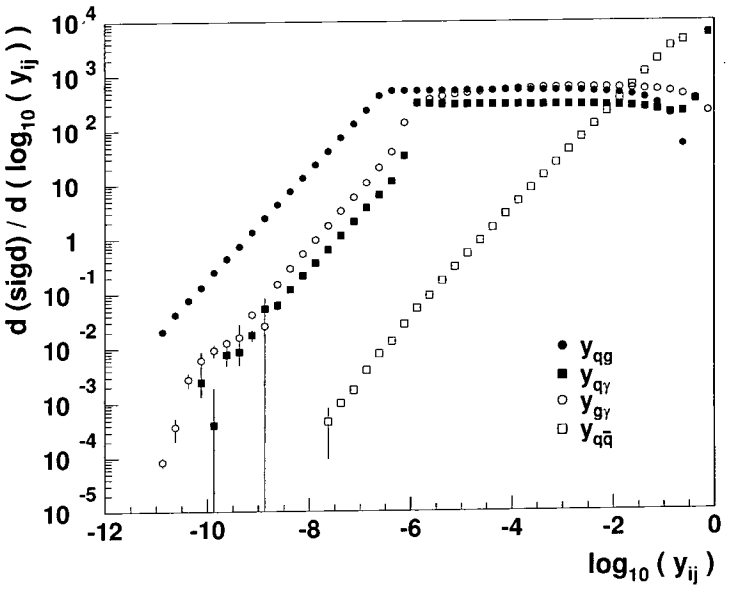

Figure 9.2: The four-parton contribution (`sigd`) to the cross section as function of $\log_{10}(y_{ij})$ for the different invariants. The parton resolution cut is $y_{\min} = 10^{-6}$ and $\alpha e_q^2 = \alpha_s C_F = 2\pi$, while $y_{\text{cut}} = 0.1$ and $z_{\text{cut}} = 0.7$.

constrained in this single collinear region appears in the denominator of the full matrix element squared and of its approximation while the invariant which is not bounded in that particular singular region appears only in the denominator of the full matrix element squared. As a consequence the difference between matrix element and approximation can be sizeable. Applying the phase space slicing method means simply ignoring these contributions – placing a strict cut at $y_{qg} = y_{\min}$ – and ignoring the contribution to the left of $\log_{10}(y_{qg}) = -6$ in Fig. 9.1. This is clearly not the right thing to do.

Although the contributions just below $y_{\min}$ may be sizeable, as the invariants tend to 0, all contributions also tend to 0. This is shown in Fig. 9.2, which represents the cross section as a function of the various y_{ij}. As there is a symmetry under the exchange of quark and antiquark the y_{1j} and y_{2j} distributions are equal.

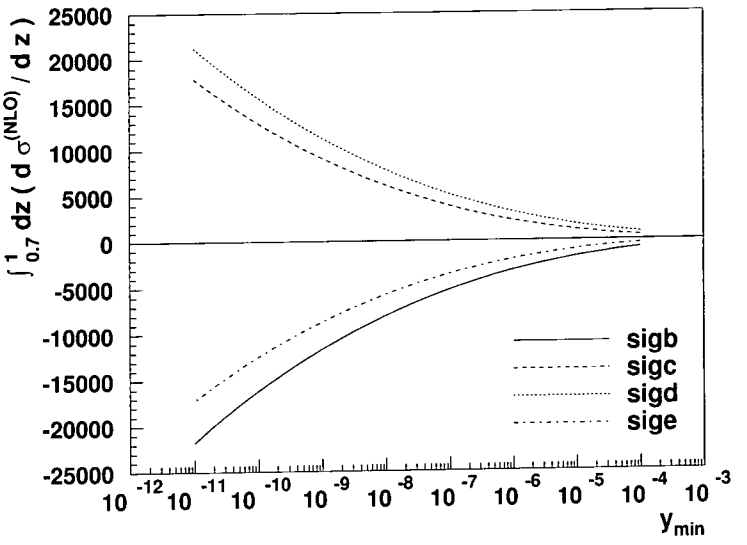

Figure 9.3: Contributions of the individual terms (`sigb`, `sigc`, `sigd`, `sige`) to the total cross section as function of $y_{\min}$ for $y_{\text{cut}} = 0.1$ and $z_{\text{cut}} = 0.7$. For clarity, only the next-to-leading order contributions are shown. Furthermore we take $\alpha e_q^2 = \alpha_s C_F = 2\pi$.

9.3 Study of the $\log(y_{min})$ dependence

As can be seen in Fig. 9.3, the size of the different contributions to the differential cross section increases dramatically as $y_{\min}$ becomes smaller. This rapid rise is due to the presence of logarithms of $y_{\min}$ in each of the contributions. In the analytic part of this calculation, we saw that the leading poles present in the different unresolved contributions (real, virtual and involving the quark-to-photon fragmentation function) were poles in $\{\frac{1}{\epsilon^3}\}$. These poles were sometimes multiplied by factors of the form $y_{\min}^{\epsilon}$. On expansion as a series in ϵ, the poles cancelled amongst each other yielding a finite result (eq.8.14). This result however contains terms proportional to logarithms of $y_{\min}$ up to a certain power being maximally equal to 3. This $\log^3(y_{\min})$ dependence of the sum of all unresolved contributions appears clearly in Fig. 9.3 by the curve representing the variation of `sigc` with variations of $y_{\min}$.

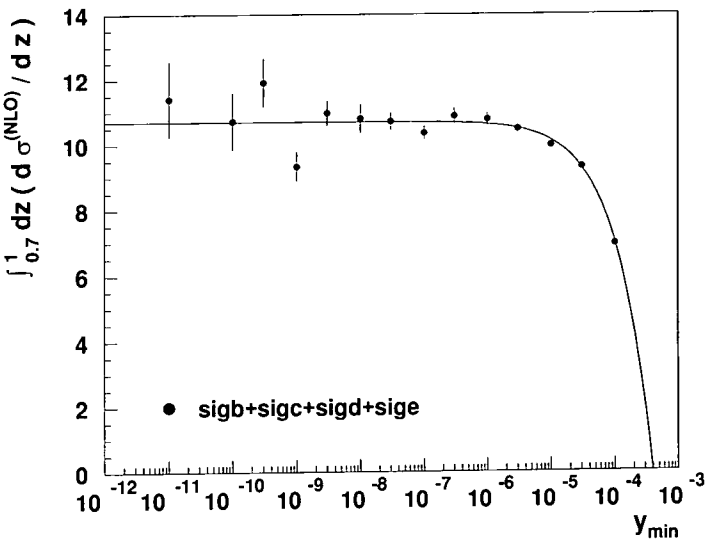

Figure 9.4: The sum of all next-to-leading order contributions to the total cross section as function of $y_{\min}$ for $y_{\text{cut}} = 0.1$ and $z_{\text{cut}} = 0.7$. Moreover, we took $\alpha e_q^2 = \alpha_s C_F = 2\pi$. The solid line is a fit of the form $c_1 + c_2\, y_{\min} \ln^2 y_{\min}$.

The final cross section which is obtained as the sum of all theoretically resolved and unresolved contributions *must* of course be independent of $y_{\min}$, as the introduction of this parameter is an artifact of the calculation. Consequently, we expect the presence of a similar $\log^3(y_{\min})$ dependence in the sum of `sigb`, `sigd` and `sige` to cancel this dependence coming from the `sigc` contribution. In this case, it appears from Fig. 9.3. that all three contributions separately contain logarithms of $y_{\min}$, including $\log^3(y_{\min})$ terms.

It can be seen from Fig. 9.4 that the sum of all resolved and unresolved contributions is clearly $y_{\min}$-independent (within the numerical errors of the calculation) providing that $y_{\min}$ is taken small enough. In practice, this means for values of $y_{\min}$ ranging between 10^{-5} to 10^{-9} for the chosen value of the experimental jet resolution parameter $y_{\text{cut}} = 0.1$. Furthermore the differential rate as a function of z illustrated in Fig. 9.5 appears also $y_{\min}$–independent. Hence, these two results demonstrate the consistency of our approach

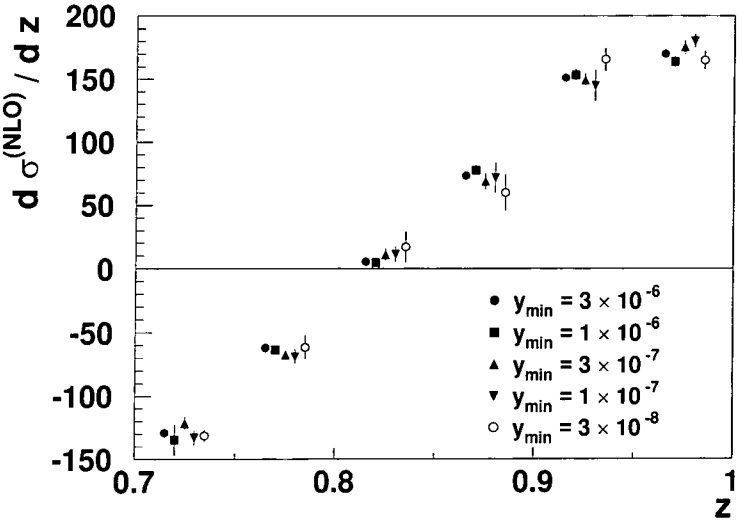

Figure 9.5: The differential cross section as function of z for different values of $y_{\min}$ and $y_{\text{cut}} = 0.1$. Only the next-to-leading order contributions are included, we again take $\alpha e_q^2 = \alpha_s C_F = 2\pi$. All points were evaluated in the respective bin centres, the results for different values of $y_{\min}$ have been shifted across the bin only for better visibility.

to perform the calculation of the NLO photon +1 jet cross section – there is a region of parameter space where the choice of the unphysical parameter $y_{\min}$ does not affect the physically observable cross section. This is actually an extremely powerful check of our calculation. Not only have the explicit poles cancelled as discussed in Chapter 8, but the final numerical result does not depend on the parameter introduced to isolate the divergences. Each individual term has a very strong dependence on $y_{\min}$, but the sum of all terms is flat in $y_{\min}$. For $y_{\min} = 10^{-8}$, the magnitude of the individual terms is $\mathcal{O}(5000)$, while the final result (after enormous cancellations) is $\mathcal{O}(10)$. Of course, in some contributions the logarithms appear explicitly, while in `sigd` particularly, they are generated by the Monte Carlo integration and form the largest source of error.

Concerning the figure displaying the $y_{\min}$ dependence of each contribution to the cross section, i.e. Fig. 9.3, we notice that for large values of $y_{\min}$ the cross section deviates from

the $y_{\min}$–independent value. This is because for large $y_{\min}$ values the approximations used in the analytic calculation become less accurate. In particular, terms of $\mathcal{O}(y_{\min} \log^2(y_{\min}))$, which have been neglected, become sizeable. On the other hand, for values of $y_{\min}$ below 10^{-9} the errors on the result become important due to the necessity of cancelling large logarithms numerically. The total result becomes therefore less stable numerically for such small values of $y_{\min}$. A reasonable choice of $y_{\min}$, which does not lead to problems of numerical instability is therefore $y_{\min} = 10^{-6}$. This value of $y_{\min}$ will be used in the remainder of this thesis to compare the results of the calculated γ +1 jet rate at $\mathcal{O}(\alpha\alpha_s)$ with the measured rate.

In conclusion, after having outlined how the numerical part of the calculation has been performed, we have demonstrated that the results of this next-to-leading order calculation of the photon +1 jet rate were independent of the theoretical cut $y_{\min}$ for values of $y_{\min}$ ranging between 10^{-5} to 10^{-9}. The value $y_{\min} = 10^{-6}$ has been chosen to determine the next-to-leading order non perturbative quark-to-photon fragmentation from a comparison between the results of this calculation and the data. This determination together with a study of the experimental cut (y_{cut})-dependence of the results shall be carried out in the next chapter.

Chapter 10

Final results

In the previous chapter, we have proven the consistency of our approach evaluating the photon +1 jet rate at order $\alpha\alpha_s$. We have shown that the results of the numerical program evaluating this rate were $y_{\min}$ independent. Having this numerical program available, it is now possible to determine the non-perturbative quark-to-photon fragmentation function up to this order from a comparison between the results of this program and the experimental data from the ALEPH Collaboration at CERN. Section 10.1 is dedicated to this determination while a prediction for the integrated photon +1 jet rate for z greater than 0.95 will be presented in Section 10.2.

10.1 A NLO determination of $D_{q\to\gamma}(z,\mu_F)$

In Chapter 8, we saw that the non-perturbative quark-to-photon fragmentation function $D_{q\to\gamma}(z,\mu_F)$ is part of the next-to-leading order photon +1 jet rate, which can be expressed in the following way,

$$\frac{1}{\sigma_0}\frac{\mathrm{d}\sigma^{NLO}(\gamma+1\mathrm{jet})}{\mathrm{d}z} = 2F_\gamma + 2C_{qq}\otimes D_{q\to\gamma}, \tag{10.1}$$

where F_γ and C_{qq} are both finite. F_γ is the sum of the finite lowest order and next-to-leading order terms occurring in the corresponding bare differential cross section (c.f. Section 8.3) and C_{qq} is a coefficient function given by eq.(8.22).

We have also found that the non-perturbative quark-to-photon fragmentation function $D(z,\mu_F)$ could be given as an exact solution (up to $\mathcal{O}(\alpha\alpha_s)$) of a next-to-leading order evolution equation, (c.f. eq.(8.36)), which took the following form,

$$D^{(NLO)}(z,\mu_F) = A_1\left(z,\frac{\mu_F^2}{\mu_0^2}\right) + A_2\left(z,\frac{\mu_F^2}{\mu_0^2}\right)\otimes D(z,\mu_0) + D(z,\mu_0). \qquad (10.2)$$

The functions A_1 and A_2 are known functions given in eq.(8.40). The non-perturbative input function $D(z,\mu_0)$ on the other hand, is up to now unknown. It will be determined together with μ_0, the starting scale[1], in this section.

In Chapter 2, we saw that a lowest-order determination of the non-perturbative fragmentation function $D(z,\mu_F)$ could be given by,

$$D^{(LO)}(z,\mu_F) = A\left(z,\frac{\mu_F^2}{\mu_0^2}\right) + D(z,\mu_0),$$

where the A–term is an exact solution of the lowest order evolution equation, given by eq.(2.27) and a comparison with the measured photon +1 jet rate yielded a lowest-order determination of the non-perturbative fragmentation function at a starting scale μ_0, which was

$$D^{(LO)}(z,\mu_0) = \frac{\alpha e_q^2}{2\pi}\left[-P_{q\gamma}^{(0)}\ln(1-z)^2 - 1 - \ln\left(\frac{s}{2\mu_0^2}\right)\right],$$
$$\text{with} \qquad \mu_0 = 0.14 \text{ GeV}. \qquad (10.3)$$

In this parametric form, the logarithmic term in $(1-z)$ had been introduced to guarantee that the lowest-order photon +1 jet rate is well behaved as z tends to 1 (c.f. Section 2.4.4). The cut-off scale μ_0 and the other constant terms had been fitted to the data. More precisely, they had been fitted to the measured photon +1 jet rate for one particular value of the jet resolution parameter y_{cut} ($y_{\text{cut}} = 0.06$). The next-to-leading order quark-to-photon fragmentation function at a given starting scale μ_0, $D(z,\mu_0)$ will be such that the lowest order component of the photon +1 jet rate calculated at next-to-leading

[1]Recall that μ_0 can be seen as the scale below which the perturbative approach is not valid anymore.

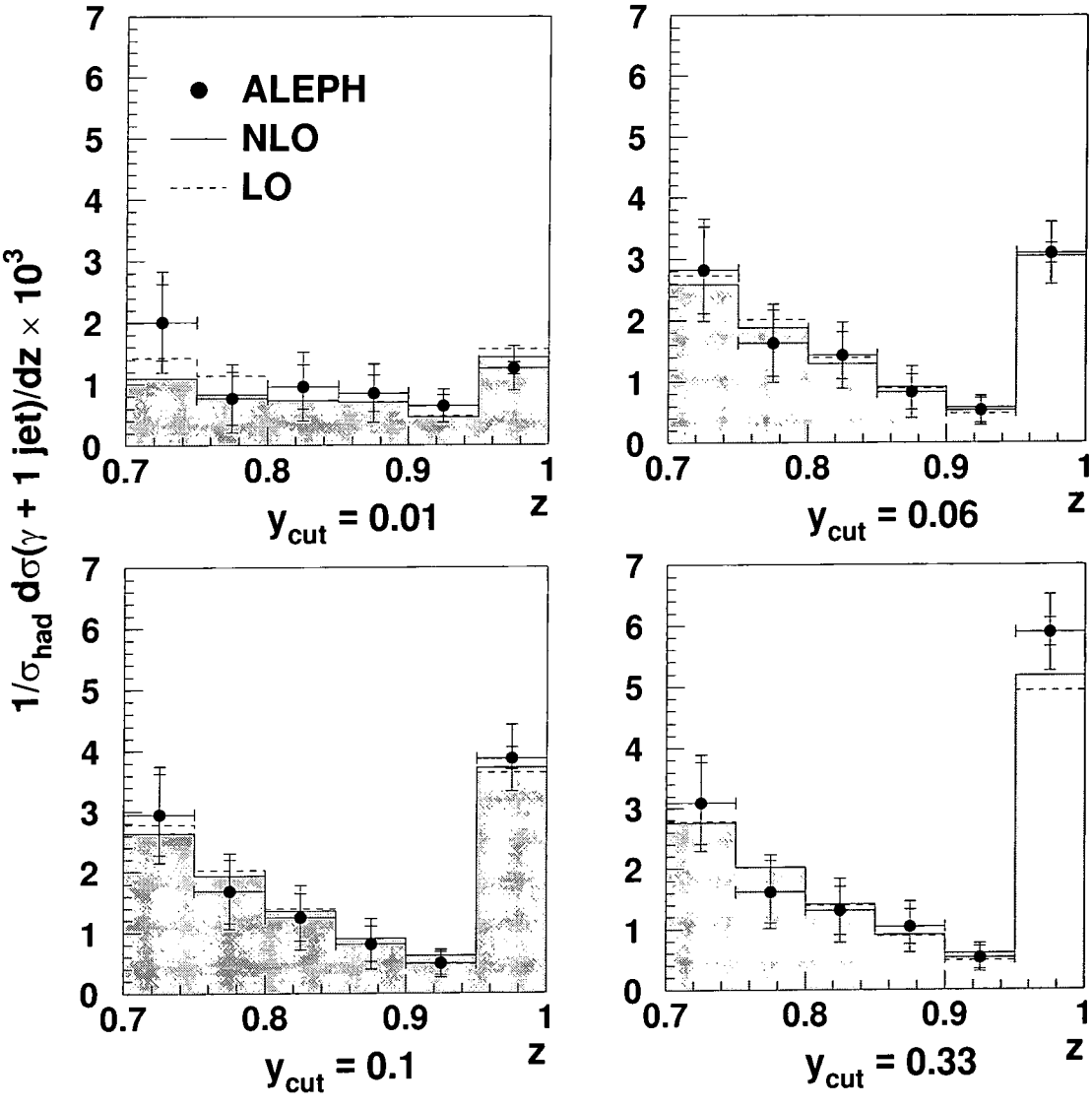

Figure 10.1: Comparison of the photon + 1 jet rate at leading and next-to-leading order with the ALEPH data. The non-perturbative quark-to-photon fragmentation function is fitted to the data for $y_{\rm cut} = 0.06$ only. The jet rates for the other values of $y_{\rm cut}$ are then predictions from the leading order and next-to-leading order calculations.

order is still well behaved as z tends to 1. A possible parametric form for $D(z, \mu_0)$ (at

NLO) therefore reads,

$$D(z,\mu_0) = \frac{\alpha e_q^2}{2\pi}\left[-P_{q\gamma}^{(0)}\ln(1-z)^2 + a_1\cdot f(z) + b_1\right] \tag{10.4}$$

with the unknown parameters being a_1, b_1 and μ_0 the cut-off scale. The strong coupling constant α_s is fixed. It is chosen to be $\alpha_s(M_Z^2) = 0.124$, the leading order value for the strong coupling constant obtained from the hadronic R–ratio.

A triple parameter fit using only the data at $y_{\rm cut} = 0.06$ yields,

$$\begin{aligned} D(z,\mu_0) &= \frac{\alpha e_q^2}{2\pi}\left[-P_{q\gamma}^{(0)}\ln(1-z)^2 + 20.8\,(1-z) - 11.07\right], \\ &\text{with} \quad \mu_0 = 0.64 \text{ GeV}. \end{aligned} \tag{10.5}$$

The resulting values of this fit obtained with $\chi^2 = 0.27/3$ have been used to evaluate the photon +1 jet rate calculated up to next-to-leading order for different values of $y_{\rm cut}$ ($y_{\rm cut}$=0.01, 0.1 and 0.33). The obtained rates are compared with the the leading order predictions and the ALEPH data given in six z-bins ($0.7 < z < 1$) in Fig. 10.1.

Consistent results are found over the whole range of $y_{\rm cut}$ showing the universality of the non-perturbative quark-to-photon fragmentation function $D(z,\mu_F)$. Furthermore, from Fig. 10.1, it can be seen that any $y_{\rm cut}$ dependence of the photon +1 jet rate is adequately described by the perturbative calculation.

10.1.1 The form of $D_{q\to\gamma}(z,\mu_F)$

A comparison between the determinations of $D_{q\to\gamma}(z,\mu_F)$ at leading and next-to-leading order is shown in Fig. 10.2. The fragmentation functions displayed as functions of z are the solutions of the respective evolution equations with the corresponding non-perturbative input distributions $D(z,\mu_0)$ fitted at μ_0 . Both inputs are proportional to the electromagnetic coupling constant and the quark charge; more precisely, they are proportional to $(\alpha e_q^2)/2\pi$.

Unlike the corresponding photon +1 jet rates at leading order and next-to-leading order which are, by construction, completely independent of the choice of the factorization

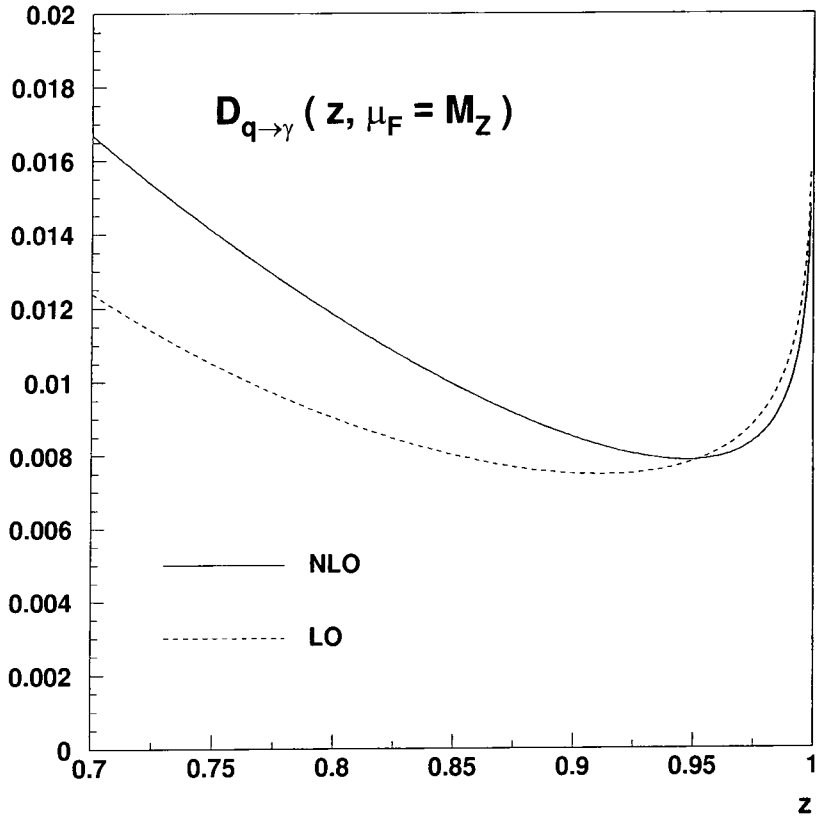

Figure 10.2: The quark-to-photon fragmentation functions at leading and next-to-leading order as functions of z only shown for a quark of unit charge. The factorization scale μ_F is taken equal to M_Z in both cases (see text).

scale μ_F, the fragmentation functions are sensitive on this choice. As the mass of the Z-boson is the only hard scale in the problem, we chose to display these fragmentation functions at the factorization scale $\mu_F = M_Z$. The next-to-leading order quark-to-photon fragmentation function is a universal, process-independent quantity, which has been unknown up to now. It appears in all processes involving quarks and photons in the final state, and could be used to re-evaluate those processes, which so far have only been evaluated using model dependent assumptions for this fragmentation function. Most prominent examples for such processes are the prompt photon cross section at hadron colliders and

the photon pair cross section at LHC. As mentioned in Section 1.2.4, the precise evaluation of the latter process is crucial to determine whether a Standard Model Higgs-boson of intermediate mass can be detected at LHC.

10.2 The integrated rate for $z > 0.95$

The measured and calculated integrated rates above $z = 0.95$ can be displayed as a function of $y_{\rm cut}$ and the results of this comparison are shown in Fig. 10.3. The leading-order curve provides an adequate description of the data as mentioned in Section 2.6.4. The next-to-leading order curve describes the data well and provides even a better agreement between theory and experiment than the leading-order curve over the whole range of $y_{\rm cut}$.

At the end of Section 2.2, after having presented the results of previous analyses of the photon $+n$ jet rates, where a "two step" procedure was used to isolate the photon, we mentioned that within this approach large negative next-to-leading order corrections were required to obtain a reasonable agreement between the theoretical and experimental results. From Fig. 10.3 this appears clearly not to be the case when the photon is clustered inside the jets simultaneously with the other partons and where the photon inside the photon-cluster is called *isolated* if it carries at least 95% of the electromagnetic energy of the photon-jet. This confirms the suggestion made in [46], that the large effects present in the previous analysis were simply a consequence of the procedure used previously to isolate the photon. Using the safer democratic approach instead, the next-to-leading order corrections are of reasonable size.

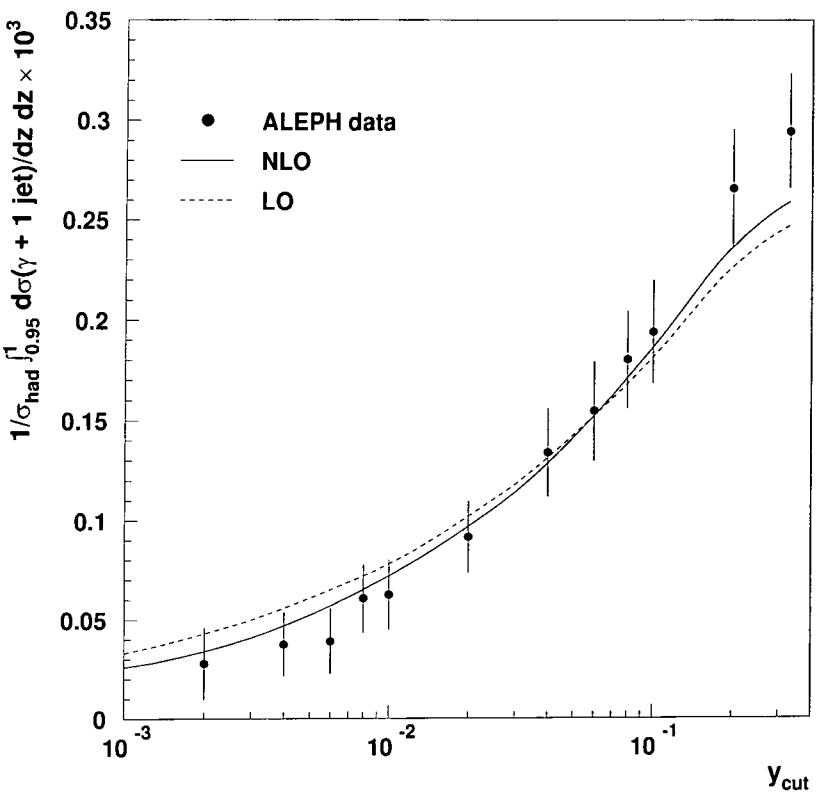

Figure 10.3: The integrated photon +1 jet rate above $z = 0.95$ as function of $y_{\rm cut}$, compared with the full leading-order and next-to-leading order calculations including respectively the leading-order and next-to-leading order determined quark-to-photon fragmentation functions, $D_{q\to\gamma}(z, \mu_F)$.

Chapter 11

Summary and conclusions

In this dissertation we have performed the calculation of the photon +1 jet rate at $\mathcal{O}(\alpha\alpha_s)$ which represents a first step towards the evaluation of jet observables at next-to-next-to-leading order. To achieve this task, despite the presence of soft and collinear singularities arising in various contributions to this jet rate, we separated this calculation into an analytical part, which contains all the divergences and a finite numerical part. The introduction of a theoretical resolution parameter $y_{\min}$ enabled us to realise this separation for all four, essentially different, contributions involving a photon or the fragmentation process in the final state, c.f. Fig. 3.1. In particular it enabled us to decompose the four particle final state phase space into theoretically resolved, single unresolved and double unresolved regions, as defined in Fig. 3.4. This decomposition of the four-particle final state phase space represents one of the most difficult tasks achieved in performing this calculation.

Indeed, due to the large particle multiplicity in the final state, we found that the expected boundaries from an analysis of the single unresolved (soft or collinear) regions in the three-particle final state phase space (c.f. Section 1.5.3) had to be modified to properly define the single unresolved regions in the four-particle final state phase space. More precisely, the theoretical separation criterion $y_{\min}$ had to be multiplied by the triple invariant defining the three colour connected or electromagnetically connected particles,

as explained in Section 4.2. Once this was carried out, the known simple collinear and simple soft approximations of matrix elements and phase space (c.f. Section 1.5.3) could be used to determine (in Chapter 4) the single unresolved real contributions to the photon +1 jet rate from the four parton process at order $\alpha\alpha_s$.

In the double unresolved regions of the 4-particle final state phase space, which we first had to define in Section 3.2, these approximations of matrix elements and phase space were previously unknown. Indeed, in Chapter 5, prior to the evaluation of the double unresolved contributions (triple collinear, soft/collinear and double collinear), we had to first define the corresponding triple collinear, soft/collinear and double collinear limits of the 4-particle matrix elements and phase space. Once these approximations had been found, the evaluation of the double unresolved contributions, for which an elaborate presentation is given in Chapter 5, was rather detailed and involved. In particular, the triple collinear contribution could only be evaluated using various subtle properties of the hypergeometric series.

All analytically calculated unresolved contributions presented in Chapter 5, 6 and 7 respectively, were combined in Chapter 8 to yield a result that still contained double and single poles in ϵ in addition to the physically important finite component (eq.(8.9)). A fifth essentially different contribution to the photon +1 jet rate at $\mathcal{O}(\alpha\alpha_s)$ displayed in Fig. 3.1, is given by the tree level $q\bar{q}$ production process with the bare next-to-leading order quark-to-photon fragmentation function "attached" to one of the quarks. The pole part of the sum of the unresolved contribution is to be factorized into this bare fragmentation function, yielding a finite physical photon +1 jet rate. These pole parts must therefore be universal functions. Indeed, we found (first by inspection of our result and subsequently by more general arguments) that the coefficient of the $\{\frac{1}{\epsilon^2}\}$ pole is given by the convolution of two leading order Altarelli-Parisi splitting functions $(P^{(0)}_{q\gamma} \otimes P^{(0)}_{qq})$ and that the residue of the $\{\frac{1}{\epsilon}\}$ pole is given by the next-to-leading order quark-to-photon splitting function $P^{(1)}_{q\gamma}$. To find that when all contributions are summed together the $\{\frac{1}{\epsilon}\}$ left-over singularity is precisely given by this next-to-leading order splitting function provides us with one of the most stringent checks of the correctness of the analytic part of the calculation of the

photon +1 jet differential cross section at $\mathcal{O}(\alpha\alpha_s)$.

Once the factorization of the left-over collinear singularities into the perturbative counter term of the bare next-to-leading order fragmentation function is realised, as described in Section 8.2, the non-perturbative quark-to-photon fragmentation function $D_{q\to\gamma}(z,\mu_F)$ and the jet rate becomes finite and dependent on the factorization scale μ_F. Requiring that the bare next-to-leading order quark-to-photon fragmentation function is independent of this scale enabled us to derive a next-to-leading order evolution equation and an exact (up to $\mathcal{O}(\alpha\alpha_s)$) solution of it in Section 8.4. When implemented into the photon +1 jet rate, it leads to a μ_F independent differential cross section.

All these contributions were then implemented into a FORTRAN program which evaluated the photon +1 jet rate at $\mathcal{O}(\alpha\alpha_s)$. As motivated in Section 9.2, the hybrid subtraction method (defined in Section 1.5) had to be used to evaluate the resolved real contributions. Outside any singular region, for each event selected by the jet algorithm, the "full" matrix element squared is evaluated while inside any of those regions the difference between the complete 4-particle matrix element squared and its approximation (used in the analytical part of the calculation) are considered instead. Consequences of the application of this method on the behaviour of the invariants $\{y_{ij}\}$ constrained in the singular regions were shown in Figs. (9.1,9.2).

The most stringent test on the consistency of our approach and the correctness of the results obtained is provided by Fig. 9.4, where it is shown that the results of the numerical program are independent of the choice of the theoretical slicing parameter $y_{\min}$. This result was obtained after a numerical cancellation of large logarithms of $y_{\min}$ taken up to the third power had been realized.

Finally, in Chapter 10 we have presented a determination of the process independent non-perturbative quark-to-photon fragmentation function up to $\mathcal{O}(\alpha\alpha_s)$ using our next-to-leading order calculation and the existing data from the ALEPH Collaboration. The fit was obtained using only the data for $y_{\rm cut} = 0.06$. A comparison between the calculated and the measured photon +1 jet rate at other values of the experimental jet resolution parameter $y_{\rm cut}$ showed clearly (in Fig. 10.1) that any $y_{\rm cut}$ dependence of this jet rate is

adequately described by our next-to-leading order perturbative calculation. A further comparison between the calculated and measured integrated rates for values of z greater than 0.95 – i.e. "isolated "photon +1 jet events – was displayed in Fig 10.3. The theoretical next-to-leading order curve (function of $y_{\rm cut}$) was found to describe well the data and to provide a better agreement between theory and experiment than the curve yielded by the leading order calculation of the photon +1 jet rate for all values of $y_{\rm cut}$ considered.

In summary, we have presented a complete calculation of the photon +1 jet rate at $\mathcal{O}(\alpha\alpha_s)$. Several new concepts and calculational methods, which could directly be applied to the evaluation of jet observables at next-to-next-to-leading order, were developed throughout this calculation. As a direct result, we obtained a new determination (at order $\alpha\alpha_s$) of the process independent non-perturbative quark-to-photon fragmentation function which could be used for a re-evaluation of processes involving final state photons, such as one important background process to the detection (via its photon pair decay mode) of the Higgs-boson of the Standard Model of Particle Physics.

Appendix A

Special functions

In this appendix we have collected the definitions and properties of special functions which we have used in different parts of the calculation throughout this dissertation. A complete list of the most commonly used definitions and properties can be found in [71] and [72].

A.1 The Gamma function $\Gamma(x)$

The function $\Gamma(x)$ can be defined by,

$$\Gamma(x) \;=\; \int_0^1 \mathrm{d}y\; e^{-y}\, y^{x-1}\,, \qquad (x \;>\; 0)\,.$$

It has the following properties:

$$\begin{aligned}
\Gamma(x+1) &= x\,\Gamma(x)\,,\\
\Gamma(n+1) &= n!,\\
\Gamma(1) &= 1\quad, \qquad \Gamma(\tfrac{1}{2}) = \sqrt{\pi},\\
\Gamma(2\,x) &= \frac{2^{2x-1}}{\sqrt{\pi}}\,\Gamma(x)\,\Gamma(x+1/2), \qquad \text{(A.1)}\\
\Gamma(z-n) &= (-1)^n\,\frac{\Gamma(1-z)\Gamma(z)}{\Gamma(-z+n+1)}\,. \qquad \text{(A.2)}
\end{aligned}$$

An alternative, but equivalent definition for the Gamma function is the so-called Euler representation

$$\Gamma(z) = \lim_{n\to\infty} \frac{1.2.3..n}{z\,(1+z)(2+z)..(n+z)} n^z.$$

The advantage of this definition is that it enables one to write the Gamma function in an exponential form,

$$\Gamma(1+z) = \exp\Big\{ -z\,\gamma_E + \sum_{n=0}^{\infty} \frac{(-z)^j}{j}\,\zeta(j)\Big\}, \tag{A.3}$$

where $\zeta(j)$ is the j th Riemann Zeta function and γ_E the Euler constant.

Throughout this thesis we used the above definition to expand in ϵ the Γ functions obtained as a result of the phase space integrals. Moreover, some frequently used combinations of Γ functions and their ϵ expansion are

$$\frac{\Gamma^2(1-\epsilon)}{\Gamma(1-2\epsilon)} = 1 - \epsilon^2\,\frac{\pi^2}{6} - 2\epsilon^3\zeta_3, \tag{A.4}$$

$$\frac{\Gamma^3(1-\epsilon)\Gamma(1+\epsilon)}{\Gamma(1-2\epsilon)} = 1 - 2\epsilon^3\zeta_3. \tag{A.5}$$

A.2 The Beta function $B(\alpha,\beta)$

The Beta function $B(\alpha,\beta)$ is defined by the following integral,

$$\begin{aligned} B(\alpha,\beta) &= \int_0^1 \mathrm{d}t\; t^{x-1}(1-t)^{y-1}\,, \\ &= \frac{\Gamma(\alpha)\Gamma(\beta)}{\Gamma(\alpha+\beta)} \qquad Re(\alpha), Re(\beta) > 0\,. \end{aligned} \tag{A.6}$$

In some cases, we can relax the constraint $Re(\alpha), Re(\beta) > 0$, we have

$$\int_0^1 \mathrm{d}b\; b^{\beta-1}(1-b)^{\alpha-1} = \frac{\Gamma(\alpha)\Gamma(\beta)}{\Gamma(\alpha+\beta)}, \tag{A.7}$$

for $Re(\alpha) > 0$ and $Re(\beta) < 0$ with $Re(\alpha+\beta) < 1$.
Indeed, considering the substitution $u = \frac{1}{b}$, the relation (A.7) can be written as

$$\int_1^{\infty} u^{-\beta\,-\alpha}(u-1)^{\alpha-1}(1-u)^0,$$

which is equal to

$$\frac{\Gamma(\alpha)\Gamma(\beta)}{\Gamma(\alpha+\beta)} \underbrace{F_{21}(0,+\beta;\alpha+\beta;1)}_{=1},$$

according to the definition (A.10) and the identity (A.14).

A.3 The Hypergeometric function $F_{21}(a,\ b;\ c;\ z)$

A.3.1 Definitions

The hypergeometric function $F_{21}(a,b;c;z)$ can be defined by the hypergeometric series

$$F_{21}(a,\ b\ ;c\ ;z)\ =\ \sum_{n=0}^{\infty}\frac{(a)_n(b)_n}{(c)_n\Gamma(n+1)}\,z^n, \tag{A.8}$$

$$\text{where}\ \begin{cases}(l)_0=1\\ (l)_n=\frac{\Gamma(n+l)}{\Gamma(l)}\end{cases}.$$

The hypergeometric series terminates if a or b is equal to a negative integer number or to zero. For $c=-n$, with n being a natural number, it is undeterminate. If we exclude these values of $a,\ b,\ c$ the hypergeometric series converges in the unit circle $|z|<1$. If $Re(c-a-b)>0$, then

$$F_{21}(a,\ b;\ c;\ 1)\ =\ \frac{\Gamma(c)\Gamma(c-a-b)}{\Gamma(c-a)\Gamma(c-b)}, \tag{A.9}$$

otherwise $F_{21}(a,\ b;\ c;\ 1)$ is divergent.

The hypergeometric function $F_{21}(a,\ b;\ c;\ z)$ can also be defined by its integral representation

$$F_{21}(a,b;c;z)\ =\ \frac{\Gamma(c)}{\Gamma(b)\Gamma(c-b)}\int_0^1 \mathrm{d}t\ t^{b-1}(1-t)^{c-b-1}(1-tz)^{-a},$$
$$Re(c)>Re(b)>0\ . \tag{A.10}$$

Furthermore, the function $u\equiv F_{21}(a,\ b;\ c;\ z)$ satisfies a differential equation called the hypergeometric equation [71],

$$z(1-z)\,\frac{\mathrm{d}^2u}{\mathrm{d}z^2}\ +\ [c-(a+b+1)z]\,\frac{\mathrm{d}u}{\mathrm{d}z}\ -abu\ =0\,. \tag{A.11}$$

In fact, let us denote by $F_{21}(a,b;c;z) \equiv F$, $F' \equiv \frac{dF}{dz}$ and $F'' \equiv \frac{d^2F}{dz^2}$ the hypergeometric series and its first two derivatives with respect to its argument z. To show that $F_{21}(a,b;c;z) \equiv F$ satisfies the following equation

$$z(1-z)F'' + [c - (a+b+1)z]F' - abF = 0,$$

we expand F and its derivatives in infinite series including the powers of z present in the hypergeometric differential equation. More precisely, we consider

$$\begin{aligned}
F_{21}(a,b;c;z) &= \sum_{n=0}^{\infty} \frac{\Gamma(a+n)\Gamma(b+n)\Gamma(c)}{\Gamma(c+n)\Gamma(n+1)\Gamma(a)\Gamma(b)} z^n, \\
\frac{dF_{21}(a,b;c;z)}{dz} &= \sum_{n=0}^{\infty} \underbrace{\frac{(a+n)(b+n)}{(c+n)}} \frac{\Gamma(a+n)\Gamma(b+n)\Gamma(c)}{\Gamma(c+n)\Gamma(n+1)\Gamma(a)\Gamma(b)} z^n, \\
z\frac{dF_{21}(a,b;c;z)}{dz} &= \sum_{n=0}^{\infty} \underbrace{n} \frac{\Gamma(a+n)\Gamma(b+n)\Gamma(c)}{\Gamma(c+n)\Gamma(n+1)\Gamma(a)\Gamma(b)} z^n, \\
z\frac{d^2F_{21}(a,b;c;z)}{dz^2} &= \sum_{n=0}^{\infty} n \underbrace{\frac{(a+n)(b+n)}{(c+n)}} \frac{\Gamma(a+n)\Gamma(b+n)\Gamma(c)}{\Gamma(c+n)\Gamma(n+1)\Gamma(a)\Gamma(b)} z^n, \\
z^2\frac{d^2F_{21}(a,b;c;z)}{dz^2} &= \sum_{n=0}^{\infty} \underbrace{n(n-1)} \frac{\Gamma(a+n)\Gamma(b+n)\Gamma(c)}{\Gamma(c+n)\Gamma(n+1)\Gamma(a)\Gamma(b)} z^n,
\end{aligned} \tag{A.12}$$

where in the above equations we wrote F', zF', zF'' and z^2F'' as the infinite series of F multiplied by some factor proportional to $\{n\}$ which are underlined. Inserting these identities the hypergeometric equation becomes,

$$n\frac{(a+n)(b+n)}{(c+n)} - n(n-1) + c\frac{a+n)(b+n)}{(c+n)} - (a+b+1)n - ab = 0$$

which is satisfied.

A.3.2 Various properties of the hypergeometric series

In the evaluation of the triple collinear contributions (in Chapter 5) we needed to use various properties of the hypergeometric functions. In what follows, we shall list the ones which follow from the definition of the hypergeometric series $F_{21}(a, b; c; z)$, while more subtle properties of it will be explicitly proven.

a. Some elementary relations

$$F_{21}(a,\, b;\, c;\, z) \;=\; F_{21}(b,\, a;\, c;\, z)\,,$$

$$F_{21}(-a,\, b;\, b;\, z) \;=\; (1-z)^a \tag{A.13}$$

$$F_{21}(0,\, b,\, c;\, z) \;=\; 1\,. \tag{A.14}$$

b.Relations between contiguous hypergeometric functions

$$(c-a-b)F-(c-a)F(a-1)+b(1-z)F(b+1) \;=\; 0, \tag{A.15}$$

$$(b-a)(1-z)F-(c-a)F(a-1)+(c-b)F(b-1) \;=\; 0, \tag{A.16}$$

$$[a-1-(c-b-1)z]+(c-a)F(a-1)-(c-1)(1-z)F(c-1) \;=\; 0, \tag{A.17}$$

where F denotes $F_{21}(a,b;c;z)$ and $F(a\pm 1)$,$F(b\pm 1)$ and $F(c\pm 1)$ stands for $F_{21}(a\pm 1,b;c;z)$,$F_{21}(a,b\pm 1;c;z)$ and$F_{21}(a,b,c\pm 1,z)$ respectively.

c. Some other useful relations between hypergeometric functions of different arguments

- A Relation between $F(z)$ and $F(1-z)$:

$$F_{21}(a,b;c;z) = A_1F_{21}(a,b;a+b-+1;1-z)+A_2(1-z)^{c-a-b}F_{21}(c-a,c-b,c-a-b+1;1-z), \tag{A.18}$$

where $A_1=\frac{\Gamma(c)\Gamma(c-a-b)}{\Gamma(c-a)\Gamma(c-b)}$ and $A_2=\frac{\Gamma(c)\Gamma(a+b-c)}{\Gamma(a)\Gamma(b)}$.

- A quadratic transformation[1]:

In performing the calculation of the triple collinear contribution to the differential cross section, for terms involving $\{\frac{1}{s_{13}s_{14}}\}$ we have used the relation

$$F_{21}\left(1,b;2b;\frac{4z}{(1+z)^2}\right) \;=\; (1+z)^2F_{21}(1,3/2-b;b+1/2;z^2), \tag{A.19}$$

[1]All these relations and further ones are cited in [71]. We have here limited ourselves to those which we explicitly used in the development of the calculation presented in this dissertation.

which holds for all values of z. In the following we shall prove the equality of these two series on a term by term basis, independently of the value of z. Furthermore, we shall also show that it is justified to expand the resulting hypergeometric function in infinite series to perform the v integration, (as in eq.(5.33)), although this series diverges at 1.

The relation (A.19) between two infinite series is correct if the two series satisfy the following two criteria:

(a) They have the same value and the same first derivative at zero, which is trivially the case here.

(b) They satisfy the same hypergeometric differential equation.

We therefore have to see whether $(1+z)^{-2}\, F_{21}\left(1, b; 2b; \frac{4z}{(1+z)^2}\right) \equiv u$ fulfills

$$E \equiv z^2(1-z^2)\,\frac{\mathrm{d}^2u}{\mathrm{d}^2z^2} + \left[b + 1/2 - (2+3/2-b)z^2\right]\,\frac{\mathrm{d}u}{\mathrm{d}z^2} - (3/2-b)u = 0\,, \quad \text{(A.20)}$$

which is the differential equation satisfied by $F_{21}(1, 3/2-b; b+1/2; z^2)$. Defining $y = \frac{4z}{(1+z)^2}$, and considering $F' = \frac{\mathrm{d}u}{\mathrm{d}y}$ and $F'' = \frac{\mathrm{d}^2u}{\mathrm{d}y^2}$, the above equation reads

$$\begin{aligned} E \;=\; & F \times \left[(1-z^2)\left[\frac{3z}{2} + \frac{1}{2}(1+z)\right] - \left[b + \frac{1}{2} - \left(\frac{7}{2} - b\right)z^2\right](1+z) - \left(\frac{3}{2} - b\right)z(1+z)^2\right] \\ & + \frac{4z}{(1+z)^2}F' \times \left[-\frac{1}{2}(1-z^2)(2-z) - (1-z^2)(1-z)\right] \\ & + F' \times \left[2\left[b + \frac{1}{2} - \left(\frac{7}{2} - b\right)z^2\right]\frac{(1-z)}{(1+z)} - (1-z)^2\right] \\ & + F''\left[\frac{4z}{(1+z)^2} - \frac{16z^2}{(1+z)^4}\right](1-z^2). \end{aligned} \quad \text{(A.21)}$$

The idea is then to make this differential equation to look like the one satisfied by $F_{21}\left(1,\ b;\ 2b;\ \frac{4z}{(1+z)^2}\right)$ which is,

$$\frac{4z}{(1+z)^2}F'' - \frac{16z^2}{(1+z)^4}F'' - (1+b+1)\frac{4z}{(1+z)^2}F' - bF = 0\,.$$

When we proved that $F_{21}(a, b; c; z)$ satisfies the hypergeometric equation (A.11), we expanded F and its derivatives in infinite series including the powers of z eventually

present in the hypergeometric equation. Following the same idea here, the equation (A.20) yields

$$
\begin{aligned}
E &\equiv \sum_{n=0}^{\infty} E_n, \\
E_n &= (2b+n)(1+z)\left[(1-z^2)\left[\frac{3z}{2}+\frac{1}{2}(1+z)\right]-\left[b+\frac{1}{2}-\left(\frac{7}{2}-b\right)z^2\right](1+z)\right. \\
&\quad \left.-\left(\frac{3}{2}-b\right)z(1+z)^2\right] \\
&\quad +n(1-z^2)(1+z)\left[-\frac{1}{2}(1-z^2)(2-z)\;-\;(1-z^2)(1-z)\right] \\
&\quad (1+n)(b+n)\left[2\left[b+\frac{1}{2}-(\frac{7}{2}-b)z^2\right]\frac{(1-z)}{(1+z)}\;-(1-z)^2\right] \\
&\quad +\left[n(1+n)(b+n)-n(n-1)(2b+n)\right](1-z^2)(1+z). \qquad \text{(A.22)}
\end{aligned}
$$

But this equation for E is still not equal to zero.

However, one has to remember that there is some arbitrariness in the way one groups the terms together. By this statement we mean here the following. There are two possible procedure to express zF' (for example) in an infinite series proportional to the infinite series defining F (as in eq.(A.8)). Either one includes the factor z in the infinite series and obtains

$$
z\frac{\mathrm{d}F_{21}(a,b;c;z)}{\mathrm{d}z} = \sum_{n=0}^{\infty} \underbrace{n} \frac{\Gamma(a+n)\Gamma(b+n)\Gamma(c)}{\Gamma(c+n)\Gamma(n+1)\Gamma(a)\Gamma(b)} z^n,
$$

or one considers z as a factor multiplying the infinite series only, in which case one finds instead

$$
z\frac{\mathrm{d}F_{21}(a,b;c;z)}{\mathrm{d}z} = z\sum_{n=0}^{\infty} \underbrace{\frac{(a+n)(b+n)}{(c+n)}} \frac{\Gamma(a+n)\Gamma(b+n)\Gamma(c)}{\Gamma(c+n)\Gamma(n+1)\Gamma(a)\Gamma(b)} z^n.
$$

The underlined factors proportional to n in the above expressions of the two infinite series being different, inserting one or the other way of writing zF' in the hypergeometric equation does not yield the same contribution to E_n. In a way this relation (A.22) is not unique.

After some algebraic manipulations we found that the identity (A.21) becomes equal to zero when one considers

$$
\begin{aligned}
E \;=\; & F \times \left[(1-z^2)\left[\frac{3z}{2}+\frac{1}{2}(1+z)\right]-\left[b+\frac{1}{2}-\left(\frac{7}{2}-b\right)z^2\right](1+z)-\left(\frac{3}{2}-b\right)z(1+z)^2\right] \\
& +\frac{4z}{(1+z)^2}F' \times \left\{\left[-\frac{1}{2}(1-z^2)(2-z)\;-\;(1-z^2)(1-z)\right](1+z)\right. \\
& \left.+\underbrace{\frac{3}{2}(z^2-z)(1+z)^2\;+\;b(z-1)(1+z)^2}\right\} \\
& +F' \times \left\{\left[2\left(b+\frac{1}{2}-\left(\frac{7}{2}-b\right)z^2\right)\frac{(1-z)}{(1+z)}\;-(1-z)^2\right]-\underbrace{6(z^3-z^2)\;+\;4b(z^2-z)}\right\} \\
& +F''\left[\frac{4z}{(1+z)^2}\;-\;\frac{16z^2}{(1+z)^4}\right](1-z^2)(1+z), \qquad \text{(A.23)}
\end{aligned}
$$

where we have added and subtracted the underlined terms in comparison with eq.(A.21). By doing so, these terms then get shifted from one infinite sum, F', to the other, yF' . As a result E_n finally becomes

$$
\begin{aligned}
E_n \;=\; & (2b+n)(1+z) \times \left[(1-z^2)\left[\frac{3z}{2}+\frac{1}{2}(1+z)\right]-\left[b+\frac{1}{2}-\left(\frac{7}{2}-b\right)z^2\right](1+z)\right. \\
& \left.-\left(\frac{3}{2}-b\right)z(1+z)^2\right] \\
& +n(2b+n)(1+z)(1-z^2) \times \left\{\left[-\frac{1}{2}(1-z^2)(2-z)\;-\;(1-z^2)(1-z)\right](1+z)\right. \\
& \left.+\underbrace{\frac{3}{2}(z^2-z)(1+z)^2\;+\;b(z-1)(1+z)^2}\right\} \\
& +(1+n)(b+n) \times \left\{\left[2\left(b+\frac{1}{2}-\left(\frac{7}{2}-b\right)z^2\right)\frac{(1-z)}{1+z}\;-(1-z)^2\right]\right. \\
& \left.-\underbrace{6(z^3-z^2)\;+4b(z^2-z)}\right\} \\
& +\left[n(1+n)(b+n)-n(n-1)(2b+n)\right](1-z^2)(1+z),
\end{aligned}
$$

which is equal to zero. This statement ends the proof of the validity of relation between two hypergeometric series of arguments $\{z^2\}$ and $\{\frac{4z}{(1+z)^2}\}$ on a term by term basis.

In evaluating the terms of the triple collinear contribution involving $\{\frac{1}{y_{13}y_{14}}\}$, i.e. in deriving I' in eq.(5.32), we have expanded the hypergeometric series $F_{21}(1,1+\epsilon;1-\epsilon;Z^2)$, obtained applying the quadratic relation mentioned above, in infinite series. Furthermore we have used this expansion to perform the v integration and obtained eq.(5.32). It is worth noting however, that according to the definition of the hypergeometric series, (c.f. Section A.3.1), at $Z=1$, a value of Z in the range of integration of the v integral, this series diverges. In what follows we shall prove that this divergence is integrable and therefore does not affect the validity of the integration in eq.(5.33).

For this purpose we show that

$$I'_\delta \equiv \int_{v'-\delta}^{v'+\delta} \mathrm{d}v\, v^{-\epsilon-1}\,(1-v)^{-\epsilon-1}\frac{1}{(1+Z)^2}\,F_{21}\left(1,1/2-\epsilon,1-2\epsilon,\frac{4Z}{(1+Z)^2}\right) \qquad \text{(A.24)}$$

vanishes for $\delta \to 0$, where $v' = \frac{1-t}{[1-t(1-z)]}$ is the value of v for $Z=1$.

For Z^2 close to 1, it is convenient, using (A.18), to write the hypergeometric function of argument $w \equiv \frac{4Z}{(1+Z)^2}$, as a function of $1-w$,

$$\begin{aligned} F_{21}\left(1,1/2-\epsilon,1-2\epsilon,w\right) &= A_1 F_{21}\left(1,1/2-\epsilon,3/2+\epsilon,1-w\right), \\ &\quad + A_2(1-w)^{-1/2-\epsilon}\underbrace{F_{21}\left(-2\epsilon,1/2-\epsilon,1/2-\epsilon,1-w\right)}_{=w^{2\epsilon}} \end{aligned}$$

where $A_1 = \frac{\Gamma(1-2\epsilon)\Gamma(-1/2-\epsilon)}{\Gamma(-2\epsilon)\Gamma(1/2-\epsilon)}$ and $A_2 = \frac{\Gamma(1-2\epsilon)\Gamma(1/2+\epsilon)}{\Gamma(1)\Gamma(1/2-\epsilon)}$.

$F_{21}\left(1,1/2-\epsilon,3/2+\epsilon,1-w\right)$ vanishes for $\delta \to 0$. Furthermore, in the second term, choosing $v = v' + \delta e^{i\theta}$ with $\theta \in [-\pi, 0]$ and expanding w in power series in δ it becomes

$$w = 1 - \frac{1}{16}\frac{(1-t(1-z))^4}{z^2\,t^2\,(1-t)^2}\,\delta^2\,e^{2i\theta} + 0(\delta^3).$$

Neglecting $0(\delta)$ terms, I'_δ yields

$$\begin{aligned} I'_\delta &= \int_{-\pi}^{0} i\,\delta\,e^{i\theta}\mathrm{d}\theta (v')^{-\epsilon-1}(1-v')^{-\epsilon-1}\frac{1}{4} \\ &\quad \times A_2\left[\frac{1}{16}\,\frac{(1-t(1-z))^4}{z^2\,t^2\,(1-t)^2}\,\delta^2\,e^{2i\theta}\right]^{-1/2-\epsilon} \\ &= 4^{2\epsilon}\frac{\Gamma(1-2\epsilon)\Gamma(1/2+\epsilon)}{\Gamma(1)\Gamma(1/2-\epsilon)}\left[\frac{tz(1-t)}{(1-t(1-z))^2}\right]^{\epsilon}\delta^{-2\epsilon} \end{aligned}$$

$$\times \int_{-\pi}^{0} \mathrm{d}\theta e^{i\theta} [e^{2i\theta}]^{-1/2-\epsilon}.$$

In order to guarantee that $\arg\left([e^{i\theta}]^2\right) \in [-\pi, \pi]$ the θ integral becomes

$$\int_{-\pi}^{-\frac{\pi}{2}} \mathrm{d}\theta\, e^{i\theta} \left[e^{2i\theta+2i\pi}\right]^{-1/2-\epsilon} + \int_{-\frac{\pi}{2}}^{0} \mathrm{d}\theta\, e^{i\theta} \left[e^{2i\theta}\right]^{-1/2-\epsilon} = -\frac{1}{i}\epsilon\pi^2 + 0(\epsilon^4).$$

I'_δ then gives

$$I'_\delta = [-\epsilon\pi^2 + 0(\epsilon^3)] \left(1 + \frac{\pi^2\epsilon^2}{3}\right) \left[\frac{tz(1-t)}{(1-t(1-z))^2}\right]^{\epsilon} (\delta)^{-2\epsilon}$$

which vanishes for $\delta \to 0$.

Hence, we have then proven that the integrand of the v integral in eq.(5.32) does not have any non integrable singularity at 1. We were therefore allowed to expand $F_{21}(1, 1+\epsilon; 1-\epsilon; Z^2)$ in an infinite series and to pursue the evaluation of the triple collinear contribution using this expansion.

A.4 The Di- and Trilogarithms: $\mathrm{Li}_2(y)$, $\mathrm{Li}_3(y)$ and $S_{12}(y)$

The ϵ expansion of hypergeometric functions often yields Di- and Trilogarithmic functions. In the following section, we shall summarize the definitions and the most commonly used properties of these polylogarithmic functions. Again, we limited ourselves to the relations used in this thesis. A complete table of these functions and their properties can be found in [72].

The Dilogarithm $\mathrm{Li}_2(y)$ and the Trilogarithm $\mathrm{Li}_3(y)$ can be both defined via an integral or via an infinite sum. The Dilogarithm $\mathrm{Li}_2(y)$ is given by

$$\mathrm{Li}_2(y) = -\int_0^1 \mathrm{d}x\, \frac{\ln(1-xy)}{x} = \int_0^y \mathrm{d}x \frac{\ln(1-x)}{x}. \tag{A.25}$$

The Trilogarithm $\mathrm{Li}_3(y)$ is defined by

$$\mathrm{Li}_3(y) = \int_0^1 \mathrm{d}x\, \frac{\ln(x)\ln(1-xy)}{x} = \int_0^y \frac{\mathrm{Li}_2(x)}{x}, \tag{A.26}$$

whereas the Trilogarithm $S_{12}(y)$ is defined by

$$S_{12}(y) = \frac{1}{2}\int \mathrm{d}x\, \frac{\ln^2(1-xy)}{x} = \frac{1}{2}\int_0^y \mathrm{d}x \frac{\ln^2(1-x)}{x}. \tag{A.27}$$

The Dilogarithm $\mathrm{Li}_2(y)$ and the Trilogarithm $\mathrm{Li}_3(y)$ can also be defined as infinite sums

$$\mathrm{Li}_2(y) = \sum_{n=1}^{\infty} \frac{y^n}{n^2}, \tag{A.28}$$

$$\mathrm{Li}_3(y) = \sum_{n=1}^{\infty} \frac{y^n}{n^3}. \tag{A.29}$$

The shape of these three functions is depicted in Fig.(A.1).

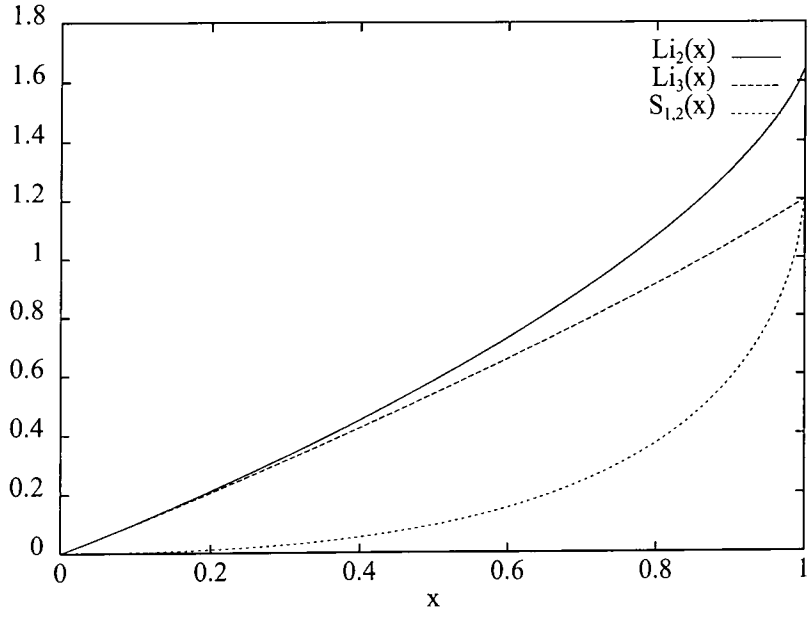

Figure A.1: Di- and Trilogarithms

A.4.1 Some commonly used relations between polylogarithms of different arguments

To reduce the size of the answer in Chapter 5 we made extensive use of the following relations between polylogarithms of different arguments [72]:

$$
\begin{aligned}
\mathrm{Li}_2(1-y) &= -\mathrm{Li}_2(y) - \ln(y)\ln(1-y) + \zeta_2\,, \\
\mathrm{Li}_2\left(-\frac{1-y}{y}\right) &= \mathrm{Li}_2(y) + \ln(y)\ \mathit{ln}(1-y) - \frac{1}{2}\ln^2(y) - \zeta_2\,, \\
\mathrm{Li}_2\left(-\frac{y}{1-y}\right) &= -\mathrm{Li}_2(y) - \frac{1}{2}\ln^2(1-y)\,, \\
\mathrm{Li}_3(1-y) &= -S_{12}(y) - \ln(1-y)\mathrm{Li}_2(y) \\
&\quad -\frac{1}{2}\ln(y)\ln^2(1-y) + \zeta_3\,, \\
\mathrm{Li}_3\left(-\frac{y}{1-y}\right) &= S_{12}(y) - \mathrm{Li}_3(y) + \ln(1-y)\mathrm{Li}_2(y) + \frac{1}{6}\ln^3(1-y)\,, \\
\mathrm{Li}_3\left(-\frac{1-y}{y}\right) &= S_{12}(y) - \mathrm{Li}_3(y) + \ln(1-y)\mathrm{Li}_2(y) + \frac{1}{6}\ln^3(y)\,, \\
&\quad +\zeta_2\ln\left(\frac{y}{1-y}\right) + \frac{1}{2}\ln(y)\ln(1-y)\ln\left(\frac{1-y}{y}\right)\,, \\
S_{12}(1-y) &= -\mathrm{Li}_3(y) + \ln(y)\mathrm{Li}_2(y) + \frac{1}{2}\ln(1-y)\ln^2(y) + \zeta_3\,, \\
S_{12}\left(-\frac{1-y}{y}\right) &= -\mathrm{Li}_3(y) + \ln(y)\mathrm{Li}_2(y) + \frac{1}{2}\ln^2(y)\ln(1-y) \\
&\quad -\frac{1}{6}\ln^3(y) + \zeta_3\,, \\
S_{12}\left(-\frac{y}{1-y}\right) &= S_{12}(y) - \frac{1}{6}\ln^3(1-y)\,,
\end{aligned}
\tag{A.30}
$$

where $\zeta_2 = \mathrm{Li}_2(1) = \frac{\pi^2}{6}$ and $\zeta_3 = \mathrm{Li}_3(1) = S_{12}(1) = 1.20205690315959...,$.

A.4.2 Numerical implementation

The power series defining the polylogarithms are only slowly convergent. To evaluate those numerically in an efficient manner, instead of the definitions above we shall consider the series expansions given below. Introducing $u \equiv -\ln(1-x)$, the dilogarithm $\mathrm{Li}_2(x)$ can be expressed as [72]

$$\mathrm{Li}_2(x) = \int_0^u \frac{t}{e^t - 1} \mathrm{d}t,$$

where the integrand in the above expression is the generating function of the *Bernouilli numbers* [73]. Therefore

$$\mathrm{Li}_2(x) = \sum_{n=0}^{\infty} B_n \frac{u^{n+1}}{(n+1)!}. \tag{A.31}$$

In a similar fashion, starting from eq.(A.27) and performing the same change of integration variables as before, after a simple integration the function $S_{12}(x)$ yields,

$$S_{12}(x) = \frac{1}{2} \sum_{n=0}^{\infty} (n+1) B_n \frac{u^{n+2}}{(n+2)!}. \tag{A.32}$$

Finally for the trilogarithm $\mathrm{Li}_3(x)$ given in (eq.A.26), using the expansion of $\mathrm{Li}_2(x)$, letting $t = 1 - exp[-z]$ and performing the z-integration, we obtain,

$$\mathrm{Li}_3(x) = \sum_{p=0}^{\infty} \sum_{q=0}^{\infty} \frac{1}{(q+1)!} B_q B_{p-q} [(p-q+1)q] \frac{u^{p+1}}{(p+1)!}. \tag{A.33}$$

We have used these series expansion truncated to a finite order to compute the polylogarithms for $x < 1/2$. For arguments outside this range, one of the relation (A.30) has been applied first. To be more precise, we have used these truncated series in a slightly modified form. As the Bernouilli numbers are rapidly increasing, we have considered equivalent series whose arguments, instead of being Bernouilli numbers are ratio of two consecutive Bernouilli numbers.

A.5 The "+" function

In the evaluation of the contributions involving the quark-to-photon fragmentation function we encountered another type of special functions, namely the "+" *functions*. "+"

functions are really distributions, and are as such only defined when convoluted with smooth functions. If $h(t)$ is a given smooth function, we have

$$\int_0^1 \mathrm{d}t\, h(t)\,[g(t)]_+ \equiv \int_0^1 \mathrm{d}t\, [h(t)-h(1)]\, g(t). \tag{A.34}$$

The singular behaviour of $h(t)g(t)$ as $t \to 1$ is compensated by a contribution at $t=1$, such that the convolution integral, $\int_0^1 \mathrm{d}t\, h(t)\,[g(t)]_+$ is finite. In Chapter 7, we have encountered convolution integrals of the form

$$\int_z^1 \frac{\mathrm{d}t}{t}\, h\left(\frac{z}{t}\right)[g(t)]_+ ,$$

with, $h(z) = P(z)$ and,

$$[g(t)]_+ = \frac{1}{(1-t)_+},\ \left(\frac{\ln(1-t)}{(1-t)}\right)_+,\ \left(\frac{\ln^2(1-t)}{(1-t)}\right)_+ .$$

Using the definition (A.34), we can rewrite these three convolution integrals as follows:

$$\begin{aligned}
\int_z^1 \frac{\mathrm{d}t}{t}\, \frac{P\left(\frac{z}{t}\right)}{(1-t)_+}, &= P(z)\ln(1-z) + \int_z^1 \frac{\mathrm{d}t}{t}\, \frac{\left[P\left(\frac{z}{t}\right) - tP(z)\right]}{1-t} \\
\int_z^1 \frac{\mathrm{d}t}{t}\, P\left(\frac{z}{t}\right)\left(\frac{\ln(1-t)}{(1-t)}\right)_+ &= \frac{1}{2}P(z)\ln^2(1-z) + \int_z^1 \frac{\mathrm{d}t}{t}\, \frac{\left[P\left(\frac{z}{t}\right) - tP(z)\right]}{1-t}\ln(1-t) \\
\int_z^1 \frac{\mathrm{d}t}{t}\, P\left(\frac{z}{t}\right)\left(\frac{\ln^2(1-t)}{(1-t)}\right)_+ &= -\frac{1}{3}P(z)\ln^3(1-z) \\
&\quad + \int_z^1 \frac{\mathrm{d}t}{t}\, \frac{\left[P\left(\frac{z}{t}\right) - tP(z)\right]}{1-t}\ln^2(1-t).
\end{aligned} \tag{A.35}$$

Appendix B

Analytic Phase Space integrals

Throughout this thesis we needed to integrate various matrix element squared over the two-particle, three-particle and four-particle phase spaces. Their derivations in terms of the invariants $\{s_{ij}\}$ is completed here below.

B.1 The Gram Determinant $\Delta(p_a, p_b, .., p_j)$

When one writes the n-particle phase spaces in terms of the invariants s_{ij}, the required Jacobian is related to the Gram Determinant Δ defined by

$$\Delta(p_a, p_b .., p_j) = \begin{pmatrix} p_a \cdot p_a & p_a \cdot p_b & \cdots & p_a \cdot p_j \\ p_b \cdot p_a & p_b \cdot p_b & \cdots & p_b \cdot p_j \\ . & . & & . \\ . & . & & . \\ . & . & & . \\ p_j \cdot p_a & p_j \cdot p_b & \cdots & p_j \cdot p_j \end{pmatrix}. \tag{B.1}$$

It satisfies the following properties:

$$\begin{aligned} \Delta(a, b, ..) &= \Delta(b, a, ..), \\ &= \Delta(a, b + \lambda a, ..), \end{aligned}$$

$$= \Delta(-a, b, ..).$$

B.2 The two-particle phase space

The two-particle phase space of a particle with mass $\sqrt{M^2}$ decaying into two massless particles with momenta $\vec{P}_i$ and energy E_i is given by

$$\int \mathrm{d}P_2^{(d)}(M, p_1, p_2) = (2\pi)^{2-d} \int \mathrm{d}R_2^d(M, p_1, p_2)$$

and

$$\begin{aligned} \int \mathrm{d}R_2^{(d)}(M, p_1, p_2) &= \int \frac{\mathrm{d}^{d-1}p_1}{2E_1} \int \frac{\mathrm{d}^{d-1}p_2}{2E_2}\, \delta^d(q - p_1 - p_2) \\ &= \int \frac{\mathrm{d}^{d-1}p_1}{2E_1}\, \delta({p_2}^2) \Big|_{\substack{p_2 = q - p_1 \\ E_1 = |\vec{p_1}|}}. \end{aligned}$$

We can choose a particular frame in which $q^\mu = (M, 0, 0, 0, ..)$, ${p_1}^\mu = (E_1, E_1, 0, 0, ..)$. The dots stand for d-dimensional zeros. Rewriting the remaining $\mathrm{d}^{d-1}p_1$ integral as a radial-angular integral gives

$$\int \mathrm{d}R^{(d)}(M, p_1, p_2) = \frac{1}{2} \int \mathrm{d}E_1\, \mathrm{d}\Omega_{d-1}\, {E_1}^{d-3}\, \delta({p_2}^2),$$

where

$$\int \mathrm{d}\Omega_d = \int_0^{2\pi} \mathrm{d}\theta_1 \int_0^{\pi} \mathrm{d}\theta_2 \sin\theta_2 ... \int_0^{\pi} \mathrm{d}\theta_{d-1} \sin^{d-2}\theta_{d-1},$$

and the volume of the d-dimensional hypersphere

$$\int \mathrm{d}\Omega_d = \frac{2\pi^{d/2}}{\Gamma(d/2)} \equiv V_d. \tag{B.2}$$

Furthermore we have

$$p_2^2 = (q - p_1)^2 = M^2 - 2E_1 M \equiv s_{01},$$

with

$$E_1 = -\frac{s_{01} + M^2}{2M},\ \mathrm{d}E_1 = -\frac{\mathrm{d}s_{01}}{2M},$$

and therefore

$$\int \mathrm{d}R_2^{(d)}(M,p_1,p_2) \;=\; \frac{1}{4M}\int -\mathrm{d}s_{01}\left(\frac{M^2-s_{01}}{2M}\right)^{d-3}\;\frac{\delta(s_{01})}{4M}\;\mathrm{d}\Omega_{d-1}.$$

Considering also that

$$s_{12}=(p_1+p_2)^2 \;=\; M^2-s_{01},$$

leads to the following expression for the d-dimensional two-particle phase space:

$$\int \mathrm{d}P_2^{(d)}(M,p_1,p_2) \;=\; (2\pi)^{2-d}\int \mathrm{d}R_2^{(d)}(M,p_1,p_2),$$

with

$$\int \mathrm{d}R^{(d)}(M,p_1,p_2) \;=\; \int (s_{12})^{\frac{d-4}{2}}\;\frac{\mathrm{d}\Omega_{d-1}}{2^{d-1}}\;\mathrm{d}s_{12}\;\delta(s_{12}-M^2)\,. \tag{B.3}$$

B.3 The three-particle phase space

The three-particle phase space of a particle with mass $\sqrt{M^2}$ decaying into three massless particles with momenta $\vec{P}_i$ and energy E_i is given by

$$\int \mathrm{d}P_3^{(d)}(M,p_1,p_2,p_3) \;=\; (2\pi)^{3-2d}\int \mathrm{d}R_3^{(d)}(M,p_1,p_2,p_3),$$

and

$$\int \mathrm{d}R_3^{(d)}(M,p_1,p_2,p_3) \;=\; \int \frac{\mathrm{d}^{d-1}p_1}{2E_1}\;\frac{\mathrm{d}^{d-1}p_2}{2E_2}\;\delta({p_3}^2)\;\Big|_{\substack{p_3\,=\,q-p_1-p_2\\ E_1\,=\,|\vec{p_1}|,E_2\,=\,|\vec{p_2}|}}.$$

We can consider a particular frame in which $q^\mu=(M,0,0,0,..)$, ${p_1}^\mu=(E_1,E_1,0,0,..)$, ${p_2}^\mu=(E_2,E_2\cos\theta_{12},E_2\sin\theta_{12},0,..)$. The dots in q^μ and ${p_1}^\mu$ represent d-dimensional zeros, while in ${p_2}^\mu$ they stand for $d-2$ unspecified angles in d-dimension. The three-particle phase space then yields

$$\int \mathrm{d}R_3^{(d)}(M,p_1,p_2,p_3) \;=\; \frac{1}{4}\int \mathrm{d}E_1\;\mathrm{d}E_2\;\mathrm{d}\theta_{12}\;\mathrm{d}\Omega_{d-1}\;\mathrm{d}\Omega_{d-2}\left(E_1\;E_2\;\sin\theta_{12}\right)^{d-3}\delta({p_3}^2),$$

where $\int \mathrm{d}\Omega_d$, $\mathrm{d}\Omega_d$ are defined in (B.2). Also

$$\Delta(q,p_1,p_2) \;=\; \Delta(p_1,p_2,p_3)=\frac{1}{4}s_{12}s_{13}s_{23} \;=\; M^2{E_1}^2{E_2}^2\sin^2\theta_{12},$$

and

$$\mathrm{d}E_1\ \mathrm{d}E_2\ \mathrm{d}\theta_{12}\ = \left(16M^2\ s_{12}s_{13}s_{23}\right)^{1/2}\ \mathrm{d}s_{12}\ \mathrm{d}s_{13}\mathrm{d}s_{23}.$$

The three-particle phase space becomes

$$\int \mathrm{d}R_3^{(d)}(M,p_1,p_2,p_3)\ =\ \frac{1}{4\ 2^{d-1}}\int (s_{12}s_{13}s_{23})^{\frac{d-4}{2}}\ \mathrm{d}s_{12}\ \mathrm{d}s_{13}\mathrm{d}s_{23}\mathrm{d}\Omega_{d-1}\ \mathrm{d}\Omega_{d-2}$$
$$\delta(s_{12}+s_{13}+s_{23}-M^2)\ (M^2)^{\frac{2-d}{2}}. \qquad \text{(B.4)}$$

Using the dimensionless invariants $y_{ij} \equiv \frac{s_{ij}}{M^2}$ three-particle phase space also reads

$$\int \mathrm{d}P_3^{(d)}(M,p_1,p_2,p_3)\ =\ (2\pi)^{3-2d}\int \mathrm{d}R_3^{(d)}(M,p_1,p_2,p_3),$$

with

$$\int \mathrm{d}R_3^{(d)}(M,p_1,p_2,p_3)\ =\ \frac{1}{4\ 2^{d-1}}\int (y_{12}y_{13}y_{23})^{\frac{d-4}{2}}\ \frac{\mathrm{d}\Omega_{d-1}}{2^{d-1}}\ \mathrm{d}\Omega_{d-2}$$
$$\delta(y_{12}+y_{13}+y_{23}-1)\ (M^2)^{d-4}\ \mathrm{d}y_{12}\ \mathrm{d}y_{13}\mathrm{d}y_{23}. \qquad \text{(B.5)}$$

B.4 The four-particle phase space

The four-particle phase space of a particle with mass $\sqrt{M^2}$ decaying into four massless particles with momenta $\vec{P}_i$ and energy E_i reads

$$\int \mathrm{d}P_4^{(d)}(M,p_1,p_2,p_3,p_4)\ =\ (2\pi)^{4-3d}\int \mathrm{d}R_4^{(d)}(M,p_1,p_2,p_3,p_4),$$

and

$$\int \mathrm{d}R_4^{(d)}(M,p_1,p_2,p_3,p_4) = \int \frac{\mathrm{d}^{d-1}p_1}{2E_1}\ \frac{\mathrm{d}^{d-1}p_2}{2E_2}\ \frac{\mathrm{d}^{d-1}p_3}{2E_3}\ \delta({p_4}^2)\ \Big|_{\substack{p_4\ =\ q-p_1-p_2-p_3 \\ E_1\ =\ |\vec{p_1}|,E_2\ =\ |\vec{p_2}|,E_3\ =\ |\vec{p_3}|}} \equiv {R_4}^{(d)}.$$

We can choose a particular frame in which

$$\begin{aligned}
q^\mu &= (M,0,0,0,..),\\
{p_1}^\mu &= (E_1,E_1,0,0,..),\\
{p_2}^\mu &= (E_2,E_2\cos\theta_{d-1},E_2\sin\theta_{d-1},..),\\
{p_3}^\mu &= (E_3,E_3\cos\theta_{d-2},E_3\sin\theta_{d-2}\cos\theta_{d-3},E_3\sin\theta_{d-2}\sin\theta_{d-3},..).
\end{aligned}$$

$\theta_{d-1}, \theta_{d-2}$ and θ_{d-3} are the 3 Euler angles between p_1, p_2 and p_3. In q^μ and ${p_1}^\mu$ the dots stand for zeros in d-dimensions, in ${p_2}^\mu$ they stand for $d-2$ unspecified angles in d-dimensions, while in ${p_3}^\mu$ the dots stand for $d-3$ unspecified angles in d-dimensions. The 4-particle phase space then reads

$$\begin{aligned}\int \mathrm{d}R_4{}^{(d)} &= \frac{1}{8}\int \mathrm{d}\Omega_{d-1}\,\mathrm{d}\Omega_{d-2}\mathrm{d}\Omega_{d-3}\mathrm{d}E_1\,\mathrm{d}E_2\,\mathrm{d}E_3\,\mathrm{d}\theta_{d-1}\,\mathrm{d}\theta_{d-2}\,\mathrm{d}\theta_{d-3}\,\delta({p_4}^2)\\ &\quad\Big(E_1\,E_2\,E_3\,\sin\theta_{d-1}\,\sin\theta_{d-2}\Big)^{d-3}\,\sin^{d-4}\theta_{d-3},\end{aligned}$$

where $\int \mathrm{d}\Omega_d$, $\mathrm{d}\Omega_d$ are defined in (B.2).

Furthermore considering

$$\Delta(q,p_1,p_2,p_3) = \Delta(p_1,p_2,p_3,p_4) = -M^2{E_1}^2{E_2}^2{E_3}^2\sin^2\theta_{d-1}\sin^2\theta_{d-2}\sin^2\theta_{d-3} \equiv \Delta_4,$$

and

$$\begin{aligned}\mathrm{d}s_{12}\,\mathrm{d}s_{13}\,\mathrm{d}s_{14}\,\mathrm{d}s_{23}\mathrm{d}s_{24}\,\mathrm{d}s_{34} &= 2^6M^3{E_1}^2{E_2}^2{E_3}^2\mathrm{d}E_1\,\mathrm{d}E_2\,\mathrm{d}E_3\,\mathrm{d}\theta_{d-1}\,\mathrm{d}\theta_{d-2}\mathrm{d}\theta_{d-3}\\ &= 2^6M^2\,(-\Delta_4)^{1/2}\,E_1\,E_2\,E_3\,\mathrm{d}E_1\,\mathrm{d}E_2\,\mathrm{d}E_3\\ &\quad \sin\theta_{d-1}\,\sin\theta_{d-2}\,\mathrm{d}\theta_{d-1}\,\mathrm{d}\theta_{d-2}\mathrm{d}\theta_{d-3}\,,\end{aligned}$$

the four-particle phase space finally yields

$$\int \mathrm{d}P_4^{(d)}(M,p_1,p_2,p_3,p_4) = (2\pi)^{4-3d}\int \mathrm{d}R_4^{(d)}(M,p_1,p_2,p_3,p_4),$$

with

$$\begin{aligned}R_4^{(d)} &= \frac{(\Delta_4)^{-1/2}}{M^2\,2^9}\int \mathrm{d}\Omega_{d-1}\,\mathrm{d}\Omega_{d-2}\,\mathrm{d}\Omega_{d-3}\,\delta(s_{12}+s_{13}+s_{14}+s_{23}+s_{24}+s_{34}-M^2)\\ &\quad\left(\frac{-\Delta_4}{M^2}\right)^{\frac{d-4}{2}}\mathrm{d}s_{12}\,\mathrm{d}s_{13}\mathrm{d}s_{14}\mathrm{d}s_{23}\mathrm{d}s_{24},\mathrm{d}s_{34},\end{aligned} \tag{B.6}$$

where Δ_4 is given by

$$\begin{aligned}+\Delta_4 &= \frac{1}{16}\Big[{s_{12}}^2{s_{34}}^2 + {s_{13}}^2{s_{24}}^2 + {s_{14}}^2{s_{23}}^2\\ &\quad -2\Big(s_{12}s_{23}s_{34}s_{14} + s_{13}s_{23}s_{24}s_{14} + s_{12}s_{24}s_{34}s_{13}\Big)\Big].\end{aligned} \tag{B.7}$$

Bibliography

[1] Y. Ne'eman, Nucl. Phys **26** (1961) 22;
M. Gell-Mann, Phys. Rev. **126** (1962) 1067;
M. Gell-Mann and Y. Ne'eman, *The eightfold way*, Benjamin (New York, 1964).

[2] M. Gell-Mann, Phys. Lett. **8** (1964) 214;
G. Zweig, CERN preprints CERN-TH-401 (1964), CERN-TH-412 (1964).

[3] O.W. Greenberg, Phys. Rev. Lett. **13** (1964) 598;
M.Y. Han and Y. Nambu, Phys. Rev. **139B** (1965) 1006.

[4] H. Fritsch, M. Gell-Mann and H. Leutwyler, Phys. Lett. **47B** (1973) 365.

[5] G. Sterman, *Introduction to Quantum Field Theory*, Cambridge University Press (Cambridge, 1993).

[6] G. Sterman, Phys. Rev. **D17** (1978) 2773, 2789.

[7] F. Bloch and A. Nordsieck, Phys. Rev. **52** (1937) 54;
T. Kinoshita, J. Math. Phys. **3** (1962) 650;
T.D. Lee and M. Nauenberg, Phys. Rev. (1964) 1549.

[8] J.C. Collins, *Renormalization*, Cambridge University Press (Cambridge, 1984).

[9] J.C. Collins and D.E. Soper, Ann. Rev. Nucl. Part. Sci. **37** (1987) 383.

[10] K. Koller, T.F. Walsh and P.M. Zerwas, Z. Phys. **C2** (1979) 197;
E. Laermann, T.F. Walsh, I. Schmitt and P.M. Zerwas, Nucl. Phys. **B207** (1982) 205.

[11] P. Aurenche et al., Z. Phys. **C29** (1985) 459;
E.L. Berger, E. Braaten and R.D. Field, Nucl. Phys **B239** (1984) 52.

[12] J.F. Owens, Rev. Mod. Phys. **59** (1987) 465;
D.W. Duke and J.F. Owens, Phys. Rev. **D26** (1982) 1600.

[13] P. Aurenche et al. and C. Seez et al., Contributions to the Large Hadron Collider Workshop, (Aachen, October 1990).

[14] R.K. Ellis, W.J. Stirling and B.R. Webber, *QCD and Collider Physics*, Cambridge University Press (Cambridge, 1996).

[15] M. Carena and P.M. Zerwas, in *Physics at LEP2*, Vol. 1, G. Altarelli, T. Sjörstrand and F. Zwirner (eds.), CERN (Geneva, 1996).

[16] E. Fermi, Z. Phys. **88** (1934) 61.

[17] T.D. Lee and C.N. Yang, Phys. Rev. Lett. **104** (1956) 254.

[18] R.P. Feynman and M. Gell-Mann, Phys. Rev. **109** (1958) 193, **111** (1958) 362.

[19] F. Halzen and A.D. Martin, *Quarks and Leptons*, J. Wiley and Sons (New York, 1984).

[20] G. Hanson et al., Phys. Rev. Lett. **35** (1975) 1609.

[21] TASSO Collaboration: R. Brandelik et al., Phys. Lett. **B86** (1979) 243;
MARK-J Collaboration: D.P. Barber et al., Phys. Rev. Lett. **43** (1979) 830;
PLUTO Collaboration: Ch. Berger et al., Phys. Lett. **B86** (1979) 418;
JADE Collaborotion: W. Bartel et al., Phys. Lett. **91** (1980) 142.

[22] JADE Collaboration: W. Bartel et al., Phys. Lett. **B115** (1982) 338.

[23] S. Bethke, Contribution to the Durham Workshop on Jet Studies at LEP and HERA J. Phys. **G17** (1991) 1441.

[24] G. Sterman and S. Weinberg, Phys. Rev. Lett. **39** (1977) 1436.

[25] W.T. Giele and E.W.N. Glover, Phys. Rev. **D46** (1992) 1980.

[26] JADE Collaboration: S. Bethke et al., Phys. Lett. **B213** (1988) 235.

[27] Y. Dokshitzer, Contribution to the Durham Workshop on Jet Studies at LEP and HERA, J. Phys. **G17** (1991) 1441.

[28] N. Brown, Contribution to the Durham Workshop on Jet Studies at LEP and HERA, J. Phys. **G17** (1991) 1441.

[29] W.T. Giele, Doctoral Thesis, Leiden (1989).

[30] Z. Kunszt and D.E. Soper, Phys. Rev. **D46** (1992) 192.

[31] R.K. Ellis, D.A. Ross and A.E. Terrano, Nucl. Phys. **B178** (1981) 421.

[32] S. Catani and M.H. Seymour: Phys. Lett. **B378** (1996) 287, Nucl. Phys. **B485** (1997) 291.

[33] Z. Kunszt and P. Nason, in *Z physics at LEP 1*, Vol. 1, G. Altarelli, R. Kleiss and C. Verzegnassi (eds.), CERN (Geneva, 1989).

[34] K. Fabricius, I. Schmitt, G. Kramer and G. Schierholz, Z. Phys. **C11** (1981) 315.

[35] W.T. Giele, E.W.N. Glover and D.A. Kosower, Nucl. Phys. **B403** (1993) 633.

[36] E. Mirkes and D. Zeppenfeld, Phys. Lett. **B380** (1996) 205.

[37] E.W.N. Glover and M.R. Sutton, Phys. Lett. **B342** (1995) 375.

[38] A. Ali and F. Barreiro, Phys. Lett. **118B** (1982) 155;
A. Ali and F. Barreiro, Nucl. Phys. **B236** (1984) 269;
D.G. Richards, W.J. Stirling and S.D. Ellis, Phys. Lett. **119B** (1982) 193;
D.G. Richards, W.J. Stirling and S.D. Ellis, Nucl. Phys. **B229** (1983) 317;
N.K. Falck and G. Kramer, Z. Phys. **C42** (1989) 459;
Z. Kunszt, P. Nason, G. Marchesini and B.R. Webber in "Z physics at LEP 1", CERN 89-08, vol. 1, eds. G. Altarelli, R. Kleiss and C. Verzegnassi (CERN, Geneva, 1989).

[39] F.A. Berends and W.T. Giele, Nucl. Phys. **B313** (1989) 595;
A. Bassetto, M. Ciafaloni, and P. Marchesini, Phys. Rep. **100** (1983) 201;
M. Mangano and S. Parke, Phys. Rep. **200** (1991) 301.

[40] G. Altarelli and G. Parisi, Nucl. Phys. **B126** (1977) 298.

[41] C.F. Weiszäcker, Z. Phys. **88** (1934) 612;
E.J. Williams, Phys. Rev. **45** (1934) 729.

[42] Z. Bern, L. Dixon and D.A. Kosower, Proceedings of the Zeuthen Workshop on "QCD and QED in Higher Orders", Rheinsberg, 1996, Nucl. Phys. Proc. Suppl. **51C** (1996) 243.

[43] OPAL Collaboration: P.D. Acton et al., Z. Phys. **C54** (1992) 193.

[44] DELPHI Collaboration: P. Abreu et al., Z. Phys. **C53** (1992) 555.

[45] G. Kramer and H. Spiesberger, *Matrix element calculation of quark bremsstrahlung in* $O(\alpha\alpha_s)$, DESY 92-022 (1992), contribution to the Workshop on Photon Radiation from Quarks, Annecy, France, 1991.

[46] E.W.N. Glover and W.J. Stirling, Phys. Lett. **B295** (1992) 128.

[47] Z. Kunszt and Z. Trócsányi, Nucl. Phys. **B394** (1993) 139.

[48] M.H. Seymour, Z. Phys. **C56** (1991) 116.

[49] A.G. Morgan and E.W.N. Glover, Z. Phys. **C62** (1994) 311.

[50] G. Altarelli, R.K. Ellis, G. Martinelli and S.Y. Pi, Nucl. Phys. **B160** (1979) 301.

[51] G. Curci, W. Furmanski and R. Petronzio, Nucl. Phys. **B175** (1980) 27;
W. Furmanski and R. Petronzio, Phys. Lett. **97B** (1980) 437.

[52] D.J. Gross and F. Wilczek, Phys. Rev. Lett. **30** (1973) 1342;
H.D. Politzer, Phys. Rev. Lett. **30** (1973) 1346;
W.E. Caswell, Phys. Rev. Lett. **33** (1974) 244;
O.V. Tarasov, A.A. Vladimirov and A.Yu. Zharkov, Phys. Lett. **93B** (1980) 429;
T. van Ritbergen, J.A.M. Vermaseren and S.A. Larin, NIKHEF preprint 97-001.

[53] Particle Data Group: Phys. Rev. **D54** (1996) 1.

[54] M. Glück, K. Grassie and E. Reya, Phys. Rev. **D30** (1984) 1447.

[55] E. Witten, Nucl. Phys. **B120** (1977) 129;
R.J. DeWitt, L.M. Jones, J.D. Sullivan, D.E. Willen and H.W. Wyld, Jr., Phys. Rev. **D19** (1979) 2046 [Erratum **D20** (1979) 1751].

[56] M. Glück, E. Reya and A. Vogt, Phys. Rev. **D48** (1993) 116.

[57] E. Berger, Xiao-Feng Guo and Jian-Wei Qiu, Phys. Rev. **D53** (1996) 1124.

[58] P. Aurenche, P. Chiappetta, M. Fontannaz, J.P. Guillet and E. Pilon, Z. Phys. **C56** (1992) 589.

[59] L. Gordon, M. Glück, E. Reya and W. Vogelsang, Phys. Rev. Lett. **73** (1993) 388.

[60] P. Aurenche, P. Chiappetta, M. Fontannaz, J.P. Guillet and E. Pilon, Nucl.Phys. **B399** (1993) 34.

[61] B.R. Webber, Contribution to the Durham workshop on Jet Studies at LEP and HERA J. Phys. **G17** (1991) 1441.

[62] ALEPH collaboration: D. Buskulic et al., Z. Phys. **C69** (1996) 365.

[63] J.A.M Vermaseren, Symbolic Manipulation with FORM, Computer Algebra Netherlands, Amsterdam, 1991

[64] E.W.N. Glover (private communication)

[65] G. 't Hooft and M. Veltman, Nucl. Phys. **B153** (1979) 365.

[66] Z. Bern, L. Dixon, D.C. Dunbar and D.A. Kosower, Nucl. Phys. **B425** (1994) 217.

[67] P.J. Rijken and W.L. van Neerven, Nucl. Phys. **B487** (1997) 233.

[68] W.A. Bardeen, A.J. Buras, D.W. Duke and T. Muta, Phys. Rev. **D18** (1978) 3998.

[69] E.B Zijlstra and W.L. van Neerven, Nucl. Phys. **B383** (1992) 525.

[70] G.P. Lepage, J. Comp. Phys. **27** (1978) 192.

[71] A. Erdelyi (ed.), *Higher Transcendental Functions, vol. 1*, Bateman Manuscript Project, Mc Graw-Hill (New York, 1953).

[72] A. Devoto and D.W. Duke, Riv. Nuovo Cimento **7**, Vol.**6** (1984) 1.

[73] M. Abramowitz and I. A. Stegun, *Handbook of Mathematical functions*, National Bureau of Standards Applied Mathematics Series **55** (1964).